



Remote Sensing of Surface Urban Cool and Heat
Island Dynamics in Erbil, Iraq, between 1992 and 2013

Thesis submitted for the degree of
Doctor of Philosophy
at the University of Leicester

by

Azad Othman Rasul (MSc)

Department of Geography
University of Leicester

2016

Remote Sensing of Surface Urban Cool and Heat Island Dynamics in Erbil, Iraq,
between 1992 and 2013.

Azad Rasul

Abstract

The variation between surface and air temperature within a city and its surrounding area is a result of variations in surface cover, thermal capacity and 3-dimensional geometry. This study examines the spatiotemporal formation of the daytime Surface Urban Cool Island (SUCI) and night-time Surface Urban Heat Island (SUHI) effect in Erbil, Iraq, as a case study for cities in semi-arid climates more generally. It furthermore quantifies the influence of rapid urban expansion on the urban heat/cool island effect over a 20 year period.

Satellite images acquired by Landsat 4, 5, 7 and 8 between 1992 and 2013 are used to retrieve Land Surface Temperature (LST). Normalised Ratio Scale (NRS) is applied to the multi-mission Landsat data, which is used to adjust the temperature range for different acquisition times of images within the same temporal range. In addition, LST data from the Moderate Resolution Imaging Spectroradiometer (MODIS) on board Aqua and Terra from January 2003 to December 2014 are analysed. In order to establish the drivers of the observed patterns of LST and SUCI/SUHI, the relationships of LST with wetness, greenness, NDVI, soil moisture and other variables are assessed.

The results indicate that during the daytime in summer, autumn and winter, densely built-up areas had lower LST acting as cool islands (SUCI) compared to the non-urbanised area around the city. In contrast, at night-time, Erbil experienced higher LST and demonstrated a significant SUHI effect. The mean LST of the newly urbanised and vegetated areas between 1992 and 2013 decreased by 2.28°C and 7.29°C respectively. Soil moisture (wetness) is the main marker of the SUCI/SUHI effect, whilst urban expansion may cause a decrease of daytime LST in dry climate zones. The NRS method is appropriate for detecting temperature trends greater than 2°C in Landsat data.

Dedication

This thesis is dedicated to my parents, my wife (Dr Khawlah), sons (Anas, Aviar and Muhammad), sister and brothers. I am grateful to all of you.

Acknowledgements

I would like to express my very great appreciation to my supervisors Professor Heiko Balzter and Dr Claire Smith for providing me sufficient guidance, useful critiques and support to complete this research. I would like to acknowledge the Human Capacity Development Program (HCDP) for their financial support. I express my gratitude to Professor Kevin Tansey (Head of Department) and Professor Alexis Comber (Thesis Chairs), for their valuable suggestions and productive comments that provided assistance in completing this thesis. I greatly appreciated the assistance provided by Dr Virginia Nicola-Perea, Adam Cox for his technical support, and other academic staff who contributed to the success of this research. I wish to acknowledge the support before commencing the research from Professor Sulaiman Ismail (Salahaddin University).

Much gratitude goes to the USGS, for providing the research with liberates Landsat images and the Oak Ridge National Laboratory Distributed Active Archive Centre (ORNL DAAC), for providing the research with MODIS products of the case study area. I would moreover like to acknowledge the R Development Core Team who continuously improve and support this liberate available software.

I appreciate technical ideas and knowledge we have shared with all CLCR colleagues Ajoke Onojeghuo, Alex Cumming, Ana Maria Pacheco-Pascagaza, Andrea Hurtado Mendoza-Rosales, Dr Bashir Adamu, Dr Beth Cole, Dr Claire Burwell, Chloe Barnes, Dr Ehsan Khalefa, Hao Wang, James Wheeler, Isah Hamisu, Dr Marc Padilla-Parellada, Maryam Pourshamsi, Dr Narissara Nuthammachot, Nkeiruka Nneti, Dr Paul Arellano, Dr Pedro Rodriguez-Veiga, Dr Polyanna Bispo, Dr Prem Pandey, Peshawa Najmaddin, Rahel Hamad, Dr Ramesh Ningthoujam, Saad Ibrahim, Dr Sara Johnson, Thomas Potter, Valentin Louis, Yahaya Zayyana Ibrahim, and the list continues.

I am definitely much thankful to my family members who always support me in difficult times. I am likewise grateful to my friend Zana Ghazi (Soran University), who assisted with valuable support. Finally, a special gratitude goes to my wife Dr ‘Khawlah’ for all her patience and support throughout the duration of my research.

Table of contents

Abstract.....	i
Dedication.....	ii
Acknowledgements.....	iii
Table of contents.....	iv
List of tables.....	ix
List of figures.....	x
List of acronyms and abbreviations	xiii
Chapter 1 : Introduction and Thesis Overview	1
1.1 Introduction.....	2
1.2 Urban Heat Island	2
1.2.1 Defining Urban Heat and Cool Islands	2
1.2.2 Causes of Urban Heat Islands	3
1.2.3 Factors Which Affect an Urban Heat Island	4
1.2.4 Urban Heat Island Intensity	7
1.2.5 Impacts of the UHI.....	7
1.2.6 Types of Urban Heat Islands.....	8
1.3 Thermal Remote Sensing.....	10
1.3.1 The Electromagnetic Spectrum	10
1.3.2 Reflectance Properties of the Surfaces.....	12
1.3.3 Optical Remote Sensing.....	12
1.3.4 Blackbody Theory.....	12
1.3.5 The Estimation of Land Surface Temperature	13
1.4 Thesis Structure	20
Chapter 2 : Literature Review.....	22
2.1 Introduction.....	23
2.2 Atmospheric Urban Heat Island	23

2.3 Urban Thermal Remote Sensing.....	25
2.3.1 Atmospheric Correction.....	25
2.3.2 Emissivity Correction	27
2.3.3 Methods of Retrieved Land Surface Temperature	28
2.3.4 Using Land Surface Temperature from Remote Sensing Data.....	29
2.3.5 Determination of Urban Area	30
2.4 Surface Urban Heat Island.....	31
2.4.1 Satellite Measurements of Urban Heat Island.....	31
2.4.2 Urban Heat Island in Arid and Semi-Arid Climate.....	33
2.4.3 Thermal Urban Studies in Areas Relatively Close to the Study Area ..	34
2.5 Cool Islands	35
2.6 Technique and Statistics Used in Urban Heat Island Studies.....	36
2.6.1 Methods to Compare Multi-Temporal LST Images	36
2.6.2 Determining the Urban Heat Island	37
2.6.3 Statistical Analyses of Urban Heat Islands	37
2.6.4 Models for Simulation Surface Temperature and Urban Heat Island...38	
2.7 Factors Which Affect UHI and LST.....	39
2.7.1 Influence of Urbanisation and City Expansion on Temperature.....	40
2.7.2 Influence of Vegetation on Temperature	42
2.7.3 Soil Moisture and Water Body.....	43
2.8 Gaps in Literature	44
2.9 Research Questions and Objectives.....	44
2.9.1 Research Questions	44
2.9.2 Aims of the Research	45
2.9.3 Objectives of the Research.....	45
Chapter 3 : Study Area.....	46
3.1 Introduction.....	47

3.2 Geology of the Study Area	48
3.2.1 Pleistocene Units and Alluvium.....	48
3.2.2 Bakhtiary Formation	48
3.3 Soil of the Study Area.....	50
3.4 Topography of the Study Area	51
3.5 Climate of the Study Area	52
3.5.1 Air Temperature	52
3.5.2 Air Pressure.....	54
3.5.3 Winds	55
3.5.4 Relative Humidity	56
3.5.4 Cloud Cover	56
3.5.5 Precipitation	57
3.6 Vegetation and Green Area	59
3.7 Growth of the City	60
3.8 Building Components in Erbil.....	61
3.9 Population of the City	62
Chapter 4 : Spatial Variation of the Daytime Surface Urban Cool Island during the Dry Season in Erbil, from Landsat 8.....	64
4.1 Introduction and Rationale	65
4.2 Data and Methodology	66
4.2.1 Data and Pre-Processing	66
4.2.2 Retrieval of LST.....	72
4.2.3 Identification of the Surface UCI and UHI Intensity	73
4.2.4 Calculating Wetness, Greenness and Brightness Components.....	73
4.2.5 Calculating Built-up and Vegetation Indices	74
4.3 Results.....	75
4.3.1 SUCI in the City.....	75

4.3.2	Variation of LST with Land Use / Land Cover	76
4.3.3	Variation of SUCI and SUHI in Selected LULC Classes	76
4.3.4	Spatial Variation of Wetness, Brightness and Greenness Components	77
4.3.5	Relationship between Land Surface Temperature and Wetness, Brightness and Greenness in Different LULC Classes	79
4.3.6	Spatial Variation of LST in Districts of the City	80
4.3.7	Relationship Between LST and Built-up and Vegetation Index.....	83
4.4	Discussion.....	84
4.5	Summary.....	85
Chapter 5 :	The Temporal Variation of Surface Urban Cool and Heat Islands in Erbil.	86
5.1	Introduction and Rationale	87
5.2	Data and Methodology	88
5.2.1.	Data	88
5.2.2	Methodology	90
5.3	Results.....	93
5.3.1	Diurnal Variation of LST and SUCI/SUHI.....	93
5.3.2	Seasonal Variation of LST and SUCI/SUHI.....	95
5.3.3	Interannual Variation of LST and SUCI/SUHI.....	100
5.3.4	Key Determinants of LST	101
5.3.5	Relationships Between LST and NDVI, fsm, ET and LE	103
5.4	Discussion.....	105
5.5	Summary.....	106
Chapter 6 :	Changes of the Urban Heat/Cool Island Effect in the Urban Expansion Zone of Erbil, Between 1992 and 2013	108
6.1	Introduction and Rationale	109
6.2	Data and Methodology	110
6.2.1	Data and Pre-Processing	110
6.2.2	Methodology	112

6.3 Results.....	115
6.3.1 Normalised Ratio Scaled Land Surface Temperature.....	115
6.3.2 Effect of Vegetated Land on Land Surface Temperature	119
6.3.3 Decreasing LST of Urbanised Area from 1992 to 2013	122
6.3.4 Changes of LST for Different Types of LULC Change	124
6.4 Discussion.....	126
6.5 Summary.....	128
Chapter 7 : General Discussion, Conclusions and Research Contributions	129
7.1 Introduction.....	130
7.2 Original research contributions.....	130
7.3 General Discussion	131
7.4 Conclusions.....	133
7.5 Limitations of the Research	135
7.6 Future Research Directions.....	136
Appendices.....	138
Bibliography	147

List of tables

<i>TABLE 1-1: TYPICAL INFRARED SENSORS FOR RETRIEVE LAND SURFACE TEMPERATURE.....</i>	<i>14</i>
<i>TABLE 2-1: A SUMMARY OF UHII/UCII IN DIFFERENT AREAS OF THE WORLD.</i>	<i>24</i>
<i>TABLE 4-1: IMAGES USED IN CHAPTER 4.....</i>	<i>68</i>
<i>TABLE 4-2: LAND SURFACE TEMPERATURE IN ERBIL AND ITS SURROUNDINGS DURING SUMMER 2013.</i>	<i>75</i>
<i>TABLE 4-3: MEAN NDBI FOR DIFFERENT LULC CLASS IN THE STUDY AREA.</i>	<i>83</i>
<i>TABLE 5-1: SUMMARY OF MODIS IMAGE PRODUCTS USED IN CHAPTER 5.</i>	<i>89</i>
<i>TABLE 6-1: IMAGES USED IN CHAPTER 6.....</i>	<i>111</i>
<i>TABLE 6-2: MEAN, SD, VARIANCE AND Δ LST IN DEGREE CELSIUS FOR DIFFERENT METHOD FROM LANDSAT IMAGES.</i>	<i>119</i>
<i>TABLE 6-3: LAND SURFACE TEMPERATURE AND NDVI IN S.A. PARK IN 1992, 2002 AND 2013.....</i>	<i>121</i>
<i>TABLE 6-4: CHANGE IN LST OF THE AREA URBANISED FROM 1992 TO 2013.....</i>	<i>124</i>
<i>TABLE 6-5: URBAN EXPANSION IN THE STUDY AREA.</i>	<i>124</i>
<i>TABLE 6-6: PIXEL SAMPLES OF LULC CHANGE WITH MEAN LST, NDVI AND ISA.....</i>	<i>125</i>

List of figures

FIGURE 1.1: ISOTHERM OF LONDON'S ATMOSPHERIC HEAT ISLAND FOR SIX NIGHTS DURING THE SUMMER OF 2000.....	3
FIGURE 1.2: THE CATEGORIES OF UHIS.....	4
FIGURE 1.3: THE ELECTROMAGNETIC SPECTRUM	11
FIGURE 1.4: THESIS STRUCTURE.....	20
FIGURE 2.1: FACTORS OF URBAN HEAT ISLAND (UHI).....	40
FIGURE 3.1: MAP OF IRAQ, KURDISTAN REGION AND TRUE COLOUR LANDSAT OF THE STUDY AREA.....	47
FIGURE 3.2: TERTIARY AND QUATERNARY ROCK UNITS IN IRAQ.....	49
FIGURE 3.3: GEOLOGICAL MAP OF ERBIL BASIN.....	49
FIGURE 3.4: SOIL TYPES IN THE ERBIL GOVERNORATE.....	50
FIGURE 3.5: ELEVATION OF THE STUDY AREA.....	51
FIGURE 3.6: ANNUAL MEAN TEMPERATURE OF ERBIL GOVERNORATE FROM 1973 TO 2011.....	53
FIGURE 3.7: MONTHLY TEMPERATURE IN ERBIL.....	53
FIGURE 3.8: WIND SPEED AND DIRECTION (%) OF ERBIL CITY.....	55
FIGURE 3.9: MONTHLY CLOUDINESS OF ERBIL.....	57
FIGURE 3.10: MONTHLY PRECIPITATION OF ERBIL FROM 1993 TO 2012	58
FIGURE 3.11: TIME SERIES OF ANNUAL PRECIPITATION FROM 1941 TO 2011.....	58
FIGURE 3.12: SAMI ABDUL-RAHMAN PARK IN ERBIL.....	60
FIGURE 3.13: URBAN TRANSFORMATION STAGES OF ERBIL CITY UNTIL 2007.....	61
FIGURE 3.14: BUILDING TYPES IN ERBIL.....	62
FIGURE 4.1: IMAGE LANDSAT 5 OF STUDY AREA OF 31 JULY 1992.....	68
FIGURE 4.2: GENERAL METHODOLOGY FLOWCHART ADOPTED IN THIS STUDY.....	69
FIGURE 4.3: SAMPLES OF SELECTED LULC WITH THE TRUE COLOUR LANDSAT OLI.....	70
FIGURE 4.4: SAMPLES OF SELECTED LULC IN ERBIL.....	71
FIGURE 4.5: MEAN LST, SUCI AND SUHI IN THE LULC CLASSES DURING SUMMER 2013.....	76
FIGURE 4.6: MEAN WETNESS, GREENNESS AND BRIGHTNESS FOR EACH LULC CLASS DURING SUMMER 2013.....	77
FIGURE 4.7: WETNESS, GREENNESS AND BRIGHTNESS OF THE STUDY AREA DURING SUMMER 2013.....	78
FIGURE 4.8: CORRELATION COEFFICIENT BETWEEN LST AND WETNESS, BRIGHTNESS AND GREENNESS DURING SUMMER 2013.....	79
FIGURE 4.9: LST OF THE DISTRICTS OF ERBIL, AT 7:40 DURING SUMMER 2013.....	81
FIGURE 4.10: LST OF DISTRICTS OF ERBIL DURING SUMMER 2013.....	82
FIGURE 4.11: RELATIONSHIP OF LST WITH NDVI AND NDBI DURING SUMMER 2013.....	83
FIGURE 5.1: AVERAGE LAND SURFACE TEMPERATURE OF THE CITY AND THE RURAL AREAS.....	94
FIGURE 5.2: AVERAGE LAND SURFACE TEMPERATURE OF THE CITY AND THE RURAL AREAS.....	94

FIGURE 5.3: DIURNAL VARIATION OF AVERAGE 2014 LAND SURFACE TEMPERATURE AND SURFACE URBAN COOL ISLAND/ SURFACE URBAN HEAT ISLAND DURING THE DAY AND NIGHT.	95
FIGURE 5.4: DIURNAL VARIATION OF AVERAGE LAND SURFACE TEMPERATURE IN DIFFERENT SEASONS OVER 12 YEARS FROM AQUA AND TERRA MODIS AND SURFACE URBAN COOL ISLAND / SURFACE URBAN HEAT ISLAND.....	97
FIGURE 5.5: SEASONAL VARIATION OF AVERAGE LAND SURFACE TEMPERATURE OVER 12 YEARS.	98
FIGURE 5.6: LST OF THE STUDY AREA FROM MODIS AQUA 8 DAY COMPOSITE IMAGE (A2014209)..	99
FIGURE 5.7: ANNUAL VARIATIONS OF LAND SURFACE TEMPERATURE AND SURFACE URBAN COOL ISLAND / SURFACE URBAN HEAT ISLAND FROM 2003 TO 2014.....	100
FIGURE 5.8: NDVI, SOIL MOISTURE CONSTRAINT, EVAPOTRANSPIRATION AND LATENT HEAT FLUX IN THE CITY AND RURAL AREA FROM 2003 TO 2014.	102
FIGURE 5.9: RELATIONSHIP OF LAND SURFACE TEMPERATURE WITH NDVI, SOIL MOISTURE CONSTRAINT FACTOR, EVAPOTRANSPIRATION AND LATENT HEAT FLUX FROM 12 YEARS MODIS DATA.	104
FIGURE 5.10: LAND SURFACE TEMPERATURE AGAINST SEASONAL NDVI, FROM 12 YEARS MODIS DATA.	104
FIGURE 6.1: LOCATION OF PIXEL SAMPLES OF LULC CHANGE.....	112
FIGURE 6.2: LST OF ERBIL BASED ON DIFFERENT METHOD FROM LANDSAT IMAGES..	116
FIGURE 6.3: DAYTIME LST OF ERBIL BASED ON DIFFERENT METHOD FROM LANDSAT IMAGES..	117
FIGURE 6.4: COMPARE LST OF ERBIL BASED ON THE DIFFERENT METHODS OF NORMALIZING LANDSAT IMAGES..	118
FIGURE 6.5: MEAN LST AND NDVI OF S.A. PARK FROM 1992 TO 2013 FROM LANDSAT.	120
FIGURE 6.6: THE CHANGE OF NDVI AND LST _{NRS} OF S.A. PARK FROM 1992 TO 2013.	121
FIGURE 6.7: DECREASE IN LST IN THE AREA THAT WAS URBANISED	123
FIGURE A. 1: MODIS TERRA LST DAYTIME PRODUCT (MOD11A2.A2002153).....	138
FIGURE A. 2: MODIS TERRA LST NIGHT-TIME PRODUCT (MOD11A2.A2006089).....	138
FIGURE A. 3: LANDSAT 8 BAND 10 FOR 01-07-2013.	139
FIGURE A. 4: METADATA OF LANDSAT 4 (LT41690351992213XXX02).....	139
FIGURE A. 5: METADATA OF LANDSAT 7 (LE71690352002208GS00).....	140
FIGURE A. 6: METADATA OF LANDSAT 8 (LC81690352013182LGN00).....	140
FIGURE A. 7: LANDSAT 8 TRUE COLOUR ATMOSPHERICALLY CORRECTED WITH QUAC METHOD.	141
FIGURE A. 8: RADIANCE IMAGE OF LANDSAT 8 BAND 10 ATMOSPHERICALLY CORRECTED WITH THERMAL ATMOSPHERIC CORRECTION METHOD.....	142
FIGURE A. 9: USING ARCGIS FOR CREATE LST MAP OF DISTRICTS OF ERBIL	143
FIGURE A. 10: R SCRIPT FOR PROCESSING LST MODIS PRODUCTS.....	143
FIGURE A. 11: R SCRIPT FOR PRODUCE LST OF URBANISED AREAS FROM 1992 TO 2013.....	144
FIGURE A. 12: EXTRACTED NDVI DATA FOR THE CITY AND SURROUNDING FOR DIFFERENT SEASONS AS EXCEL FILE.....	144
FIGURE A. 13: STATISTICAL OUTPUT OF LST OF 2002 FROM LANDSAT FOR THE STUDY AREA WITHIN ENVI SOFTWARE.....	145
FIGURE A. 14: LST OF PIXEL SAMPLES OF LULC CHANGE.....	145

*FIGURE A. 15: RADIANCE ATMOSPHERICALLY CORRECTED FROM SINGLE CHANNEL AND THERMAL
ATMOSPHERIC CORRECTION..... 146*

*FIGURE A. 16: LST ATMOSPHERICALLY CORRECTED FROM SINGLE CHANNEL AND THERMAL ATMOSPHERIC
CORRECTION..... 146*

List of acronyms and abbreviations

$^{\circ}\text{C}$	<i>Degree Celsius</i>
<i>3-d</i>	<i>Three Dimensional</i>
<i>ACRON</i>	<i>Atmosphere CORrection Now</i>
<i>ANEM</i>	<i>adjusted normalised emissivity method</i>
<i>ASTER</i>	<i>Advanced Spaceborne Thermal Emission Reflection Radiometer</i>
<i>ATREM</i>	<i>Atmosphere Removal Algorithm</i>
<i>AUHI</i>	<i>Atmospheric Urban Heat Island</i>
<i>AVHRR</i>	<i>Advanced Very High Resolution Radiometer</i>
<i>BI</i>	<i>brightness index</i>
<i>BLUHI</i>	<i>Boundary Layer Urban Heat Island</i>
<i>BSh</i>	<i>Subtropical Semiarid</i>
<i>CBEM</i>	<i>classification based emissivity method</i>
<i>CLUHI</i>	<i>Canopy Layer Urban Heat Island</i>
<i>Csa</i>	<i>Mediterranean climate</i>
<i>e.g.</i>	<i>for example</i>
<i>EBM</i>	<i>emissivity bounds method</i>
<i>EELM</i>	<i>Emissive Empirical Line Method</i>
<i>EM</i>	<i>electromagnetic</i>
<i>Eq.</i>	<i>Equation</i>
<i>ERTS</i>	<i>Earth Resources Technology Satellite</i>
<i>ET</i>	<i>Evapotranspiration</i>
<i>ETM+</i>	<i>Enhanced Thematic Mapper Plus</i>
<i>FFT</i>	<i>fast Fourier transformation</i>
<i>FLAASH</i>	<i>Fast Line-of-sight Atmospheric Analysis of Spectral Hypercube</i>
<i>fsm</i>	<i>Soil Moisture Constraint Factor</i>
<i>GBE</i>	<i>grey-body emissivity</i>
<i>GIS</i>	<i>Geographical Information Science</i>
<i>GV</i>	<i>Green Vegetation</i>
<i>GVI</i>	<i>greenness index</i>
<i>GWR</i>	<i>Geographically Weighted Regression</i>

<i>GWRK</i>	<i>combined GWR residual kriging</i>
<i>HATCH</i>	<i>High-accuracy Atmospheric Correction for Hyperspectral Data</i>
<i>HCDP</i>	<i>Human Capacity Development Program</i>
<i>IAR</i>	<i>Internal Average Reflectance</i>
<i>IMW</i>	<i>improved mono-window</i>
<i>IR</i>	<i>Infrared Radiometer</i>
<i>ISA</i>	<i>impervious surface area</i>
<i>ISAC</i>	<i>in-scene atmospheric composition</i>
<i>ISSTES</i>	<i>iterative spectrally smooth temperature emissivity separation</i>
<i>K</i>	<i>Kelvin</i>
<i>LC</i>	<i>Land Cover</i>
<i>LE</i>	<i>Latent heat flux</i>
<i>LMSA</i>	<i>linear mixture pixel analysis</i>
<i>LSE</i>	<i>Land Surface Emissivity</i>
<i>LSMM</i>	<i>linear spectral mixture model</i>
<i>LST</i>	<i>Land surface temperature</i>
<i>LULC</i>	<i>Land Use Land Cover</i>
<i>m</i>	<i>Metre</i>
<i>MAS</i>	<i>MODIS airborne simulator</i>
<i>MIR</i>	<i>mid-infrared</i>
<i>MLR</i>	<i>Multiple Linear Regression</i>
<i>MMD</i>	<i>min-max difference</i>
<i>MNDWI</i>	<i>Modified Normalised Difference Water Index</i>
<i>MODIS</i>	<i>Moderate resolution imaging spectroradiometer</i>
<i>NASA</i>	<i>National Aeronautics and Space Administration</i>
<i>NBEM</i>	<i>NDVI based emissivity method</i>
<i>NDBaI</i>	<i>Normalised Difference Bareness Index</i>
<i>NDBI</i>	<i>Normalised Difference Built-up Index</i>
<i>NDVI</i>	<i>Normalised Difference Vegetation Index</i>
<i>NDWI</i>	<i>Normalised Difference Water Index</i>
<i>NEM</i>	<i>normalisation emissivity method</i>
<i>NIR</i>	<i>Near-infrared</i>
<i>nm</i>	<i>Nanometre</i>

<i>NOAA</i>	<i>National Oceanic and Atmospheric Administration's</i>
<i>NOR</i>	<i>emissivity normalisation</i>
<i>NO_x</i>	<i>nitrogen oxide</i>
<i>NRS</i>	<i>Normalised Ratio Scale</i>
<i>OCIE</i>	<i>oasis cold island effect</i>
<i>OLI</i>	<i>Operational Land Imager</i>
<i>ORNL -</i>	
<i>DAAC</i>	<i>Oak Ridge National Laboratory Distributed Active Archive Centre</i>
<i>PBMs</i>	<i>physically based methods</i>
<i>PCA</i>	<i>Principal component analysis</i>
<i>QA</i>	<i>quality assessment</i>
<i>QUAC</i>	<i>quick atmospheric correction</i>
<i>RE</i>	<i>emissivity re-normalisation method</i>
<i>REF</i>	<i>reference channel method</i>
<i>RH</i>	<i>relative humidity</i>
<i>RK</i>	<i>Residual Kriging</i>
<i>RT</i>	<i>Radiative Transfer</i>
<i>RTE</i>	<i>Radiative transfer equation</i>
<i>S.A. Park</i>	<i>Sami Abdul-Rahman Park</i>
<i>SA-C-VW</i>	<i>Semi-arid Cool Very Warm</i>
<i>SAVI</i>	<i>Soil-Adjusted Vegetation Index</i>
<i>SD</i>	<i>Standard Deviation</i>
<i>SEMs</i>	<i>Semi-empirical methods</i>
<i>SHIM</i>	<i>surface urban heat island model</i>
<i>SLC</i>	<i>Scan Line Corrector</i>
<i>SR</i>	<i>spectral ratio</i>
<i>St error</i>	<i>Standard error</i>
<i>SUCI</i>	<i>Surface Urban Cool Island</i>
<i>SUHI</i>	<i>Surface Urban Heat Island</i>
<i>SW</i>	<i>Split window</i>
<i>SWIR</i>	<i>shortwave infrared</i>
<i>TC</i>	<i>Tasselled Cap</i>
<i>TCT</i>	<i>Tasselled Cap transformation</i>

<i>TCZs</i>	<i>thermal climate zones</i>
<i>TES</i>	<i>Temperature–Emissivity Separation</i>
<i>TIR</i>	<i>Thermal infrared</i>
<i>TIROS</i>	<i>Television Infrared Observation Satellite</i>
<i>TIRS</i>	<i>Thermal Infrared Sensor</i>
<i>TISI</i>	<i>Temperature-independent spectral indices</i>
<i>TM</i>	<i>Thematic Mapper</i>
<i>TOA</i>	<i>top of atmosphere</i>
<i>TSRM</i>	<i>two-step physical retrieval method</i>
<i>TTM</i>	<i>two-temporal method</i>
<i>TVX</i>	<i>temperature/vegetation index</i>
<i>UCII</i>	<i>Urban Cool Island Intensity</i>
<i>UHI</i>	<i>Urban Heat Island</i>
<i>UHII</i>	<i>Urban Heat Island Intensity</i>
<i>UHSs</i>	<i>Urban Heat Sinks</i>
<i>USGS</i>	<i>United States Geological Survey</i>
<i>VIS</i>	<i>visible</i>
<i>WI</i>	<i>wetness index</i>
<i>WRF</i>	<i>Weather Research and Forecasting</i>
ΔT	<i>temperature difference</i>
μm	<i>Micrometer</i>

Chapter 1 : Introduction and Thesis Overview

1.1 Introduction

This chapter presents an overview of the existing knowledge on the topic of research (Urban Heat Island), thermal remote sensing and establishes the research questions and objectives of the research. It commences with definitions, factors and the impacts of UHI to provide readers with more knowledge regarding the topic and its importance.

1.2 Urban Heat Island

When the city is warmer than the surrounding rural area - especially at night time - a phenomenon occurs which is known as an “urban heat island” (UHI). Luke Howard first recognised the UHI in London (Howard, 1833). The results indicated that, at night, the city on average was 2.1°C warmer than in the countryside while during the day it is 0.19°C cooler (Landsberg, 1981, Bonan, 2002). This difference between city temperatures and rural temperatures is referred to in this thesis as ΔT .

1.2.1 Defining Urban Heat and Cool Islands

Urbanisation brings a substantial and fundamental change to the nature of the local surface and atmosphere. A list of micro and medium climates exist due to changes in radiation, thermal properties, humidity, and aerodynamic properties (Roth *et al*, 1989). An UHI is an urban area that generates higher temperatures than its non-urbanised surroundings (Wetherick *et al*, 2001; Weng *et al*, 2004; Farina, 2012). In contrast, Urban Cool Islands (UCI), equivalent to negative UHI, have lower temperatures than their rural surroundings (Guoyin and Mingyi, 2009; Shigeta *et al*, 2009; Miao *et al*, 2009). The term 'island' stems from the shape of the temperature pattern and the pattern of isotherms which resembles an island (Farina, 2012; Figure 1.1). Generally, the intensity of this phenomenon increases as a result of the growth of a city and the rise in the number of residents. The term UHI/UCI refers to air temperature and here to the atmospheric urban heat island. In this thesis, SUHI and SUCI are used to identify surface temperature heat/cool islands. UHII and UCII refers to urban heat island and urban cool island intensity or maximum value (section 1.2.4).

Numerous researchers have confirmed that the SUHI intensities during the day are greater than at night (Roth *et al*, 1989). On the other hand, cities in arid and semi-arid areas probably demonstrate SUCIs on a daily basis (section 1.2.6.2).

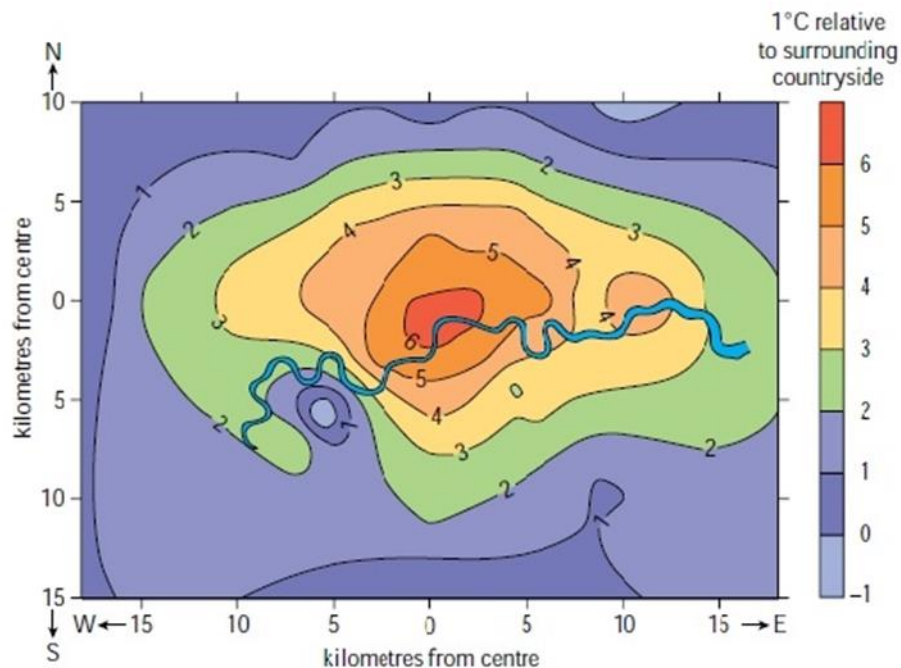


Figure 1.1: Isotherm of London's atmospheric heat island for six nights during the summer of 2000. (Vowles G., 2013)

1.2.2 Causes of Urban Heat Islands

Robinson and Ann (1999) enumerated seven hypothetical causes of the UHI effect.

- Absorbing long-wave radiation by urban surfaces in view of the sky and re-emitting it into the polluted atmosphere above the city causes an increase in counter radiation (i.e. back radiation).
- The effect buildings on decreasing sky view causes the reduction of long-wave radiation loss.
- The effect of canyon geometry on the albedo causes wide absorption of shortwave radiation (Figure 1.2).
- Low wind speeds in the canopy (tall buildings and narrow sidewalks) negatively affect sensible heat loss.
- Characters of urban material cause frequent storage heat during the day, which is released at night.

- Anthropogenic heat sources input more heat into the urban atmosphere and surface.
- Converting green areas to impervious surfaces in the cities causes a decrease of evaporation and transpiration and hence higher temperature.

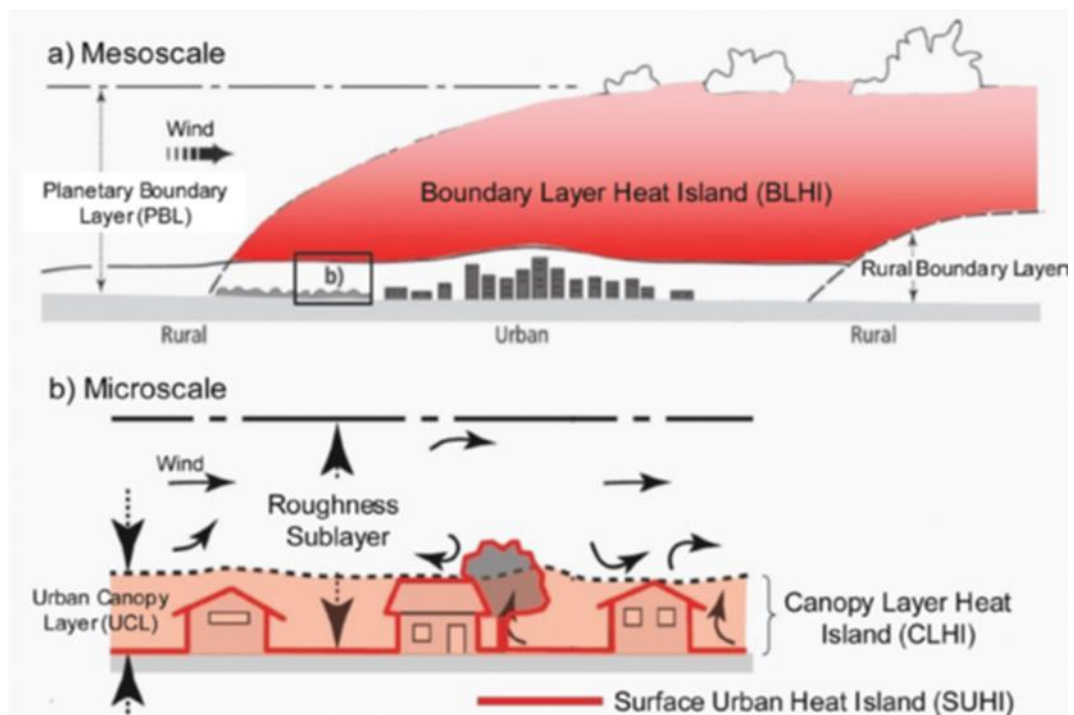


Figure 1.2: The categories of UHIs (Srivanit and Hokao, 2012, modified after Voogt, 2004).

1.2.3 Factors Which Affect an Urban Heat Island

1.2.3.1 Urban heat island and population

Generally, population size of the city has a clear relationship with ΔT between city and surrounding rural areas. Under transparent skies, UHI intensity is positively related to the logarithm of population (Oke, 1973; Zhao *et al*, 2014). Large cities in Europe are a few degrees cooler than comparable cities in North America (Bonan, 2002). The temperature variation (ΔT) between urban and rural areas and population (P) are related as:

$$\text{Europe: } \Delta T = 3.02 \log_{10}(P) - 3.29 \quad 1.1$$

$$\text{North America: } \Delta T = 5.21 \log_{10}(P) - 11.24 \quad 1.2$$

1.2.3.2 Urban heat island and weather

Characteristics of the UHI depend on weather conditions. A ΔT between urban and rural areas is generally smallest in cloudy and windy situations and largest in clear, calm conditions. The strong winds transport characteristics of rural areas into the city while the effect of clouds lessens the urban warming effect (Kidder and Essenwanger, 1995). For example, the atmospheric humidity of rural areas of St. Louis, Missouri is higher than urban areas from 0700 to around midnight then the urban site is more humid. Wind is another factor as strong winds decrease UHI due to the fact that they effectively mix heat through the atmosphere (Bonan, 2002).

1.2.3.3 Urban heat island and urban geometry

The temperature variations between the urban and rural areas depend on urban geometry factors (i.e. size, shape and direction of buildings and streets) and the nature of urban surfaces (i.e. albedo, heat capacity, thermal conductivity and wetness) (Bonan, 2002). The street geometry and its distribution within the city area play an essential role in creating patterns of the street surface temperature and 'surface heat island' (Barring, Mattsson and Lindqvist, 1985). The change in these features transforms the radiation balance, the storage of heat and the dividing of energy into latent and sensible heat (Landsberg, 1981; Oke, 1982; Oke, 1987).

Below rooftop level, which is called the 'urban canopy layer', buildings, roads and vegetation in cities generate a microclimate. The nature of the immediate surroundings (especially site materials and geometry) controls the climate of urban canopy (Oke, 1976). Shade from buildings in this layer can create cooler local temperatures than nearby open areas. In a city, vegetated lawns and parks are able to have large latent heat fluxes relative to the rest of the urban fabric (Bonan, 2002).

Sky view factor suitably indicates the effect of urbanisation on UHI intensity (Yamashita *et al*, 1986). The centre of the urban canyon is only exposed to a portion of the sky due to tall buildings which block some of it. The fraction of the sky for a substantially long street is:

$$\psi = \cos(a) \quad 1.3$$

where a is the angle defined by street width W and building height H as $\tan(a) = 2H/W$. The portion of the cold sky that is blocked by the urban buildings increases as a result

of a rise in the ratio of H/W. The buildings surrounding the street absorb more of the emitted longwave radiation limiting the amount that can escape to the atmosphere (Bonan, 2002). Sky view factor is strongly related to ΔT between urban and rural areas. The magnitude of the effective urban surface temperature warming will increase as a result of more sky view seen.

In the architecture of arid and semi-arid areas, a courtyard is a common element of buildings (Etzion, 1990). The courtyard behaves in the same manner as an urban canyon. In the large courtyard, the sky view factor increases and the air becomes warmer during the day due to more solar radiation reaching the ground and it is cooler at night. While in the small courtyards, solar radiation did not reach the surface therefore the air is cool in the morning and mildly warm at night compared with rooftop level (Bonan, 2002).

1.2.3.4 Urban heat island and surface cover/radiative exchange

Impervious surfaces such as asphalt and concrete absorb, store and re-radiate more heat energy than vegetated surfaces (Celestian and Martin, 2004). For example, the surface of a parking lot is usually hotter than nearby fields due to higher radiative forcing and greater heat storage (Bonan, 2002).

Numerous studies have demonstrated the importance of vegetated landscapes in amending the UHI. There is a strong relationship between the reduction of temperature and the presence of large green areas in a city (Wong and Yu, 2005). A big park – with a size of around 150 ha – can cool air temperature by around 6°C at night when compared to surrounding areas. Small size parks – sized around 2 ha – can only cool the air by about 2°C. The influence of a large park can extend 1000 m from its boundary whereas the small size may only extend 30 m from the boundary (Upmanis *et al*, 1998; Bonan, 2002).

A large amount of impervious surface in the city is a consequence of urban development and is considered to be an important contributor of the UHI effect. Limiting the amount of impervious surface in the cities is important to mitigate UHI, storm-water management, water recharge and habitat preservation (Lee and French, 2009). The daytime surface temperature can be linearly related to the percentage of impervious surface (Landsberg, 1979). Hard impervious surfaces such as asphalt and concrete have a warming effect while vegetated surfaces have a cooling effect. The

climate and ΔT is influenced due to these local landscapes in the cities. In cities with less vegetated area and greater impervious surfaces, the difference between urban and rural temperature increases (Carlson and Arthur, 2000; Bonan, 2002).

1.2.3.5 Numerical models of the energy balance of urban

The physical factors of the UHI can be explained with numerical models of the energy balance of urban surfaces that apply to the urban boundary layer above rooftops. A bulk formation can represent the energy balance of the urban as:

$$(1 - r)S \downarrow + L \downarrow = L \uparrow + H + \lambda E + G \quad 1.4$$

where $S \downarrow$ is the incoming solar and $L \downarrow$ is longwave radiation, r is albedo, $L \uparrow$ is emitted longwave radiation, H is sensible heat, λE is latent heat and G is heat storage (Terjung and O'Rourke, 1980a; Terjung and O'Rourke, 1980b). There is also the effect of anthropogenic heat which is an additional term to this standard equation.

1.2.4 Urban Heat Island Intensity

Urban Heat Island Intensity (UHII) is identified as the highest variation between urban and suburban/rural (ΔT_{u-r}) surface air temperatures (Roth *et al.*, 1989; Chow *et al.*, 2012; Zhao *et al.*, 2013; Menberg *et al.*, 2013). In contrast, Urban Cool Island Intensity (UCII) is the negative variation between temperatures of urban areas and their surroundings, when the latter are hotter than the former (Clinton and Gong, 2013). The intensity of UHIs depend on factors such as weather, a city's morphology, time of temperature measurement, and the classification of rural areas surrounding the city (Chow *et al.*, 2012). The intensity of the urban canopy layer (UCL) heat island (Figure 1.2) increases with the cloudless sky and calm wind, and it usually takes the daily cycle form. If conditions permit, in UCL heat island is at its lowest at midday and at its highest during the night, especially the hours immediately after sunset (Roth *et al.*, 1989).

1.2.5 Impacts of the UHI

For cold climates, and in winter, the UHI has some positive effects. Increasing temperatures cause enhanced comfort, reduced energy demands (i.e. for heating), a lengthened agricultural season, and the thawing of snows and ice on roads (Robinson

Peter and Ann, 1999; EPA, 2009). However, it has numerous negative effects on the urban inhabitants and environment during summer as discussed below:

- **Increased energy consumption:** according to Lee *et al* (2014), increased temperatures exacerbate energy demands in cities, which include the requirement of air conditioning to keep buildings cool. The use of air conditioners in both the residential and the commercial sector increases the UHI intensity (Golden *et al*, 2006; Chow *et al*, 2012). Therefore, pressure on electricity increases during summer afternoons, which is the period of peak demand. Generally, whenever the temperature increases by 0.6°C, electricity consumption rises on average between 1.5 and 2% (EPA, 2009).
- **Air quality and greenhouse gases:** the emission of greenhouse gases and air pollution increases as a result of rising energy demands (Tarle, 2010). Therefore, these emissions negatively affect the physical condition of people and contribute to air troubles, including acid rain. In addition, carbon dioxide emitted from power plants that work by fossil fuel contributes to global climate changes (EPA, 2009). Sarrat *et al* (2006) ascertained that the urban effect during both day and night has a profound influence on Parisian regional pollutants, namely ozone and nitrogen oxide (NO_x). The combination of heat and penurious air quality has severe implications for people with cardio-respiratory diseases.
- **Human health and comfort:** during the hot summer season, the UHI effect influences urban residents, reducing thermal comfort while increasing the risk of heatstroke, exhaustion, and heat-related mortality. In addition, it increases the effect of heat waves on inhabitants who are sensitive to high temperatures, such as the elderly, children and the sick (EPA, 2009; Su, Foody and Cheng, 2012; Chapman *et al*, 2013; Steeneveld *et al*, 2014).

1.2.6 Types of Urban Heat Islands

There are different categories of UHIs (Figure 1.2):

1.2.6.1. Surface Urban Heat Island: it is defined by higher temperatures of urban surfaces compared with rural surrounding surfaces. Studies of SUHI generally use land surface temperature (LST) images that are obtained from airborne and satellite thermal infrared remote sensing (Srivanit and Hokao, 2012). In contrast with Atmospheric

Urban Heat Islands (AUHIs), SUHIs are greatest during the day when solar inputs are highest and least at night, when long-wave losses occur (Roth *et al*, 1989). As a result of the variation of the sun's intensity, land cover and weather, the intensity of the SUHI changes with the seasons and typically it is greatest in the summer (EPA, 2009).

Researching the temperature of the surface is one of the substantial fields of the study of urban atmospheres. The surface temperature regulates the temperature of the lowest layer of air and the surface energy balance. Furthermore, by determining the climate inside buildings it affects the comfort of residents (Srivanit and Hokao, 2012).

1.2.6.2. Surface Urban Cool Island: it is defined by lower temperature of urban surface compared with rural surrounding surfaces. In contrast to cities in the temperate zone, during the daytime arid and semi-arid urban areas have lower LSTs than their surroundings. For instance, in Dubai the average LST in urban areas was 5°C lower than in rural ones. The reason is due to the presence of a dry desert environment in Dubai (Frey *et al*, 2012). SUCI and SUHI are chosen as the subject of this study.

1.2.6.3. Canopy Layer Urban Heat Island (CLUHI): it is defined by higher air temperature of the urban canopy layer compared with rural surrounding areas. CLUHI refers to the air near the surface, which expands to approximately the height of buildings (Voogt, 2004). Thus, it is the layer of air in which human beings reside. This type is more common in the AUHI observation (Farina, 2012; EPA, 2009). Usually, the CLUHI is observed through measuring the air temperature and dense sampling points from installed stations or automobile surveys (Roth *et al*, 1989; Voogt and Oke, 2003; EPA, 2009; Srivanit and Hokao, 2012). The important features of data from permanent meteorological stations provide high temporal resolution and coverage of the place over the long period, conversely it does not provide great spatial details. Mobile measurements of temperature address this limitation, however they do not provide a synchronous display over the urban area (Srivanit and Hokao, 2012) and may be deficient in temporal resolution. Patterns of air temperature inside the city have a strong correlation with the latter's development (Roth *et al*, 1989). Usually, an AUHI is at its strongest during the night and weakest during the day (EPA, 2009) as for the SUHI but weaker in magnitude.

1.2.6.4. Boundary Layer Urban Heat Island (BLUHI): it is defined by higher air temperature of the urban boundary compared with rural surrounding areas. This is another type of AUHI, which is located above the CLUHI. During the day, its thickness attains 1 km or more, while it shrinks to only 100 m or less during the night (Voogt,

2004). This type of UHI is potentially more visible at night. It can be measured and observed using specific platforms of remote sensing such as long towers, radiosonde, balloon and aircraft (Voogt and Oke, 2003).

1.2.6.5. Oasis Cool Island Effect: it is defined by a lower temperature of an oasis compared with arid surrounding. Oasis is a landscape in arid regions, which is assisted by natural water sources in deserts. It is capable of exhibiting the cool island effect (Taha *et al*, 1991, Wen *et al*, 2005, Potchter *et al*, 2008, Li *et al*, 2011). For instance, in the Tarim Basin in China, oasis cold intensity attained -9.08°C during summer (Hao and Li, 2016).

1.2.6.6. Urban Cool Island in parks and water body: it is defined by lower temperature in green spaces and water body in urban compared to other class of land use (e.g. built-up and industrial areas). Generally, the air temperature in green sites can be cooler than non-green sites (Bowler *et al*, 2010). The results of studying several parks indicated that temperature is cooler in larger parks and those containing trees (Bowler *et al*, 2010), whereas the UCI of the parks is determined by the characteristics of the parks (Chang *et al*, 2007). Moreover, large parks can have a significant oasis effect.

1.3 Thermal Remote Sensing

This section provides basic knowledge of the electromagnetic spectrum, blackbody theory and the techniques of retrieval LST.

1.3.1 The Electromagnetic Spectrum

The electromagnetic (EM) spectrum describes the complete set of wavelengths of light (Figure 1.3). It commences from the shortest wavelengths (gamma rays and x-rays) to the longest wavelengths that are used in telecommunications (microwaves). There is a series of terms commonly used in remote sensing to label the several spectral regions. Typically, the names and spectral ranges are as follows:

1- The visible (VIS) region commences from 0.4 to 0.7 μm . This spectral region corresponds with the fraction of electromagnetic radiation that is detected by human eyes. It includes the three main colours, the blue from 0.4 to 0.5 μm , green from 0.5 to 0.6 μm and red from 0.6 to 0.7 μm (following Chuvieco and Huete, 2010).

2- The near infrared (NIR) region commences from 0.7 to 1.2 μm . This part of the spectrum is just beyond the human eye. The capability to discriminate green vegetation gives it spatial interest. In this region, healthy vegetation has a high reflectance that decreases with growth of a plant disease and its damage (Tempfli *et al*, 2009).

3- The mid-infrared (MIR) region commences from 1.2 to 8 μm . MIR situated between the NIR and thermal infrared regions. From 1.2 to 3 μm is called shortwave infrared (SWIR) region. The region from 1.3 to 2.5 μm is mainly useful for estimating soil and vegetation moisture content while the 3 to 5 μm range is useful for perceiving high-temperature sources.

4- The thermal infrared (TIR) region typically commences from 8 to 14 μm . This region is the emitted energy from Earth's surface, which is useful to map surface temperatures. The peak wavelength of thermal emission of land surface at (300 K) is situated at 10 μm . As well, a human body releases 'heat energy', with a maximum at $\lambda \approx 10 \mu\text{m}$. The thermal region has been valuable to detect vegetation stress and clouds, and to assess environmental contamination (Tempfli *et al*, 2009; Chuvieco and Huete, 2010).

5- The microwave region (>1 mm) is a very long wavelength region that is transparent to cloud cover and forest canopies. It is definitely useful in the analyses of soil moisture and surface roughness (Chuvieco and Huete, 2010).

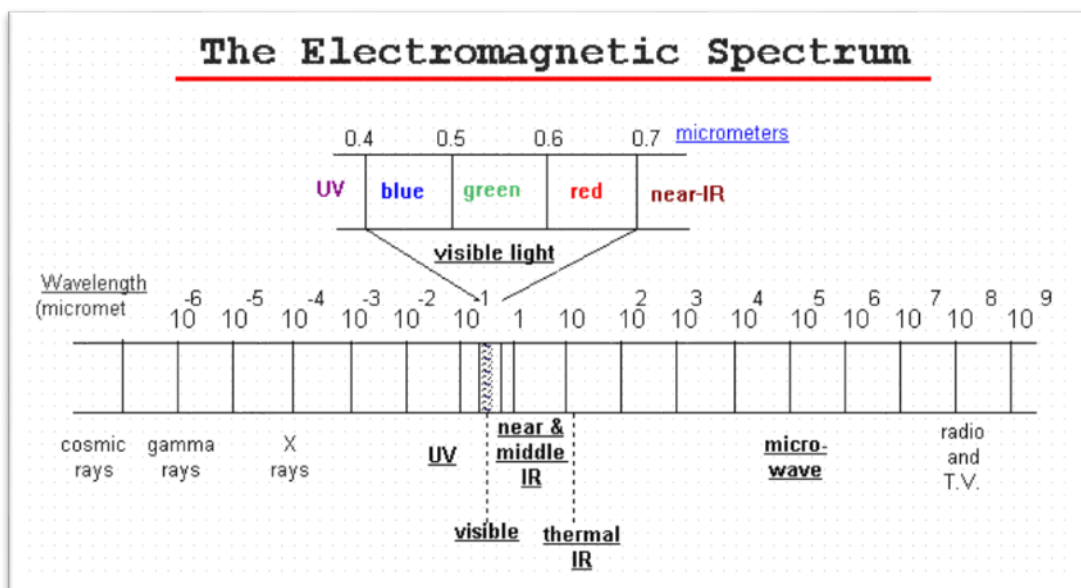


Figure 1.3: The electromagnetic spectrum (Crum, 2016)

1.3.2 Reflectance Properties of the Surfaces

The reflectance spectra of natural and artificial surfaces are significantly variable in the visible. The dry leaf simply differentiates from green leaves. The absorption of healthy plants is definitely strong in visible range and less intense in green (550 nm). In red, it increases again and toward 670 nm it decreases (Tupin *et al*, 2014). The spectral signature of soil depends on surface conditions because in contrast to the vegetation only a slight amount of electromagnetic energy is transmitted amid the soil (Chuvieco and Huete, 2010). The soil that is wet and contains more humus is dark. From blue to red range the reflectance of soil increases very slowly and in the NIR region it attains a plateau. Several white soils and artificial materials, such as concrete and asphalt, have a higher reflectance in the blue range (Tupin *et al*, 2014).

1.3.3 Optical Remote Sensing

The advantages of using remote sensing are that it is possible to cover large areas in less time and it is relatively cheaper than field measurements (Song *et al*, 2002). Instruments for optical remote sensing are sensitive to the energy of the light that is received. Thus, characteristics of atmosphere, vegetation or the oceans are determined through the measurement of this energy (Tupin *et al*, 2014). Apollo 9 acquired the first optical multispectral images that were used in creating a map of earth features (Rees and Rees, 2013). The use of remote sensing for SUHI began in 1972, when NASA launched Earth Resources Technology Satellite (ERTS, later renamed Landsat 1). From that time, an advanced remote sensing stage commenced and it is considered as being a milestone in the history of remote sensing observations (Lauer *et al*, 1997; Elachi and Van Zyl, 2006). Multispectral images such as Landsat, SPOT and World View use 5 to 7 bands to measure the reflectance of the features (Ustin and Xiao, 2001; Lee *et al*, 2004).

1.3.4 Blackbody Theory

Planck's law is one of the physical laws that governs the behaviour of electromagnetic radiation. This theory can characterise the spectral distribution of electromagnetic radiation emitted by a blackbody – a perfect emitter – as the following:

$$M_{n,\lambda} = \frac{2\pi hc^2}{\lambda^5 \left\{ \exp\left(\frac{hc}{\lambda kT}\right) - 1 \right\}} \quad 1.5$$

where $M_{n,\lambda}$ is radiant spectral exitance in $W/m^2/sr/\mu m$

h is Planck constant ($6.626 \times 10^{-34}Ws^2$);

k is Boltzmann's constant ($1.38 \times 10^{-23}Ws^2K^{-1}$);

c is speed of light;

λ is wavelength in metres;

T is blackbody temperature (in Kelvin).

The equation can be found in any standard physics book.

This law signifies the maximum emittance that a body can attain. Due to molecular agitation, all material with a temperature above absolute zero (0 K) emit electromagnetic energy. A material that is able of absorbing and re-emitting all electromagnetic energy that is received is called a blackbody. In reality, blackbodies do not actually exist and materials emit lower levels than the blackbody. It could be expressed in the following way:

$$M = \varepsilon(\lambda) M_{n,\lambda} \quad 1.6$$

where $\varepsilon(\lambda)$ is the spectral emissivity, varies between 0 and 1 (Tupin, Inglada and Nicolas, 2014) and with wavelength.

1.3.5 The Estimation of Land Surface Temperature

Remote sensing can quantify the average temperature of the pixel that for succinctness is referred to as the land surface temperature (LST). Both infrared and microwave sensors have been used to detect LST. Infrared thermal sensors provide high spatial resolution (i.e. 90 m for ASTER), however their limitation is they are only capable under transparent sky situations. In contrast, passive microwave sensors provide lower spatial resolution and lower precision while they are capable to use in all-weather situations because they are only slightly affected by atmospheric influences.

Since usually the size of atmospheric elements such as smoke and biomass burned aerosols are smaller than microwave or infrared wavelengths; the atmospheric effects of small particles in this region are insignificant (Chuvienco and Huete, 2010). However, 1 K retrieval precision that is required in practical applications cannot be attained by any one of these types. The most reliable LST data are from MODIS that can attain this

precision only for homogeneous surfaces such as water surface and sandy land while in reality having 1 km of homogeneous land surface is quite rare (Liang *et al*, 2012). Table 1-1 demonstrates typical infrared sensors. Mainly there are three LST retrieval approaches: the single-channel algorithm, the split-window algorithm and the multichannel algorithm.

Table 1-1: Typical Infrared Sensors for land surface temperature.

Sensor	Channel(s)	Spectral range (μm)	Spatial Resolution (m)	Typical Algorithm
Landsat 8	10	10.6–11.2	100	Split-window algorithm
	11	11.5–12.5		
ETM+/Landsat 7	6	10.4–12.5	60	Single-channel algorithm
TM/Landsat 5	6	10.4–12.5	120	Single-channel algorithm
AVHRR/NOAA	3	3.55–3.93	1100	Split-window algorithm
	4	10.30–11.30	1100	TISI algorithm
	5	11.50–12.50	1100	
MODIS/Aqua;Terra	20	3.66–3.84	1000	Split-window algorithm
	22	3.929–3.989	1000	Day/night algorithm
	23	4.02–4.08	1000	
	29	8.4–8.7	1000	
	31	10.78–11.28	1000	
	32	11.77–12.77	1000	
ASTER/Aqua	33	13.185–13.485	1000	
	10	8.125–8.475	90	TES algorithm
	11	8.475–8.825	90	
	12	8.925–9.275	90	
	13	10.25–10.95	90	
AATSR/ENVISAT	14	10.95–11.65	90	
	6	Central wavelength: 10.85 & 12.0	1000	Split-window algorithm
	7	Channel width: 0.9 & 1.0	1000	
SLSTR/Sentinel-3	S7	Central wavelength: 3.74, 10.85 & 12.0	1000	Split-window algorithm
	S8	Channel width: 0.38, 0.9 & 1.0	1000	
	S9		1000	

ABI/GOES-R	14, 15	Central wavelength: 11.2 & 12.3	2000	Split-window algorithm
SEVIRI/MSG	9, 10	Central wavelength: 10.8 & 12.0	3000	Split-window algorithm
IRMSS/CBRES-1	9	10.4–12.5	300	Single-channel algorithm
MERSI/FY-3	5	Central wavelength: 11.25	1000	Single-channel algorithm
IRMSS/HJ-1B	4	10.5–12.5	300	Multi-channel algorithm
S-VISSR/FY-2	IR1	10.3–11.3	5000	Split-window algorithm
	IR2	11.5–12.5	5000	
VIRR/FY-3	3	3.55–3.93	1100	Split-window algorithm
	4	10.3–11.3	1100	TISI algorithm
	5	11.5–12.5	1100	

1.3.5.1 Single-Channel Algorithms

Algorithms in this approach can estimate LST and Land Surface Emissivity (LSE) from sensors with single thermal infrared channels such as Landsat TM. It includes Radiative Transfer Equations, Single-Channel Algorithm and Generalised Single-Window Algorithms.

The Radiative Transfer Equation Method

The LST can be derived in this method through a reverse of the Planck function while supposing that the LSE is known. In cases where atmospheric temperature and humidity are known, we can simulate upward radiance, downward radiance and transmittance by applying an atmospheric transfer equation. The advantage of this approach is the capability to use it at any geographic location. The shortcoming of this method is the complexity of the computational processes and usual unavailability of real time atmospheric temperature and humidity information that is necessary in atmospheric simulations (DiStasio Jr. and Resmini, 2010; Liang *et al*, 2012). These algorithms also need emissivity which is not always well known.

The Single-Channel Algorithm

A single-window algorithm was proposed by Qin *et al* (2001) for retrieving LST from a TM image. The upward and downward radiance was expressed approximately

by introducing the average atmospheric temperature T_a . The linear approximation of the Planck function is possible to calculate at room temperature assuming that the average temperature of atmospheric upward radiance and downward radiance are equal (Liang *et al*, 2012). This algorithm is stated as:

$$T_s = \frac{[a(1 - C - D) + (b(1 - C - D) + C + D)T_6 - DT_a]}{C} \quad 1.7$$

where T_6 is the brightness temperature of the sixth TM channel, $a = -67.355351$, $b = 0.458606$, $C = \varepsilon_6\tau_6$, and $D = (1 - \tau_6) [1 + \tau_6(1 - \tau_6)]$. ε_6 is LSE and τ_6 is atmospheric transmittance of the sixth channel.

The LSE, atmospheric transmittance and average temperature are required in this algorithm. The limitation of this algorithm is that the standard atmospheric profile data represents the average results of large samples thus effects of the real atmospheric circumstances cannot be revealed (Liang *et al*, 2012).

Generalised Single-Channel Algorithms

A generalised single-channel algorithm was proposed by Jiménez-Muñoz and Sobrino (2003). The advantage of this approach is it can be used with any thermal infrared data to retrieval LST, the equation is expressed as:

$$T_s = \gamma \left\{ \frac{1}{\varepsilon} + [\phi_1 L_\lambda^{at-sensor} + \phi_2] + \phi_3 \right\} + \delta \quad 1.8$$

$$\gamma = \left\{ \frac{c_2 B_\lambda(T_o)}{T_o^2} \left[\frac{\lambda^4}{c_1} B_\lambda(T_o) + \lambda^{-1} \right] \right\}^{-1} \quad 1.9$$

$$\delta = -\gamma B_\lambda(T_o) + 1 \quad 1.10$$

where $L_\lambda^{at-sensor}$ is the at-sensor radiance, ε is the land surface emissivity, λ is the equivalent wavelength, $c_1 = 1.19104 \times 10^8 \text{ W m}^{-2} \text{ sr}^{-1} \mu\text{m}^4$ and $c_2 = 14388 \mu\text{m K}$. T_o is the reference temperature. ϕ_1 , ϕ_2 and ϕ_3 are simple functions of atmospheric water content (w).

This algorithm is more accurate than the single-channel algorithm as it is only requires LSE and atmospheric water content parameters. The results of this algorithm were acceptable for atmospheric content ranges between 0.5 to 2 g/cm², resulting in an error between 1-2 K. For water content greater than 3 g/cm², the errors of the results became unacceptable (Liang *et al*, 2012).

1.3.5.2 Split-Window Algorithms

A split-window algorithm was first proposed by McMillin (1975) for estimating sea surface temperature. The influence of the atmosphere is removed through the combination of brightness temperature from two channels. The typical split-window algorithm can be expressed as follows:

$$T_s = a_0 + a_1 T_i + a_2 T_j \quad 1.11$$

where $a_i (i = 1, 2)$ is a coefficient, T_i and T_j are the brightness temperatures of the two channels. Actually, the derivation of the split-window algorithm is extremely complex. However, it is widely used as an empirical equation as a result of its simple structure (Liang, Li and Wang, 2012). Sea surface temperature attained using this method for MODIS-Terra images has a reported precision of 0.3 K (Nicolòs *et al.*, 2007).

The sea surface temperature split-window algorithm, has been used to measure land surface temperature by numerous researchers, Prince (1984) was one of the first to apply it. This algorithm can be expressed as:

$$T_s = [T4 + 3.33(T4 - T5)] \left(\frac{3.5 + \varepsilon_4}{4.5} \right) + 0.75T5(\varepsilon_4 - \varepsilon_5) \quad 1.12$$

where $T4$ and $T5$ are the brightness temperatures of the fourth and fifth channels of the AVHRR, respectively, and ε_4 and ε_5 are the corresponding LSEs.

Wan and Dozier (1996) proposed a generalised split-window algorithm for retrieving land-surface temperatures from MODIS data. This generalised split-window algorithm has been used for creating MODIS global LST products and it has been significantly verified. This algorithm for MODIS can be expressed as:

$$T_s = C + \left(A_1 + A_2 \frac{1 - \varepsilon}{\varepsilon} + A_3 \frac{\Delta\varepsilon}{\varepsilon^2} \right) \frac{T_{31} + T_{32}}{2} + \left(B_1 + B_2 \frac{1 - \varepsilon}{\varepsilon} + B_3 \frac{\Delta\varepsilon}{\varepsilon^2} \right) \frac{T_{31} + T_{32}}{2} \quad 1.13$$

where A_i , B_i and C are coefficients; $\varepsilon = (\varepsilon_{31} + \varepsilon_{32})/2$; $\Delta\varepsilon = \varepsilon_{31} - \varepsilon_{32}$; ε_{31} and ε_{32} are the emissivity of MODIS channels 31 and 32, respectively.

Prata (2002) used Split Window Algorithm for AATSR data. It can be expressed as:

$$LST = a + b(T_{11} - T_{12})^{n(\theta)} + (b + c)T_{12} \quad 1.14$$

where T_{11} and T_{12} are the AASTR nadir BTs for the 11 μm and 12 μm channels and the term a, b, and c are coefficient which depend on fractional vegetation, biome, water vaper and angle.

1.3.5.3 Multichannel Algorithms

Multichannel algorithms can estimate LST and LSE from sensors with multi thermal infrared channels such as MODIS, ASTER, AVHRR and Landsat 8. These approach algorithms are capable of retrieving LSE and LST concurrently.

The Temperature-Independent Spectral Index Method

Temperature-independent spectral indices (TISI) defined by Becker and Li (Becker and Li, 1990) can be used to retrieve LST and LSE from the day and night data from the channels 3, 4, 5 of NOAA AVHRR. TISI for night-time observations are defined as:

$$TISI_n = M \frac{L_3(T_{g3n})}{L_4(T_{g4n})^{\alpha 4} L_5(T_{g5n})} \quad 1.15$$

where $L_3(T_{g3n})$, $L_4(T_{g4n})$ and $L_5(T_{g5n})$ are the radiances in the night observation on AVHRR channels 3, 4 and 5, respectively, and T_{g3n} , T_{g4n} and T_{g5n} are the corresponding land surface brightness temperatures. M is a constant number, and $\alpha 4$ is used to remove the impact of LST on the TISI.

The TISI in day observations are expressed as:

$$TISI_d = M \frac{L_3(T_{g3d})}{L_4(T_{g4d})^{\alpha 4} L_5(T_{g5d})} \quad 1.16$$

where $L_3(T_{g3d})$, $L_4(T_{g4d})$ and $L_5(T_{g5d})$ are the radiances in the day time observation on AVHRR channels 3, 4 and 5, respectively, and T_{g3d} , T_{g4d} and T_{g5d} are the corresponding land surface brightness temperatures.

Several researchers improved this algorithm; however it is still extremely complex and entails numerous assumptions that limit its application (Liang *et al*, 2012).

The MODIS Day/Night Algorithm

A physical algorithm was proposed by Wan and Li (1997) to retrieve LST and LSE from MODIS day and night data. Based on day/night observations of the seven infrared MODIS channels, for the solution land-surface and atmospheric parameters, 14 equations are created from which LST and LSE can be derived. Geometric corrections are necessary to reference the two scenes in day and night observations (Liang *et al*, 2012).

The Integrated Retrieval Algorithm

An integrated retrieval or the two-step retrieval algorithm proposed by Ma *et al* (2000) for the MODIS airborne simulator (MAS) was then been applied to MODIS data (Ma *et al*, 2002). In the first step, the values of parameters are derived using a regression method; in the second step, the initial values are adjusted by Tikhonov's regularised method (Hansen, 1998).

The results of Ma *et al* (2000; 2002) indicate that this method effectively retrieved atmospheric temperature, humidity, LSE and LST, while it cannot be applied to acquire LST on a global scale (Liang *et al*, 2012).

Algorithms for Hyperspectral Data from Meteorological Satellites

A statistical regression algorithm (Smith and Woolf, 1976) is normally used to acquire the initial values of LST, LSE, and atmospheric conditions. Then for deriving an optimal estimate for each parameter, an iteration method is used (Liang *et al*, 2012). Susskind *et al* (2003) proposed algorithms for computing land surface parameters and atmospheric parameters for AIRS/AMSU/HSB data, and for the retrieval of LST, LSE, temperature and humidity profiles from AIRS data.

To estimate the LST from remote sensing data, the ideal technique can be chosen by bearing in mind the complexity of the method, the availability of atmospheric information, emissivity data and characteristics of the sensor. Future research should focus on improvement of methods to simultaneously derive LST and LSE from hyperspectral TIR instruments, multiple spectral channel observation of a scene over time and from combination of TIR and microwave data. Methods need to consider aerosol and cirrus effects (Li *et al*, 2013).

1.4 Thesis Structure

This thesis comprises of seven chapters. The chapters are generally categorised into three parts (Figure 1.4). The first part includes Chapters 1 to 3 which exhibit context and background information. The second part is concerned with the methodology used for this study and presents the findings of the research. The third part demonstrates general discussion, founded conclusions and research contributions to UHI studies. Each chapter will be identified below.

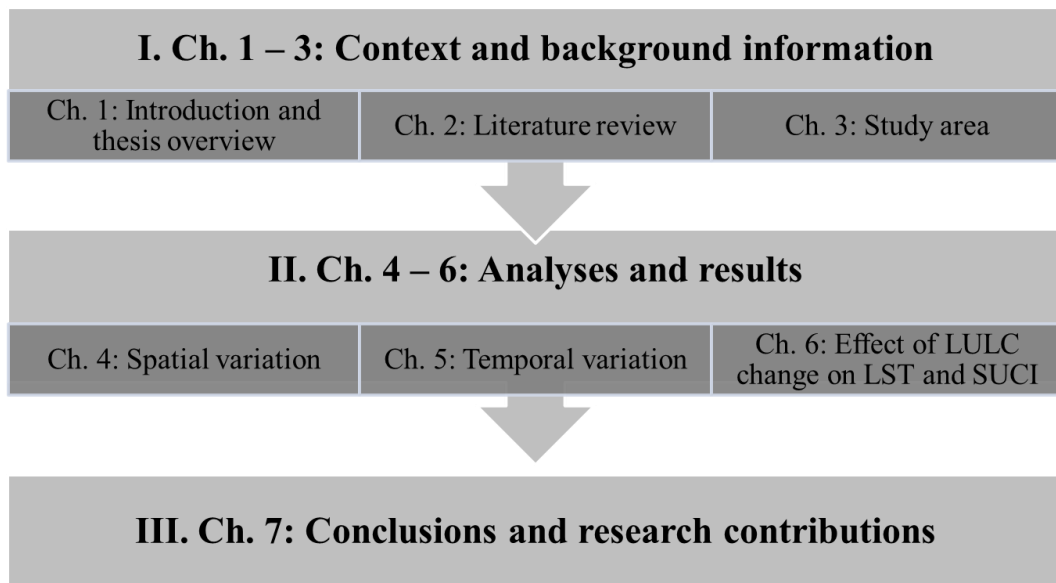


Figure 1.4: Thesis structure.

Chapter 1: the chapter presents an overview background on UHI and thesis structure as an introduction to the research. The causes, types and influences of UHI are discussed. It also includes concepts of thermal remote sensing and methods to derive LST from remote sensing sensors.

Chapter 2: the chapter presents a review of literature on both atmospheric and surface UHI research. It provides a chronological presentation of studies in LST and UHI. Methods for atmospheric and emissivity correction and determination of urban areas for UHI are given in this chapter. The review provides UHI studies in different areas with a variety of results for both daytime and night-time. This chapter concludes with gaps in literature, objectives and research questions.

Chapter 3: the chapter provides a description of the study area which is necessary for the comprehension of the nature of the environment of the study site. The geology,

soil type, topography, green area, building components and the population of Erbil are presented. The chapter moreover is focused on climatic elements of the city including temperature, air pressure, winds, relative humidity, cloud cover and precipitation.

Chapter 4: the chapter provides an assessment of spatial variation of the daytime SUCI during the summer dry season in Erbil, from Landsat 8. The methods used in this chapter are described including the retrieval of LST from Landsat 8, identification of SUCI, and the usefulness of wetness, greenness and brightness components. The chapter provides results of spatial variations within Erbil.

Chapter 5: the chapter provides an assessment of temporal variations of the surface urban cool/heat island in Erbil, from MODIS data. The chapter includes diurnal, seasonal, and interannual variation for 12 years. It provides results of the temporal variation and relationship between LST and some factors such as Normalised Difference Vegetation Index (NDVI) and soil moisture.

Chapter 6: this chapter presents SUCI/SUHI changes in the urbanised and vegetated areas from 1992 to 2013 based on multi Landsat sensors. It is divided in three sections: the effect of vegetated land; the effect of urbanisation on SUCI/SUHI; and the LST change in pixels that represent different Land Use/Land Cover (LULC) change. Methods of retrieval of LST and calculating impervious surface area (ISA) have been presented. In this chapter the 'Normalised Ratio Scale Temperature' technique, is been proposed for modifying the temperature from satellite images captured in different times.

Chapter 7: the chapter summarising the new research contributions of this thesis to UHI and urban climate studies, with discussion and conclusions from the results of Chapters 4, 5 and 6 of this thesis. The conclusions are based on each research question, which has been identified in Chapter 2. The chapter concludes with the considerations of limitations of the research and directions of future research according to limitations and results from this thesis.

Chapter 2 : Literature Review

2.1 Introduction

Surface temperature is one of the crucial topics in urban climatology studies. The comfort of the urban inhabitants is influenced by surface temperature through modified air temperature of the lowest layer of the urban atmosphere (Srivanit and Hokao, 2012). Land surface is a complex feature that could be described as a combination of green vegetation, water surfaces, impervious surface materials and exposed soils. As a result of this complexity, LST varies spatially. Impervious surface differs considerably between urban and suburban areas and it is a main contributor to the SUHI effect (Zhang *et al*, 2008).

As a result of human-induced changes to surface climate, UHI intensity could increase (Zhao *et al*, 2014). Since the early 1900s, the UHI intensity of thousands of urban areas around the world have been assessed (Stewart and Oke, 2009) and continues to remain an extensive area of study within urban climatology (Souch and Grimmond, 2006). The growth and strength of the heat island areas during this time bring challenges in energy, the health of urban residents, water supplies, urban infrastructure and social comfort (Ukwattage and Dayawansa, 2012). In addition, it exacerbates heat waves and creates a negative effect on life expectancy (Tan *et al*, 2010).

This chapter reviews literature on remote sensing concepts and methods relating to urban climate, surface temperature, emissivity and atmospheric correction. It has a particular emphasis on surface urban heat/cool island and factors to determine LST. The purpose of this review was to identify current research gaps in the SUHI field and use them in formulating research questions and objectives for this study.

2.2 Atmospheric Urban Heat Island

Atmospheric UHI is computed by examining variations of air temperature between an urban and surrounding rural area at the same time and with the similar geographic characteristics. Statistical analysis of weather station data, in situ data or computer simulation models have been generally used to perform atmospheric UHI studies (Memon *et al*, 2009). Most UHI studies have reported positive UHIIs (Kim and Baik, 2005; Lemonsu and Masson, 2002) however occasionally UCIIs (negative UHIIs) are reported (Montávez *et al*, 2000; Hafner and Kidder, 1999) (Table 2-1).

Table 2-1: A summary of UHII/UCII in different areas of the world. SUHI/SUCI refers to surface temperature. UHI/UCI refer to air temperature.

Type	Study area	Climate	Reference study	Approach	UHII/ UCII°C
Daytime SUCI	Abu Dhabi, UAE	Bwh: Subtropical Desert	Lazzarini <i>et al</i> (2013)	Satellite data	-6
	Dubai, UAE	Bwh: Subtropical Desert	Frey <i>et al</i> (2007)	Satellite data	-5
Daytime SUHI	Beijing, China	Dwa: Hot Summer Continental	Hung <i>et al</i> (2005)	Satellite data	10
	Vancouver, Canada	Csb: Warm-summer Mediterranean	Roth <i>et al</i> (1989)	Satellite data	7.5
Daytime UCI	Atlanta, USA	Cfa: Humid Subtropical	Hafner and Kidder (1999)	Modeling	-0.5
	Granada, Nicaragua	Aw: Tropical Savanna	Montavez <i>et al</i> (2000)	Weather station data	-2.0
Daytime UHI	Hong Kong, China	Cfa: Humid Subtropical	Memon <i>et al</i> (2009)	Weather station data	10.5
	London, UK	Cfb: Marine West Coast	Kolokotroni and Giridharan (2008)	Weather station data	8.6
Nighttime SUHI	Birmingham, UK	Cfb: Marine West Coast	Tomlinson <i>et al</i> (2012)	Satellite data	5
	Atlanta, USA	Cfa: Humid Subtropical	Hafner and Kidder (1999)	Modeling	1.2
Nighttime UHI	Łódź, Poland	Cfb: Marine West Coast	Klysik and Fortuniak (1999)	Weather station data	12
	Mexico city, Mexico	Cwb: Oceanic Subtropical Highland	Jauregui (1997)	Weather station data	7.8

Jauregui (1997) found that the atmospheric UHI of Mexico was more frequently observed (75%) at night than during the daytime. The maximum night time of UHI intensity was 7.8°C in February, which is a dry month, at a time of calm and clear sky nights. Harlan *et al* (2006) showed that higher temperature strongly correlated with densely populated neighbourhoods, sparse of vegetation and reducing open spaces in the city.

It is clear that significant SUHI and to some extent SUCI effects are already observed for major cities. The use of LST is important and appropriate for Erbil where

atmospheric temperature data are not available. The next section describes urban thermal remote sensing in more detail.

2.3 Urban Thermal Remote Sensing

Thermal remote sensing concentrates on observing the variations of land surface temperature in the urban areas as a consequence of surface energy balance. LST combines the influences of surface radiative effects, surface moisture, thermal admittance and surface emissivity. The TIR data are providing an incessant and concurrent view of the complete city and registers the radiative energy emitted from a variety of surfaces such as building roofs, paved surfaces, vegetation, bare soil and water body (Srivanit and Hokao, 2012). Thermal infrared remote sensing has been applied widely in environmental and urban climate research. Essentially, it has been used for analysing LST patterns, assessing UHI and relating LST with surface energy fluxes (Weng, 2009).

2.3.1 Atmospheric Correction

The atmosphere affects the intensity of thermal infrared radiation through scattering, absorption, refraction and re-radiation. These atmospheric effects have to be removed or corrected from the brightness temperature (Voogt and Oke, 2003; Gao *et al*, 2006) for reasonable LST data to be obtained from the instrument signals. Ignoring atmospheric correction means assuming that atmospheric effects are the same in all places, while in reality, water vapour and pollutant contents vary horizontally in urban areas. Errors related to atmospheric effects are around 1 K (Roth, Oke and Emery, 1989), although probably higher in wet tropical regions. If the atmospheric correction is neglected or is incorrectly, estimated surface temperature SUHI intensity may be incorrectly derived (Voogt and Oke, 2003; Barsi *et al*, 2003).

One of the commonly applied methods of correcting thermal infrared (multi and hyperspectral) images is the In-Scene Atmospheric Composition (ISAC) method proposed by Young *et al* (2002) that is employed in ENVI software as Thermal Atmospheric Correction. ISAC merely uses the scene data for approximating atmospheric transmissivity and upwelling radiance. For processing and analysis TIR spectral images, this method can be used with confidence (DiStasio Jr. and Resmini, 2010).

In general, atmospheric correction methods for a TIR image are divided into two main approaches. The first one is Radiative Transfer (RT) modelling, where the atmospheric column is modelled using the radiative transfer equation and is frequently adjusted with known atmospheric situations. The advantage of this method is the possibility to use it at any geographic location and it does not require a prior knowledge of the scene (DiStasio Jr. and Resmini, 2010). For the readers benefit, it is noted that in the visible, the example of this approach is the Atmosphere Removal Algorithm (ATREM) by Gao *et al* (1993) which is used to retrieve “scaled surface reflectance” spectra where horizontal surfaces have Lambertian reflectance. Other examples are the Atmosphere CORrection Now (ACORN), the Fast Line-of-sight Atmospheric Analysis of Spectral Hypercubes (FLAASH) and the High-accuracy Atmospheric Correction for Hyperspectral Data (HATCH) by Qu *et al*, (2000).

The second main approach is In-Scene methods (for thermal images), which are from space at-aperture radiance data in the hyperspectral cube that can be used to recompense for the atmosphere. A benefit of this method is that they obtain the true situation of the atmosphere at the time of data collection. However, the complexity of these methods includes the input parameters of the correction algorithm which must be identified correctly. Other examples of this approach include The Emissive Empirical Line Method (EELM) (DiStasio Jr. and Resmini, 2010) and The Internal Average Reflectance (IAR) method by Kruse (1988) that calculates the average spectrum of a scene. The flat field correction method (Roberts *et al*, 1986) which assumes there is an area in the scene that has spectrally neutral reflectance is another example. Radiative reflectance spectra of other pixels in this sense can be driven by using the mean spectrum of the flat field (Gao *et al*, 2006). The quick atmospheric correction (QUAC) is one of the powerful methods (for optical images) that only requires approximate specification of sensor band location and their radiometric calibration. The advantage of the method is that it is much faster when compared to physical-based methods (Bernstein *et al*, 2012).

In addition, there are hybrid approaches to atmospheric corrections that combine radiative modelling and empirical approaches (Clark *et al*, 1995). This method allows deriving laboratory-like reflectance spectra (Gao *et al*, 2006).

2.3.2 Emissivity Correction

“The emissivity, ε , is the ratio of the radiance emitted by a body and the radiance emitted by a blackbody at the same temperature” (Li *et al.*, 2013). Gillespie *et al.* (1999) states that the emissivity over land is not identifiable in advance although considerable progress has been made lately. The surface of urban and rural areas has different emissivity. Typically, the average surface emissivity in urban areas is lower by around 2% compared to the typical rural areas (Arnfield, 1982). In the case of not doing emissivity correction and neglecting this difference, it can retrieve the temperature of urban-rural with differences up to 1.5°C or more. Therefore, the urban heat island effect can typically be underestimated (Roth *et al.*, 1989). Land Surface Emissivity (LSE) is a vital surface parameter and can be acquired from the space by TIR sensors with various resolutions and accuracies (Weng, 2009; Li *et al.*, 2013). In literature, many methods have been proposed to retrieve LSE from space. However, they differ in advantages, limitations and application conditions.

The first category of methods is the semi-empirical methods (SEMs). The illustrative methods of this category are the classification based emissivity method (CBEM) (Snyder *et al.*, 1998; Peres and DaCamara, 2005) and NDVI based emissivity method (NBEM) (Van de Griend and Owe, 1993; Sobrino and Raissouni, 2000). In circumstances, where the area is classified accurately and the emissivity of each class is well known, typically CBEM can produce LSE accurately (Gillespie *et al.*, 1999). On the other hand, because the NDVI threshold method is simple it has been applied easily and successfully with different sensors (Li *et al.*, 2013). As a result of the uncertainty of the classifications in CBEM (i.e. for mixed pixels and changes from one type to another) the LSE derived through this method has the problem of discontinuity. Compared with other classification methods; this method contains several progresses while it still does not succeed to indicate considerable changes in the LSE, especially for sparse vegetation areas (Liang *et al.*, 2012).

The second category of methods is multi-channel methods. One type included in this category is emissivity spectrum character-based methods that determine the LSE from the characteristics of emissivity spectra. The example of this type is a two-temporal method (TTM) by Watson (1992), which assumes the emissivity has a flat spectrum for specific wavelengths. The grey-body emissivity (GBE) method by Barducci (1996) assumes the emissivity spectrum is smooth. Borel (1997) proposed the

iterative spectrally smooth temperature emissivity separation (ISSTES) method. The emissivity bounds method (EBM) by Jaggi *et al* (1992) applies a priori information about the distribution range of emissivity.

Another type of Multi-channel method is the reference channel method (REF). It was proposed by Kahle *et al* (1980) and presumed that in one channel the emissivity is constant for all pixels. Gillespie, in 1985, described a normalisation emissivity method (NEM) which has been used subsequently by Realmuto (1990). It assumes that the emissivity is constant in all N channels for a given pixel. Temperature–Emissivity Separation (TES) algorithm is another Multi channel method that hybridises NEM, spectral ratio (SR) and min-max difference (MMD). It was initially proposed for retrieving LST and LSE from ASTER satellite images. It contains the advantages of the NEM method, the spectral contrast method, and the MMD method (Liang *et al*, 2012). Becker and Li (1990) proposed the temperature-independent spectral indices (TISI) method that is a pure mixture of channel emissivity (Sobrino *et al*, 2002; Li *et al*, 2013).

The third category of LSE methods is physically based methods (PBMs). The examples of the PBMs are the TISI-based method (Becker and Li, 1990; Li and Becker, 1993), the physical-based day/night operational method by Wan and Li (1997) and the two-step physical retrieval method (TSRM) by Ma *et al* (2000) that uses the principal component analysis (PCA) technique.

Mainly infrared spectral information has been used for multichannel algorithms. In contrast, mainly visible and near-infrared information has been used by classification and NDVI based approach (Liang *et al*, 2012). Sobrino *et al* (2002) revealed that from the five methods (TISI, NOR, REF, RE, ALPHA) that are used for finding emissivity, TISI and NOR supply the best results. In addition, in the study of Majumdar (2012), the best results of emissivity for estimation of LST were provided by the Emissivity Normalisation method that was selected for emissivity correction in this research.

2.3.3 Methods of Retrieved Land Surface Temperature

Chapter 1 demonstrated in more detail the various methods proposed for retrieval of LST from thermal remote sensing data. Du (2015) categorised them into three groups: the single-channel algorithm, multi-channel methods (e.g. the split-window algorithm and the temperature and emissivity separation method) and multi-time

methods (e.g. the temperature-independent spectral indices method, two-temperature method and the physical day and night algorithm).

The radiative transfer equation (RTE) method has been used for retrieving LST, which is used in radiosonde field data and radiative transfer code as MODTRAN (Sobrino *et al*, 2004). In addition, the National Aeronautics and Space Administration (NASA) provided equations to derive brightness temperature from a digital number of thermal bands of Landsat. However, Qin *et al* (2001) developed a mono-window algorithm based on a thermal radiative transfer equation, for retrieving LST from the only one thermal band of the sensors. This method avoids the reliance on radiosonde in the RTE method and required two atmospheric parameters; transmittance and mean atmospheric temperature. The generally accepted level for LST estimation is 1.5°C while Qin *et al* reported the probable error of this algorithm is 1.1°C in the image (Qin *et al*, 2001; Sobrino *et al*, 2004). Wang *et al* (2015) presented an improved mono-window (IMW) algorithm to retrieval LST from Landsat 8 Thermal Infrared Sensor (TIRS) band 10 data.

A single-channel algorithm was developed by Jiménez-Muñoz and Sobrino (2003) which is suitable for retrieving LST from sensors with only one infrared window channel which uses only the atmospheric water vapour content (Sobrino *et al*, 2004). In Sobrino *et al* (2004), the results indicated that the rmsd value was 0.6, 2 and 0.9°C for using radiative transfer equation, mono-window and single-window, respectively. The split window (SW) algorithm is an example of multichannel method used for two thermal channels based on the different atmospheric absorption behaviour of two radiometric channels (Ulivieri *et al*, 1994). Du (2015) developed this method for retrieving LST from Landsat 8 TIRS images. But such methods rely on good retrieval calibration between two channels used.

2.3.4 Using Land Surface Temperature from Remote Sensing Data

In order to ascertain surface temperature through radiation the traditional technique of aerial surveillance is commonly used (Albrecht, 1952; Combs, 1961; Lorenz, 1962). Thereafter, Wark *et al* (1962) and Rao and Winston (1963) attempted to utilise satellites to measure surface temperatures. Through data obtained from the Television Infrared Observation Satellite (TIROS II), they found that measuring surface temperature is possible in clear and dry areas (Lenschow and Dutton, 1964). Primarily,

LST and SUHI have been derived from the National Oceanic and Atmospheric Administration's (NOAA) Advanced Very High Resolution Radiometer (AVHRR) data (Weng, Lu and Schubring, 2004). After that, Landsat's Thematic Mapper (TM) and Landsat's Enhanced Thematic Mapper Plus (ETM+) were widely employed to retrieve surface temperatures (Sobrino *et al*, 2004; Weng *et al*, 2004; Chen *et al*, 2006; Srivastava *et al*, 2009; Shahmohamadi *et al*, 2012). Srivastava *et al* (2009) estimated surface temperature in the Singhbhum Shear Zone of India. The results indicated that emissivity has a strong relationship with the reflectance of ETM+ band 3. They compared field data with estimated LST from different algorithms. It was found that the use of Valor's emissivity and single channel equations increase the accuracy of the result and is closer to field truth temperature.

2.3.5 Determination of Urban Area

In urban climatic literature, there is considerable confusion in defining and classifying places as urban and rural. This confusion arises from researchers relying on typical dictionary meanings of "urban" and "rural" to define and classify their study sites (Stewart and Oke, 2009). There are different methods that have been used to select urban and rural areas, for example digitally or supervised classification is the way to divide the study area to urban, rural and other classes. Another approach that is less successful is classification based on the size of population of the place (Voogt and Oke, 2003). Satellite detected night-time light images can also be used to distinguish between urban and rural areas (Gallo and Owen, 1998).

In 2003, the Normalised Difference Built-up Index (NDBI) was proposed as a new method for mapping built-up area automatically. This method was applied in practice to extract data for a built-up area of Nanjing city in eastern China (Zha *et al*, 2003). It was able to distinguish between built-up and vegetated or green and wet surroundings for the city of Nanjing, however it is unable to distinguish between built-up and bare and dry soil that surrounds the city. Therefore, this method was not suitable for the city sites of this research (Erbil) and similar cities located in the dry environment climate.

Xu (2007) used Thematic-oriented Index Combination Technique to extract built-up area from Landsat image. He used the results of NDBI, MNDWI and Soil-adjusted

Vegetation Index (SAVI) as three new bands instead of normal bands for supervised classification.

Many researchers have attempted to extract ISA at sub-pixel level. Ji and Jensen (1999) used sub-pixel analysis and a layered classification to select ISA for coastal and urban environments. In 2001, Flanagan and Civco improved this method to produce impervious surface fraction estimates using artificial neural networks. Small (2001; 2002) used a linear spectral mixture model (LSMM) which acquires vegetation, low and high albedo endmembers to divide fractions for New York City. Later in 2003, a linear mixture pixel analysis (LMSA) was employed by Wu and Murry to select impervious distribution (Zhang *et al*, 2008).

Stewart (2009) proposed “local climate zones” (LCZs) as a sample system for classifying UHI zones at the local scale, within the canopy layer, to address the issue of confusion in classifying urban and rural areas. Urban and rural landscapes are divided as standard into 17 classes; each class has its own description by the construction and land cover properties (Stewart *et al*, 2014).

2.4 Surface Urban Heat Island

Surface UHII is determined by variations of surface temperature between urban and surrounding rural areas with similar geographic characteristics. Remote sensing sensors, thermal images and field data have all been used to assess the SUHI of urban areas.

2.4.1 Satellite Measurements of Urban Heat Island

The temperature of the urban area and SUHI can be derived from remote sensing images as a captivating and possibly valuable source (Roth *et al*, 1989; Zhang *et al*, 2008). Satellite sensors have been used to obtain the surface temperature of urban areas and to study the spatial variations of UHIs and their development (Watson, 2012). Rao (1972) reported the first study of SUHI based on imagery data. Through the study of surface temperature patterns of the mid-Atlantic coast of USA, he utilised thermal Infrared Radiometer (IR) data of the Improved TIROS Operational Satellite (ITOS-1). The research found that patterns of surface temperature vary from one city to another and the centre of the city is the warmest part (Watson, 2012). Matson *et al* (1978) and Price (1979) detected the UHI by utilising satellite data. Since then, the SUHI and

surface temperature have been observed through utilising different sensors such as satellites, aircrafts, and ground-based sensors. Later, in 1989, Roth *et al* studied the thermal urban climates (Voogt and Oke, 2003).

The AVHRR sensor has been used to discern the surface temperature (Ottlé and Vidal-Madjar, 1992; Gutman, 1999; Pinheiro *et al*, 2006) and to analyse the regional-scale of UHI effects (Lopezgarcia *et al*, 1991; Lee, 1993; Streutker, 2002). Gallo *et al* (1993) used it to assess the UHI in 31 cities based on NDVI. Airborne acquired high-resolution images were also used to assess the thermal determiners of urban surfaces such as sky view factor and surface materials (Voogt and Oke, 2003). The Advanced Spaceborne Thermal Emission Reflection Radiometer (ASTER) is another sensor of the TIR image that collects both daytime and night-time data and has been used for determining the UHI effect in many cities (Nichol and Wong, 2005; Binyan *et al*, 2008; Nichol *et al*, 2009; Liu and Zhang, 2011). Tiangco *et al* (2008) used ASTER to analyse the nocturnal UHI in Metro Manila. The inverse relationship between temperature and NDVI was found, which is the study also suggested that increasing green areas in cities could limit the UHI effect.

Landsat images are widely used to investigate the growth of SUHIs and to assess the relationship between LST and LULC. Xu, Qin and Lv (2008) used Landsat to compare SUHI and Land Cover (LC) changes. The result showed growth in SUHI and a strong relationship between SUHI patterns and urban areas. Bajaj, Inamdar and Vaibhav (2012) in monitoring the growth of the UHI in Ahmedabad, India, confirmed that temperature is higher in built-up areas. Furthermore, it showed the increasing percentage of the built-up area from 38% in 1999 to 45% in 2011 which has led to an increase in the UHI intensity and a decrease of temperatures in areas with high NDVI. A similar study used Landsat data to compare the development of a UHI between city centre and the new area of Tianjin, China, has shown that due to an increase of built-up areas in 2008, SUHIs became greater in 2008 compared to 1986 (Mo *et al*, 2011). Li *et al* (2012) used Landsat images to illustrate the impact of LULC changes on SUHI patterns in the biggest cities in China, including Shanghai. The research produced significant results, including that there had been an increase in the built-up area by 219.5%, with decreasing agricultural areas and bare lands. It also mentioned the presence of gradients for LST from the city centre to the rural surroundings. In addition, seasonal variation of the average UHII between the city centre and suburban areas reached its peak in the summer and rose again in the spring, while UHII was weak in

the winter and autumn. Ukwattage and Dayawansa (2012), after analysing the impact of urbanisation on the UHI of Colombo city, Sri Lanka, showed a considerable change in the spatial division of the UHI, which expanded from its initial north-western confinement towards the south.

Clinton and Gong (2013) used MODIS at 1 km special resolution with high temporal resolution to investigate UHIs and Urban Heat Sinks (UHSs) of cities on a global scale. The results confirmed that development, land cover, and size of city have the greatest effect on thermal difference. Conversely, factors such as the population and structure of the city have a limited effect. Furthermore, MODIS data has been used to analyse daily differences of LST and UHI in Abu Dhabi. Standard nocturnal UHIs were found in the city, while during the day the city centre was cooler than its surroundings (Lazzarini *et al*, 2013).

In 2013, Landsat 8 was launched with two thermal bands that give the chance for this research to apply TIRS data in spatial investigation of LST and SUCI on Erbil. The effect of LULC change on LST has been widely assessed for cities in the humid climate while in cities located in semi-arid environments requires more focus to be better quantified and understood. Unfortunately calibration problems with Landsat 8 TIRS have restricted its use (chapter 4).

2.4.2 Urban Heat Island in Arid and Semi-Arid Climate

SUHI studies pay more attention to urban areas located in tropical, mediterranean and cold climatic regions whereas arid regions with extreme high temperatures have been less focused on (Al-Ali, 2015). Some of the few UHI studies in the literature based in arid regions were carried out in Phoenix and Tucson, Arizona by Hsu (1984); Brazel and Balling (1986); Tarleton and Katz (1995), Kuwait City by Nasrallah *et al* (1990) and the Al Ahsa oasis by Al-Ali (2015). The effect of land cover on UHII of the Al Ahsa oasis in Saudi Arabia has been assessed by using both ground data and satellite images. The results showed that UHII in summer time was higher than in winter and at night than during the day. The highest UHII (10.5°C) was recorded in Al Hufuf and Al Mubarraz oasis cities while UCII (-6.4°C) was recorded, at night in summer time, in the small villages and vegetated areas (Al-Ali, 2015). The limitation of approach is such research is in comparing urban area with nearby towns to study UHI and ignoring the bare soil and desert sand surrounding the city that has high LST in arid and semi-arid

regions. In semi-arid regions, the importance of changing aridity soil moisture in the rural areas in modifying heat islands has not been studied extensively.

2.4.3 Thermal Urban Studies in Areas Relatively Close to the Study Area

Satellite data have been used to investigate the LST and UHIs in some countries near to the study area. An analysis of the SUHI of Dammam city in the Kingdom of Saudi Arabia (Habib, 2007) was the first published study in this field within Arabic literature. Results indicated that the lack of high buildings with a concentration of gardens in the city centre reduced the temperature while the heat islands are concentrated over industrial zones and new neighbourhoods in the east and west of the city. Likewise, it was suggested that reconstruction of desert areas led to reduced temperatures. The limitation of this study is that it is focused on using LST data uncorrected for the atmosphere in the analysis.

Amiri *et al* (2009) used Landsat 4, 5, and 7 to investigate the relationship between LST and LULC in Tabriz, Iran, finding that changes that have occurred due to urbanisation could be observed in the pixels, showing a transfer of surface characteristics from a dense plantation with low temperature to sparse vegetation with high temperature. While determining the SUHI of the metropolitan city of Tehran, Iran, the difference of UHII in daytime between the urban and rural area was 12°C (Shahmohamadi *et al*, 2012). Saleh (2011) determined the impact of urban expansion of the Iraqi capital Baghdad. The results indicate that there was a strong inverse relationship between the surface temperature and NDVI and the daily variation of temperature in water and forest areas was less than the residential and commercial areas. Ghazal and Hassoon (2012) aimed to derive the surface temperature in a part of the province of Sulaimania in Kurdistan, and found that there are a similarity between the results obtained by both high and low gains of band 6 of Landsat 7. Therefore, they created the map of distribution on top of atmosphere (TOA) surface temperature for the study area by using the average of band 61 and 62.

During the period of this research, Khalid (2014) performed master's research entitled 'Urban Heat Island in Erbil City' at Lund University. The study observed higher values of minimum air temperature, for winter and autumn, in an Erbil weather station compared to weather stations in the rural areas, which indicative of the atmospheric UHI. In terms of Surface LST, only one Landsat 7 image was used in the

study and the result indicates low LST associated with high NDVI and high LST located with low NDVI such as Industrial Area. In addition, there are still considerable gaps (section 2.8) within the literature that require consideration and provide novelty to the current research. In particular, temporal variations of heat islands have not been investigated strongly in semi-arid climates.

2.5 Urban Cool Islands

The general conviction that the air temperature in green sites can be cooler than non-green sites was confirmed by many studies on the temperature of parks (Bowler *et al.*, 2010). To explain the effect of parks on the temperature of cities in detail, more research is necessary on the design of urban green area, distribution and type of greening. Studies on many parks indicated that the temperature is cooler in larger parks and those with trees (Bowler *et al.*, 2010). On average, larger parks are cooler than smaller ones but not always, while the UCI of the parks is more related to the characteristics of the parks (Chang *et al.*, 2007). The results from the study indicate that 61 parks in Taipei city were confirmed as UCIs whereas around one-fifth of parks with $\geq 50\%$ paved coverage and little tree and shrub cover, have been warmer than their urban surrounding at midday during the summertime (Chang *et al.*, 2007). Several studies have confirmed that this so-called “oasis” exhibits the cold island effect (Taha *et al.*, 1991; Wen *et al.*, 2005; Potchter *et al.*, 2008; Li *et al.*, 2011). The results of the study of the Tarim Basin in China indicated that all oases exhibited an oasis cold island effect (OCIE). The highest OCIE intensity was -9.08°C recorded in summer; OCIE intensity of autumn and spring were -4.24 and -3.85°C respectively. Factors that affected the OCIE were farmland and water areas while natural vegetation, such as forest and grassland had a negligible influence (Hao and Li, 2016). In some environments such as arid, semi-arid, arctic and subarctic, cities have been reported as UCIs (negative UHI) during certain times of the day or during particular seasons (Steinecke, 1999; Hafner and Kidder, 1999).

The result of investigating the LST of Athens in Greece by using MODIS data found that during the daytime the LST of bare soil and sparse vegetation rose faster than urban areas (Keramitsoglou *et al.*, 2011). During the dry season the daytime SUHI intensity in some cities such as Mexico City and Reykjavik is very weak and sometimes exhibits a cold island. In contrast, the air temperature UHI remains present throughout

the year (Cui and De Foy, 2012; Steinecke, 1999). In Okayama City in Japan, during the daytime, the air temperature of the central area was 1 to 2°C lower than that of the residential area and the surface temperature recorded UCI (Shigeta *et al*, 2009). As a result of low thermal inertia, urban places in arid areas have the capability of showing both nocturnal SUHIs and diurnal SUCIs (Clinton and Gong, 2013). The amount of soil moisture has an effect because evaporation via latent heat reduces land surface temperature. As such, the investigation proved the existence of UCIs in Dubai compared with the desert areas. Not only residential districts but also industrial areas had lower temperatures than sand zones (Frey *et al*, 2005; Frey *et al*, 2012).

To date, plenty of research has investigated UHI and UCI in green spaces and water bodies within cities whereas only a few studies have investigated Surface Urban Cool Island across a whole urban area so it requires greater comprehension. Usually, research of atmospheric UHI uses measured air temperature of some points in and around the city that not represent the study area entirely. However, because SUHI studies usually use remote sensing data it represents the temperature of the whole of the study area with some consistency.

2.6 Technique and Statistics Used in Urban Heat Island Studies

In the literature, different kinds of technique, statistic methods and models have been used to quantify, illustrate and analyse temperature difference (ΔT) between the urban and rural areas and to select key determining parameters. Some of these techniques are described below.

2.6.1 Methods to Compare Multi-Temporal LST Images

In the literature, various techniques have been applied for analysing the temporal change of satellite based LST. Some researchers directly compare two or more LST images without any modification (Abdullah, 2012). This approach lacks scientific rigour because the atmospheric situation is not the same at the time of image acquisition. Having a high temperature in the second image compared to the first one, for example, does not mean the temperature has increased because it is possible that at that time the temperature was high for other reasons. A technique to account for this and to better establish the Urban Heat Island effect is through the normalisation of the temperature based on the mean and standard deviation in high and low temperature

areas (Streutker, 2002; Zhang *et al*, 2007). The third technique is common normalisation of temperature based on min and max LST of the same image in the same way as for NDVI (Carlson and Arthur, 2000; Khandelwal *et al*, 2011).

In the literature, there is a necessity to apply new techniques to make satellite images comparable to detect variation in LST from images obtained from different times. In this study, a Normalised Ratio Scale (NRS) technique is proposed to normalise the value of each pixel-based ratio to make the LST images from different times comparable and at the same time maintaining the original values. This is described in Chapter 6.

2.6.2 Determining the Urban Heat Island

Researchers used various methods to assess UHI; for instance, Saitoh *et al* (1996) have used automobile collected weather data while Tran *et al* (2006) have used satellite data to assess maximum SUHI. Hafner and Kidder (1999) have used a model to assess both SUHI and AUHI. Kim and Baik (2005) have used weather station data to analyse maximum atmospheric UHI while Tran *et al* (2006) assessed SUHI. UHI was determined in some studies as a comparison of the mean and maximum temperature between urban and rural areas. Others compared temperature during times such as a season, a month, a year or some days. In some cases, it was selected as temperature changes over time (Mochida *et al*, 1997). Moreover, Magee *et al* (1999) selected UHI as the average changed temperature for both the urban and the rural areas (Rizwan *et al*, 2008).

2.6.3 Statistical Analyses of Urban Heat Islands

For the city of Indianapolis in the USA, Weng *et al* (2004) conducted pixel by pixel correlation analysis by calculating Pearson's correlation coefficients between surface temperatures on the one hand, and NDVI, Green Vegetation (GV), and impervious surface fractions on the other hand. The results indicated that LST tends to correlate negatively with NDVI values and GV fraction values for all LULC types. At the same time, LST and impervious fraction values were positively correlated (Weng *et al*, 2004; Weng and Lu, 2008).

The linear regression technique has been used extensively in UHI studies to show the relationship between LST and NDVI values (Weng *et al*, 2004; Sun and Kafatos, 2007; Weng and Lu, 2008; Schwarz *et al*, 2012). A linear statistical model has been applied to find the relationship between different meteorological variables (namely, cloud, speed of wind, and relative humidity) and the UHI of Hamburg, Germany (Hoffmann *et al*, 2012). Szymanowski and Kryza (2009) conducted Multiple Linear Regression (MLR) to state the land-use situation of the UHI, but inaccurate results have been obtained when the process tended towards non-stationary variables such as the impact of the wind. The common character of meteorological data is non-stationary, hence the application algorithm can be largely limited in case the technique is unable to manipulate it. According to Szymanowski and Kryza (2012) and Su *et al* (2012), Geographically Weighted Regression (GWR) is better suited when compared with MLR and other conventional regression analyses. GWR shows the relationship between temperature and land covers more clearly and it is more successful in the spatial modelling of UHI. Su *et al* (2012) used GWR in studying the UHI in Taoyuan County, Taiwan, and it showed a significant non-stationary spatial relationship between LST and land covered types.

The Residual Kriging (RK) method has been used to create a map of mean air temperature in the summer time in order to model a UHI in Birmingham in the United Kingdom (Tomlinson *et al*, 2013). For spatial modelling of the UHI, Szymanowski and Kryza (2012) suggested the combined GWR residual kriging (GWRK) method as an alternative to the extensively used MLR model. The RK technique presented the most accurate results when compared with the MLR for assessing the capacity to estimate the air temperature in Wroclaw, Poland (Szymanowski and Kryza, 2009). Similarly, Florio *et al* (2004) emphasised that the kriging models anticipate temperature better than the MLRs. RK errors are neutral while regression models are inclined to give partially predicted values. RK and GWR methods have been also applied for LSTs (e.g. Mukerjee *et al* 2015; Kalota 2016).

2.6.4 Models for Simulation Surface Temperature and Urban Heat Island

A number of numerical and physical models have been developed to study the LST of urban areas, for instance, energy balance model (Oke *et al*, 1999), laboratory models (Cenedese and Monti, 2003), three-dimensional simulations (Saitoh, Shimada

and Hoshi, 1996) and the Gaussian model (Streutker, 2002). Amongst these models, statistical analysis is used widely to link LST to the surface characteristics (Weng, 2009). A satellite-based model has been used effectively in determining the surface temperature of Hong Kong (Nichol and Wong, 2005). While a numerical model was used by Lemonsu and Masson (2002) to exhibit the temperature of four areas of Paris. Poreh (1996) has used a small-scale physical model in studying UHI and related factors. Johnson *et al* (1991) proposed a surface urban heat island model (SHIM) and it has been used by Oke *et al* (1991). Carlson *et al* (1981) coupled remotely sensed data with a 1-dimensional atmospheric model to estimate energy balance fluxes and surface properties. Hafner and Kidder (1999) used a 3-dimensional numerical model on the city of Atlanta (Voogt and Oke, 2003). Rajasekar and Weng (2009) used a fast fourier transform (FFT) - a non-parametric model - with MODIS imagery to drive UHI and related variables.

2.7 Factors Which Affect UHI and LST

There are different reasons for variations of temperature between urban and rural areas. The most significant reason is the surface differences in the thermal characteristics of the radiation and reduction in evapotranspiration cooling in urban (Streutker, 2002; Zhao *et al*, 2014). Local background climate of the cities determines the effect of these factors. Urban warming happens if the cities are aerodynamically smoother than nearby rural areas and urban heat dispersion is relatively less efficient (and vice versa). Daytime ΔT is increasing in humid climates while decreasing in dry climates (Zhao *et al*, 2014). In addition, many controllable and uncontrollable factors have a role in generation UHI (Figure 2.1). These factors furthermore could be categorised as temporary influence factors (cloud cover and wind speed), permanent influence factors (building materials and green areas), and cyclical variables (solar radiation and anthropogenic heat sources) (Rizwan *et al*, 2008).

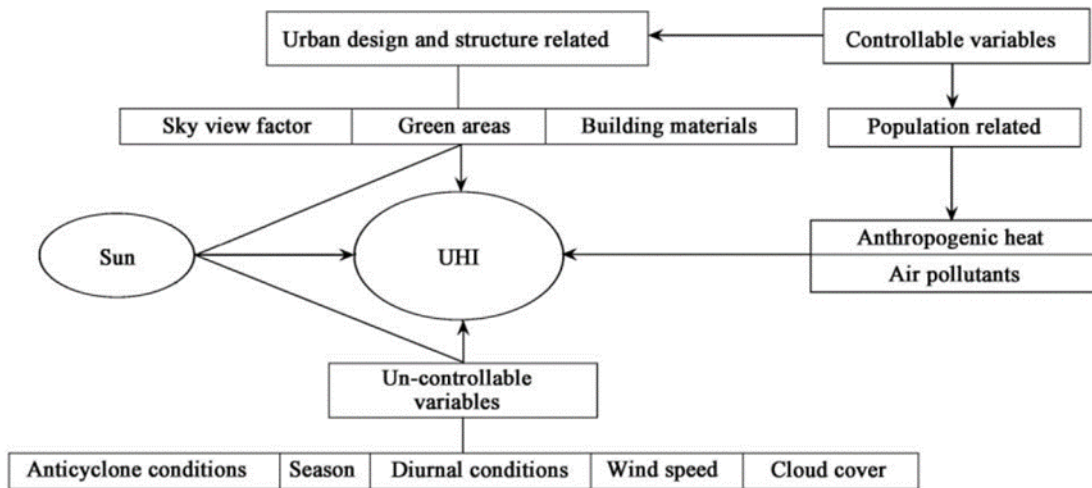


Figure 2.1: Factors of Urban Heat Island (UHI) (Rizwan *et al*, 2008).

2.7.1 Influence of Urbanisation and City Expansion on Temperature

Land surface temperature has been examined extensively to assess the effect of urbanisation as a main land use land cover (LULC) change. In urban areas, anthropogenic heat is another source that influences temperature besides solar radiation (Youneszadeh, 2013). For monitoring LULC change, remote sensing data are an appropriate technique to assess changes which occur pre-urban and after urbanisation (Zha *et al*, 2003). Due to alterations of natural surfaces, urbanisation commonly increases in surface temperature in urbanised areas and it may decrease the level of atmospheric humidity (Mallick and Kerle, 2009; Sofer and Potchter, 2006). Increasing aspects of urbanisation such as population, pollution and urban expansion all influence climatic elements in cities (Shahmohamadi *et al*, 2010) while the world still demonstrates extraordinary urban growth. The number of world cities with one million or more habitants was 77 in 1950, it rose to 501 in 2015, and it is expected that it could be 663 cities by 2030 (DESA, 2014). Numerous research on cities with different environmental and physical characteristics indicate that urbanisation leads to increased surface and air temperature (Weng, 2001; Kalnay and Cai, 2003; Baker *et al*, 2004; Zhou *et al*, 2004; Amiri *et al*, 2009; Grossman-Clarke *et al*, 2010). In terms of the effect of urban expansion on cities located in subtropical climates, Weng (2001) found out that urban development and decreasing biomass in the Zhujiang Delta in China, during 1989 to 1997, increased surface radiant temperature by 13.01°C on average. Baker *et al* (2002) examined the urbanisation effect of Phoenix, Arizona (USA) as a city situated in

a subtropical desert climate. They used temperature data from 1948 to 2000 at Sky Harbor Airport. The research indicated that because of urbanisation, night-time minimum temperature and average daily temperature increased by 5°C and 3.1°C for each one respectively. The model simulation of the impact of LULC change in Phoenix, Arizona (USA) on four summer extreme heat events suggests that night-time temperature increased by up to 10°C in new urban developments. Furthermore, when urbanisation occurred in an irrigated agricultural area the maximum air temperature increased by 2-4 °C. Replacing desert land with urban development only increased daytime temperature by 1°C (Grossman-Clarke *et al*, 2010). In cities similar to Erbil that are located in semi-arid climates, the effect of LULC in Turkey indicated that urbanisation and industrialisation has led to increasing minimum temperature (Tonkaz and Cetin, 2007).

Most research in China reported that urbanisation has led to increased temperature. Results of Jiang and Tian (2010) research on Beijing from 1995 to 2000 showed that urbanisation moved pixels from cool to hot surface in temperature/vegetation (TVX) techniques. In another study, the impact of urbanising forest was to raise LST by 3.4°C and urbanised agricultural land increased LST by 1.9°C. While in Guizhou Province in Southwest China urbanisation increased LST between 1.1 and 1.5°C. Temperature variation between cities, and rural areas increased by urbanisation, has led to strengthened UHI in some cities. Analyses of increases of UHI in Tehran metropolitan indicated that urbanisation aspects directly influenced the rise in daytime surface UHI by 12°C as the difference between the maximum surface urban and rural temperature (Shahmohamadi *et al*, 2010). Srivani and Hokao (2012) reported that urbanisation has led to an increase in the average LST in Bangkok metropolitan area from $26.01 \pm 5.89^{\circ}\text{C}$ to $37.76 \pm 2.84^{\circ}\text{C}$ in 2009. A more extensive UHI effect of Shanghai is one consequence of urbanisation and it is highlighted as a direct reason of additional hot days and heat waves that increases heat-related mortality in the city (Tan *et al*, 2010).

The effect of urban expansion of cities located in green and wet background was illustrated well by many studies. However, there is the necessity to explain the effect of LULC change on SUCI/SUHI in semi-arid climates.

2.7.2 Influence of Vegetation on Temperature

Vegetation is different from urban materials in terms of radiative, aerodynamic, thermal and moisture properties. The vegetation's ability to produce shade, coolness, and air filtration make them appropriate means for environmental design (Oke *et al*, 1989). A key process of urban greening that reduces temperature is evapotranspiration, which cools the leaf and the air temperature through increased latent heat (Bowler *et al*, 2010). Moreover, trees can intercept solar radiation and reduce the surface and air warming through creating the shade (Oke *et al*, 1989). Most studies on urban green area and multiple parks broadly confirm that green sites in the cities can be cooler than non-vegetated area. Green areas act to increase the cooling of the daytime temperature if the park is large and contains trees (Bowler *et al*, 2010; Gago *et al*, 2013).

In assessing the UHI in New York City, Susca *et al* (2011) found that the temperature in the most vegetated areas averages 2°C lower than less vegetated areas. Results of some research indicated that the cooling influence of green areas in the city exceed vegetated areas to surrounding built-up and commercial areas (Ca *et al*, 1998; Yu and Hien, 2006). Because vegetation such as trees, grass and forests have a strong cooling effect in the city, it can be used to decrease temperatures and mitigate UHIs (Onishi *et al*, 2010). Qiu *et al* (2013) suggested that urban temperature could be reduced by 0.5 to 4.0°C by vegetation and urban agricultural evapotranspiration. In addition, the result of simulation by Taha (1997) suggests that air temperature could decrease by 2°C as a consequence of increasing vegetation in the cities. This decrease may reach 4°C in some circumstances due to propitious meteorological conditions and the possibility of evaporation soil-vegetation systems.

Kaufmann *et al* (2003) statistically quantified the influence of interannual variations of vegetation on surface temperature in North America and Eurasia. The result demonstrates that increasing terrestrial vegetation leads to a reduction in temperature. In addition, models can be used to simulate the effect of vegetation fractional change on urban areas. A Weather Research and Forecasting (WRF) model used for UHI in Mexico City found that during the night both the surface and atmospheric UHI and daytime surface UHI reduced with increases of vegetation (Cui and De Foy, 2012). Studies have shown that the relationship between temperature and vegetation indices can be used to assess the influence of vegetation on surface temperature. Jenerette *et al* (2007) found that a Soil-adjusted Vegetation Index

correlates strongly and positively with considerable variation of surface temperature in Phoenix in the USA. The NDVI index was widely used as an indicator of urban-rural differences in surface properties (Voogt and Oke, 2003). Abdollahi *et al* (2008) used NDVI to examine the environmental effect of vegetation cover in Yazd province, Iran. The result indicates that because of a 36.2% decrease in total vegetation the emitted surface temperature rose considerably. On the other hand, to mitigate the effect of UHI in the urban area planting more vegetation is a widely proposed technique (Yu and Hien, 2006; Gago *et al*, 2013; Skelhorn, 2013). Skelhorn (2013) assessed the effect of increasing green spaces in Manchester in the UK on the microclimate of the city. The result of the most effective scenario of adding 5% mature trees led to reductions of around 0.7°C and 1.7°C for air temperature and surface temperature in the urban case study, respectively. While in the suburban case study, an increase of 5% in mature deciduous trees can reduce the mean hourly surface temperature by 1°C in each hour between 10 am and 5 pm.

2.7.3 Soil Moisture and Water Body

In meteorology, ecology and hydrology applications, surface soil moisture is an essential variable (Zhao *et al*, 2013). One of the causes of UHI is variations in moisture between the city and countryside (Stewart, 2011). Taha (1997) states that the moisture is changed considerably by the urban surface. However, the vast majority of human involvement in the creation of moisture, such as the irrigation of urban green areas, mainly occurs in greener residential areas and urban parks (Souch and Grimmond, 2006). In general, reduced vegetation abundance causes limited evapotranspiration compared to the countryside where there is a superior availability of surface moisture (Smith, 2010). In addition, soil moisture is one of the substantial parameters in controlling LST and the surface energy balance in cities (Piringer *et al*, 2002; Weng, 2009). Qiu *et al* (2013) reported that the temperature of a water body in the urban area can be between 2 and 6°C less than the temperature of nearby built areas, and the temperature of up to 2,826 m³ nearby space could be decreased 1°C with a water body of 16 m².

Several UHI studies compared LST with indices (e.g. NDVI and NDWI) to assess the relationship between vegetation, water body and temperature while greenness and wetness components from the Tasselled Cap (TC) technique were not used. On the

other hand, the relationship between vegetation and surface temperature for different seasons requires more investigation and comprehension.

2.8 Gaps in Literature

During the review in relevant literature, the following gaps and areas were discovered that require more focus:

- A search of the literature revealed few studies which investigated spatiotemporal variation of UHI in semi-arid climates.
- To date, there are few studies that have investigated Urban Cool Island and it requires greater comprehension.
- There is a necessity to examine and explain in more detail the effect of LULC change on SUCI/SUHI in semi-arid climates.
- Several UHI studies compared LST, NDVI and NDWI to assess relationship between vegetation, water body and temperature while greenness, wetness components from TC technique were not used.
- The relationship between vegetation and surface temperature for different seasons required more quantification and comprehension.
- There is a gap in methods to make multi satellite images comparable to detected variation in LST.

2.9 Research Questions and Objectives

Based on the above literature review and gaps in literature, the following questions and objectives can be considered as ‘very important’.

2.9.1 Research Questions

This research attempts to answer the following questions for Erbil:

1. How does the land surface temperature and surface urban cool island vary spatially over the study area?
2. How does the land surface temperature and surface urban cool/heat island vary temporally over the study area?
3. What are the main determinant variables of the SUCI/SUHI in Erbil?

4. What is the effect of LULC change on LST and SUCI/SUHI in semi-arid climates such as Erbil?

These research questions will be addressed to attain the following aims and objectives.

2.9.2 Aims of the Research

The overall aim of this research is to study and quantify the spatiotemporal variation of SUCI/SUHI in Erbil as a semi-arid city, explore factors influencing its variation and assess the effect of urban expansion on SUCI/SUHI.

2.9.3 Objectives of the Research

Specific objectives of this research are:

1. To quantify the spatial variation of the SUCI in Erbil, as a case study of a semi-arid climate.
2. To quantify the temporal variation of the SUCI/SUHI in the study area.
3. To establish the key determinant factors and patterns of the spatiotemporal distribution of LST and SUCI/SUHI.
4. To assess the effect of LULC change on LST and the occurrence of SUCI over a long-time period (from the 1990s to 2010s).

Chapter 3 : Study Area

3.1 Introduction

Erbil (also named Arbil and Hawler in Kurdish language) is the capital of the Kurdistan Region and is the central city in the north of Iraq. The city lies 412 m above mean sea level (Sharif, 1998). It is located between 43°57'E to 44°03'E and 36°08'N to 36°14'N (Figure 3.1). During the past two decades, the infrastructure and inhabitants of the city have experienced extensive growth.

The city has a semi-arid continental climate and is classified as subtropical semiarid (BSh) in the Köppen classification of climate. It has a dry and warm summer and a rainy and cool winter. The amount of rain fluctuates from year to year, the average annual precipitation from 1993 to 2012 was 380.26 ± 108.88 mm and the majority of it falls between December and March whereas the summer is the dry season. The annual air temperature is 21.85°C and July and August are the hottest months of the year; air temperature during these months may reach 49°C (MSDEG, 2014). Residential land use is the most dominant land use type in the city comprising buildings built from concrete blocks.

In this chapter, key characteristics of the study area are described to assist reader awareness of the nature of the study site. It includes physical characteristics such as geology, soil type, topography, climatic elements and human characteristics including building components and the population characteristics of Erbil.

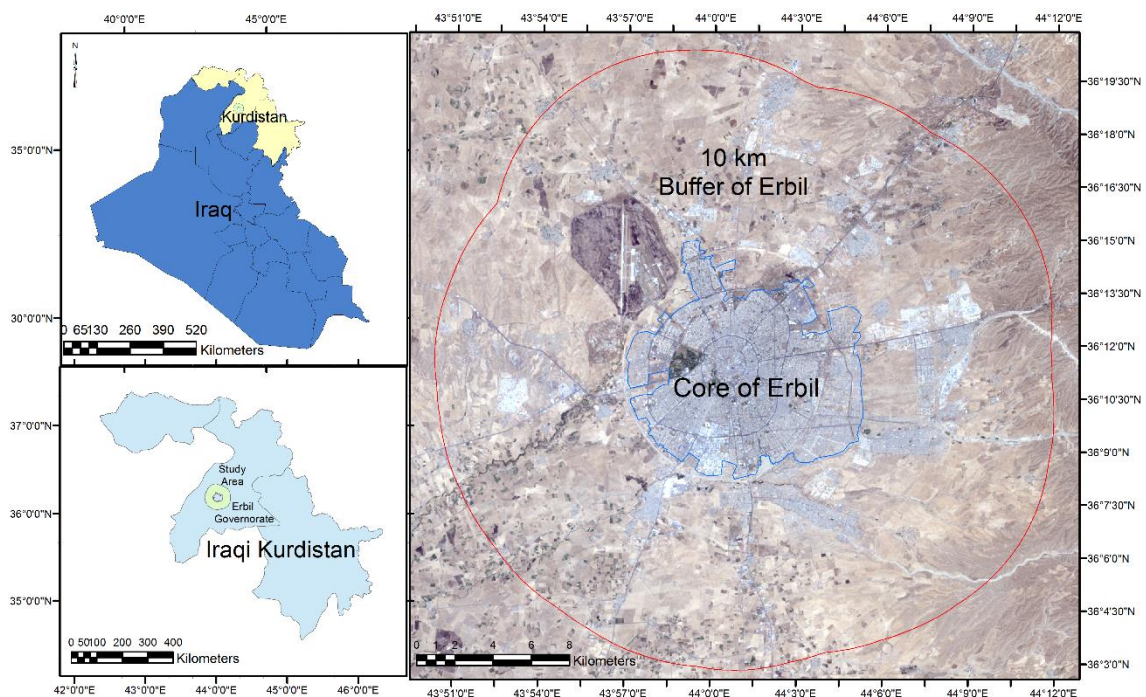


Figure 3.1: Map of Iraq, Kurdistan Region and true colour Landsat image of the study area.

3.2 Geology of the Study Area

The study area consists of recent deposits in layers (alluvial) covering the upper Bakhtiari formation. The thickness of these layers varies according to geological factors: the topography and the elevation of the area from the average of sea level (SETS, 2015). In the following section, the characteristics of the two main geological layers are discussed.

3.2.1 Pleistocene Units and Alluvium

Over the Erbil Plain, the Quaternary deposits are common. Mainly Pleistocene deposits consist of gravels, soils, and conglomerates with some clay, sands and silt. The new deposits consist of alluvial fans, river terraces, slope and flood plain deposits (Figure 3.2 and 3.3). The thickness of these deposits is more than 100 m in some places across the study area. These coarse-grained materials are assisting to reserve the groundwater. The thickness of coarse alluvial deposits might exceed 150 m and it consists of fine-grained clay embedded with sandy silty layers, which is combined with stony, gravelly strata (Dizayee, 2014).

3.2.2 Bakhtiary Formation

The Bakhtiary Formation returns to the Pliocene age and is overlain by Quaternary terrace gravels in the valleys and alluvium. It contains of thickly-bedded conglomerates, shale and sandstones. The thickness of the Bakhtiary Group (Upper and Lower) differs while at Erbil Plain it attains more than 1,800 m (Dizayee, 2014). In Iraq, the name Mukdadiya is used instead of Upper Bakhtiary and the name Bai Hassan formation is used to refer to the Lower Bakhtiary (Karim *et al*, 2015).

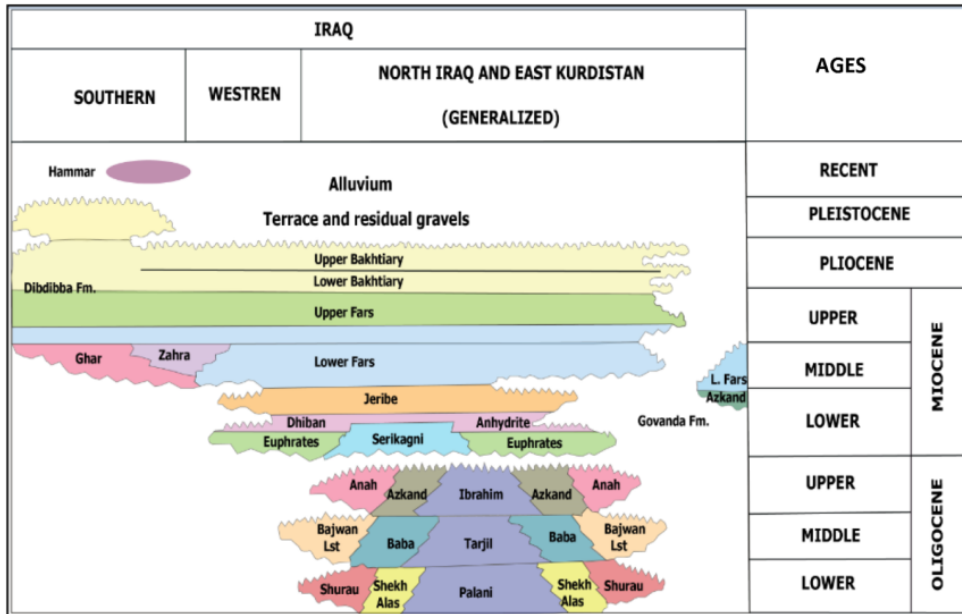


Figure 3.2: Tertiary and Quaternary rock units in Iraq (following Dizayee, 2014)

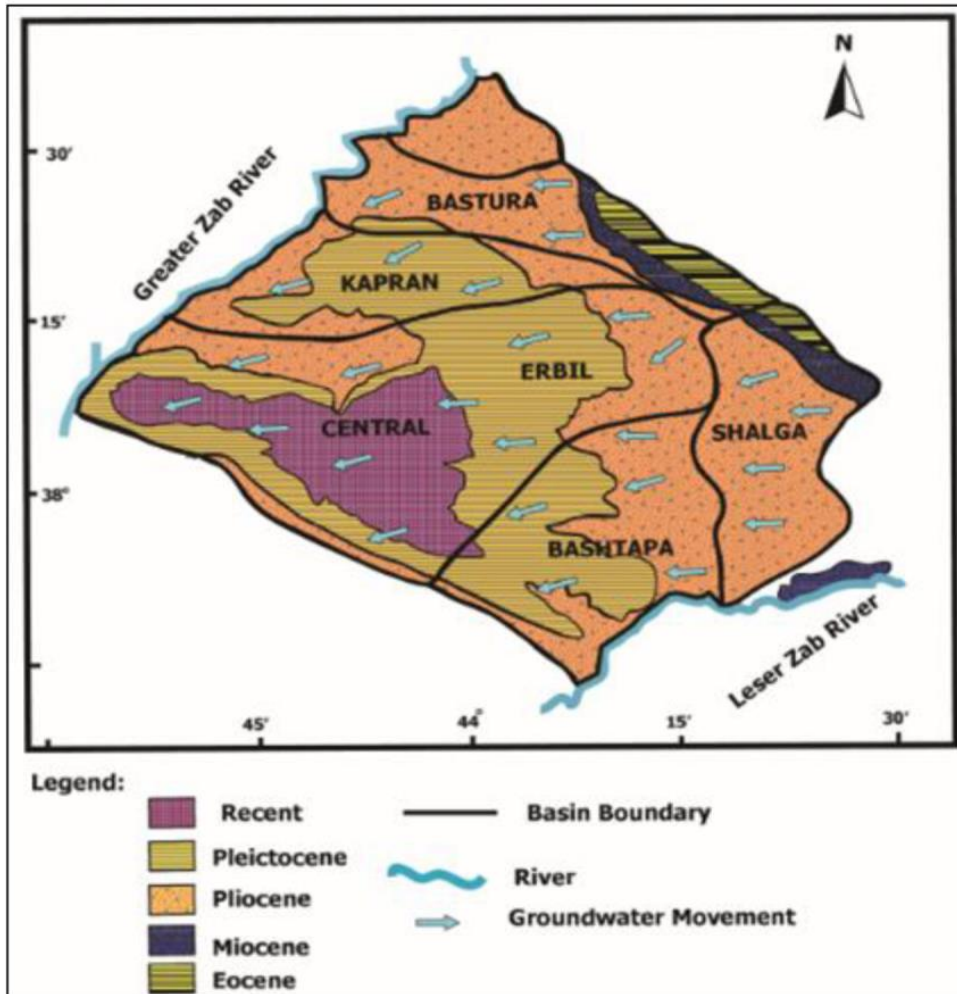


Figure 3.3: Geological map of Erbil Basin (following Dizayee, 2014)

3.3 Soil of the Study Area

The soil is vital to the life and contains a surface layer of the earth, which formed due to the weathering of rocks. It varies in thickness, texture, structure, composition and colour from place to place. The capability of heat storage of soil depends on the proportion of water, air, organic matter and soil minerals. Dry soil will have low heat storage compared to the wet soil (Ragnarsdóttir and Banwart, 2015).

Erbil is built-up on the Erbil Plain and it has dark brown soil that is appropriate for agriculture (Figure 3.4). Having good structure, large depth and rich in organic materials makes it one of the best soils. The average depth of soil in Erbil Plain is 140 cm. The texture of soils in the plains area, for example in Erbil Governorate, contains loamclay, sand, loam silt and siltclay (Kahraman, 2004).

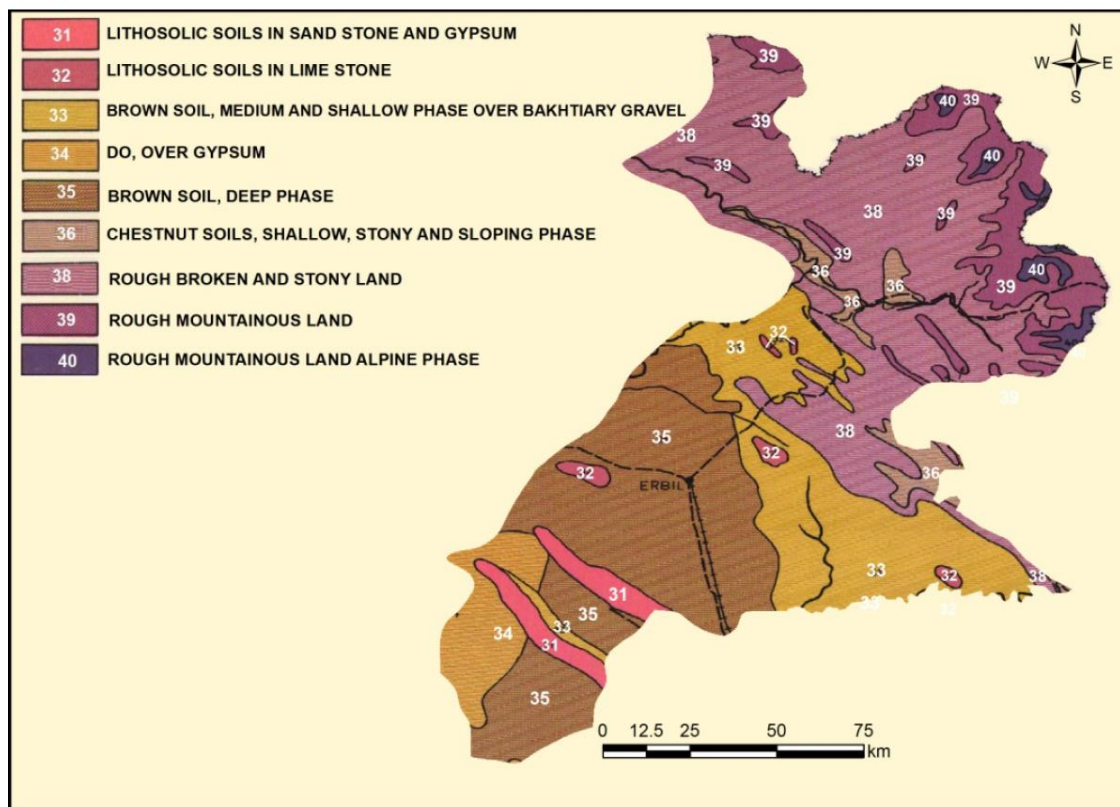


Figure 3.4: Soil types in the Erbil Governorate (following Zakaria et al, 2013)

In Assyrian periods, this plain was the centre of the world and the oldest permanently populated city in the world is Erbil. The old city located on a high flat is surrounded by rich land. These cities are probably among the oldest agricultural land areas with well-developed soils in the world. Gravel, sandstone and mudstone are underlying the brown soil in the area (Buringh, 1960).

3.4 Topography of the Study Area

Erbil city lies on Erbil Plain. It is bordered by the Upper Zab in the northeast and by the Lower Zab at Altın Köprü in the south. In the south-western the Erbil Plain was separated from the Makhmur Plain by a long anticlinal hill. The valley of the Chami Bastora is the north-eastern boundary (Ur *et al*, 2013).

Local topography is a factor that is affecting UHI intensity (Khalid, 2014). The average elevation of the study area is 454 m, the minimum height is 319 m located in the southwest and the maximum height is 878 m in the northeast of the study area. The detailed elevation for the study area is presented in Figure 3.5. Generally, the elevation of the area increases from south to northeast.

Geographically the plain is not uniform. It comprises flat alluvial plains, valleys of rivers, rolling gravel hills and the Zagros foothill regions. In general, the terrain of the area is undulating. Large amounts of water from the Erbil Plain drains via Chami Bastora into the Upper Zab in the north side and below Erbil drains via Chami Shiwasor or Chami Kurdara (Ur *et al*, 2013).

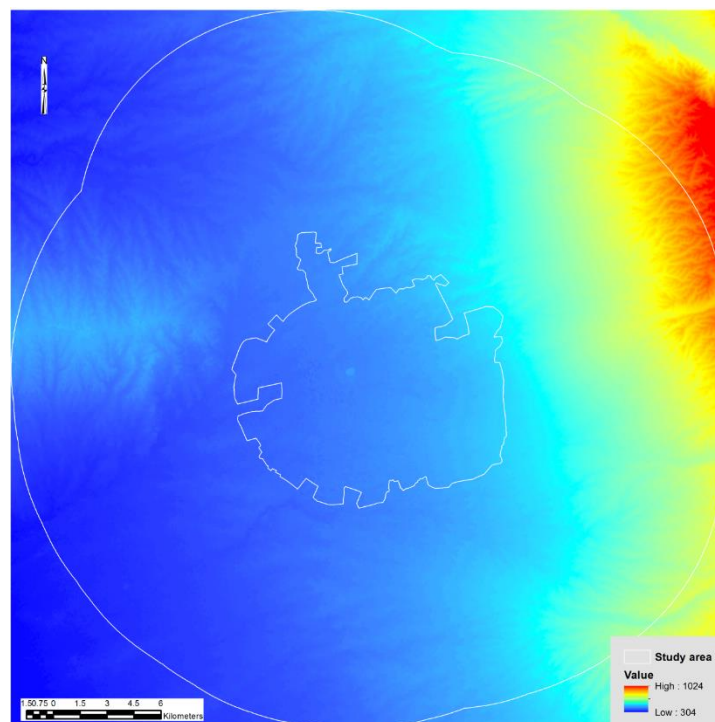


Figure 3.5: Elevation of the study area (USGS, 2016).

3.5 Climate of the Study Area

The majority of the Kurdistan Region and the north part of the Erbil Governorate have a hot-summer mediterranean climate (Csa) while the centre of the city and south part of the Erbil Governorate has a subtropical, hot, semi-arid climate (BSh). For the reason that climatic elements are crucial in this study, they are described in more detail.

3.5.1 Air Temperature

Temperature is one of the most important climatic elements influencing local conditions (Sharif, 1998). In the study area, four seasons can be recognised. Winter and summer are usually longer than spring and autumn. The later seasons will be longer in the north and northeast of the Erbil governorate (Hasan, 2006). The temperature of Erbil is hot and extreme in the summer, cold in winter and mild in spring (Figure 3.7). The mean annual temperature of the Erbil Governorate is $18.35 \pm 0.97^{\circ}\text{C}$ (Hama *et al*, 2014). However, the mean temperature of Erbil city is 21.85°C . The seasonal average temperature is 9.0, 19.2, 33.5 and 22.9°C for winter, spring, summer and autumn, respectively (Hasan, 2006). In the Erbil Governorate, there is an inverse relationship between air temperature and elevation (Hameed, 2013). Therefore, the temperature of the city is higher compared to the mountain areas in the north and northeast part of Erbil. The area is considered as continental, therefore both annual and diurnal temperature ranges are influenced by continentality (Malinowski, 2002).

In terms of temperature, in Erbil city from 1975 to 2011 mean minimum temperature increased by 0.055°C per year and average air temperature by 1.95°C in 35 years. At the monthly level, December ($0.084^{\circ}\text{C}/\text{year}$) and February ($0.085^{\circ}\text{C}/\text{year}$) demonstrated the highest increase of minimum temperature. However, the slope trend of maximum temperature was less compared to minimum values (0.016) for the same period. In some months the trend was negative, for instance, November showed a trend of -0.052°C per year while May and June demonstrated a positive trend (Khalid, 2014).

However, in terms of air temperature of the Erbil Governorate, the trend of mean temperature from 1973 to 2011 was 0.056°C per year (Figure 3.6). Based on the Mann-Kendall trend test this increase was significant ($p < 0.05$). It means in 39 years, the average temperature of the area increased by 2.18°C .

The annual range of temperature was 26.8°C; hence, it demonstrates the continental feature of the study area. According to the Khromov continentality index, the continental percentage of the Erbil is 88.1%. The monthly range of temperature increases in wet seasons and decreases in dry season. The daily range of temperature increases in sunny and calm winds and decreases in rainy and windy days (Sharif, 1998).

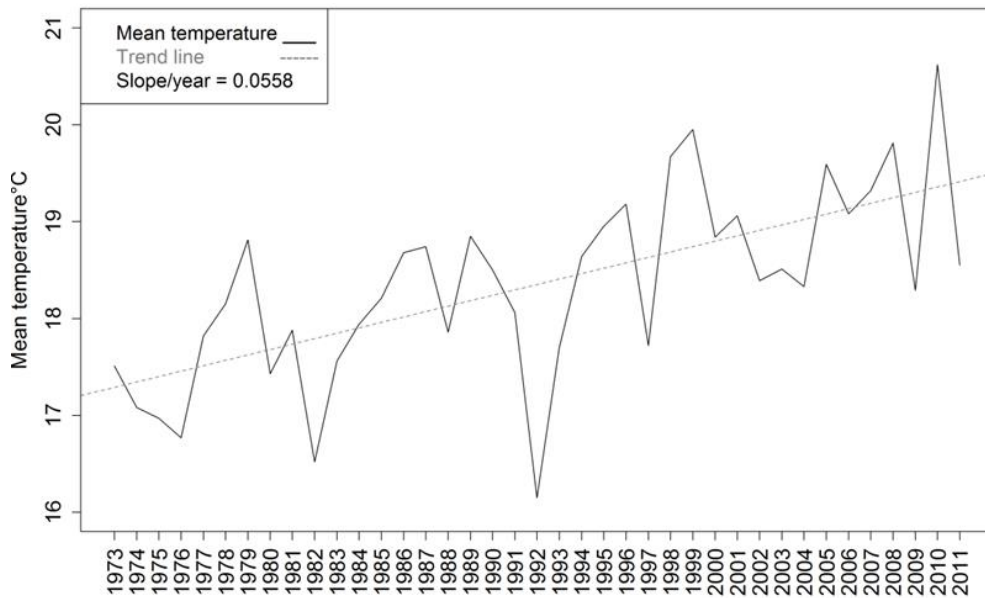


Figure 3.6: Annual mean temperature of Erbil Governorate from 1973 to 2011. (Source of data: Hama et al, 2014).

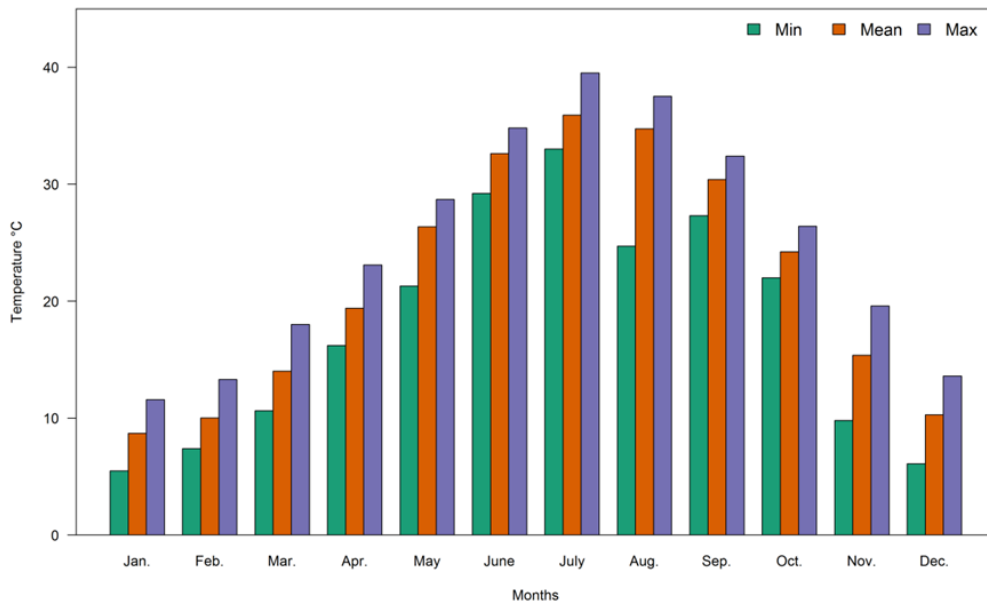


Figure 3.7: Monthly temperature in Erbil (MSDEG, 2014).

3.5.2 Air Pressure

The annual average air pressure of Erbil is 1011.45mb (Figure 3.8). The average air pressure in the winter (January) is 1020.05mb and it decreases to 999.83mb in the summer (July) (MSDEG, 2014). The highest air pressure is usually recorded in January while it was not the coldest month. Whereas, July is the hottest month and shows the lowest pressure. Moreover, the annual range of pressure is 20.22mb (Sharif, 1998). In the summer time, the area is strongly affected by subtropical high pressure. By contrast, during the winter subtropical high pressure is interrupted by periodic low-pressure systems. Mediterranean low pressures travel from west to the east through the Kurdistan Region which brings winter precipitation to the study area (Malinowski, 2002). In this season, the Mediterranean Sea becomes the main centre of low pressure and this strongly affects the Kurdistan Region. This low pressure is influenced by the main direction of the wind moving to the east and northeast. These low pressures are the main reason for the majority of the atmospheric processes that are happening in the winter such as precipitation, wind direction and the temperature fluctuations. The average number of these low pressure systems in the Kurdistan Region is 39.2 and they stay in the area for an average of 63.6 days (Hasan, 2006). As a result of these fluctuations, there is a wide variation in the amount of precipitation from year to year.

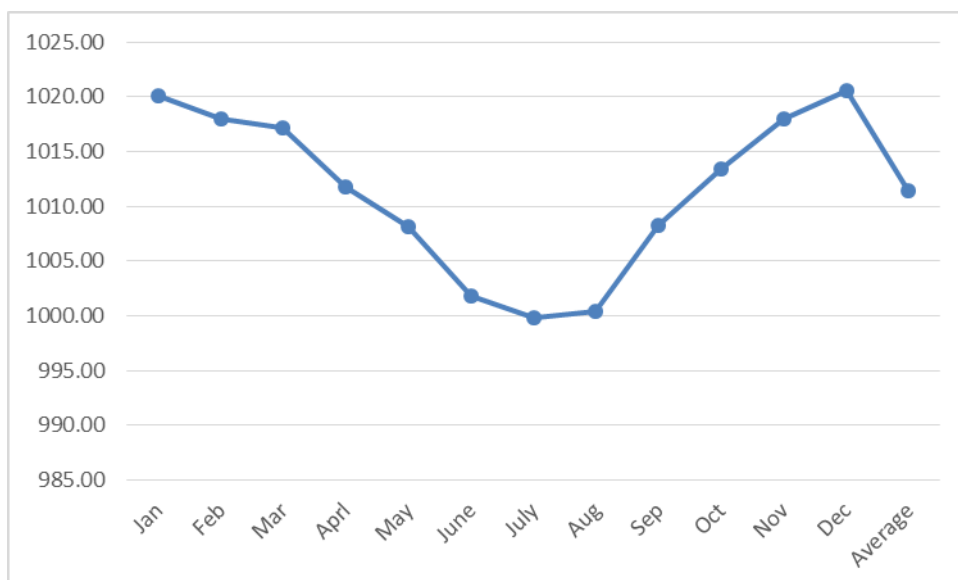


Figure 3.8: Monthly mean sea level air pressure in mb of Erbil from 1993 to 2000.

3.5.3 Winds

The important role of wind in the climate is transferring the character of temperature and humidity (Hasan, 2006). The movement of wind in the city centre is differing from the wind movement in the surrounding regions. The tall buildings in the city affect the speed, direction and wind stream (Sharif, 1998). Wind speed is one of the factors that influence UHI intensity (Khalid, 2014). UHI intensity will increase with calm wind. The mean speed of wind in the city is around 2.45 m/s in Erbil (MSDEG, 2014).

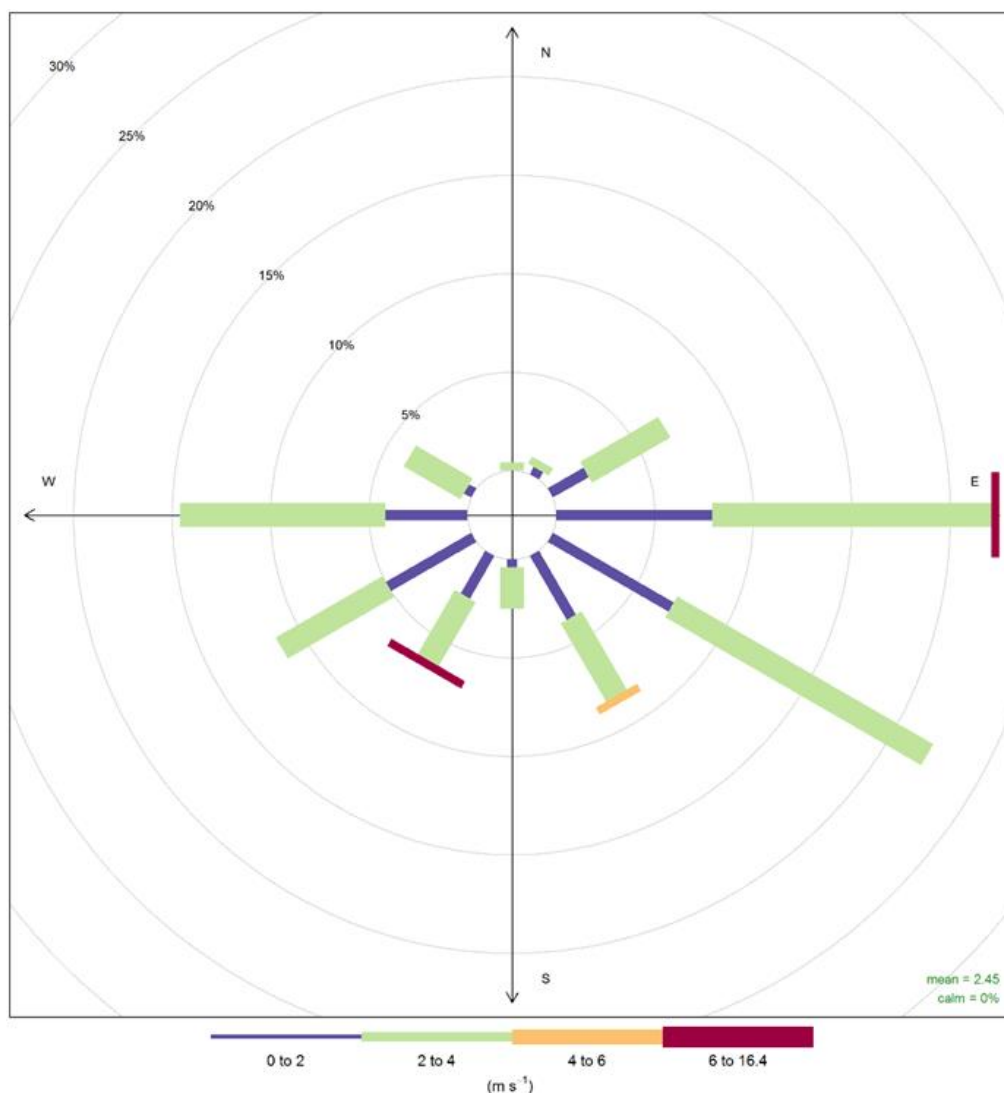


Figure 3.9: Wind speed and direction (%) of Erbil city. Sampled from years of data (1993:2012). The circles are % occurrence in the directions shown.

The east and southeast winds are the main wind direction in the city and they represent 22% of all winds. Another most common wind in the city is a western wind

and it makes up 14% of all the winds. This wind is more prevalent in summer months, especially during August (20%). Finally, southwest wind is the third most common wind (Figure 3.9).

In terms of wind speed, the wind in the city centre is slow and the number of calm days are higher. The strongest wind in the area, during the year is coming in the spring months (Sharif, 1998).

As the study area is located in the north part of the world, the temperature commonly increases with the southern wind group and decreases with the northern wind group. The eastern and western winds cause decreasing temperature in the winter and cause more warming in the summer.

3.5.4 Relative Humidity

The relative humidity (RH) depends on air temperature and the amount of water vapour in the air (Sharif, 1998). The relationship between RH and temperature is inverse and increasing temperature causes decreased RH for the same water vapour content. In contrast, there is a positive relationship between RH and precipitation.

High atmospheric humidity may reduce the potential radiative cooling of the surface and it may likely cause an increase in the heat island intensity (Voogt, 2002). The average RH of Erbil is 48.74%. It is high in the raining season and attains 75.16% in January. In contrast, it decreases in the dry season (summer) and experiences the lowest percentage (24.37%) in July (MSDEG, 2014).

3.5.5 Cloud Cover

Cloud cover leads to a rise in temperature of cities however it decreases the ΔT between urban and rural areas. The average number of cloudy days over Erbil is low and is around 33 days annually. The lower cloudiness creates a great opportunity to investigate surface temperature of the city through thermal satellite instruments. The highest average cloudy months are December (4.5 days) and January (4.4 days, Figure 3.10). Generally, summer months in the city are very clear. The average number of cloudy days of June, July, August and September are between 0.5 and 1.1 days.

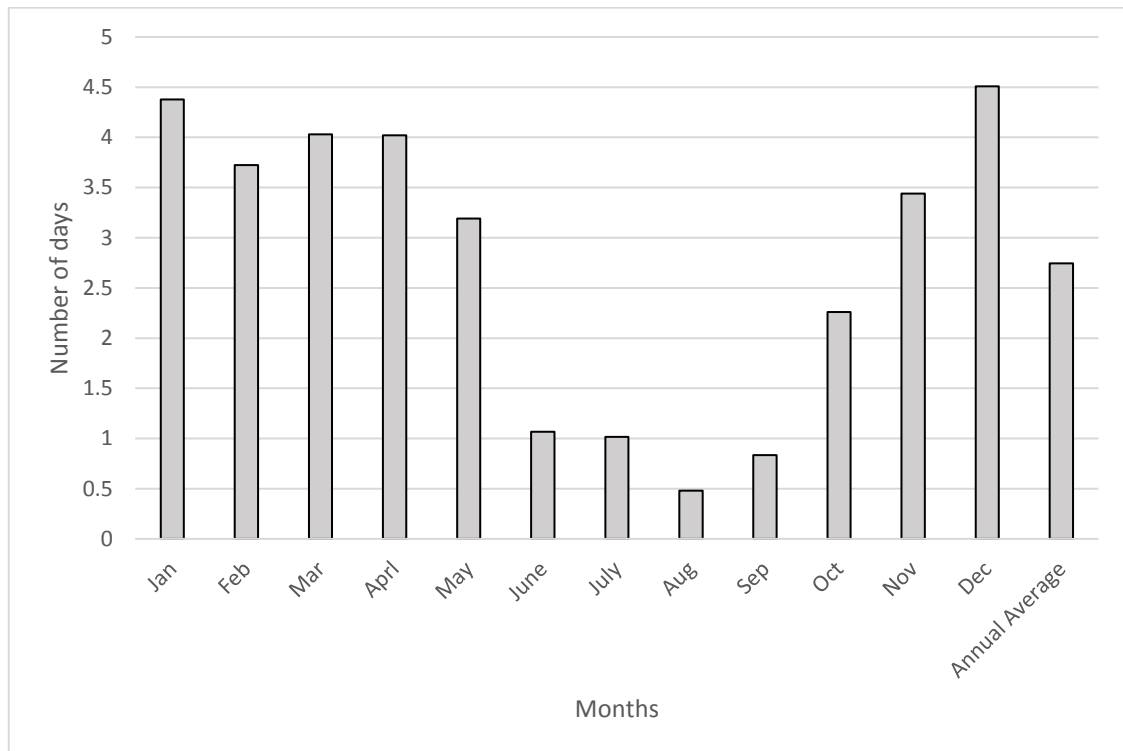


Figure 3.10: Monthly cloudiness of Erbil.

3.5.6 Precipitation

The amount of rainfall in the study area strongly fluctuates over the year. It increases from south to the north and north east with the increasing elevation. Average annual precipitation in Erbil from 1993 to 2012 was 380.26 ± 108.88 mm whereas in the south part of the Erbil Governorate it reduces to 250 mm and grows to 1200 mm in the north and north east near Iran's and Turkey's border (Hameed, 2013). The amount of rainfall in the Erbil plain is suitable for dry-farming agriculture whereas the fluctuation of rainfall and drought in some years makes agricultural activities more vulnerable. This fluctuation also causes a decreasing amount of water in the rivers and springs. In contrast, sometimes it rains 50 to 80 mm through thunderstorms in less than 24 hours. Therefore, there is a potential hazard of flash flooding in the area (Malinowski, 2002).

In recent years, rainfall in the Kurdistan Region of Iraq has decreased substantially (Hameed, 2013). The mean annual rainfall from 1941 to 2011 in the Erbil Governorate was 411.14 ± 169.19 mm. During this period, the highest amount of

annual precipitation was 872.4 mm which occurred in 1945, whereas the lowest amount of rain was 227.5 mm which fell in 1955 (Hama *et al*, 2014). The slope of time series trend for precipitation during this period in the Erbil Governorate was -1.288 mm/year (Figure 3.12).

In Erbil, rainfall usually occurs during autumn, winter and spring months whereas summer is the dry season. The highest amount of precipitation occurs in February, January and March whereas July and August are dry season periods due to the absence of precipitation (Figure 3.11).

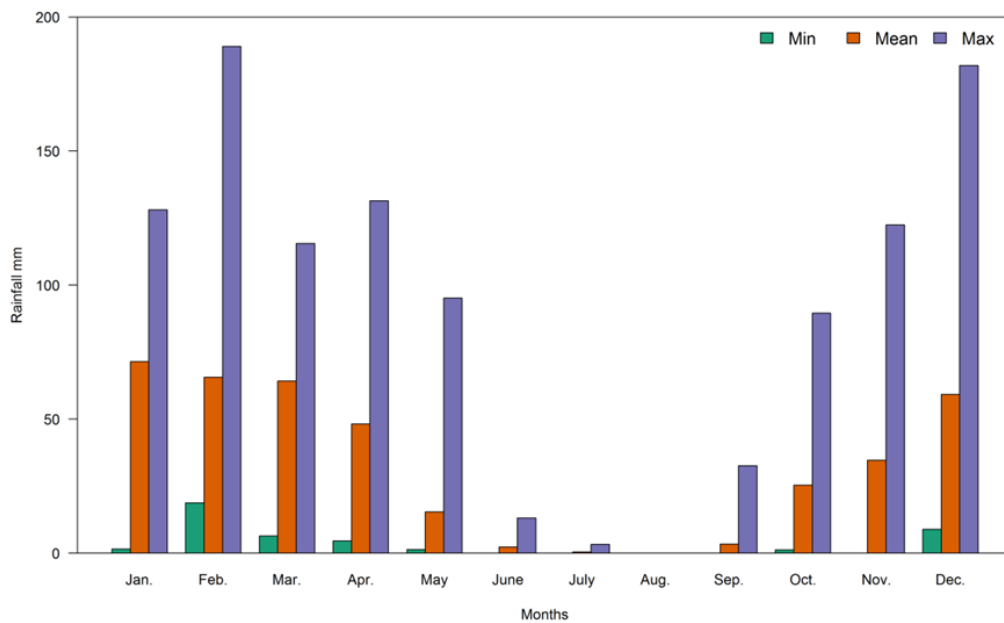


Figure 3.11: Monthly precipitation of Erbil from 1993 to 2012 (MSDEG, 2014).

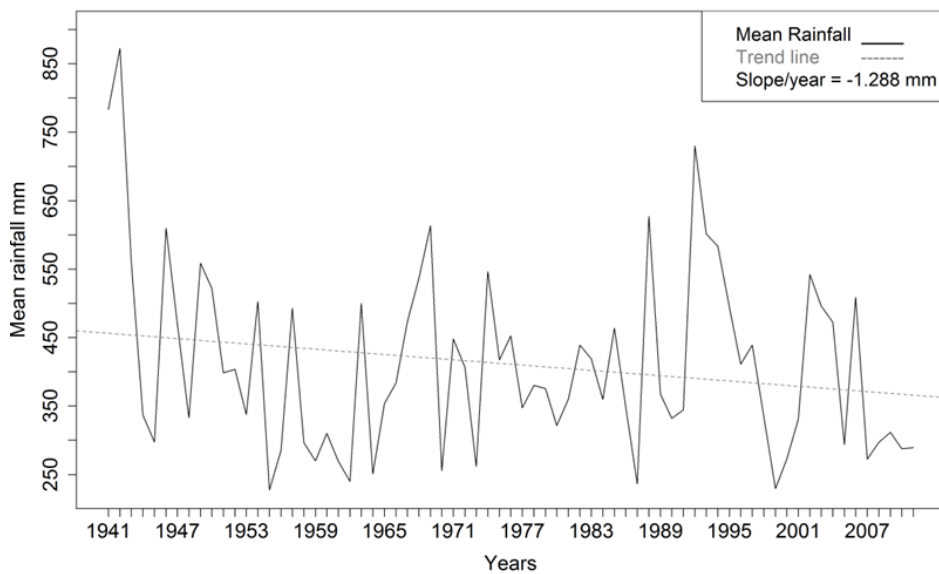


Figure 3.12: Time series of annual precipitation from 1941 to 2011 (Source of data: Hama *et al*, 2014).

3.6 Vegetation and Green Area

Vegetation can reduce surface and air temperature through shading and evapotranspiration (EPA, 2009). The variation of vegetation abundance between the urban and the rural is one of the determining factors that are affecting UHI and SUHI intensity.

In the spring, the area is characterised by extensive grasses and herbs while in the summer soil moisture is low and vegetation is rare in the rural area surrounding the city. The natural vegetation in the area is steppe grass type and it is a transition region between mountain vegetation in the north and desert vegetation in the south. In this area, the grass layer becomes higher and more dense near the mountain region in the north as a result of increasing elevation and precipitation whilst it becomes similar to desert vegetation in the south (Hasan, 2006).

Gardens inside the houses form part of the green area in the city. In the city expansion during the second half of the twentieth century, houses in the newly built areas are characterised by having large frontal garden areas. The final stage of city expansion is distinguished by the presence of smaller or no gardens (Baper *et al*, 2010).

An agroclimatic zone of the area is Semi-arid Cool Very Warm (SA-C-VW) with the character semi-arid climate with cool winter and very warm summers. The moisture-limited and temperature-limited growing period of Erbil is 190-210 and 330-365 days, respectively. The prevailing time of moisture and temperature is limited to 150-180 days (Pauw, Saba and Ali, 2015). In the rural area, winter grain such as wheat and barley are the most commonly cultivated crops and in general agriculture in the study area depends on the precipitation, rather than irrigation. Therefore, the majority of croplands are dry in the summer time. In the Erbil Governorate, 41% of the lands are arable and 93% of croplands are rain-fed (Fadhil, 2011).

The ratio of the green area to total city area in Erbil City is 12% (Erbiltourism2014, 2014). There are several gardens and parks in the city, for instance Sami Abdul-Rahman Park (S.A. Park), Minare Park, and Shanidar Park. S.A. Park is located in the west of Erbil and is the biggest green area (about 2 km²) in the city. It is divided into gardens and forest. Its gardens consist of three types: lawns, a flower quarter and a variety of trees. The forest contains 50,000 trees in different parts of the park and around 50,000 trees are planted around the park (Figure 3.13).



Figure 3.13: Sami Abdul-Rahman Park in Erbil.

3.7 Growth of the City

The old city of Erbil consists of the Erbil Citadel and the old districts surrounding it (Al-Hashimi and Bandyopadhyay, 2015). The citadel of Erbil is the core and fundamental part of the city that shaped the surrounding urban pattern as concentric rings (Ibrahim *et al*, 2015). In the second half of twentieth century, the third and fourth stages of the city expansion occurred. These new areas are shaped as a circular pattern around the centre (Baper *et al*, 2010) (Figure 3.14).

Since 2003, the city changed rapidly and experienced abundant architectural structures and great housing projects. As an example of rapid growth, the number of districts in Erbil reached 82 in 2012 while it was only eight in the 1950s. However, the rapid growth and migration means remaining housing is a serious issue in the city. Furthermore, environmental degradation, the deficiency of educational, health services and infrastructure are some of the major problems that the city is suffering from (Ibrahim *et al*, 2015). In addition, this city expansion transformed vegetated lands to built-up areas (Baper *et al*, 2010). Thus, developmental projects influenced negatively on the environment that has not been given the necessary attention (Jassim *et al*, 2013). More tall buildings and small houses characterise the final stage of city expansion (Figure 3.15).

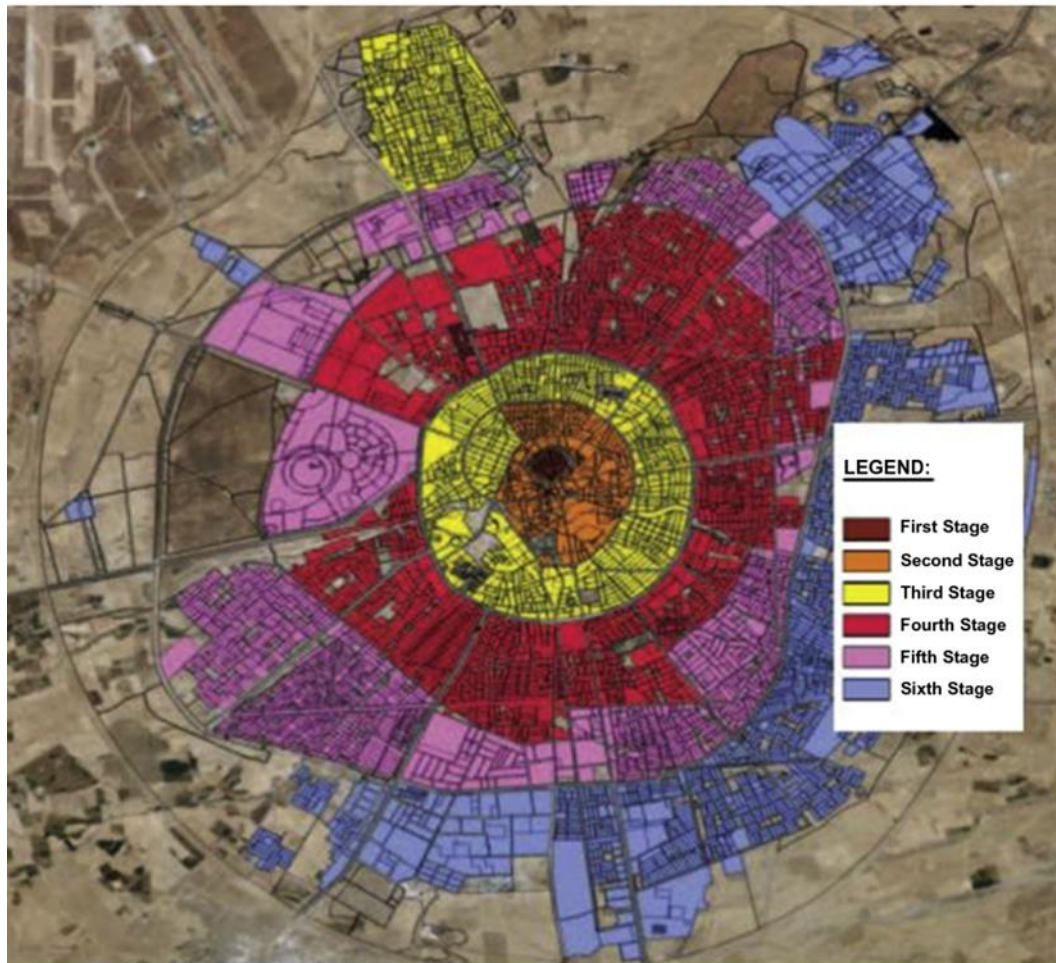


Figure 3.14: Urban transformation stages of Erbil City until 2007.

Source: (Baper *et al*, 2010).

3.8 Building Components in Erbil

In general, concrete blocks or bricks are used for making wall houses, gypsum for covering the inner and cement for covering the outer of the walls. The thickness of walls in the houses in Erbil ranges between 20 and 40 cm (Abdulrahman, 2014). The floors of buildings take a flat shape and are covered with concrete. The structure and materials of old districts that built during the second stage of city expansion differ from new districts that were built-up in the fifth and sixth stages.

For instance, houses in the Arab district that return to the second stage principally consist of one floor that is built from bricks and clay (Figure 3.15). The houses here contain rooms that surround the courtyard in the centre. The houses take a square or rectangular shape and they have one entrance. Buildings contiguous with each other and the area include narrow organic alleys. Demographically, an average of five

people reside in each family and the district has high density (Ibrahim, Mushatat and Abdelmonem, 2014).

On the other hand, the Italian Village is an example of new districts and build style in the western building style. It comprises of 659 attached and semi-attached buildings built in 2008. The area includes public service buildings that are built on one floor such as schools, shops and mosques. The green areas and open spaces here are well considered. The density of this new district has as average of four people per family which is less than Arab district (Ibrahim *et al*, 2014).



Figure 3.15: Building types in Erbil. A: Erbil Citadel (first stage), B: Qaisary Bazaar (second stage and rebuilt), C: Old buildings (second stage), D: Building in fourth stage and some of them rebuilt in the new style, E: House in Italian Village (sixth stage), F: Naz City (sixth stage).
Sources: (Hawlergov, 2012; One-thirteen, 2009; NGC, 2015; Media.tagorg, 2013).

3.9 Population of the City

Erbil is one of the oldest cities in the world that has been continuously inhabited and life in the city commenced more than 6000 years ago (Ibrahim *et al*, 2014). The population of the Erbil Governorate was 1,095,992 inhabitants in 1997 and in 2012 this

number was rose dramatically to around 1.9 million. It means the annual growth rate of the population in Erbil Governorate is 2.9% (Dizayee, 2014).

In the 19th century, the population of the city principally resided in the Citadel and the number ranged between 3,000 to 6,000 inhabitants (Ibrahim *et al*, 2015). In 2015, the population of the Erbil Governorate was estimated to be 1,530,722 inhabitants (IOM Iraq 2015).

**Chapter 4 : Spatial Variation of the Daytime Surface Urban
Cool Island during the Dry Season in Erbil, from Landsat 8**

Parts of this chapter have been published with CC-BY copyright license as:
Rasul, A., Balzter, H. and Smith, C. (2015) 'Spatial variation of the daytime Surface Urban Cool Island during the dry season in Erbil, Iraqi Kurdistan, from Landsat 8', *Urban Climate*, 14, pp. 176-186.

4.1 Introduction and Rationale

The variation between the characteristics of land cover in urban and non-urbanised areas in terms of 3-dimensional geometry of the built area, heat absorption, the building materials, surface albedo and amount of vegetation cause different air and surface temperatures within a city relative to the surrounding area. Therefore, urban expansion has the ability to cause radical variations in the nature of the surface of the urbanised area. Usually, in temperate and sub-tropical climates this urban extension causes temperatures to increase, a phenomenon known as the UHI effect. In contrast, built-up areas in semi-arid regions have been ascertained to exhibit lower surface temperatures compared to non-urbanised dry surroundings, which has been termed the Urban Cool Island (UCI) effect.

Satellite sensors can be used to derive the surface temperature of urban areas and to study the spatial variations of UHIs and their development (Watson, 2012). SUHIs and surface temperatures have been observed from different platforms including satellites, aircraft and ground-based sensors. Landsat TM and ETM+ are widely used to investigate the expansion of SUHIs and to assess the relationship between LST and LULC. Freely available and high spatial resolution of Landsat images make them to be appropriate to investigate the spatial variation of SUCI/SUHI and the effect of LULC change from different samples of classes on LST. In 2013, Landsat 8 was launched with two thermal bands that potentially give the opportunity for this research to apply TIRS data in spatial investigation of LST on Erbil.

It is notable that few investigations of the SUHI/SUCI effect in arid environments have been published. Research on the UCI effect is still in its infancy (Li *et al*, 2011) and its characteristics in semi-arid environments are still required to be superior, quantified and comprehended.

This chapter investigated and assessed spatial distribution of LST and SUCI in the city from Landsat 8 images. Variations of LST, SUCI and SUHI were assessed based on different LULC classes in the study area such as water, tree, grass, built-up, and bare soil. In another section, the distribution of LST in different districts in Erbil has been considered. To establish the main determinant factors, relationship between LST and wetness, brightness, greenness, NDVI and NDBI for different LULC classes and districts have been assessed.

4.2 Data and Methodology

In this section, data and methods that were used in this chapter are presented. It includes retrieval of LST, identifies Greenness, Wetness and Brightness Indices, and relates them to NDVI, NDBI and SUCI/SUHI intensity.

4.2.1 Data and Pre-Processing

Land surface temperature data were extracted from six Thermal Infrared Radiometer images acquired by Landsat TIRS (Landsat 8) from 1st July to 19th September 2013 (Table 4-1). These were used to retrieve LST (Path 169, Row 035). The images are level L1T data and were captured under transparent atmospheric conditions (<1 % cloud coverage). These images were provided by the United States Geological Survey (USGS), Earth Explorer website (<http://www.earthexplorer.usgs.gov/>).

As a visual comparison of Landsat true colour bands with a thermal band, Figure 4.1 for Landsat-5 indicates that low surface radiation in the thermal image is associated with urban areas of the city and green fields in the south west of the city. In contrast, high surface radiation is consistent with the bare soil land within rural areas in the north west of Erbil. The image indicates that rural areas surrounding the city show higher surface emitted radiation than urbanized and vegetated areas. The thermal image shows sensitivity to larger river beds and roads indicating that LST is sensitive to urban structures at Landsat resolution; Erbil urban structure can be greater than 100 m in extent. Hence Landsat is appropriate for observations of SUHI and SUCI.

A composite image of summertime Landsat 8 is produced by calculating the pixel-based mean of all of the six images for the thermal and Operational Land Imager (OLI) bands. This composite image is used for all of the subsequent analysis. For the

thermal bands of Landsat 8, thermal atmospheric correction was applied due to it having two thermal channels. Furthermore, Quick Atmospheric Correction (QUAC) is appropriate for atmospheric corrections of OLI Bands of Landsat 8 (Figure 4.2).

Landsat 8 data have suffered from a calibration problem, believed to be due to straylight from observations outside the observed scene, and resulting in pixel-to-pixel uncertainties of 0.8 K in band 10 and 1.75 K in band 11 (Montanaro *et al*, 2014; Barsi *et al*, 2014; Landsat User Handbook). Results from Cook *et al* 2014, suggest that band 10, and band 11 errors tend to be correlated so that atmospheric correction using both bands should have an uncertainty due to calibration which is similar to or smaller than 1.0 K. Analysing only summertime images will also mitigate relative errors since the surrounding areas to Erbil will have a similar temperature structure on analysed days. If subsequent processing to LST is performed only with band 10, then uncertainty on absolute LST should be no more than the combination of 0.8 K and 1.0 K which is approximately 1.3 K. Hence changes of less than 1.5 K should be treated with caution but larger variations should be robust to calibration errors.

Shapefiles of LULC were created based on a true colour image from Landsat 8, Digital Globe imagery (with 0.5 m resolution was acquired on 5th July 2010) and a map of Erbil's districts (was prepared by the GIS Centre of Erbil Governorate). Exemplar LULC classes were selected based on expert knowledge and definitions of local climate zones by Stewart (2011) to assess how LST varied according to LULC (Figure 4.3, 4.4). These were comprised of "Commercial Areas", "Industrial", "Airport", "Compact low-rise LCZ 3", "Sparsely built LCZ 9", "Bare soil LCZ F", "Dense trees LCZ A", "Scattered trees LCZ B", "Grass" and "Water LCZ G" (Stewart and Oke, 2012).

A map of the districts of Erbil was prepared based on Open Street Map data and the map of Erbil's districts. The digitised district boundary map was georeferenced and projected to WGS-1984 UTM zone 38N. The minimum, maximum and mean LST were calculated for each district with the Zonal Statistics Tool in ArcMap.

Table 4-1: Images used in Chapter 4.

Number	Date	Time	Cloud Cover (%)	Image Quality	Path/Raw	Spatial Resolution (m)
1	01/07/2013	07:40:58	0.01	9	169/35	30 OLI/100 TIRS
2	17/07/2013	07:40:58	0.01	9	169/35	30 OLI/100 TIRS
3	02/08/2013	07:41:00	0.02	9	169/35	30 OLI/100 TIRS
4	18/08/2013	07:41:01	0.01	9	169/35	30 OLI/100 TIRS
5	03/09/2013	07:41:02	0.03	9	169/35	30 OLI/100 TIRS
6	19/09/2013	07:40:57	0.72	9	169/35	30 OLI/100 TIRS

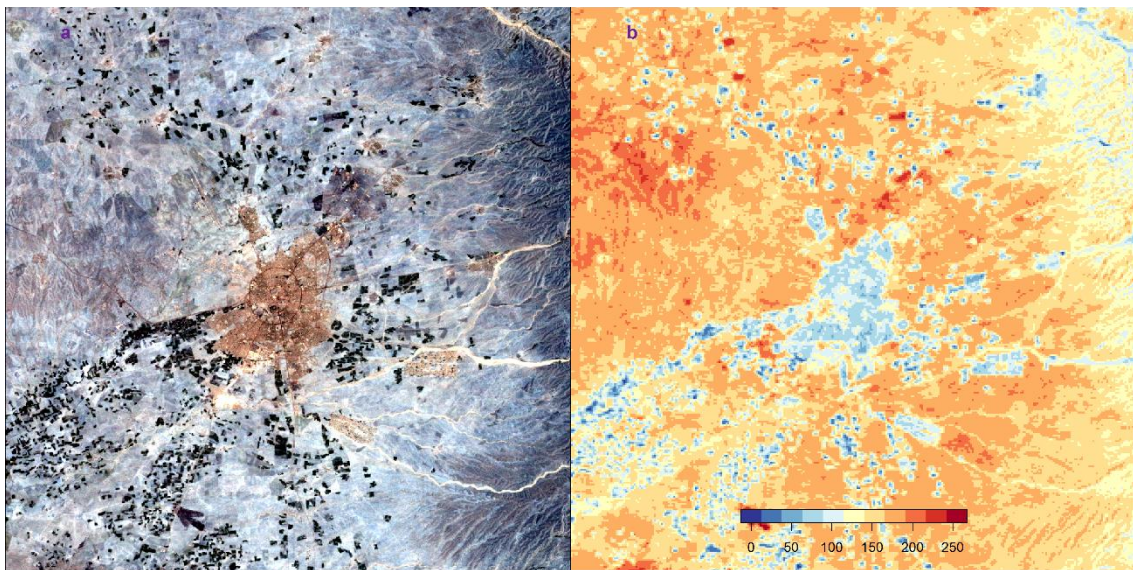


Figure 4.1: Image Landsat 5 of study area of 31 July 1992, “a” is a combination of bands 3, 2, 1 and “b” is band 6 (thermal band).

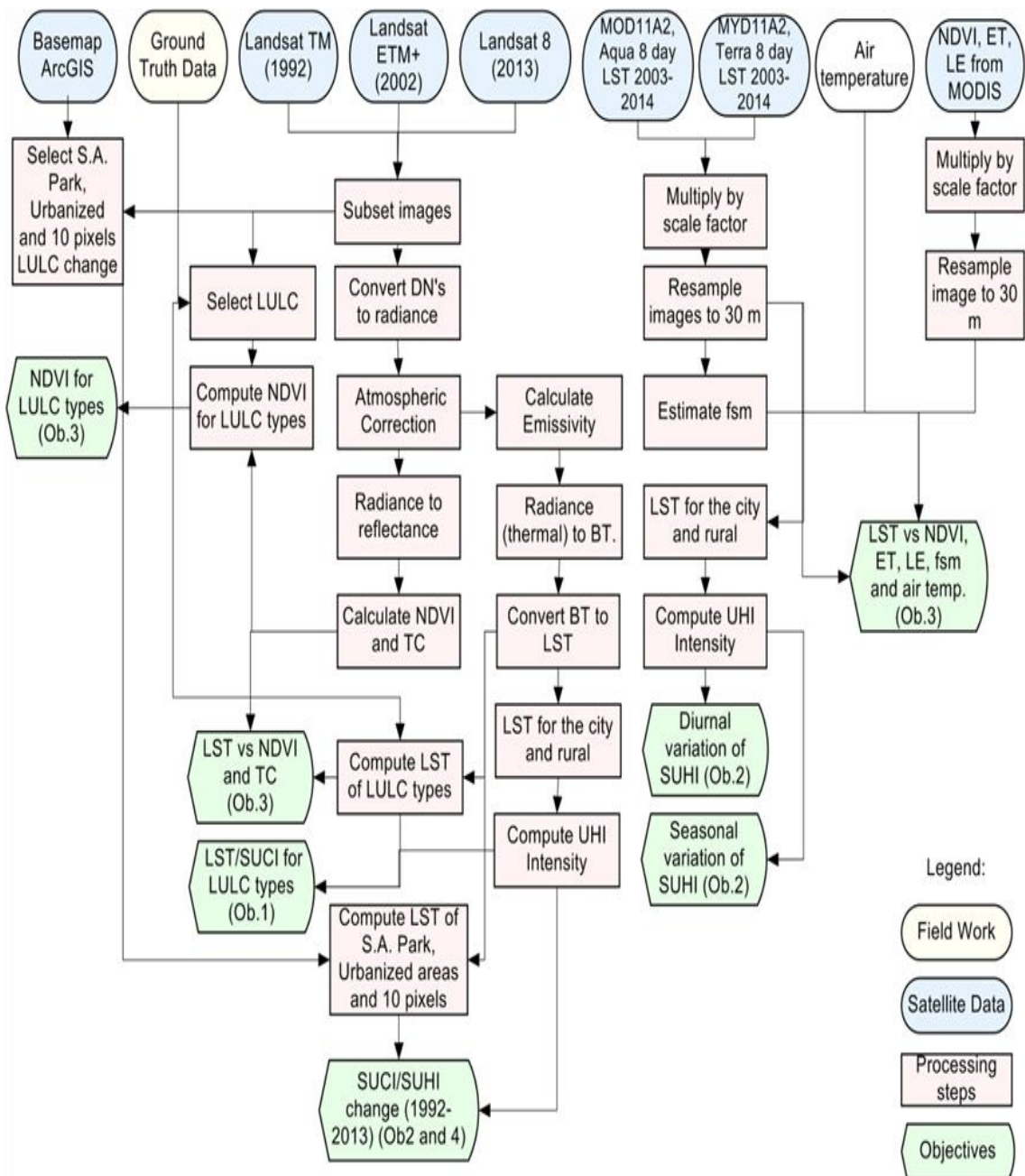


Figure 4.2: General methodology flowchart adopted in this study.

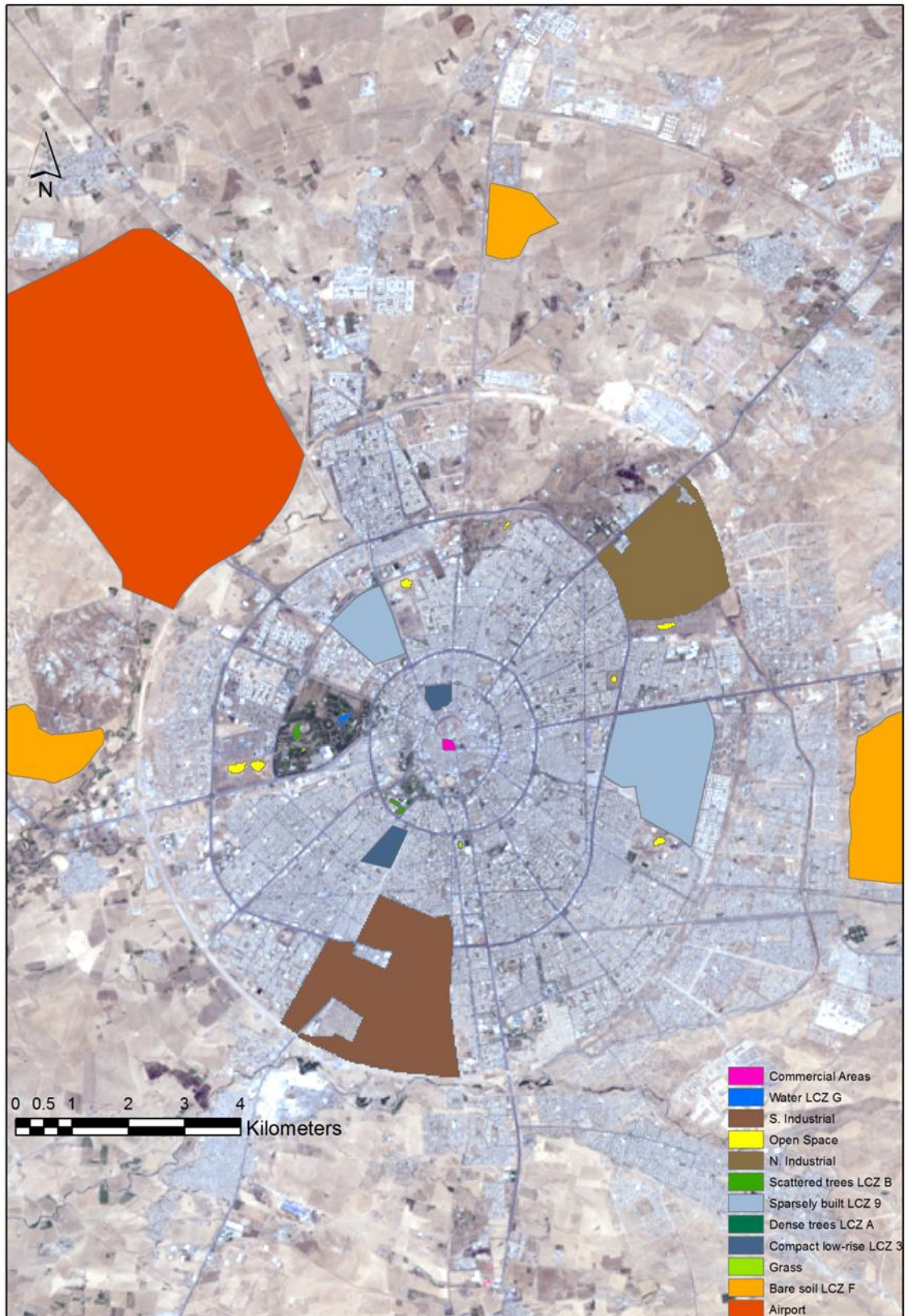


Figure 4.3: Samples of selected LULC with the true colour Landsat OLI.



Figure 4.4: Samples of selected LULC in Erbil. A: Commercial Areas, B: Airport, C: North Industrial, D: South Industrial, E: Scattered trees, F: Dense trees, G: Sparely built, H: Compact low-rise, I: Grass, J: Water, K: Open space and L: Bare soil (Image source: Esri, DigitalGlobe, GeoEye, i-cubed, Earthstar Geographics, CNES/Airbus DS, USDA, USGS, AEX, Getmapping, Aerogird, IGN, IGP, swisstopo, and the GIS User Community).

4.2.2 Retrieval of LST

The digital number of Landsat TIRS was converted to at-sensor radiance, using Eq. (4.1) (Chander and Markham 2003; USGS 2013; Landsat 7).

$$L_{\lambda} = gain * DN + offset \quad (4.1)$$

where: L_{λ} = at-sensor spectral radiance ($Watts/(m^2 * sr * \mu m)$); $gain$ = rescaling factor specific to each band from the metadata. $offset$ = rescaling factor added to each band from the metadata. DN = digital number of a given pixel.

These values were subsequently converted to at-satellite brightness temperature with Eq. (4.2):

$$TB = \frac{k2}{\ln(\frac{k1}{L_{\lambda}} + 1)} \quad (4.2)$$

where TB = brightness temperature in Kelvin, $k1$ = Landsat 4: 671.62; Landsat 5: 607.76; Landsat 7: 666.09; Landsat 8: 774.89 and $k2$ = Landsat 4: 1284.30; Landsat 5: 1260.56; Landsat 7: 1282.71; Landsat 8: 1321.08 are calibration constants from the metadata (USGS, 2013).

4.2.2.1 Emissivity correction

An emissivity correction is required to accurately derive LST from satellite imagery (Srivastava *et al*, 2009). The Emissivity Normalisation Method was applied here. It was first described by Gillespie (1985) and has been recommended by Li *et al* (1999) to calculate emissivity. The approach calculates the emissivity of the highest temperature for each pixel (Li *et al*, 2013; Zhang *et al*, 2008). Eq. (4.3) is then used to correct surface emissivity (Zhang *et al*, 2013).

$$T_s = \frac{TB}{(1 + (\lambda TB / \rho) \ln \epsilon)} \quad (4.3)$$

where T_s is land surface temperature (in Kelvin); TB is radiant surface temperature (in Kelvin); λ is the wavelength of emitted radiance (11.5 μm); ρ is $h \times c / \sigma$ ($1.438 \times 10^{-2} m K$); h is Planck's constant ($6.26 \times 10^{-34} J s$); c is the speed of light ($2.998 \times 10^8 m/sec$); σ is Stefan Boltzmann's constant ($1.38 \times 10^{-23} J K^{-1}$); and ϵ is emissivity (Farina, 2012).

An analysis of the effect of using only one or both thermal channels in the analysis is included in Appendix A15 and A16. Essentially an effect of K can result. However, the effect is an absolute bias so the analysis of relative LST in this chapter is much less affected.

4.2.3 Identification of the Surface UCI and UHI Intensity

Surface UCII and UHII is the variation between the surface temperature of an urban area and its rural surroundings (Stathopoulou and Cartalis, 2007). There is no standardised method of measuring UHII. To address the problem of confusion in classifying urban and rural areas, Stewart (2009) proposed LCZs classification. Difference in average LST between urban and rural areas (buffer around the city) is one approach that has been used to select SUHI (Hawkins *et al*, 2004; Cheval and Dumitrescu, 2009; Imhoff *et al*, 2010). A 10 km buffer zone around Erbil is used here to define the reference ‘rural’ (non-urban) surface temperature. The buffer principally represents rural areas (91.63% Open Shrublands and 6.99% Crop Lands) which contain only a small (1.33% Urban and Built-up) of urban pixels according to MODIS Land Cover Classification at 500 m resolution. Therefore, Erbil Airport and some urban pixels have only a limited influence on the average LST of rural areas. In this study, the magnitude of both SUCI and SUHI is calculated by Eq. (4.4) (Oke, 1987; Li, Mo and Dai, 2011).

$$\Delta LST = LST_u - LST_r \quad (4.4)$$

where: LST_u = mean LST of urban area; LST_r = mean LST of rural buffer area. A positive value represents a SUHI situation whilst a negative result represents SUCI intensity.

4.2.4 Calculating Wetness, Greenness and Brightness Components

One of the advantages of the Tasselled Cap Transformation (TCT) is the ability to consolidate spectral data into a few bands with a slight loss of information (Baig *et al*, 2014). The most relevant indicators for the current study, which can be acquired using TCT derived from Landsat 8, are brightness, greenness and wetness. The first feature is a brightness index, which is a weighted sum of all reflective (OLI) bands. It is related to bare or semi bare soil, natural and artificial features. Greenness is characterised by high absorption in visible bands and high reflectance in the near band.

The greenness index significantly correlates with the leaf index and a healthy biomass, while it is proven that wetness is sensitive to soil and plant moisture (Jin and Sader, 2005; Crist and Cicone, 1984; Baig *et al*, 2014). Schönert *et al* (2015) found that all correlations (r) of greenness related to green leaf area index (LAI) were statistically significant ($p = 0.01$), and ranged from 0.79 to 0.91. Akther and Hassan (2011) found that wetness indices correlated with ground soil moisture. The Brightness Indices (BI), Greenness (GVI) and Wetness (WI) are calculated using Eq. (4.5), (4.6) and (4.7), respectively (Baig *et al*, 2014). The results indicate these equations are suitable for this study. The high greenness pattern were found to be associated with vegetated areas and high wetness patterns correlated with water body and high soil moisture areas (Figure 4.6).

$$BI = (.3029 * b2) + (.2786 * b3) + (.4733 * b4) + (.5599 * b5) + (.508 * b6) + (.1872 * b7) \quad (4.5)$$

$$GV = (-.2941 * b2) + (-.243 * b3) + (-.5424 * b4) + (.7276 * b5) + (.0713 * b6) + (-.1608 * b7) \quad (4.6)$$

$$WI = (.1511 * b2) + (.1973 * b3) + (.3283 * b4) + (.3407 * b5) + (-.7117 * b6) + (-.4559 * b7) \quad (4.7)$$

where: BI = brightness index, GVI = greenness index, WI = wetness index. $b2 : b7$ = digital number of bands 2:7.

Subsequently, a few extreme values of the results of each of the Tasselled Cap components were replaced with the Replace Bad Value tool in ENVI software and then they are rescaled to [1, 100].

4.2.5 Calculating Built-up and Vegetation Indices

NDBI was proposed by Zha *et al* (2003) as a sensitive indicator of a built up area. They used this index to map the built-up area of Nanjing city in the east of China. In this example, the study area has a humid, subtropical climate and the index provided high accuracy due to the vegetated and wet surroundings; the index has limitations in built-up areas located in barren regions due to the similarity of the spectral properties in all TM bands. NDBI was calculated by using Eq. (4.8) (Zha *et al*, 2003).

$$NDBI = \frac{(\rho_{SWIR1} - \rho_{NIR})}{(\rho_{SWIR1} + \rho_{NIR})} \quad (4.8)$$

where: $NDBI$ = normalised difference built-up index, ρ_{SWIR1} is the surface reflectance of Short-wave Infrared band (6), and ρ_{NIR} is the surface reflectance of Near Infrared band (5) in Landsat OLI.

The simple and widely used vegetation index is NDVI. Compared to NDVI, GVI is a multiple linear spectral combination (e.g. four bands for MSS and six bands for TM, ETM+ and OLI) and it is a type of data transformation used to distinguish healthy vegetation. In contrast, NDVI is a ratio based index using two bands (red and near infrared) to identify healthy vegetation and green biomass variations. Both of these indices rely on the fact that vegetation has a strong absorption in the red band and a strong reflection of the radiation in the NIR band (Karnieli *et al*, 2010; Wu, 2014). Aufmuth (2001) concluded that GVI and NDVI are well correlated whereas Todd and Hoffer (1998) ascertained that when the vegetation cover is low, GVI was less affected by moisture content and soil type. To calculate NDVI, equation 4.9 was employed (Sobrino *et al*, 2004).

$$NDVI = \frac{(\rho_{NIR} - \rho_{RED})}{(\rho_{NIR} + \rho_{RED})} \quad (4.9)$$

where $NDVI$ = normalised difference vegetation index, ρ_{NIR} is the surface reflectance of band 4, and ρ_{RED} is the surface reflectance of band 3 in Landsat 4, 5 and 7 (band 5 and band 4 in Landsat 8).

4.3 Results

4.3.1 SUCI in the City

The spatial distribution of LST indicates significant variations between the urban thermal environment and its surroundings. The mean LST inside the city was $46.2 \pm 1.74^\circ\text{C}$, compared to a mean LST of $50.1 \pm 1.76^\circ\text{C}$ in the 10 km buffer zone surrounding the city. The SUCI of the city in the morning (at ~07:40) ranges from -3.5 to -4.6°C (Table 4-2).

Table 4-2: Land Surface Temperature in Erbil and its surroundings during summer 2013.

Area	Min LST °C	Max LST °C	Mean LST °C	SD LST °C
Core (city)	34.1	53.5	46.2	1.74
Buffer (10 km)	37.6	58.1	50.1	1.76

4.3.2 Variation of LST with Land Use / Land Cover

The influence of land cover on LST and SUHII was assessed by calculating zonal statistics. Figure 4.5 indicates that water bodies (Lake 1 and Lake 2) have the lowest average LST ($40.22 \pm 1.59^{\circ}\text{C}$), as would be expected (e.g. Frey *et al*, 2007, Stathopoulou and Cartalis, 2007). The highest mean LSTs were ascertained for the Airport ($53.11 \pm 2.6^{\circ}\text{C}$) and within the Barren Land category ($50.93 \pm 0.49^{\circ}\text{C}$). The mean surface temperatures for North Industrial and South Industrial areas are 48.1 ± 1.57 and $46.67 \pm 1.54^{\circ}\text{C}$, respectively. The cooling influence of vegetation is apparent from the cooler surface temperatures observed in the more vegetated zones of dense trees ($42.8 \pm 1.91^{\circ}\text{C}$) and grasses ($43.86 \pm 2.46^{\circ}\text{C}$).

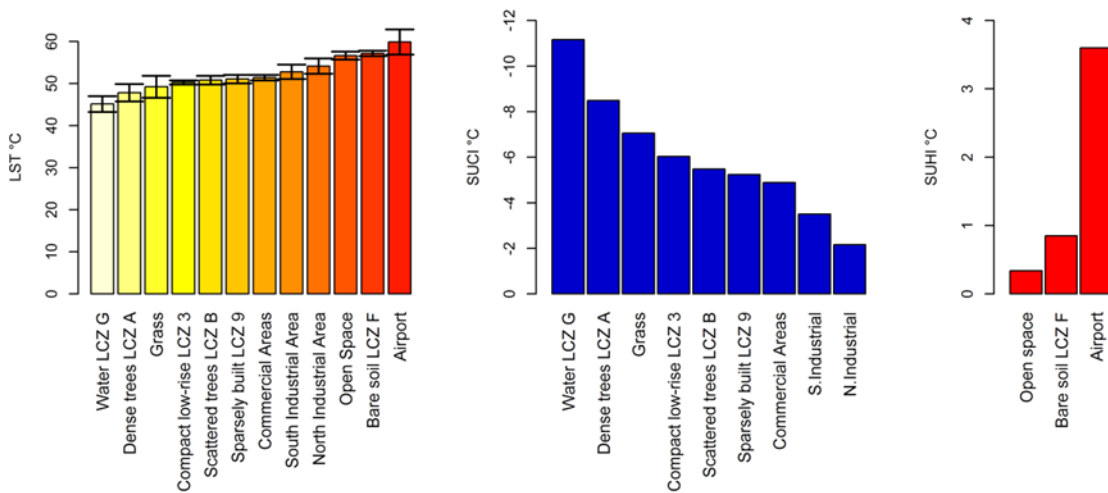


Figure 4.5: Mean LST, SUCI and SUHI in the LULC classes during summer 2013.

4.3.3 Variation of SUCI and SUHI in Selected LULC Classes

The magnitude of the SUHII/SUCII varies considerably between LULC categories (Figure 4.5). Relative warming (compared to the buffer zone) of 3.01°C is associated with the Airport class. Warming was moreover exhibited in the Bare Soil (0.83°C) and Open Area (0.4°C) classes. This warming is due to low soil moisture and limited tree and other plant cover in these areas. In contrast, a surface urban cool island was evident in all other land cover types. The greatest SUCI intensity is -9.88°C ascertained at the artificial lakes within the Sami Abdurrahman Park compared to the mean LST of the buffer of the city at the same time. Green areas experienced a significant decrease of temperature compared to the mean temperature of the city. The

SUCI intensity values of Dense Trees and Grass is -7.3°C and -6.24°C respectively. The main reasons for this variation are the low heat storage capacity and heat losses through evaporation and transpiration processes in the green areas.

4.3.4 Spatial Variation of Wetness, Brightness and Greenness Components

Wetness, brightness and greenness were calculated for the study area using the Tasseled Cap (Baig *et al* 2014). The highest values of wetness were ascertained in the Water and Dense trees classes, while Bare Soil and Open Space experienced the lowest wetness (Figure 4.7). The mean wetness of Water was 54.67 ± 9.84 and the mean wetness of Dense Trees was 47.69 ± 6.2 . However, Bare Soil and Open Space demonstrated values of 7.54 ± 4.4 and 15.09 ± 6.74 , respectively (Figure 4.6). This low wetness and soil moisture in Bare Soil and Open Space is the main reason for the increased LST in the buffer zone and Sparsely Built areas. The Grass and Dense Trees

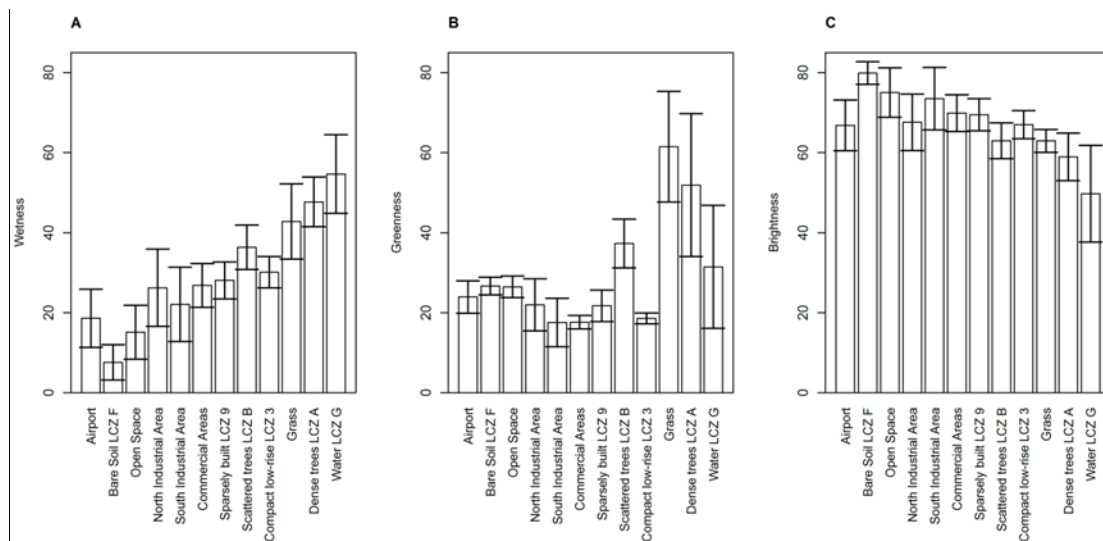


Figure 4.6: Mean wetness, greenness and brightness for each LULC class during summer 2013.

classes demonstrated the highest greenness, meanwhile the South Industrial and Commercial areas experienced the lowest greenness. The greenness of Grass class is 61.51 ± 13.81 while the greenness of Commercial was 17.63 ± 1.69 . In terms of brightness, Bare Soil and Open Space demonstrated the highest brightness while Water and Dense Trees experienced the lowest brightness. Brightness of both Bare Soil and Open Space was calculated to be 79.9 ± 2.84 and 75.05 ± 6.17 , while the brightness of

the Water and High Density Tree classes was 49.74 ± 12.11 and 58.95 ± 5.96 respectively.

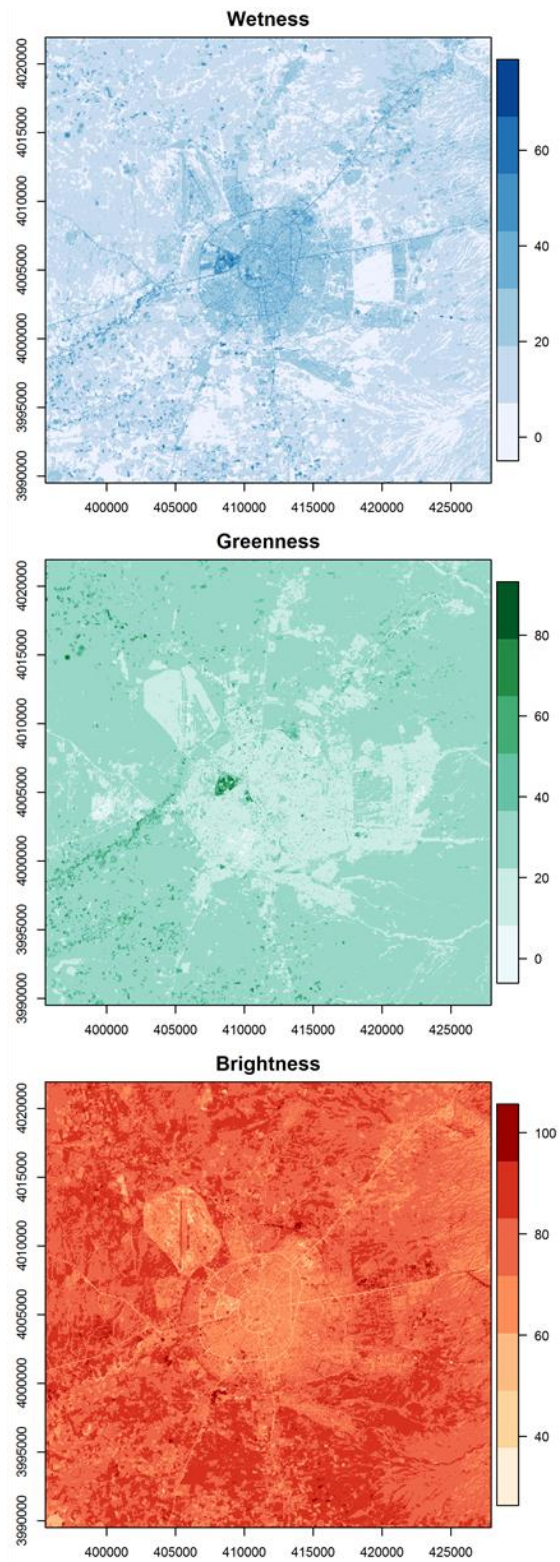


Figure 4.7: Wetness, greenness and brightness of the study area during summer 2013.

The wetness of the city centre is 27.39 ± 8.29 while the buffer is less wet (15.49 ± 6.8). The main factor explaining the decrease of LST in the city is higher soil moisture. In terms of brightness, the buffer of the city is brighter (77.32 ± 6.08) and the mean brightness of the city is 69.14 ± 5.93 . Generally, vegetation in the study area in the summer is low. The mean greenness of the city is 23.23 ± 7.52 and the buffer is more green (28.93 ± 5.29).

4.3.5 Relationship between Land Surface Temperature and Wetness, Brightness and Greenness in Different LULC Classes

4.3.5.1 Surface temperature and wetness

The wetness factor, which refers to the amount of soil moisture, corresponds well with the spatial distribution of surface temperature in the case study area. The relationship between LST and wetness index demonstrates a strong inverse relationship (Figure 4.8, $r^2 = 0.9$, $p < 0.01$). This means that as the wetness index increases the LST will decrease; for instance, in the centre of the city the wetness is 27.39 and the mean LST is 46.21°C , while in the 10 km buffer of the city the wetness decreased to 15.49, and the mean LST increased to 50.08°C .

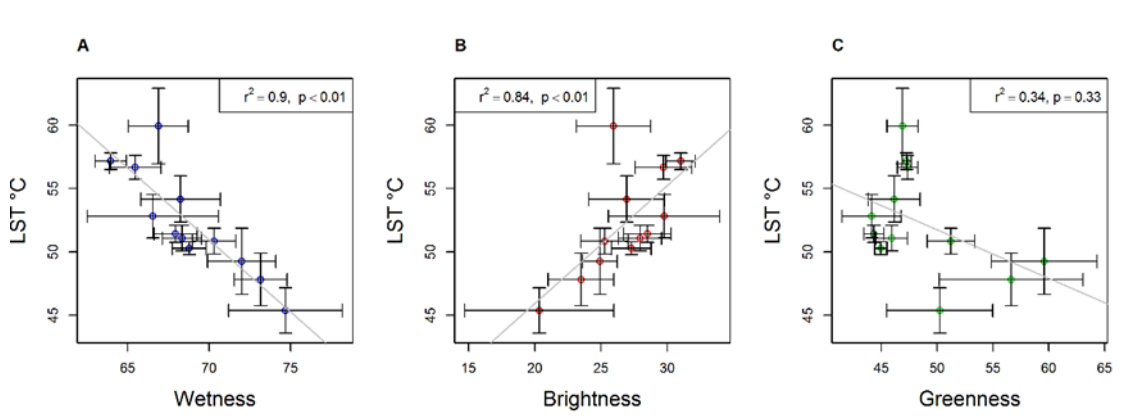


Figure 4.8: Relationship of LST with Wetness, Brightness and Greenness during summer 2013.

Each plot represents a class of LULC.

4.3.5.2 Surface temperature and brightness

The relationship between surface temperature and the Brightness Index for LULC class is a strong positive ($r^2 = 0.84$; $p < 0.01$). For instance, in the buffer zone of

the city, the brightness is 77.32 and the mean surface temperature is 50.08°C. While, in the core of the city the brightness is 69.14 and the surface temperature decreases to 46.21°C.

4.3.5.3 Surface temperature and greenness

Between surface temperature and Greenness Index, a moderate negative relationship was ascertained ($r^2 = 0.34$; $p = 0.33$). The reason for this deficiency of correspondence is the deficiency of vegetation, especially during the dry season, in the study area. However, in general areas of high greenness will exhibit lower surface temperature. In Chapter 5 and 6 the influence of vegetation on LST of Erbil will be assessed in more detail.

4.3.6 Spatial Variation of LST in Districts of the City

Figures 4.9 and 4.10 indicate that in general old districts inside the 60 m street zone recorded low values of temperature. An Urban Cool Island effect is experienced in these areas with the exception of Qalat in the centre of the city, which has a temperature of $47.4 \pm 0.93^\circ\text{C}$. The more modern built-up districts, which contain wide open space areas situated on the outskirts of the city, experienced a high average LST and low SUCI effect, for instance, Zagroz $49.83 \pm 0.9^\circ\text{C}$ in the north east and Sarbasty $48.54 \pm 1.04^\circ\text{C}$ in the west of the city (Figure 4.10).

The highest average LST exists in Zagroz ($49.83 \pm 0.9^\circ\text{C}$) and Tureq ($48.92 \pm 1.16^\circ\text{C}$). While the lowest average LST exists in Sami Abdurrahman Park, Rizgari 1 and Azadi 2, the LST was 43.43 ± 2.06 , 44.32 ± 0.31 and $44.47 \pm 0.44^\circ\text{C}$ for these areas respectively. On the other hand, the mean LST of some districts was normal and close to the average temperature of the city, for instance; Taajeel $46.34 \pm 0.83^\circ\text{C}$ and Rasty $46.29 \pm 1.31^\circ\text{C}$.

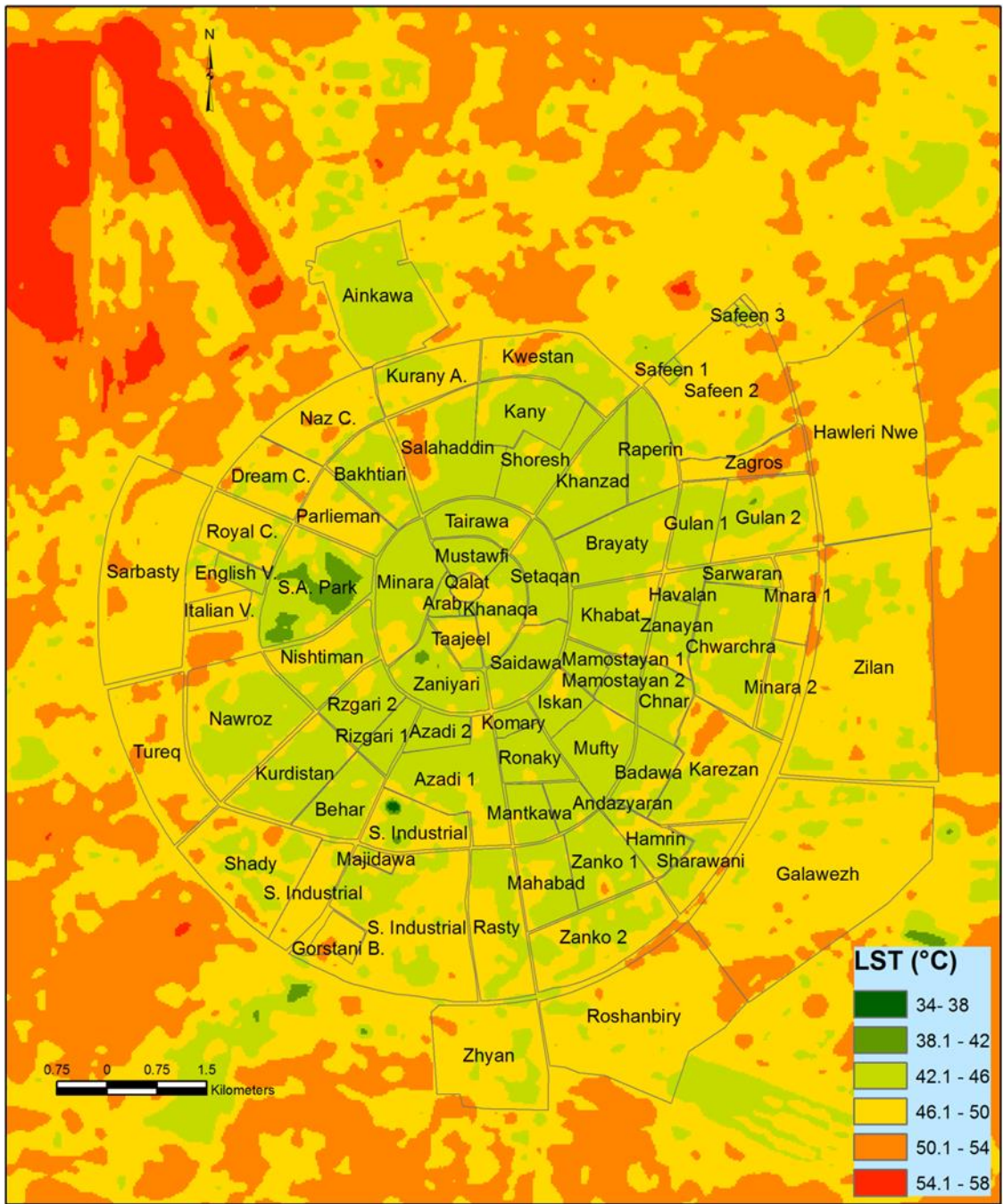


Figure 4.9: LST of the districts of Erbil, at 7:40 during summer 2013, the data derived from composite image created from Landsat TIRS.

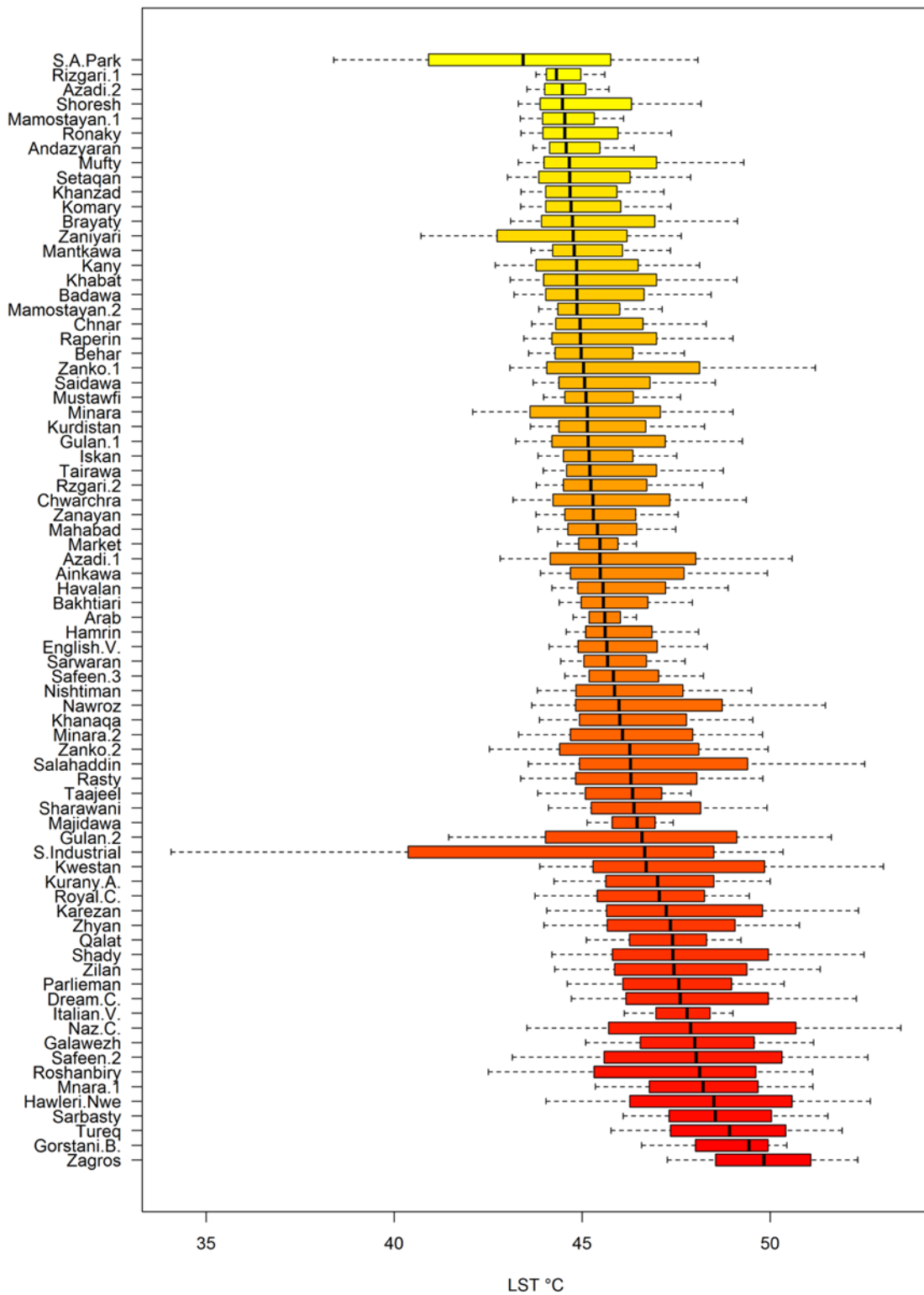


Figure 4.10: LST of districts of Erbil during summer 2013.

4.3.7 Relationship Between LST and Built-up and Vegetation Index

Regression analysis was performed between mean LST and mean NDBI and NDVI index for each district of the city. Figures 4.11 demonstrate the results of these relationships, where each point on a scatter plot represents a district in the city.

The results indicate a weak positive relationship ($r^2 = 0.34$; $p < 0.01$) between mean LST and the NDBI. Meanwhile, a weak (ignored) relationship is found between surface temperature and the NDVI because in summer time only small NDVI exist. For instance, S. M. Park with the highest green index (0.32 NDVI) demonstrated the lowest surface temperature of 43.43°C and Zaniyari with 0.18 NDVI was estimated to be 44.76°C. Due to the seasonality in NDVI, the relationship between LST and NDVI was investigated for each season in Chapter 6.

Table 4-3: Mean NDBI for different LULC class in the study area.

Class	Mean NDBI	SD NDBI
Bare Soil	0.091	0.012
Built-up Area	0.055	0.009
Water Body	-0.061	0.048
Vegetation	-0.102	0.074

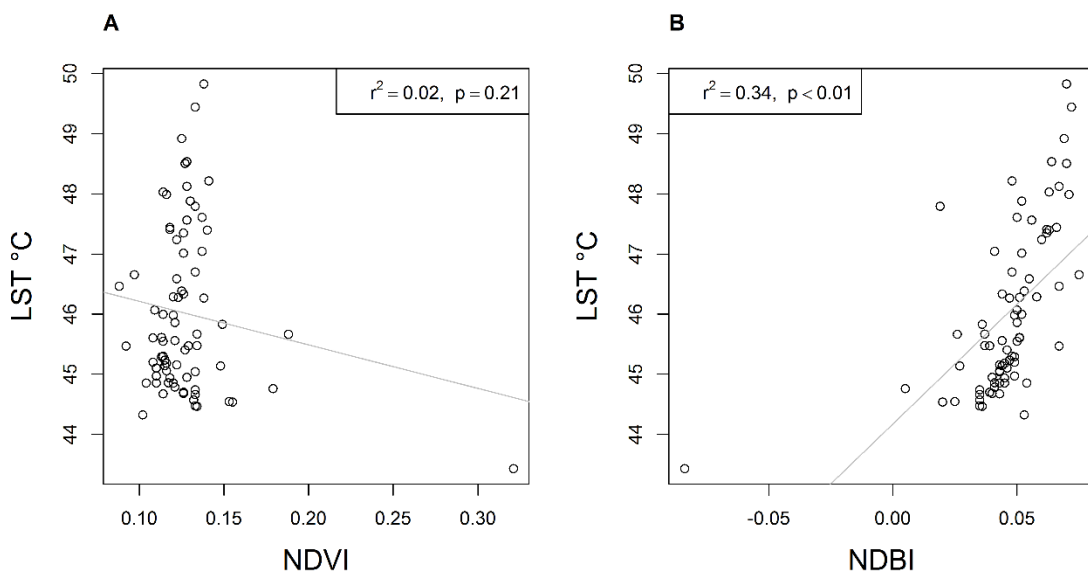


Figure 4.11: Relationship of LST with NDVI and NDBI during summer 2013. Each plot represents districts.

The results presented here demonstrate that the NDBI index is not congruent with the results from previous studies. In the study area, the NDBI index does not have the ability to distinguish well between built-up areas and barren soil. Commonly, high NDBI refers to high built-up and low bare soil. Conversely, in this research, districts with high NDBI corresponding to low built-up density, demonstrated high temperature (Table 4-3). For instance, the NDBI of Galawezh was 0.07 and its LST was 47.99°C. In contrast, Azadi 2 showed 0.04 NDBI and 44.47°C.

4.4 Discussion

In this chapter, the spatial structure of LST and SUCI of Erbil city was determined. The results indicate that during the daytime of summer, especially in the morning, the average surface temperature in built-up areas within the city boundaries is lower than the mean surface temperature in a 10 km non-urban reference zone around the city. The SUCI Intensity of the central districts in the morning (at ~07:40) ranged from -3.5 to -4.6°C. Given the calibration uncertainties this is probably an effect of approximately 4.0°C. The results of this study indicate a daytime SUCI effect which differs in this finding from other published studies of the UHI in humid and densely vegetated regions (e.g. Shahmohamadi *et al*, 2012, Tran *et al*, 2006, Dhorde and Dhorde, 2012). However, results of this research confirm results from previous studies in similar geographical areas which have pointed out the presence of a diurnal SUCI effect in arid or semi-arid climates (e.g. Frey *et al*, 2006, Li *et al*, 2011, Abdullah, 2012).

In the summer, the climate of the city of Erbil is dry and hot. In such dry environments during the daytime, the land surface on the outskirts of the city absorbs more heat than the urban area itself. Since the rural land surface is largely dry and barren in the dry season, it does not have large evaporation and transpiration effects to mitigate the temperature of the soil. Through assessing the relationship between LST and SUCI with WI, GVI, BI and vegetation indices, it was ascertained that a high bareness value is the significant factor corresponding to an increase in LST. It means that increasing bare soil and cropland without vegetation in the dry season leads to increased LST in the day-time. Likewise, the results indicate wetness is the main important factor in determining LST. The results indicate that wetness inside city

borders was higher than rural areas in this season so it leads to decreased LST in built-up areas within the city.

4.5 Summary

Variations between the energy balance of cities and their non-urban surroundings exist due to the modification of surface properties. In temperate and sub-tropical climates, these variations are manifested as the UHI effect. However, in more arid environments, artificial modifications of the environment have the ability to cause urban cooling relative to the surrounding landscape particularly during the dry season. This chapter assessed the spatial formation of the daytime SUCI effect of Erbil, as a case study of cities in semi-arid climates. Six satellite images, acquired by Landsat 8 during the period from 1st July to 19th September 2013, are used to retrieve land surface temperature, identify LULC classes and investigate the spatial variation of LST and the SUCI intensity. In order to ascertain the key drivers of the observed patterns of LST, the relationship with wetness, brightness, bareness, built-up and vegetation index maps were examined. The results indicate that densely built-up areas, such as central districts of the city, green areas and water bodies, had lower LST acting as cool islands, compared to the non-urbanised area around the city. In contrast, the airport, open spaces and new low-density housing developments on the outskirts of the city experienced higher LST and demonstrated an SUHI effect. A strong inverse relationship is evident between surface temperature and Wetness Index ($r^2 = 0.9$; $p < 0.01$). A strong positive correlation ($r^2 = 0.84$; $p < 0.01$) is apparent with the Brightness Index. In contrast, between surface temperature and the Greenness Index a moderate negative relationship was ascertained ($r^2 = 0.34$; $p = 0.33$) for dry season. The results of this chapter demonstrate that during the daytime, residential areas in the city centre recorded an LST of $46.2 \pm 1.74^\circ\text{C}$ while rural areas recorded $50.1 \pm 1.76^\circ\text{C}$. Urban cool island intensity (UCII) of the city in the morning (at ~07:40) ranged from -3.5 to -4.6°C compared to a 10 km buffer zone around the city. This study demonstrates that during the dry season in some cities, such as Erbil, the wetness index is the main determinant of the SUCI effect, and not vegetation cover.

Chapter 5 : The Temporal Variation of Surface Urban Cool and Heat Islands in Erbil

Parts of this chapter have been published with CC-BY copyright license as:
Rasul, A., Balzter, H. and Smith, C. (2016) 'Diurnal and Seasonal Variation of Surface Urban Cool and Heat Islands in the Semi-Arid City of Erbil, Iraq', *Climate*, 4(3), 42.

5.1 Introduction and Rationale

Since land surface temperature moderates the lowest layer of the atmosphere it plays an important role in the evolution of the urban climate. The comfort and health of urban residents is affected by surface temperature, which can influence internal building temperatures and energy exchange processes (Voogt and Oke, 2003). The variation between the characteristics of surface cover in urban and rural areas, in terms of 3-dimensional geometry of the built environment, heat absorption, construction materials, surface albedo and vegetation abundance cause different air and surface temperatures in a city relative to the surrounding, less urbanised area.

Lazzarini *et al* (2013) studied the daytime SUHI and LST variation in Abu Dhabi using MODIS surface temperature data. Their results indicate the existence of a daytime SUCI, in contrast to the common nocturnal SUHI. The higher apparent soil moisture within the urban area in an arid environment compared to the dry, bare surroundings has an effect on the thermal environment as a result of evaporation from the soil which reduces LST via latent heat flux cooling. Lazzarini *et al*'s study established the presence of a SUCI in Dubai compared with the surrounding desert. Both residential districts and industrial areas within arid environments recorded lower temperatures than sand (Frey *et al*, 2005).

In the previous chapter, Landsat 8 has been used for studying the spatial variation of daytime SUCI during the dry season in Erbil. The results indicated that densely built-up areas had lower LST acting as cool islands, compared to the non-urbanised area around the city. The study demonstrated that during the dry season in some cities, such as Erbil, the surface wetness is the main indicator of the SUCI effect. The current chapter extends these earlier findings to assess seasonal, interannual and diurnal patterns of LST and the SUCI/SUHI effects in Erbil.

Optimum growing temperatures imply that there is a temperature effect on vegetation whereas vegetation also influences ambient air temperature via

evapotranspiration processes. Consequently, there is a correlation between vegetation and temperature. In UHI studies, the correlation between NDVI and LST has been applied widely (Weng *et al*, 2004; Sun and Kafatos, 2007; Weng and Lu, 2008; Schwarz *et al*, 2012). Liang and Shi (2009) and Bajaj *et al* (2012) confirmed the existence of a strong linear inverse relationship. In contrast, there was no such relationship in Shanghai, China (Zhang *et al*, 2008). This disparity may relate to seasonal variations. Therefore, this chapter assess this relationship for each season based on multi MODIS images during 12 years. The long record of data, the relatively high temporal resolution of MODIS data (e.g. 1 to 2 days and four overpass times) and its free availability make it to be appropriate for studying the temporal variation of SUHI/SUHI (e.g. diurnal and seasonal).

It is noticeable that a few studies on the SUCI and SUHI effect have been published for arid and semi-arid climate regions. The nature and determinants of the Urban Cool Island effect require greater comprehension (Li *et al*, 2011), in particular a more rigorous quantification and comprehension of the SUCI/SUHI in semi-arid climates is necessary.

This chapter investigated and assessed the temporal variation of LST and SUCI/SUHI in the city from MODIS Aqua and Terra. Then, it established a main determinant, the relationship between LST and NDVI, soil moisture, evapotranspiration, latent heat flux and air temperature has also been examined. Due to the seasonality in NDVI, the relationship between LST and NDVI was investigated for each season.

5.2 Data and Methodology

In this section, the MODIS products that were used in this chapter are presented. It includes a description of the processing for LST, NDVI, ET, Latent Heat Flux (LE), and estimates of soil moisture constraint.

5.2.1. Data

In this chapter, the MODIS sensor data on board NASA's Terra and Aqua satellites are used. The resolution of LST data from MODIS is quite coarse at 1 km but because it has four overpasses per day, it is better suited for investigating the diurnal variation of LST and the long-term UHI effect than higher resolution sensors such as

Landsat 8. Using MODIS Aqua (MYD11A2) and MODIS Terra (MOD11A2), an 8 day composite for a 12 year period was selected, from January 2003 to December 2014. Several categories of MODIS products from years 2003 to 2014 are used: 16 days composite of NDVI (MOD13Q1), and 8 days composite of ET and LE (MOD16A2) (Table 5-1).

Table 5-1: Summary of MODIS image products used in Chapter 5.

Dataset	Resolution m	Product
MOD11A2	1000	LST
MYD11A2	1000	LST
MOD16A2	1000	ET and LE
MOD13Q1	250	NDVI

Data source: (ORNL DAAC, 2015)

5.2.1.1 Land Surface Temperature

The Land Surface Temperature is the radiative temperature of the land surface (Ghent *et al*, 2010). It is influenced by the albedo, the vegetation cover and the soil moisture (Copernicus, 2016). The “surface” is anything seen from space at the ground: snow and ice, the grass, or the roof of a building (NASA, 2016a). Near surface air temperature “is a measurement of the average kinetic energy of the air near the surface of the Earth” (NASA, 2016b). Usually LST is measured by remote sensing whereas air temperature is measured 1-2 m above the ground. Near surface air temperature is a consequence of complex effects of the turbulent heat transports produced by nearby heated surfaces (Unger *et al*, 2009).

An 8 day composite product with quality assessment (QA) information from both Terra (MOD11A2) and Aqua (MYD11A2) was employed in this investigation. These products were derived from the split-window method (Wan and Dozier, 1996). Only LST images with 80% or higher accuracy (i.e. pixels passed quality filter) are used and low accuracy images are excluded. However, the exclusion of images leaves a gap in the time series which requires gap filling by interpolation, hence it appears somewhat anomalous in 2008 (Figure 5.2). Pixels with zero values that represent Not Available

(NA) value are ignored in the statistical analysis. Terra passes over the study area at approximately 11:00 and 22:00 local time, while Aqua images are recorded around 02:00 and 13:00 local time. The advantage of MODIS is that the overpass times for the study area covers the late morning (11:00) provides additional information on the ones covered by Landsat (~ 8:00 am). The pass of 13:00 (nearly at the maximum of LST) provides information on how LST variation between the urban and rural areas during the time of maximum LST. It also comprises around 22:00 and midnight. The disadvantages of the MODIS overpass time for the study area is that they do not include before and after sunrise and sunset for assessing the highest SUHI at night and estimating the time of turn from daytime SUCI to night-time SUHI.

5.2.1.2 NDVI

MOD13Q1 is a product from MODIS Terra, which contains a 16-day composite NDVI index with 250 m spatial resolution and QA information. 274 MOD13Q1 collection five images from January 2003 to December 2014, were obtained for this study. 251 NDVI images with 80% or higher accuracy (i.e. pixels passed quality filter) from the quality assurance file are used and lower accuracy images are excluded.

5.2.1.3 ET and LE

MOD16A2 is a product from MODIS Terra 8 day composite, which contains Evapotranspiration and Latent Heat Flux data with a 1 km spatial resolution and quality assurance (QA) information. This product is generated using the Mu *et al* (2011) improved ET algorithm. This algorithm considers the surface energy partitioning process and atmospheric drivers of ET (Jang *et al*, 2013).

5.2.2 Methodology

5.2.2.1 Processing data

MODIS products were downloaded from daac.ornl.gov using the WGS 84 ellipsoid model in UTM projection (zone 38N) associated with quality assessment data for each image. MODIS images were processed with the Raster Package in R (R Core Team, 2014). The value of each pixel was multiplied by the scale factors $k_{LST}=0.02$,

$k_{NDVI}=0.0001$, $k_{ET}=0.1$ and $k_{LE}=0.0001$ (Wan, 2007; Solano *et al*, 2010; Mu *et al*, 2011). Anomalous ET pixel values greater than 32,700 were masked out in ENVI (Mu, 2005). In addition, LST values were converted from Kelvin to degrees Celsius. All spatial data were stacked and cropped to the study area. Statistics for subsets of the study area, stratified by the city and surrounding area were extracted and the timeSeries package (Wuertz and Chalabi, 2009) in R was used for processing the data to categorise the images into different seasons and to fill gaps by the linear interpolation method.

5.2.2.2 LST

For determining the seasonal variation, the images are categorised into four seasons based on the astronomical seasons of Erbil. Winter was defined between 22 December and 20 March, spring from 21 March to 20 June, summer from 21 June to 22 September and autumn from 23 September to 21 December. Subsequently the average of the LST and the standard deviation for 12 years for both the urban and the rural areas were calculated and displayed as a line graph. The significance of the regression model was tested with Welsh's t-test. In determining the interannual variation of LST over the 12 years, the focus is on the overall trend line of LST/SUCI/SUHI to display how LST was affected by continuous urbanisation and LULC change in the study area.

5.2.2.3 NDVI

Due to the amount of vegetation varying according to the season and the amount of precipitation, the relationship between LST and NDVI has a seasonal dependency. The NDVI MODIS data for 12 years is divided into the four seasons. Then NDVI and LST data are displayed as scatterplots with the R package ggplot2 (Wickham, 2009) and the linear regression is used to quantify this relationship.

5.2.2.4 Soil Moisture Constraint

Soil moisture is one of the main drivers of LST especially in dry climates. Yao *et al*'s (2013) algorithm to estimate Fractional Soil Moisture constraint (fsm) from land surface temperature of MODIS satellite data was applied:

$$fsm = \left(\frac{1}{DT}\right)^{DT/DT_{max}} \quad (5.1)$$

where DT is the diurnal temperature range ($LST_{\text{day}} - LST_{\text{night}}$ or $T_{\text{max}} - T_{\text{min}}$), DT_{max} is the maximum diurnal temperature (constant: 60°C). The fsm is scaled between zero and one.

5.2.2.5 Identification of the surface UCI and UHI Intensity

There are different methods of measuring UHI. Here a 10 km buffer zone surrounding the city of Erbil is selected as a ‘rural’ (non-urban) reference area. The city limit used to define urban areas and the shapefile of the city was created in ArcGIS based on high-resolution satellite imagery. Heterogeneity is one feature of the urban scene and it is difficult to have one km^2 of the same surface. It could be better to resample 1 km size of MODIS LST product to 30m, the same size of resampled Landsat thermal bands, to limit the number of mixed pixels and make Landsat and MODIS data comparable. MODIS images were resampled to a 30 m spatial resolution based on the nearest neighbour method. The easiness and preservation of original values are the advantages of this approach while its limitation is noticeable position errors (Baboo and Devi, 2010). The city boundary delimits predominantly urban areas, which contain some pixels of other LULC classes while the buffer principally represents rural areas (section 4.2.3). The intensity of SUCI and SUHI is calculated using Eq. (4.4) (Oke, 1987).

5.2.2.6 The variation between urban and rural areas

The means and standard deviations of LST, NDVI, fsm, ET and LE were calculated for both the city and rural areas. The 12-year time-series was gap-filled with linear interpolation and smoothing in R using the Kalman smoothing approach. The percentage of low quality LST images (i.e. pixels not passed quality filter) was low at night (Terra 2.5% and Aqua 2.4%) whilst it was higher for daytime data (Terra 12% and Aqua 20%). Overall, 2008 high quality MODIS LST images (538 Terra night, 538 Aqua night, 486 Terra day and 442 Aqua day) are used in this study.

5.2.2.7 Relationship of LST with NDVI, fsm, ET, LE and air temperature

The relationships between LST and the various influencing factors are presented as scatterplots. In addition linear relationship between pairs of parameters was

calculated. The significance of the regression model was tested using the Welch method.

5.3 Results

5.3.1 Diurnal Variation of LST and SUCI/SUHI

There is considerable variation of LST and SUCI/SUHI between the city and rural areas due to the variation of heat absorption and radiation during the day and night, respectively. Figure 5.1 and 5.2 indicate that generally during the day the city experiences a SUCI effect. In terms of average 12 years of LST, the magnitude of the SUCI intensity tends to be greatest ($-1.78 \pm 1.68^{\circ}\text{C}$) in the morning (11:00) although there is some seasonal variation. However, at night the situation is reversed and LST in the city is higher than the rural surroundings and a SUHI is experienced. The SUHI intensity attains its highest value, around $2.67 \pm 0.72^{\circ}\text{C}$, in the early night (~22:00 pass); this drops off during the late night. In terms of the most extreme SUCI and SUHI during these 12 years, in the morning (11:00) SUCI was -5.37°C , and in the afternoon it was -5.32°C . The highest SUHI of early night was 4.59°C and it was 4.28°C in the late night.

Figure 5.3 demonstrates the variation between the average LST and SUCI/SUHI over all seasons between the city of Erbil and the rural surroundings for the four overpass times of the MODIS satellite during 2014. At ~ 11:00, the LST of the city was $30.92 \pm 0.98^{\circ}\text{C}$, whilst the LST of the rural area was $32.44 \pm 1.46^{\circ}\text{C}$. The city experienced a daytime SUCI averaging -1.5°C , decreasing to -1.2°C by the afternoon. In contrast, at night, the surface of the rural environment radiates the heat more rapidly than the surface of the city. Consequently, the average LST of the city in 2014 at ~22:00 was $17.86 \pm 1.12^{\circ}\text{C}$ whilst in the rural area it was $14.6^{\circ}\text{C} \pm 1.09^{\circ}\text{C}$. The SUHI intensity was 3.3°C , decreasing to 3.1°C by ~02:00.

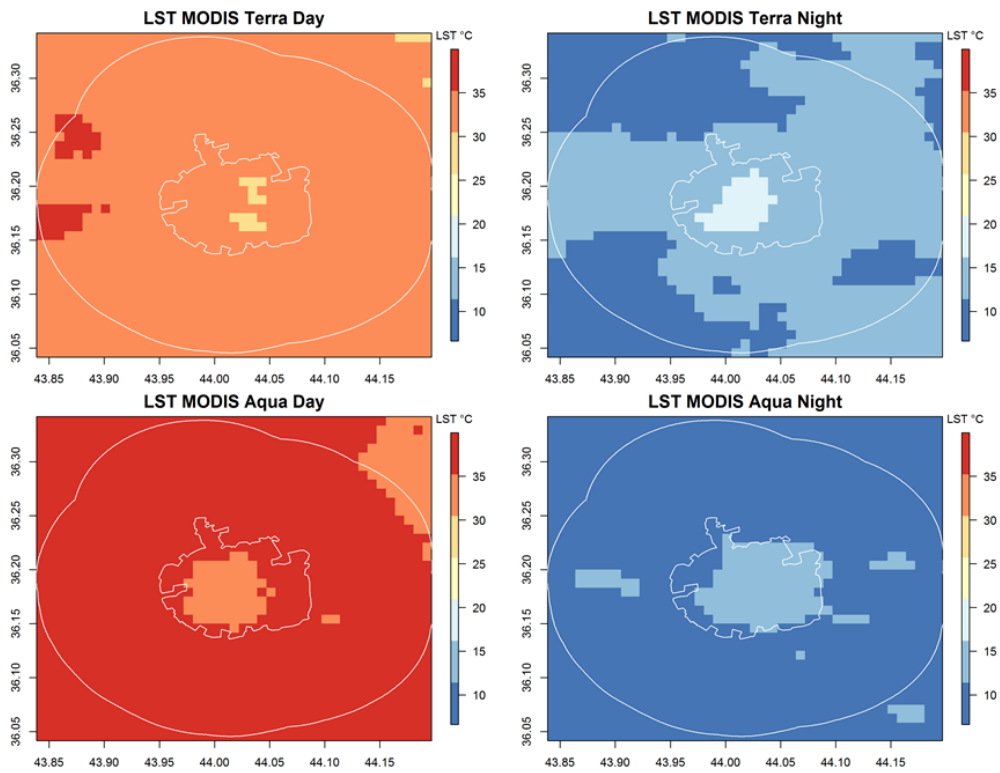


Figure 5.1: Average Land Surface Temperature of the city and the rural areas from MODIS Terra and Aqua for both day and night-time passes over 12 years from 2003 to 2014. The data is at 1 km resolution (without resample).

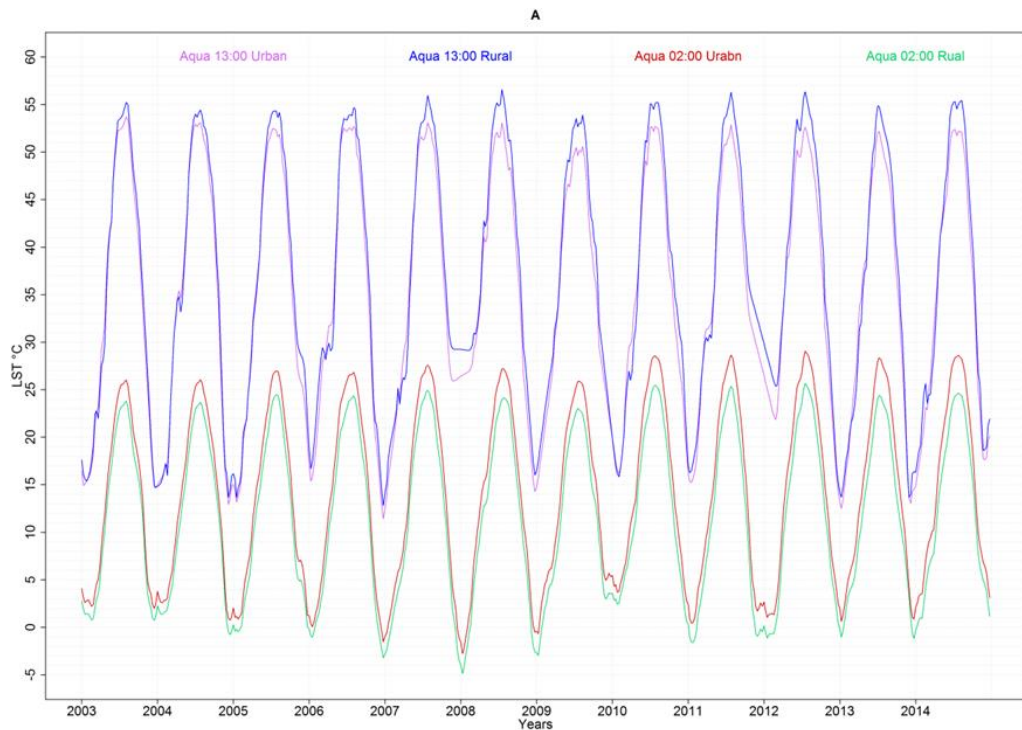


Figure 5.2: Average Land Surface Temperature of the city and the rural areas from MODIS Aqua for both day and night-time passes over 12 years from 2003 to 2014. The exclusion of bad images leaves a gap in the time series and it appears somewhat anomalous in 2008 and 2012.

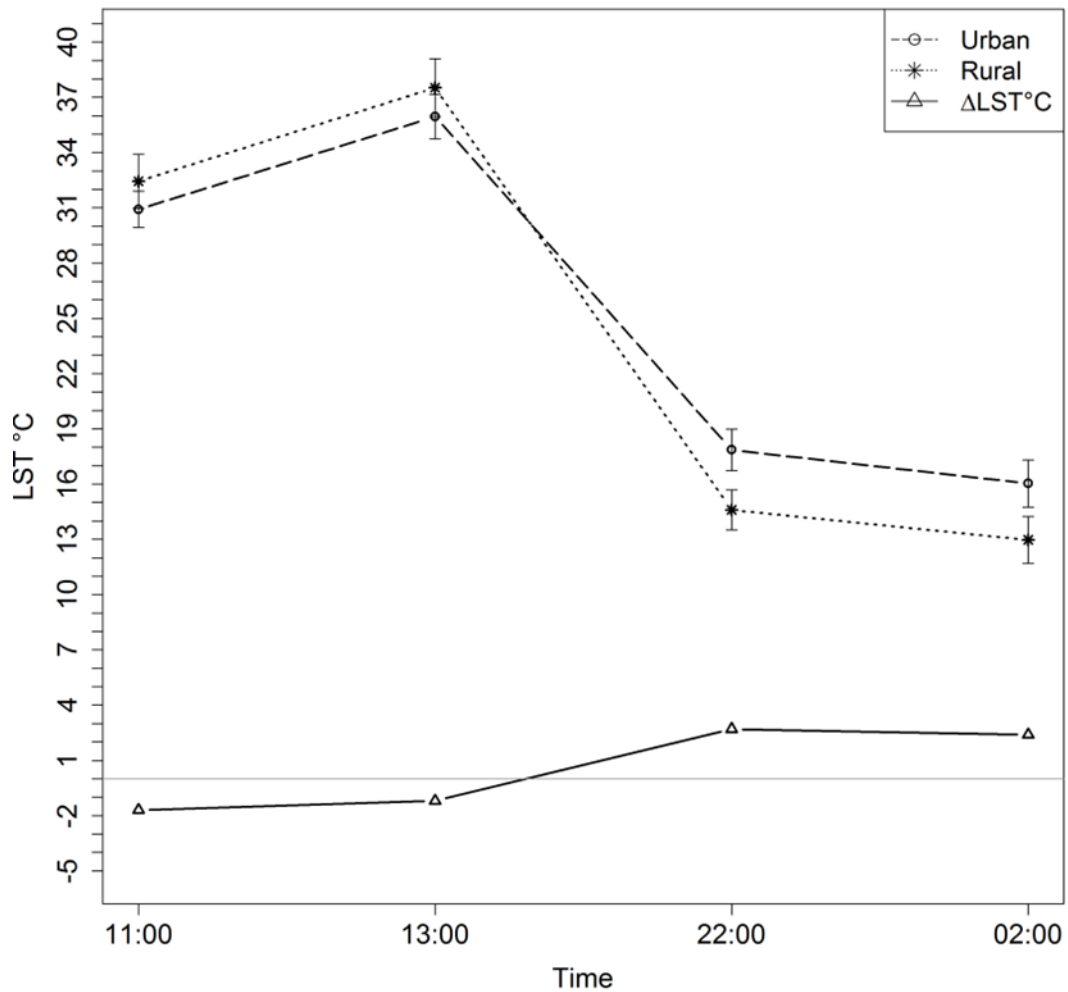


Figure 5.3: Diurnal variation of average 2014 Land Surface Temperature and Surface Urban Cool Island/ Surface Urban Heat Island during the day and night.

5.3.2 Seasonal Variation of LST and SUCI/SUHI

The city exhibits a night-time SUHI with varying intensity depending on the season (Figures 5.4, 5.5 and 5.6). In the spring and summer, the intensity of the SUHI in the study area is higher than during autumn and winter. In contrast, the intensity of the daytime SUCI (negative SUHI) is higher in autumn and summer; the incidence of a daytime SUCI decreases in winter and spring. Spring is the growing season for grasses and crops in the rural area which cools the local environment via reduced heat absorption and greater evapotranspiration and latent heat flux during this season.

In autumn, during the daytime, LST in the rural area is higher than the LST of Erbil and it exhibits a SUCI. In contrast, at night the urban areas experienced a SUHI.

In spring during the daytime, the city typically exhibited a low magnitude of SUCI (at ~13:00 the SUCI was $-0.05 \pm 0.64^{\circ}\text{C}$). During the night-time SUHI was $2.82^{\circ}\text{C} \pm 1.05$. In summer, the average of LST in the city at ~11:00 is $46.98 \pm 1.43^{\circ}\text{C}$ and the LST of the rural area is $49.76 \pm 1.30^{\circ}\text{C}$ (Table 5-2). This means that the SUCI intensity in the city is -2.78°C at 11:00, whilst during the night-time the city exhibits a SUHI with intensity 3.05°C . This is particularly problematic from a public health perspective.

Table 5-2: Diurnal variation of average Land Surface Temperature and Δ LST in different seasons over 12 years from Aqua and Terra MODIS.

Season	Time	Mean LST $^{\circ}\text{C}$ city	SD $^{\circ}\text{C}$	Mean LST $^{\circ}\text{C}$ rural	SD $^{\circ}\text{C}$	Δ LST $^{\circ}\text{C}$
autumn	11:00	33.5	1.38	36.45	1.16	-2.95
	13:00	32.2	1.73	34.59	0.94	-2.39
	22:00	12.15	1.18	9.69	0.69	2.46
	02:00	10.56	1.29	8.25	1	2.31
winter	11:00	15.62	0.46	16.61	0.64	-1.00
	13:00	20.41	0.83	21.18	0.83	-0.77
	22:00	5.1	1.11	2.9	0.48	2.21
	02:00	3.11	1.02	1.25	0.59	1.87
spring	11:00	35.1	1.43	36.58	0.97	-1.47
	13:00	39.44	0.48	39.49	0.8	-0.05
	22:00	18.93	1.37	16.11	0.72	2.82
	02:00	16.58	1.43	13.99	0.97	2.59
summer	11:00	46.98	1.43	49.76	1.3	-2.78
	13:00	50.36	1.35	52.84	1.01	-2.48
	22:00	28.41	1.27	25.36	1	3.05
	02:00	25.71	1.51	22.73	1.19	2.98

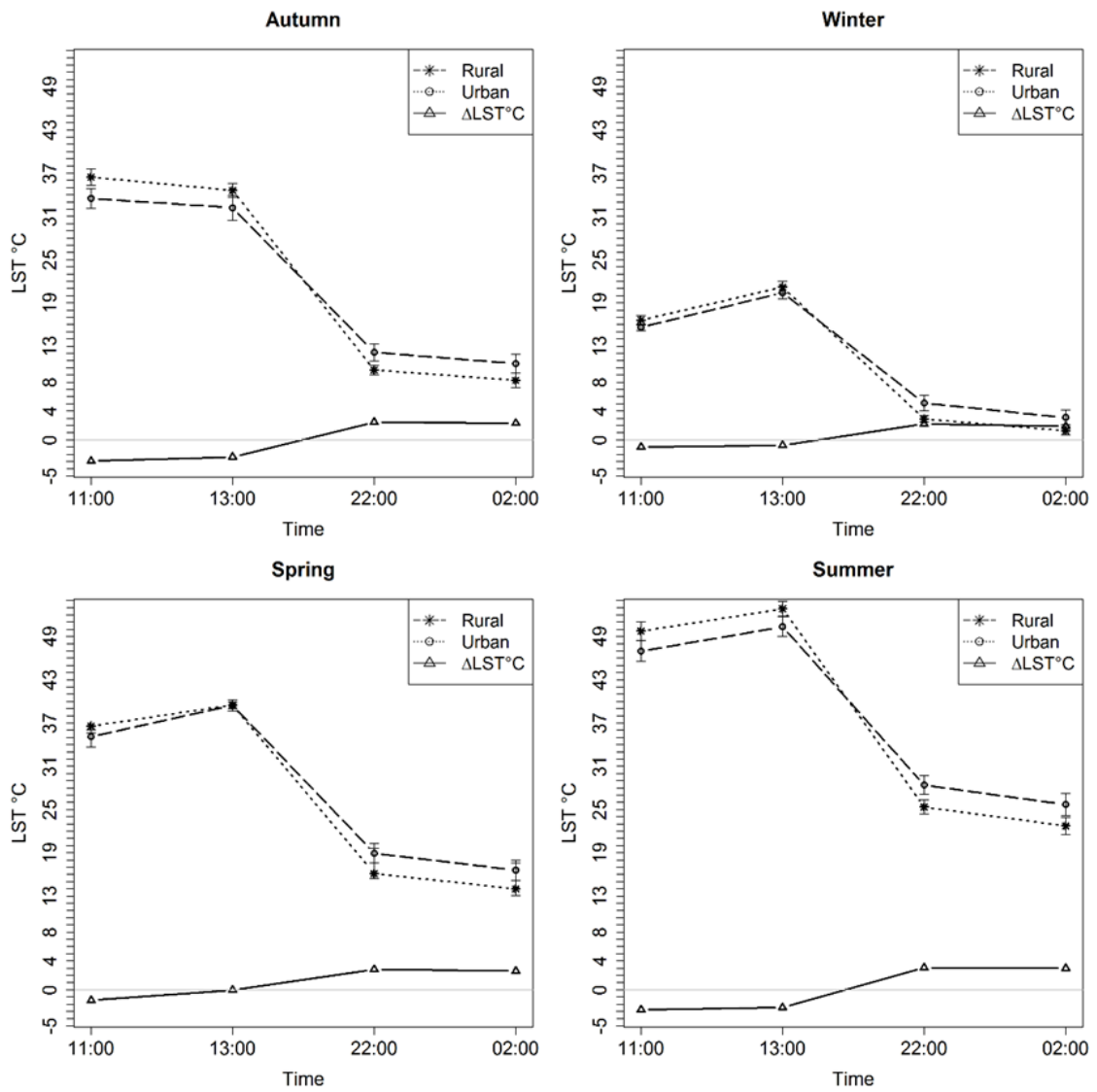


Figure 5.4: Diurnal variation of average Land Surface Temperature in different seasons over 12 years from Aqua and Terra MODIS and Surface Urban Cool Island / Surface Urban Heat Island.

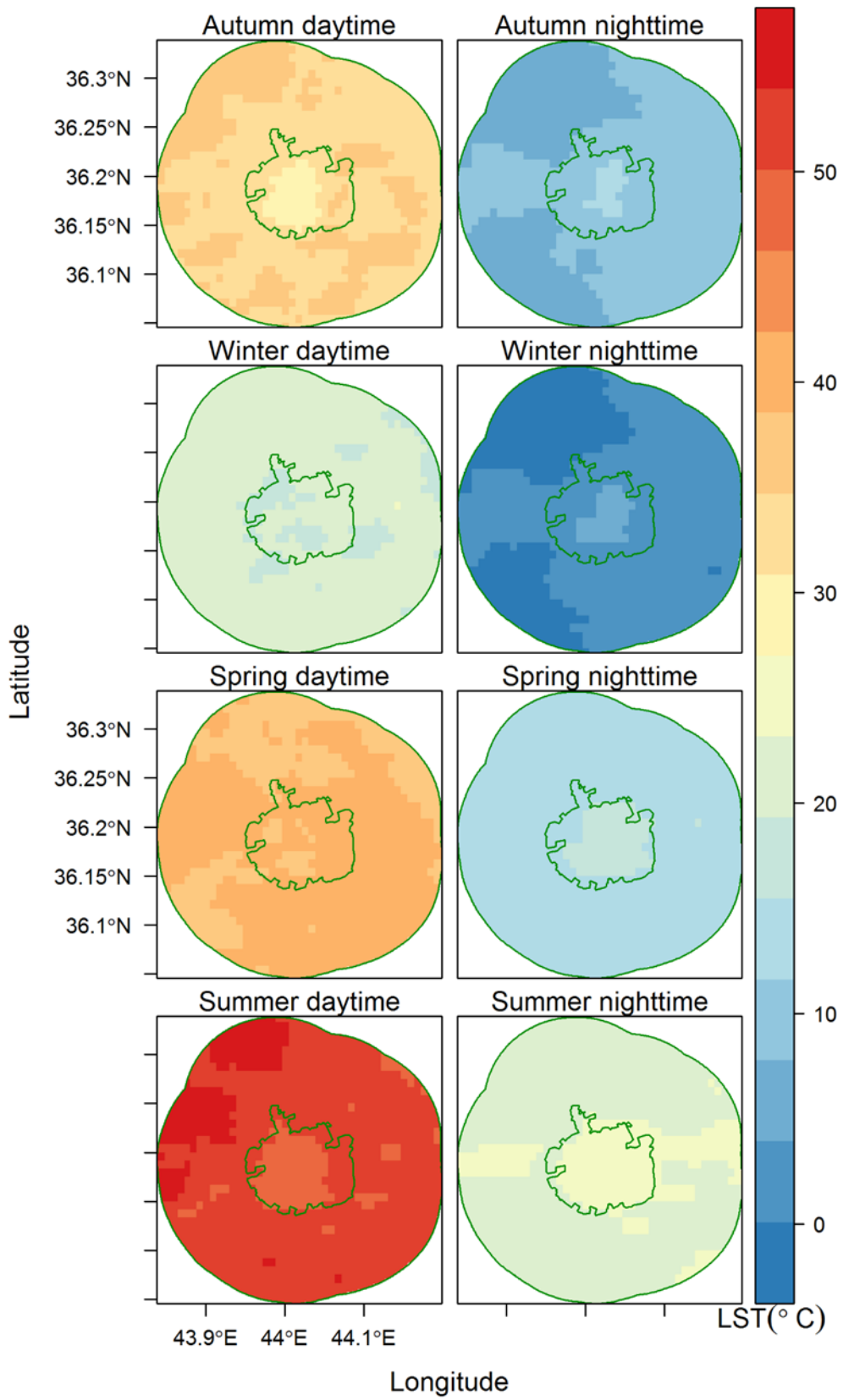


Figure 5.5: Seasonal variation of average Land Surface Temperature over 12 years, based on MODIS Aqua, the green line is the boundary of Erbil city.

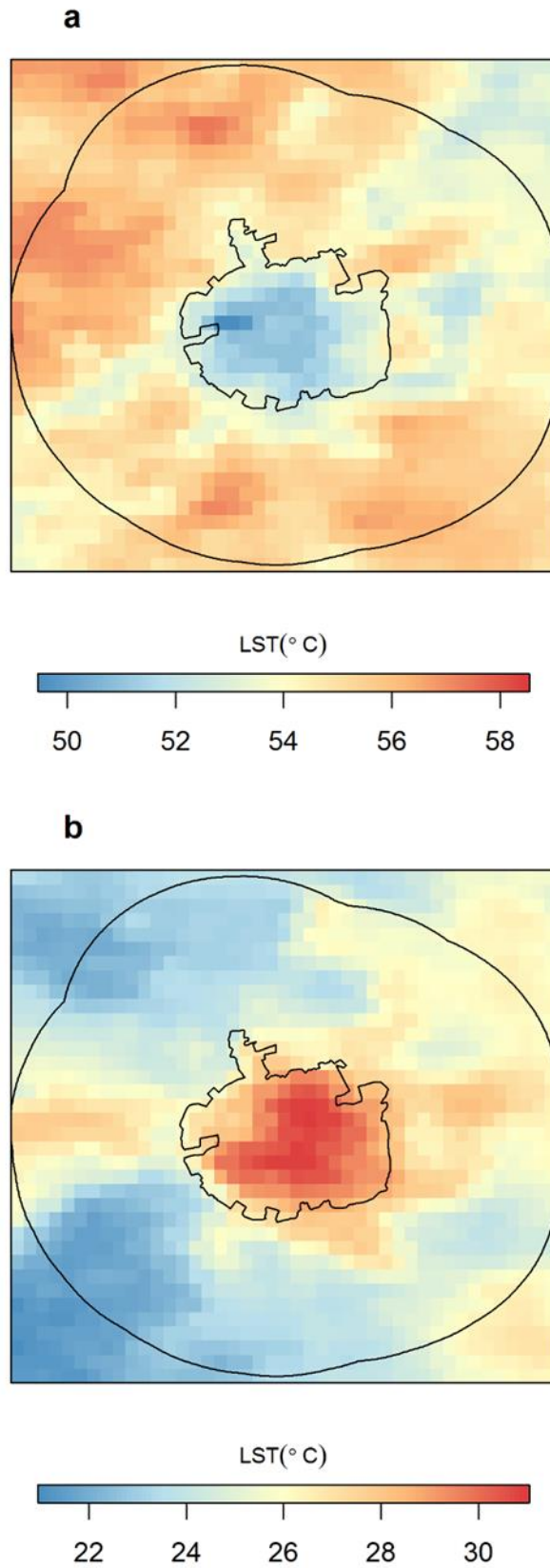


Figure 5.6: LST of the study area from MODIS Aqua 8 day composite image (A2014209) 28th July 2014. a: is daytime (SUCI) and b: is nighttime (SUHI).

5.3.3 Interannual Variation of LST and SUCI/SUHI

There is an overall increasing trend in daytime SUCI and night-time SUHI between 2003 and 2014. The slope of SUCI and SUHI per year is 0.06 and 0.1°C, respectively (Figure 5.7). The daytime SUCI trend displays significant interannual variation, the night-time SUHI fluctuates less compared to the daytime and the trend demonstrates an increase from ~ 2°C in 2003 to around 3°C in 2014.

The SUCI intensity at ~11:00 in 2003 and 2004 demonstrated the lowest intensity (−0.93 and −0.97°C respectively). However, in 2008 and 2009 the highest intensities of −2.37 and −2.2°C were recorded, respectively. During these 12 years, SUCI intensity increased at ~11:00 by 0.72°C ($p = 0.12$) and at ~13:00 by 0.85°C ($p = 0.08$). On the other hand, in 2003 and 2004, the SUHI intensity at 22:00 was 1.99 and 2.15 °C, respectively, while in 2014 it increased to 3.26°C. The trend of time series data indicates during these 12 years that night–time SUHI intensity increased significantly by 1.12 to 1.22°C ($p < 0.01$).

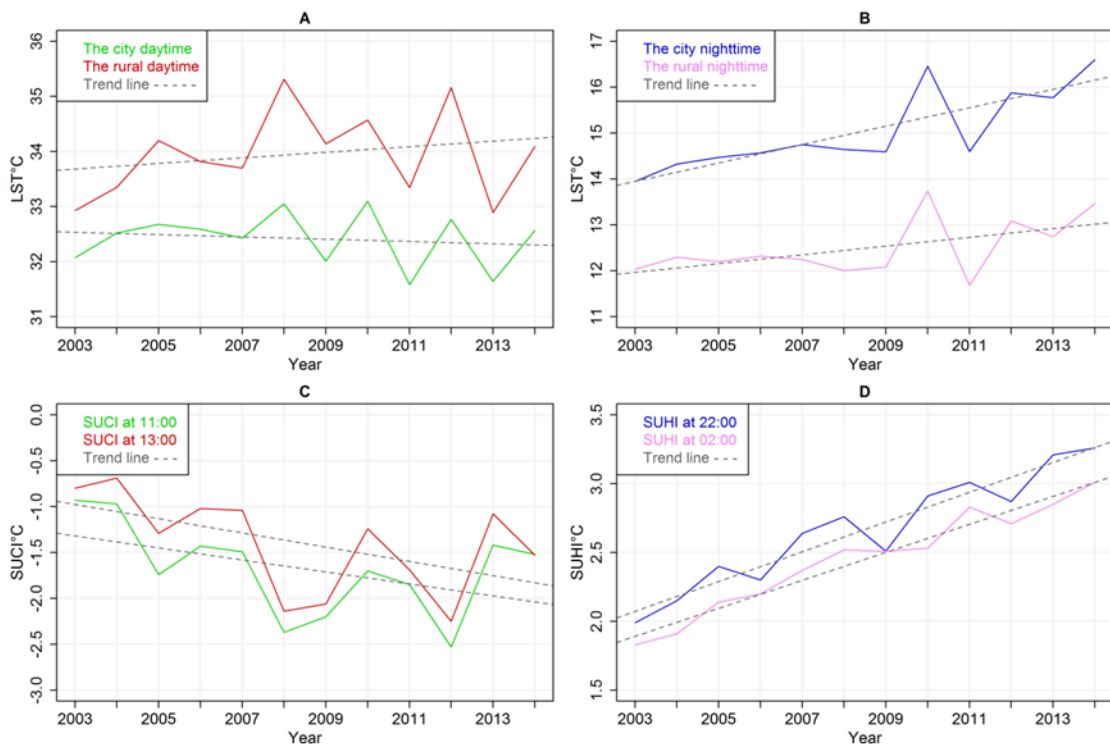


Figure 5.7: Annual variations of Land Surface Temperature and Surface Urban Cool Island / Surface Urban Heat Island from 2003 to 2014.

5.3.4 Key Determinants of LST

5.3.4.1 NDVI

In general, during the last 12 years the NDVI of the rural area was higher than the NDVI of Erbil. The average NDVI of the rural area was 0.22 ± 0.11 whereas the average NDVI of the city was 0.16 ± 0.05 (Figure 5.8, Table 5-3). Since vegetation in the study area is strongly dependent upon precipitation, the value of NDVI varies between years depending on the amount of rain. The peak NDVI value was recorded in 2003 when it was 0.57 in the rural area and 0.37 in the city. The total precipitation in that year was high (496.3 mm) compared to the annual average (386.2 mm). The lowest values of NDVI (0.12 ± 0.02) coincided with reduced precipitation in 2008 (297.5 mm). Moreover, the value of NDVI demonstrates seasonal variation. High values (0.31 ± 0.07 in the rural and 0.19 ± 0.05 in the city) occur in spring when precipitation is high and temperatures start to increase. In contrast, during the dry season (summer) the seasonal average of NDVI dropped to the lowest value with 0.14 ± 0.01 in the rural area and 0.13 ± 0.01 in the city.

Table 5-3: Min, max and mean of NDVI, fsm, LE and ET of Erbil city and rural area from 12 years MODIS data.

Parameter	Min (city)	Max (city)	Mean (city)	SD	Min (rural)	Max (rural)	Mean (rural)	SD
NDVI	0.1	0.37	0.16	0.05	0.11	0.57	0.22	0.11
fsm	0.18	0.77	0.35	0.11	0.12	0.82	0.27	0.11
LE ($\text{J m}^{-2} \text{ day}^{-1}$)	0	0.06	0.0067	0.0076	0	0.139	0.0085	0.0095
ET (mm)	0	19.5	2.19	2.44	0	45.4	2.76	3.1

5.3.4.2 Soil moisture constraint

In general, the fsm in the city is higher than the rural surroundings and it displays annual and seasonal variation. The average fsm in the city during 2003 to 2014 was 0.35 ± 0.11 and it was 0.27 ± 0.11 in the rural area (Figure 5.8, Table 5-3). The peak fsm of the city was 0.77 in December 2013 and the lowest value was 0.18 in June 2006.

Moreover, the highest value of the rural area was 0.82 in December 2013 and the lowest value (0.12) was recorded in June 2006. In general, fsm is high in the winter and autumn when it is between 0.4 to 0.7, while in the summer it reduced to between 0.1 and 0.3.

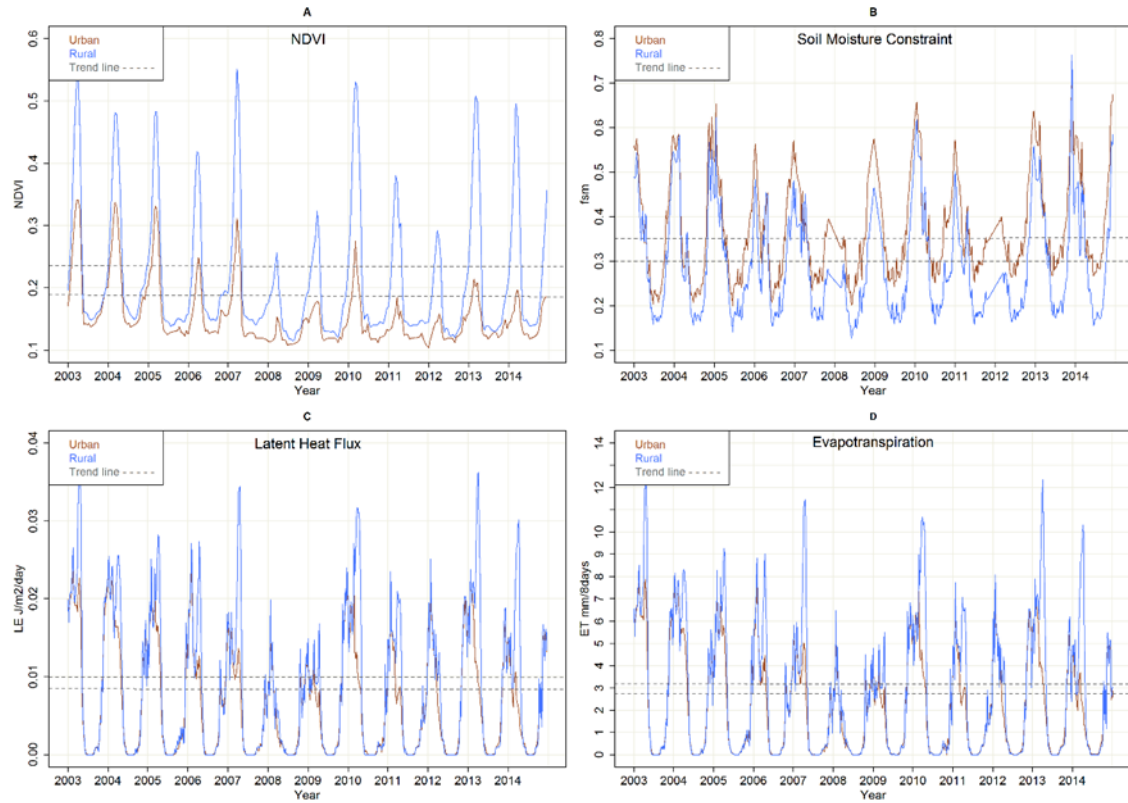


Figure 5.8: NDVI, Soil Moisture Constraint, Evapotranspiration and Latent Heat Flux in the city and rural area from 2003 to 2014.

5.3.4.3 Evapotranspiration

In general, unexpectedly, ET in the city is lower than in the rural area. The average of ET in the city is 2.19 ± 2.44 mm/8 days and 2.76 ± 3.1 mm/8 days in the 10 km surrounding rural area ($p < 0.01$). During the wet season, it is higher than in the drier season. The highest ET was in 2013 and the lowest one was in 2009.

5.3.4.4 Latent Heat Flux

In general, LE in the rural area is higher than in the city. The average of 12 years of LE in the city is 0.0067 ± 0.0076 ($\text{J m}^{-2} \text{ day}^{-1}$) and 0.0085 ± 0.0095 ($\text{J m}^{-2} \text{ day}^{-1}$) in

the rural area. The highest magnitude of LE was in 2003 and the lowest LE was in 2009.

5.3.5 Relationship Between LST and NDVI, fsm, ET and LE

Linear regression analysis was performed between mean LST and mean NDVI, fsm, Evapotranspiration and Latent Heat Flux. Figure 5.9 demonstrates the results of these relationships, where each point in a scatterplot represents an average of composite images of MODIS from 2003 to 2014.

The results indicate a weak (significant) inverse relationship ($r^2 = 0.18$; $p < 0.01$) between surface temperature and the NDVI (Figure 5.9). NDVI data in Figure 5.9 consists of 12 years NDVI for all seasons. As a result of seasonal vegetation phenology, the relationship of LST with NDVI is diverse for different seasons. The relationship converts to a positive relationship in the winter, as demonstrated in Figure 5.10. However, in general, areas of high greenness such as green spaces inside the city and cropland in the rural area will exhibit lower surface temperature. In the spring, with the abundant rain and rising air temperature, vegetation in the study area increases significantly. During this season the highest inverse ($r^2 = 0.73$, $p < 0.01$) relationship is ascertained between LST and NDVI. It means increasing NDVI is associated with decreasing LST. Whilst during the summer, which is the dry season, NDVI values drop to the lowest level and the relationship with the LST becomes a weak relationship ($r^2 = 0.02$, $p = 0.22$). During autumn, the commencing of the wet season, NDVI increases slightly and the relationship with LST is increased ($r^2 = 0.34$, $p < 0.01$). However, in the winter, the relationship between NDVI and LST during the daytime switches to a positive relationship ($r^2 = 0.37$, $p < 0.01$). In general, during the winter, vegetated areas have a higher LST compared to bare land and residential areas.

Meanwhile, a strong significant inverse relationship ($r^2 = 0.81$; $p < 0.01$) is ascertained between LST and fsm. In the majority of seasons, for instance, in the dry summer season, the relationship demonstrates that low ET and LE are associated with high LST. Moreover, the relationship of LST with ET ($r^2 = 0.51$; $p < 0.01$) and LE ($r^2 = 0.56$; $p < 0.01$) was inverted. This means that as the fsm, ET and LE indices increase, the LST will decrease; for inside the city border the fsm is 0.35 ± 0.11 , ET is 13.51 ± 0.01 and the mean LST at ~11:00 is $30.92 \pm 0.98^\circ\text{C}$, whilst in the 10 km buffer of the

city the fsm and ET decreases to 0.27 ± 0.11 and 0.83 ± 0.03 , respectively. Moreover, the mean LST increased to $32.44 \pm 1.46^\circ\text{C}$.

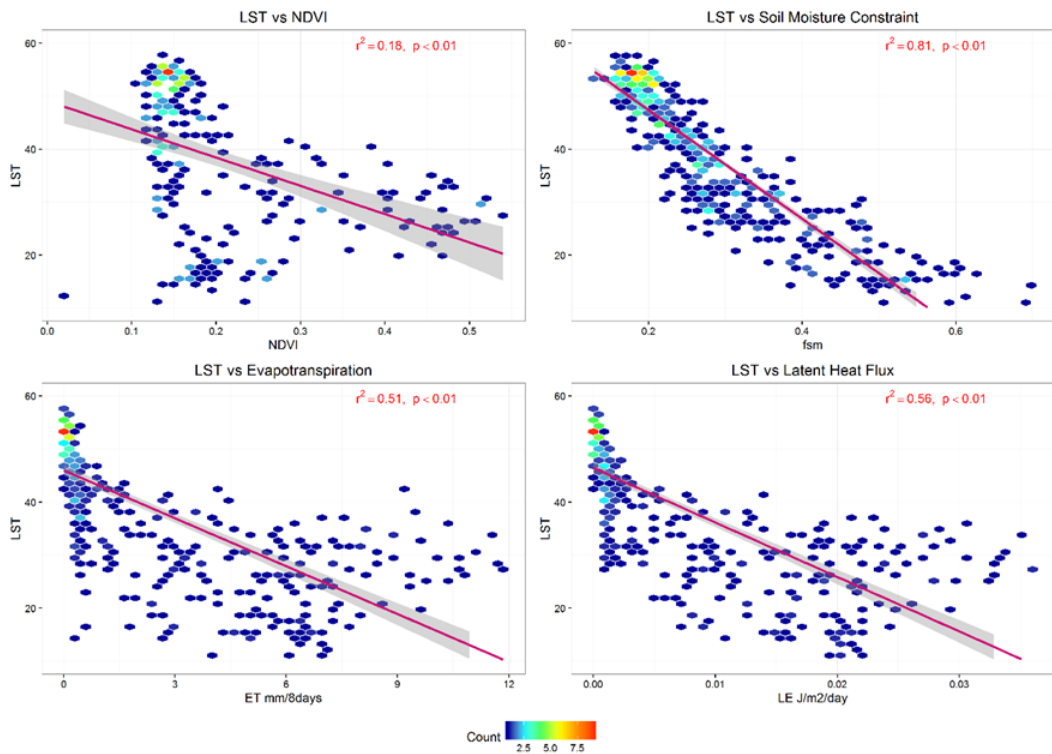


Figure 5.9: Relationship of Land Surface Temperature with NDVI, Soil Moisture Constraint Factor, Evapotranspiration and Latent Heat Flux from 12 years MODIS data.

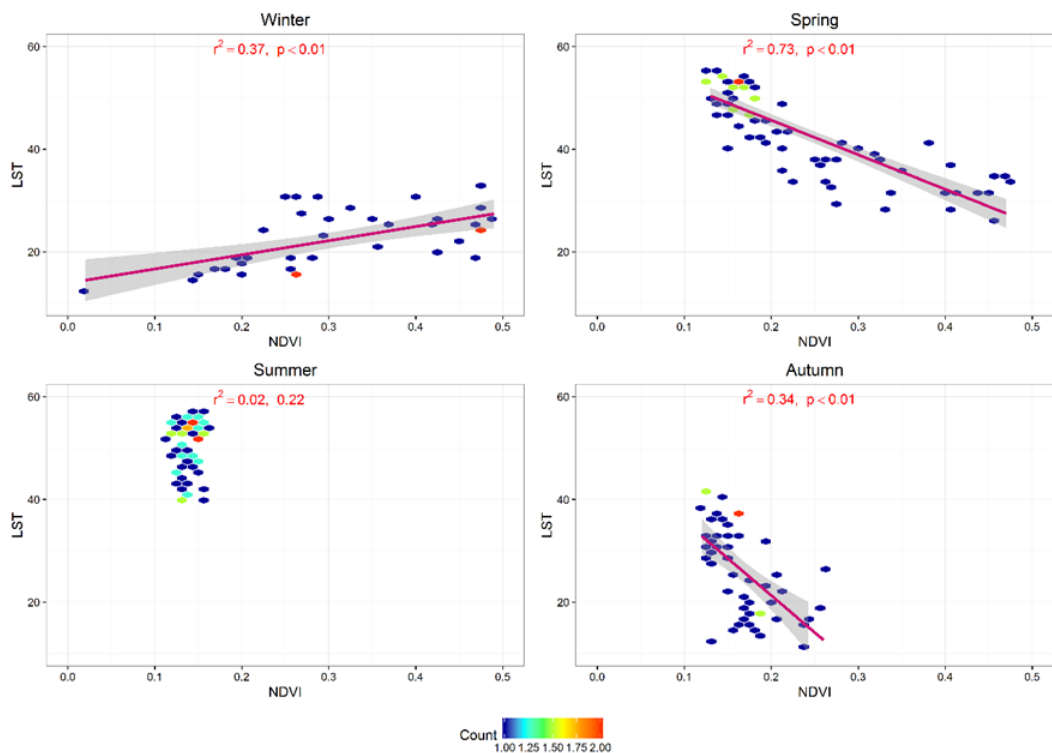


Figure 5.10: Land Surface Temperature against Seasonal NDVI, from 12 years MODIS data.

5.4 Discussion

To study the diurnal cycle of LST and SUCI/SUHI, the data of four MODIS overpasses per day were used. Roth *et al* (1989), Tran *et al* (2006) and EPA (2009) ascertained that SUHI in temperate environments is greatest during the day and lowest at night. The results presented here demonstrate a different dynamic behaviour in the semi-arid climate of Erbil, where the strongest SUHI occurs at night, confirming earlier results by Cheval *et al* (2009), contrasting with a SUCI during the day.

The seasonal variation of SUCI/SUHI indicates that the night-time SUHI is stronger in the spring and summer than the autumn and winter. This is in agreement with Li *et al* (2012) who ascertained that SUHI is higher in summer and spring while it is weaker in the winter and autumn. Similarly, Chow and Roth (2006) observed the highest UHI intensity during the dry season and lowest intensities during the wet season. However, the results presented here do not agree with the boreal study by Runnalls (2000) who found the largest UHI intensity of Vancouver, Canada to be in the autumn, followed by summer, winter and spring. On the other hand, daytime SUCI intensity in the autumn and summer is higher than the winter whilst it turns neutral in the spring. In general, during summer the effect of UHI is more important to the urban residential area. This is due to the more extreme thermal conditions, which increase illnesses and mortalities related to heat (Tan *et al*, 2010).

During the period of study, the NDVI of the rural areas was on average 0.06 higher than the NDVI of the urban areas. The result for Erbil's NDVI as a semi-arid area disagrees with results from arid studies, for instance, for Phoenix in the USA where the NDVI of the rural areas is lower than the NDVI of the urban. In Erbil, the surface wetness index (which is intended to be related to soil moisture) is the main indicator of the SUCI effect, and not vegetation cover. Nevertheless, as the vegetation in the area mainly depends on precipitation, this variation of NDVI between the city and rural areas increases significantly in spring and decreases during the dry season. In March 2010 and 2013, this variation was 0.31 while in August and September 2013 no variations were observed.

The relationship of LST and NDVI was assessed for the 12 years of MODIS data and this relationship was determined for each season. The general relationship for the 12 year period was weakly negative. Our results indicate this relationship changes significantly with the seasons, confirming the results of Yuan and Bauer (2007) and Sun

and Kafatos (2007). In the summer, it is definitely weak. The peak of the inverse relationship is located in the spring within the period of vegetation growth, meaning that in the area of high vegetation greenness LST decreases. This type of relationship confirms the results of Tiangco *et al* (2008) and Li (2011). On the contrary, during the winter, which is a relatively cold and wet season in the study area, this relationship turns positive and LST rises with increasing NDVI. These results agree with Sun and Kafatos (2007) during the winter, the results of Schultz and Halpert (1995) in the high and mid-latitudes and Haashemi *et al* (2016). The reason for this positive relationship is potentially related to vegetation water content which retains heat during the cold period; the decrease of photosynthesis may also have an influence (Haashemi *et al*, 2016).

The trend of NDVI of the urban from 2003 to 2014 was -0.00025 and the rural area was -0.00015 (Figure 5.8). It means that the NDVI of the city during this period decreased more than NDVI of the surrounding area. The reason may be related to urbanisation that may have led to some vegetation fields around the city being transformed to residential area. In terms of soil moisture, the trend of fsm of urban and rural areas was 0.00009 and -0.00002 respectively. It may suggest that the soil moisture in the city increased slightly as a result of irrigation and human activity and decreased slightly in the rural area resembling a decrease in precipitation.

5.5 Summary

Due to LST influences, the lowest layer of the atmosphere is a key driver of urban climate and it plays a significant role in physiological processes. This chapter assessed the temporal formation of the daytime SUCI and night-time SUHI effect in Erbil in Iraq, as a case study of cities in semi-arid climates more generally. LST data from the MODIS Aqua and Terra, MODIS NDVI, ET and LE are analysed, from January 2003 to December 2014. In order to establish the key drivers of the observed patterns of LST and SUCI/SUHI, the relationships of LST with NDVI, fsm, ET and LE are investigated. The results indicate that during the daytime, in summer, autumn and winter, densely built-up areas had lower LST acting as surface cool islands, compared to the non-urbanised area around the city. In contrast, at night-time Erbil experienced higher LST and demonstrated a significant SUHI effect. A strong inverse relationship is evident between surface temperature and soil moisture ($r^2 = 0.81$; $p < 0.01$). The relationship between LST and NDVI is affected by seasonality and the relationship during spring is

strongly inverted ($r^2 = 0.73$; $p < 0.01$). The results suggest that during the dry season in Erbil, soil moisture index is the main indicator of the SUCI/SUHI effect, and vegetation cover is the main factor during the spring season.

**Chapter 6 : Changes of the Urban Heat/Cool Island Effect in
the Urban Expansion Zone of Erbil, Between 1992 and 2013**

Parts of this chapter have been submitted as:

Rasul, A., Balzter, H. and Smith, C. (2016) 'Applying a Normalized Ratio Scale Technique to Assess Influences of Urban Expansion on Land Surface Temperature of the Semi-Arid City of Erbil', *International Journal of Remote Sensing*.

6.1 Introduction and Rationale

The variation between surface and air temperature within a city and its surrounding area is a result of variations in surface cover, thermal capacity and 3-dimensional geometry. Moreover, urbanisation causes a reduction of natural habitats, has the ability to modify energy flow and alter the local microclimate (Alberti and Marzluff, 2004). Researching LULC changes in an area allows for an assessment of the amount of artificial modification of the surface and other environmental variations related to human impacts (Xiao and Weng, 2007). In urban climate studies, the surface temperature is very significant (Voogt and Oke, 2003).

In previous chapters, the spatial variation of LST and SUCI in Erbil during the dry season has been examined using Landsat 8 images. The results of the research indicated that bare soil rural areas exhibited higher LST compared to densely built-up areas and the city, which act as surface cool islands during the daytime. Furthermore, the temporal variation of LST and SUCI/SUHI of the city was considered using the LST product from MODIS Aqua and Terra. The study focused on seasonal, interannual and diurnal patterns of LST and SUCI/SUHI. It confirmed that the city experienced a SUCI during the daytime and a SUHI at night-time and that the key driver of LST in the study area can be soil moisture. Erbil as a city is located in a semi-arid climate and experiences a SUCI during the daytime, therefore urban expansion is expected to correspond to a decrease in daytime LST.

The current research extends these earlier results by quantifying the decrease of the daytime LST as a consequence of urban expansion. It is important to also assess different pixel samples of LULC change to demonstrate the influence of this variation in more detail and to illustrate what type of LULC change contributes to mitigation of the night-time SUHI and makes the daytime SUCI more active in the summer-time.

The effect of LULC change on LST in cities located in semi-arid environments still requires more research to be better quantified and understood. The specific objective of this chapter is to quantify the effect of the LULC change on the LST patterns in Erbil. In this study, we propose a Normalised Ratio Scale (NRS) technique to normalise the value of each pixel-based ratio to make the LST images from different times comparable, while at the same time maintaining the original values. Through multiplying the results by an appropriate number, they have the ability to illustrate the original degree of temperature.

This chapter focused on the effect of urban expansion on LST and SUCI between 1992 and 2013. Multi sensor Landsat images have been used in this chapter. In the first section, the effect of vegetated land on LST has been considered. Then, decreasing LST of urbanised areas from 1992 to 2013 has been assessed. Finally, pixel samples of LULC change are selected to illustrate the effect of different patterns of LULC change on LST and the formation of a SUCI.

6.2 Data and Methodology

In this section, data and methods that are used in this chapter are presented. It includes pre-processing of data, calculation of Impervious Surface and application of the Normalised Ratio Scale technique.

6.2.1 Data and Pre-Processing

LST data were extracted from 11 Landsat images. Three images were acquired in 1992 (Landsat 4 and 5): two images from 2002 (Landsat 7) and six thermal images from 2013 acquired by Landsat TIRS (Landsat 8) from 1st July to 19th September 2013 were used (Table 6-1). These images were resampled to 30 m spatial resolution and were used to retrieve LST (Path 169, Row 035). The images are level L1T data and were captured under transparent atmospheric conditions (<1 % cloud coverage) and in the dry season. The United States Geological Survey (USGS), Earth Explorer website (<http://earthexplorer.usgs.gov/>) provided these images. As noted in Chapter 4, the calibration uncertainties of Landsat 8 imply a calibration uncertainty of approximately 1.3 K in the LST data generated in this thesis. Recognising also the normalisation methods applied in this chapter then the uncertainty may be reduced. However, one

should be cautious to not over-interpret changes in LST of order 1.5 K or less in absolute terms (see Chapter 4).

Table 6-1: Images used in Chapter 6.

Sensor	Date	Local Time	Cloud Cover (%)	Quality	Spatial Resolution Multispectral/Thermal
TM (L4)	31/07/1992	06:47	0.00	9	30 m/120 m
TM (L5)	08/08/1992	07:01	0.00	9	30 m/120 m
TM (L5)	24/08/1992	07:01	0.00	7	30 m/120 m
ETM+ (L7)	27/07/2002	07:27	0.00	9	30 m/60 m
ETM+ (L7)	13/09/2002	07:26	0.00	9	30 m/60 m
OLI, TIRS (LDCM)	01/07/2013	07:40	0.01	9	30 m/100 m
OLI, TIRS (LDCM)	17/07/2013	07:40	0.01	9	30 m/100 m
OLI, TIRS (LDCM)	02/08/2013	07:41	0.02	9	30 m/100 m
OLI, TIRS (LDCM)	18/08/2013	07:41	0.01	9	30 m/100 m
OLI, TIRS (LDCM)	03/09/2013	07:41	0.03	9	30 m/100 m
OLI, TIRS (LDCM)	19/09/2013	07:40	0.72	9	30 m/100 m

Composites of the Landsat images were produced for each year by calculating the pixel-based mean of the images of each year for the thermal and multispectral bands. These composite images are used for all of the subsequent analysis. For the thermal bands of Landsat 4 and 5 that have one thermal channel, a scene-specific atmospheric correction was applied (Coll *et al*, 2010), whilst for the thermal bands of Landsat 7 and 8 Thermal Atmospheric Correction method was applied. Furthermore, Quick Atmospheric Correction (QUAC) is appropriate for atmospheric corrections of Landsat multispectral bands.

A shapefile of S.A. Park and the urbanised area from 1992 to 2013 was digitised based on true colour Landsat imagery. Exemplary pixels of different LULC with the significant variation in the study area were selected based on Landsat images for each year, and DigitalGlobe imagery with 0.5 m resolution was acquired on 5th July 2010 (Figure 6.1).

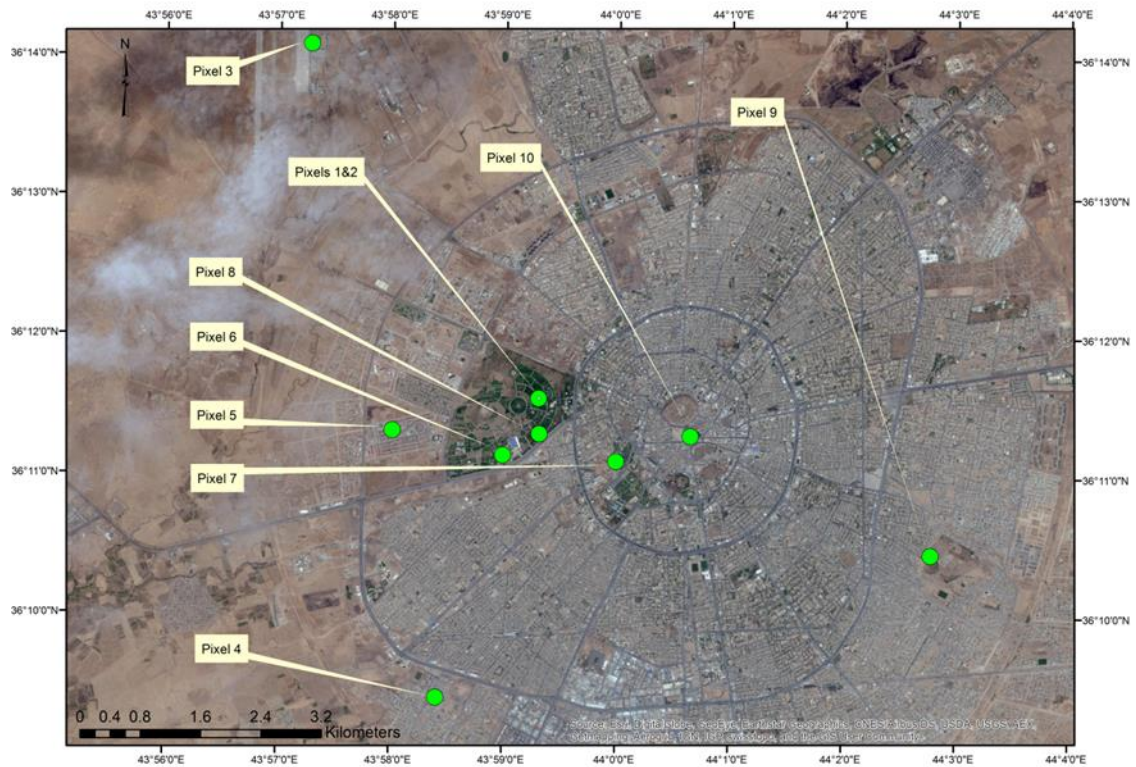


Figure 6.1: Location of pixel samples of LULC change (Image source: Esri, DigitalGlobe, GeoEye, i-cubed, Earthstar Geographics, CNES/Airbus DS, USDA, USGS, AEX, Getmapping, Aerogird, IGN, IGP, swisstopo, and the GIS User Community).

6.2.2 Methodology

6.2.2.1 Retrieval of LST

The digital number of thermal band Landsat was converted to land surface temperature, using Eq. (4.1, 4.2 and 4.3) in Chapter 4.

6.2.2.2 Calculating Impervious Surface Area (ISA) and vegetation indices

NDVI is a simple and widely used vegetation index. It is a ratio based index using two bands (red and near infrared) to identifies healthy vegetation and variations in green biomass. The index relies on the fact that vegetation has a strong absorption in the red band and a strong reflection in the NIR band (Karnieli *et al*, 2010; Wu, 2014). To calculate NDVI, equation 4.9 in Chapter 4 was employed (Sobrino *et al*, 2004).

Fractional vegetation and impervious surface cover

Fractional vegetation Fr was calculated as

$$Fr = N^{*2} \quad (6.1)$$

where N^* is a scaled NDVI from equation 6.2

$$N^* = \frac{(NDVI - NDVI_o)}{(NDVI_s + NDVI_o)} \quad (6.2)$$

and N^* is a scaled NDVI. $NDVI_s$ and $NDVI_o$ respectively are values for dense vegetation and pure bare soil (maximum and minimum NDVI of the study area or the image).

Impervious surface area (ISA) is calculated from the following equation (Carlson and Arthur, 2000):

$$ISA = (1 - Fr)_{dev} \quad (6.3)$$

where dev means the quantity is only defined for urban developed regions.

6.2.2.3 Normalised Ratio Scale

A common technique for normalising LST is based on the minimum and maximum of LST (NLST; Khandelwal *et al*, 2011), Eq 6.4:

$$LST^* = \frac{(LST - LST_o)}{(LST_s + LST_o)} \times 100 \quad (6.4)$$

where LST^* is a normalised LST. LST_s and LST_o respectively are values for maximum and minimum LST for the study area of that particular image. The range of normalised LST is between 0 and 100.

To normalise variables and to make them comparable to each other there are different methods in statistics such as Nominal Scale Variables, Ordinal Scale, Interval Scale, Ratio Scale, Difference Scale and Absolute Scale. Ratio scale preserves four properties including equality, ordinality, interval ratios, and value ratios. Due to the ratios of the intervals between the numbers they are not affected by congruence transformations, and ratio scales are unique up to a congruence or proportionality transformation ($Y = mX$). It means if one measures a group of objects on a ratio scale, and then multiplies each value by a constant, the resulting values are equally as valid as the original values. For instance, in the following example, the measurements M1, M2 and M3 are equally valid measures of a given object property, whereas M4 is not measuring the same thing (Borgatti 2016):

<i>Object</i>	<i>M1</i>	<i>M2</i>	<i>M3</i>	<i>M4</i>
<i>A</i>	22	220	11	12
<i>B</i>	22	220	11	12
<i>C</i>	22	220	11	12
<i>D</i>	23	230	11.5	13
<i>E</i>	24	240	12	14

A ratio scaled normalising of the variables above would produce:

Object	M1	M2	M3	M4
A	0.44	0.44	0.44	0.43
B	0.44	0.44	0.44	0.43
C	0.44	0.44	0.44	0.43
D	0.45	0.45	0.45	0.46
E	0.47	0.47	0.47	0.50

To make thermal satellite images comparable and maintaining original values to detect change in LST, according to review of this research, application of a new technique is necessary. Therefore, in this study, a Normalised Ratio Scale is proposed, which rescales a set of images on a ratio scale, and then multiplies each value by a suitable number in order to produce a result close to the original temperature. Each pixel value will be divided by the square root of the sum of squares of all the original pixel values (Stevens 1946; Borgatti 2016). Eq 6.5:

$$LST_{NRS} = \frac{LST}{\sqrt{\sum LST^2}} \quad (6.5)$$

where LST_{NRS} is normalised LST based on ratio scale, LST is LST of each pixel in the image. To return the outputs to numbers similar to original LST values, LST_{NRS} is multiplied by a number of the order of:

$$N = \left(\frac{\text{mean LST}}{\text{mean } LST_{NRS}} \right) \quad (6.6)$$

where mean LST is the mean LST of one image before normalisation and mean LST_{NRS} is the mean scaled LST of the same image from equation 6.5. As a result of equation 10, the constant number (N) used in this study is 50,000.

Ground truth LST measurements of the study area from 1992 (before urbanization), 2002 and 2013 (after urbanization) are unavailable. In its place, LST derived from Landsat data from 1992 was used as reference (referring to 330 pixels within the same land cover, bare soil). The results of the different normalization methods for each year compared with these estimated references are shown in Figure 6.4.

6.3 Results

6.3.1 Normalised Ratio Scaled Land Surface Temperature

In order to understand the characteristics of the new method, LST_{NRS} method (D) was compared with non-normalised method (A), rescaling images to the same minimum and maximum in 1992 (B) NLST (C). The results indicate that non-normalisation (A) was unable to show real LST change of an area at different times. As illustrated on Figure 6.3, the method shows a decrease of LST of -1.17°C in 2002 and an increase of LST of 1.91°C in 2013 compared to 1992, while in reality daytime LST decreased in both periods (Table 6-2, Figure 6.2, 6.3). Results of method (C) showed a change of LST in a wide range of high values up of to -12.54 (1992-2013). There is not much variation in the change of LST between method B and D (LST_{NRS}). Both of them were capable of illustrating the change in LST of the same place at different periods. In method A and C, the standard deviation, and variance were relatively high while they are low in method B and D as shown in Table 6-2. For 2002 and 2013 respectively (Figure 6.4), RMSE (0.44, 0.77) and bias of LST_{NRS} (-0.1 , -0.9) are relatively low. Some differences are observed between the full image and mean temperatures in all methods. For method D, 1992 and 2013 mean values were approximately 2°C apart (Table 6-2). Part of this at best can be explained by the real scene variation of vegetation leading to residual differences from the normalization procedure (calibration issues in Landsat 8 may also contribute). Therefore, results indicate that NRS is appropriate for detecting temperature but caution should be exercised for changes much less than -2°C between 1992 and 2013.

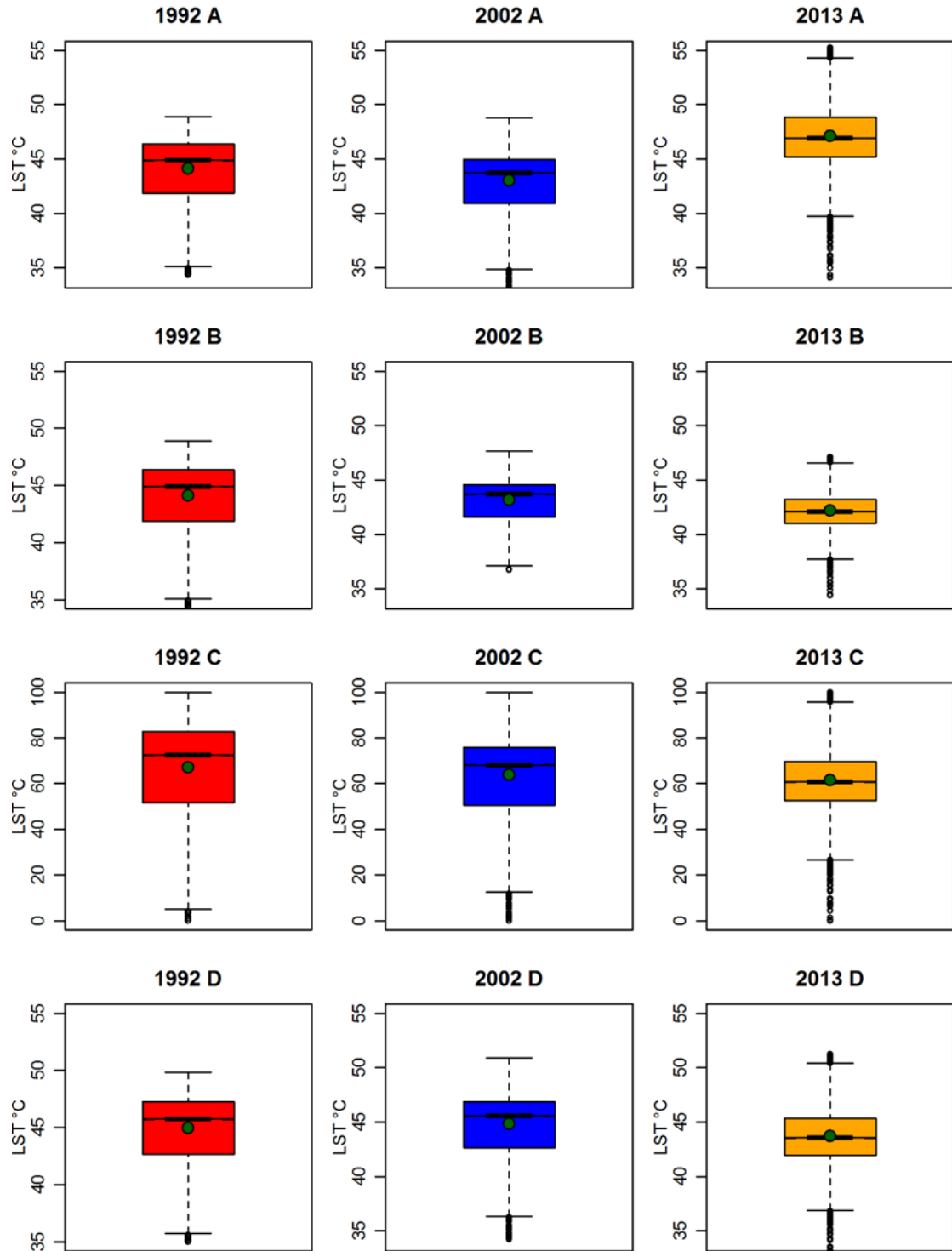


Figure 6.2: LST of Erbil based on different method from Landsat images. (A) is without normalisation, (B) is LST in rescaling images to the same minimum and maximum in 1992, (C) NLST (2000) method, (D) normalised based on NRS.

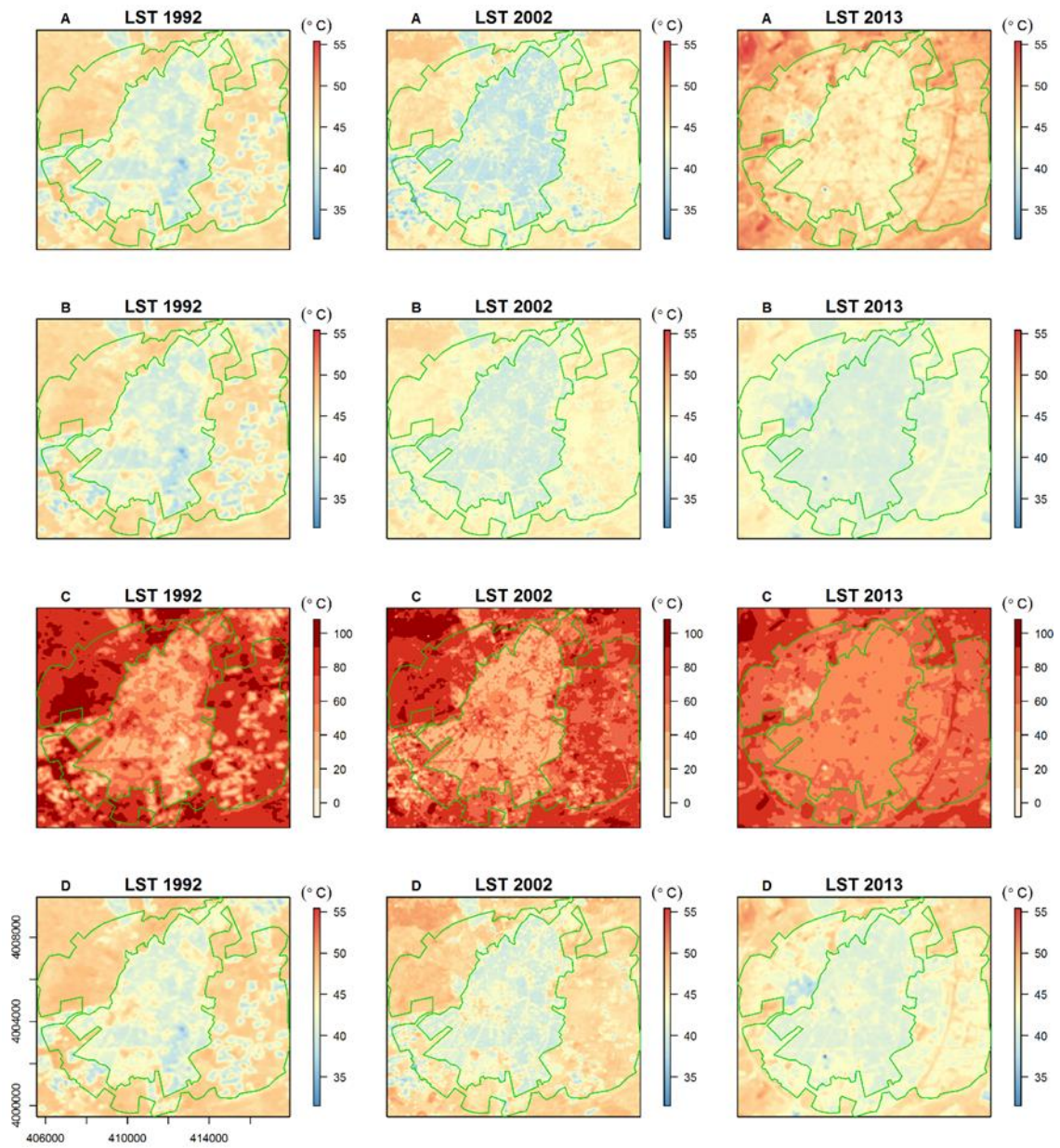


Figure 6.3: Daytime LST of Erbil based on different method from Landsat images. (A) is without normalisation, (B) is LST in rescaling images to the same minimum and maximum in 1992, (C) NLST (2000) method, (D) normalised based on NRS.

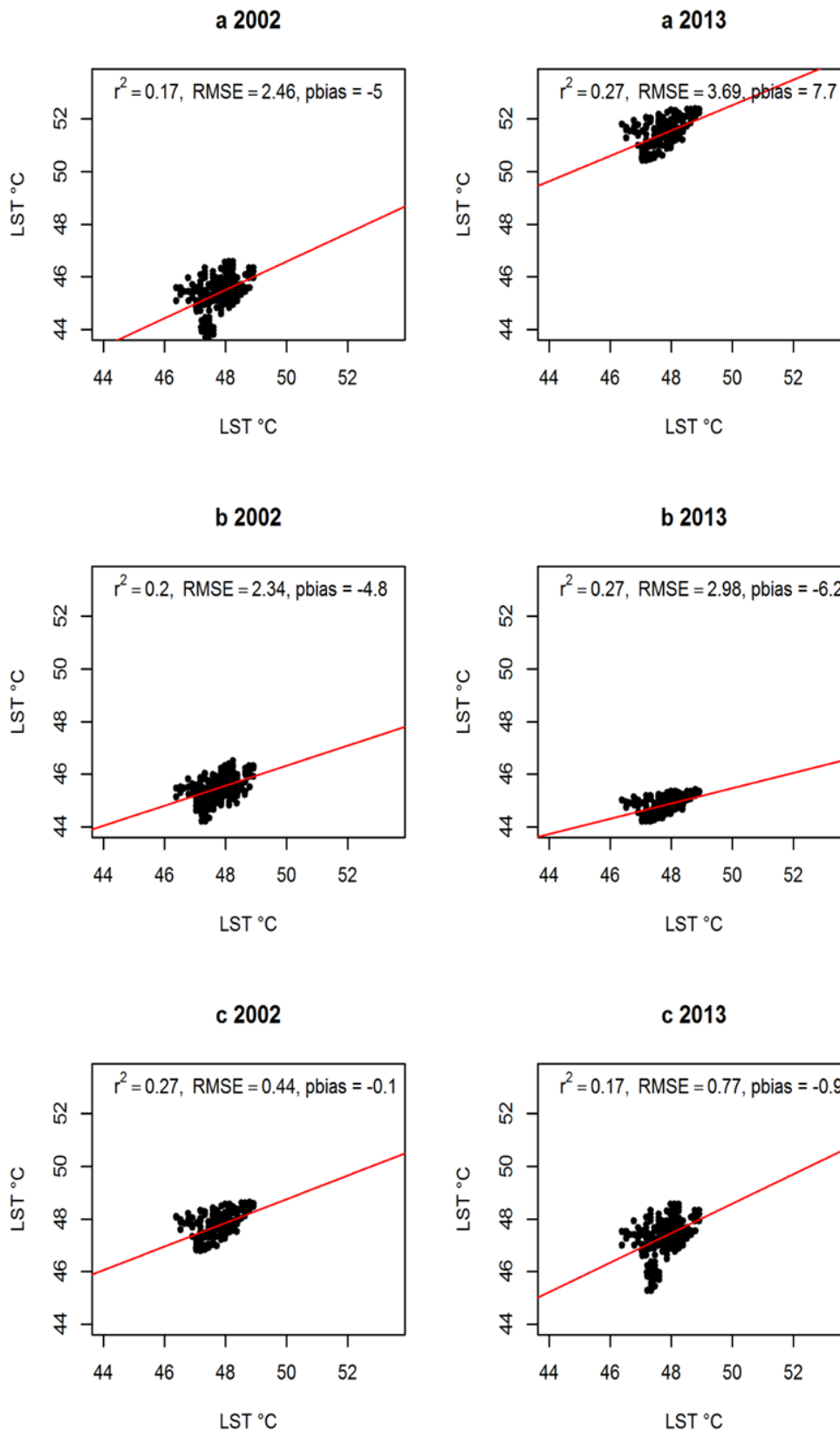


Figure 6.4: Comparison of the scaled LST of Erbil based on the different methods of normalizing Landsat images. (a) is LST without normalization, (b) is LST in rescaling images to the same minimum and maximum in 1992, (c) normalized based on NRS. X data is LST 1992 of 330 pixels with the same land cover from 1992 to 2013.

Table 6-2: Mean, SD, variance and Δ LST in degree Celsius for different method from Landsat images.

Methods	Mean LST 1992	SD mean LST	Variance LST 1992	Mean LST 2002	SD mean LST	Variance LST 2002	Mean LST 2013	SD mean LST	Variance LST 2013	Δ LST (1992,2002)	Δ LST (1992,2013)
A*	45.01	2.28	5.18	43.84	1.85	3.43	46.92	1.72	2.95	-1.17	1.91
B**	45.01	2.28	5.18	43.76	1.22	1.49	42.1	1.04	1.08	-0.95	-2.91
C***	73.28	15.67	245.5	68.93	11.62	134.94	60.74	8.12	65.91	-4.35	-12.54
D****	45.86	2.32	5.38	45.71	1.93	3.73	43.56	1.59	2.54	-0.15	-2.3

* Without normalisation, ** is LST in rescaling images to the same minimum and maximum in 1992,

*** NLST method, **** normalised based on NRS.

6.3.2 Effect of Vegetated Land on Land Surface Temperature

S.A. Park is the biggest park in Erbil and the entirety of Iraq. The location of the park is a former army base that was taken out of use in 1991. The period studied here commences in 1992 before the park was established. Large parts of this area were used for winter grain cultivation such as wheat and barley. However, due to the seasonality of precipitation in this region these areas would be occupied by bare soil or cropland without vegetation during the dry season. In 1992 the mean NDVI of S.A. Park was 0.09 ± 0.01 and the mean of LST $47.67 \pm 0.73^\circ\text{C}$ (Table 6-3, Figure 6.5 and 6.6). At the same time the mean LST of the city was $44.56 \pm 2.71^\circ\text{C}$ and S.A Park was 3.11°C warmer compared to the entire city.

In 2002, the park was partially vegetated and its NDVI increased slightly to 0.11 ± 0.08 . This variation led to a decrease in mean LST to $46.07 \pm 2.65^\circ\text{C}$ (a 1.6°C decrease). By 2013, the majority of the park had been converted to a greenspace and its mean NDVI increased to 0.32 ± 0.11 , a 0.23 increase compared to 1992. By contrast, the mean LST of the park decreased to $40.38 \pm 1.91^\circ\text{C}$. Compared with 1992, its LST decreased by 7.29°C . Consequently, decreasing LST as a result of increased vegetation causes means the park appears as a cool island between the other LULC classes in the city.

In summer 1992 the average NDVI of the park was less than 0.1 and the area was almost free of vegetation. At that time all the parts of the park exhibited high

temperature and the highest LST was on the west side of the park. In 2002, increased vegetation on the east side of the park led to decreased LST while LST in the west part was still high. In 2013 when most part of the park had been vegetated, also LST of the west side of the park has decreased significantly. Usually big parks influence temperature in close neighbouring areas. Therefore, it is possible that the influence of S.A. Park is one of the reasons for a decrease of temperature in the east and west neighbouring areas to the park.

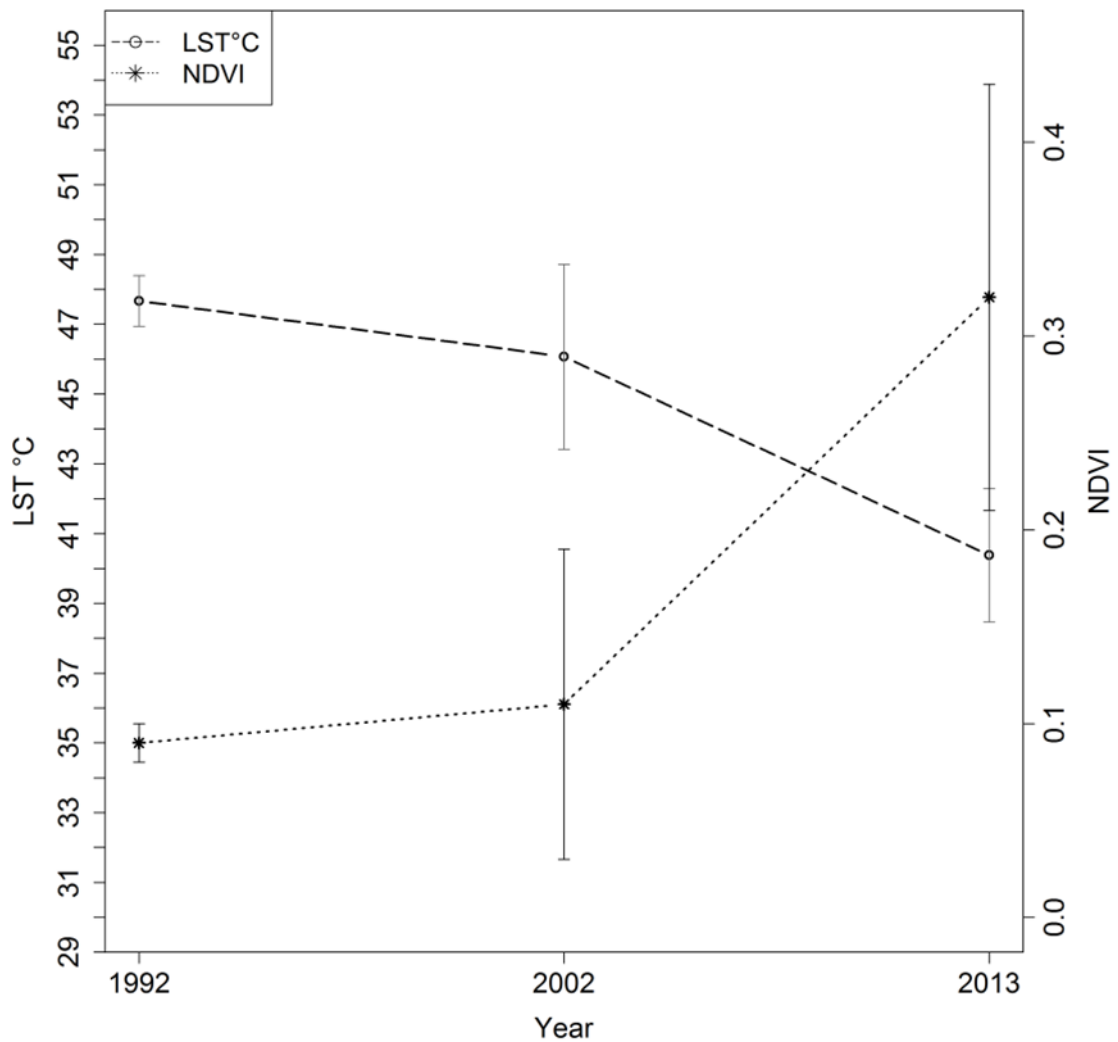


Figure 6.5: Mean LST and NDVI of S.A. Park from 1992 to 2013 from Landsat.

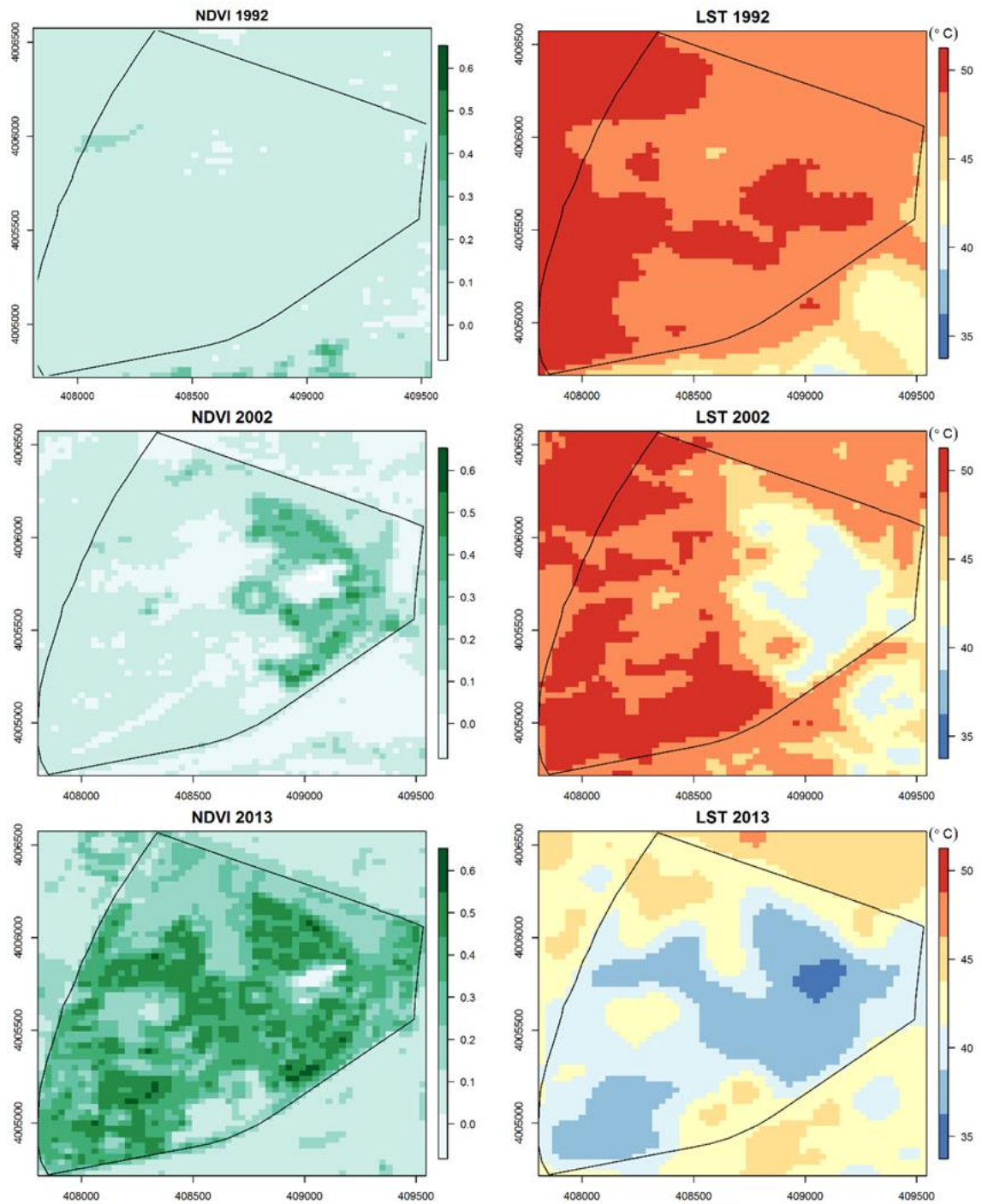


Figure 6.6: The change of NDVI and LST_{NRS} of S.A. Park from 1992 to 2013 from Landsat.

Table 6-3: Land Surface Temperature and NDVI in S.A. Park in 1992, 2002 and 2013.

Year		Min	Max	Mean	SD	Min	Max	Mean	SD
		NDVI	NDVI	NDVI	NDVI	LST (°C)	LST (°C)	LST (°C)	LST (°C)
1992	*	0.05	0.18	0.09	0.01	44.21	48.66	46.78	0.71
	**					45.05	49.58	47.67	0.73
2002	*	-0.05	0.47	0.11	0.08	39.89	46.15	43.92	1.46
	**					39.30	49.70	46.07	2.65
2013	*	-0.02	0.54	0.32	0.11	36.92	42.79	40.03	1.25
	**					35.64	44.64	40.38	1.91
Change	*	-0.07	+0.36	+ 0.23		-7.29	-5.87	-6.75	
	**					-9.41	-4.94	-7.29	

* is LST in rescaling images to the same minimum and maximum in 1992. ** is LST in NRS technique.

6.3.3 Decreasing LST of Urbanised Area from 1992 to 2013

In 1992, the area of Erbil city was 38.1 km², the mean LST of the city was 44.56 ± 2.71°C compared to the mean LST of the expanded urban area in 2013 which was 45.85 ± 2.31°C (Table 6-4, Figure 6.7). The LST of this part was 1.29°C higher than the mean LST of the city. Rapid urbanisation led to 55.3 km² around the city being transformed principally from ‘bare soil’ and ‘field without vegetation’ to ‘urban’ between 1992 and 2013. During the first decade the city only expanded by approximately 6.4 km². In the second decade, especially after 2003, the city expanded rapidly. In this period, after the political change, the government changed the investment law to advantage investment in the building sector. In 2013 the area of the city increased by 48.9 km² compared to 2002 (Table 6-5). In this year, the mean LST of the new urbanised area decreased to 43.57 ± 1.6°C, indicating that from 1992 to 2013 the daytime LST of the new urbanised area decreased by 2.28°C. This result demonstrates that the LULC change from barren soil to urban areas in cities located in semi-arid climate has the ability to cause a decrease in daytime LST.

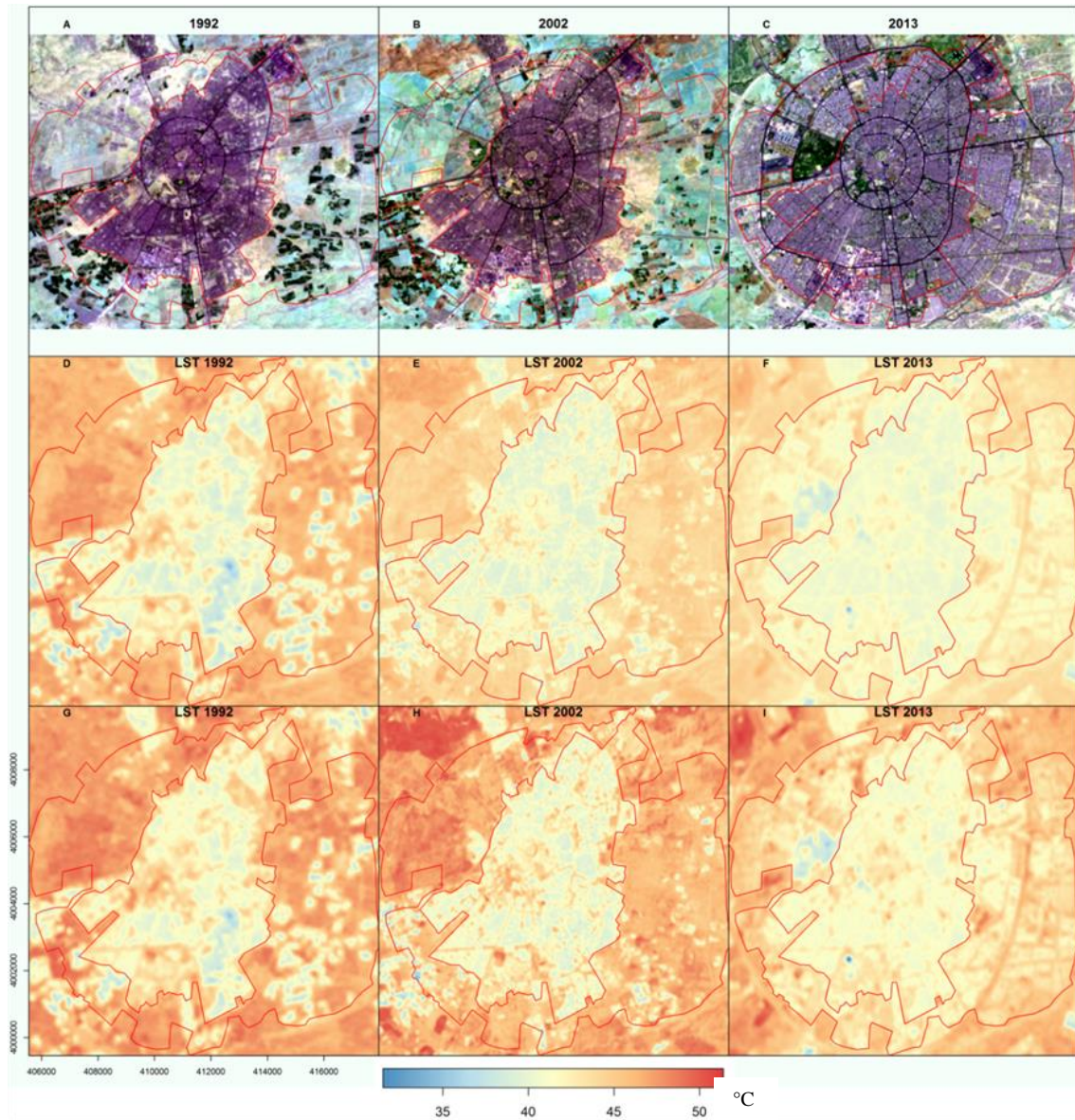


Figure 6.7: Decrease in LST in the area that was urbanised from 1992 to 2013. Bands 7, 6 and 4 as false colours from Landsat 8 (bands 7, 5 and 3 for Landsat 5 (image A) and Landsat 7 (image B)) demonstrating urban areas in brown, vegetation in dark blue, water in black and barren land in sky blue and wheat colour. D:F is LST rescaled with min and max, G:I is LST from the NRS method. Red line is boundary of urbanised area.

Table 6-4: Change in LST of the area urbanised from 1992 to 2013.

Year		Min LST °C	Max LST °C	Mean LST °C	SD LST °C
1992	*	36.38	48.89	45.01	2.28
	**	37.06	49.82	45.85	2.31
2002	*	37.15	46.50	43.76	1.22
	**	34.25	50.23	45.69	1.94
2013	*	36.92	46.04	42.10	1.04
	**	35.64	49.65	43.57	1.6
Change	*	+ 0.54	-2.85	-2.91	
	**	-1.42	-0.17	-2.28	

* is LST from rescaled based of minimum and maximum, ** is LST based of NRS method.

Table 6-5: Urban expansion in the study area.

Year	Area (km ²)
1992	38.114
2002	44.461
2013	93.398
Urbanised	55.284

6.3.4 Changes of LST for Different Types of LULC Change

After finding a decrease of LST caused by vegetation and urbanisation in the previous sections, ten pixels are selected to illustrate different types of LULC change to identify in more detail how LULC change affects LST in Erbil as an example of cities in semi-arid climates. The first group of pixels (one to eight) changed from bare land or fields without vegetation to buildings and other purposes in the residential area whilst pixel number nine changed from green to bare soil and pixel number 10 changed from buildings to vegetation (Table 6-6).

Pixel 1 was bare soil with LST = 47.67°C and in 2013 it became a part of an artificial lake (Lake 2) inside S.A. Park, the true colour of the pixel changed from grey in 1992 to dark blue in 2013. This variation causes a significant decrease in LST (35.64°C), a drop of 12.03°C. Pixel 2 changed from bare soil with ISA = 0.61 to a built-up area of Erbil International Airport with ISA = 0.94. Its LST increases to 50.23°C in 2002 from 47.54°C in 1992 then decreases to 46.92°C in 2013 (Table 6-6).

Table 6-6: Pixel samples of LULC change with mean LST_{NRS} , NDVI and ISA.

Year		<i>N1 bare to water</i>	<i>N2 bare to airport</i>	<i>N3 dry field to houses</i>	<i>N4 bare to western house</i>	<i>N5 bare to asphalt parking lot</i>	<i>N6 bare to grass-tree</i>	<i>N7 bare to tree</i>	<i>N8 bare to grass</i>	<i>N9 farm to bare soil</i>	<i>N10 commercial to grass-water</i>
1992	<i>LST °C</i>	47.67	47.54	46.03	48.36	47.27	45.86	47.4	46.84	40.1	42.37
	<i>NDVI</i>	-0.1	0.1	0.13	0.09	0.1	0.07	0.09	0.08	0.44	0.05
	<i>ISA</i>	1	0.61	0.41	0.65	0.58					0.83
2002	<i>LST °C</i>	40.91	50.23	44.91	47.49	49.45	46.76	42.28	40.2	42.26	42.53
	<i>NDVI</i>	0.01	0.04	0.09	0.05	0.07	0.05	0.28	0.46	0.21	0.01
	<i>ISA</i>		0.99	0.97	0.99	0.99					1.0
2013	<i>LST °C</i>	35.64	46.92	42.27	44.52	43.98	40.67	38.02	38.38	45.94	41.41
	<i>NDVI</i>	0.16	0.05	0.1	0.12	0.1	0.38	0.47	0.51	0.13	0.21
	<i>ISA</i>		0.94	0.89	0.88	0.89					0.76

Pixel 3 changed from field without vegetation with $ISA = 0.41$ and $LST = 46.03^{\circ}C$ in 1992 to houses within flat roofs (in the Shadi district) with $ISA = 0.89$ and $LST = 42.27^{\circ}C$ in 2013. During these two decades its LST decreased by $3.76^{\circ}C$ as a result of the urban expansion. Pixel 4 changed from bare soil with $ISA = 0.65$ and $LST = 48.36^{\circ}C$ in 1992 to houses within western style (in Italian Village) with $ISA = 0.88$ and $LST = 44.52^{\circ}C$ in 2013. The transformation of bare soil to residential area decreased the LST by $3.84^{\circ}C$. This result demonstrates that urbanisation from bare soil to urban built-up areas in cities located in the semi-arid climate can cause a decrease in its daytime LST .

Asphalt parking lots have their own microclimate due to albedo and low thermal conductivity. Impervious surfaces such as asphalt and concrete absorb, store and reradiate more heat energy than vegetated surfaces (Celestian and Martin, 2004). Pixel 5 also was bare soil in 1992 with $ISA = 0.58$ and $LST = 48.36^{\circ}C$. It changed to asphalt parking lot with $ISA = 0.89$ and $LST = 44.52^{\circ}C$ in 2013. During these periods its LST unexpectedly decreased by $3.29^{\circ}C$ as a result of the LULC change.

Three pixels represent vegetation-related LULC change. Pixel 6 changed from bare soil with $NDVI = 0.07$ to a mixed pixel of tree and grass with $NDVI = 0.38$ and its

LST decreased from 45.86°C in 1992 to 40.67°C in 2013. Pixel 7 changed from bare soil with LST = 47.4°C in 1992 to tree cover with LST = 38.02°C in 2013, whilst pixel 8 was converted to grassland and increased its NDVI from 0.08 to 0.51 and decreased its LST from 46.84°C to 38.38°C over the same time. Transferring bare soil to dense tree cover decreased the LST by 9.38°C whilst changing bare soil to grassland in S.A. Park led to a decrease in LST by 8.46°C.

In contrast, pixel 9 changed from farmland vegetation to bare soil. Its LST was 40.1°C in 1992 and it increased to 42.26°C in 2002 and 45.94°C in 2013. Pixel 10 represents variation from commercial buildings to a mixed pixel of ornamental grasses and a water fountain. Its LST was 42.37°C in 1992 and then slightly decreased to 41.41°C in 2013.

6.4 Discussion

To demonstrate the variations in LST for urbanised and vegetated areas, the NRS method was proposed and the results demonstrated that it is an appropriate technique to examine temperature variation from remote sensing data (for change greater than 2°C). LULC change from green areas such as forest and irrigated agriculture to built-up urban cover types causes an increase in air temperature and LST, as other authors have demonstrated (Weng, 2001; Amiri *et al*, 2009; Grossman-Clarke *et al*, 2010). In contrast, increasing the fractional cover of green spaces in the city is an active strategy for reducing temperatures. Analysis of the effects of establishing S.A. Park in Erbil on the local LST matched similar findings by other researchers related to vegetated area in different environments. The results indicate that the relationship between NDVI and LST during the period was an inverse relationship. Consequently, the surface of the park demonstrated a cooling of 7.29°C in LST.

Furthermore, expanding water bodies such as artificial lakes and rivers in urban areas causes a decreasing local LST. The results of the pixel changed to a new water body is consistent with Tonkaz and Cetin's (2007) research on the GAP area in Turkey. These two techniques are good procedures to reduce temperatures and the night-time SUHI in Erbil.

From 1992 to 2013, 55.3 km² were urbanised around Erbil, especially in the latter decade when the area of the city increased more than twofold. Consequently, the mean LST of these new urbanised areas decreased by 2.28°C. This result agrees with other

researchers such as Trenberth (2004) and Abdullah (2012), whilst the finding differs from the majority of previous studies on the effect of urbanisation on surface and air temperature (Weng, 2001; Kalnay and Cai, 2003; Baker *et al*, 2004; Zhou *et al*, 2004; Amiri *et al*, 2009; Grossman-Clarke *et al*, 2010). This is due to the urbanisation in the study area which occurred in semi-arid dry soil while the majority of other studies focused on the effect of urbanisation in regions within wet and green zones.

In the published literature, some authors indicate that urbanised areas cool the surface in comparison to their rural surroundings. Examples of this include reducing the incident solar radiation (Trenberth, 2004), higher thermal inertia in the built-up area, shadows cast from high-rise buildings and the moisture variation between the urban and rural areas (Buyantuyev and Wu, 2010). In some cities, convection is more efficient compared to their rural surroundings, and cooling from evaporation from trees and lawns planted in the city occurs (Zhao *et al*, 2014). The soil moisture (which is an essential variable) in Erbil is higher than in the 10 km surrounding as rural area.

LULC change in the 55.3 km² urbanised area of the rapidly growing city of Erbil has led to a transformation of the surface to materials that reduce sunlight more than natural soil and increasing green spaces, water bodies and soil moisture content. To control the local LST in Erbil and make living more comfortable, city planners of the Erbil Master Plan should be using light-coloured materials for new buildings. Another technique is to direct the future expansion of the city to areas covered by bare soil and rocks that are not suitable for agriculture in order to control the temperature of the city and not lose green land.

As a consequence of decreased LST in vegetated areas (e.g. S.A. Park), an urban cool island has been formed. Likewise, in urbanised areas in new districts located on the outskirts of the city (e.g. Chwarchra and Sharawani), the daytime surface urban heat island patterns has been transformed to daytime SUCI. Despite the decrease in surface temperature, the general temperature remained high within the city especially in the summer which demonstrates very hot temperatures. It means the city and bare soil surrounding still require more mitigation techniques such as the increase of green areas and artificial water bodies.

6.5 Summary

The variation between surface and air temperature within a city and its surrounding area is a result of variations in surface cover, thermal capacity and 3-dimensional geometry. Moreover, urbanisation causes a reduction of natural habitats, can modify energy flow and can alter the local microclimate. This research chapter has assessed and quantified the decreasing daytime LST in Erbil and the influence of rapid urban expansion on urban heat/cool island effect over a 20 year period. LULC change across this time period is also established using pixel samples. NRS for multi-sensor Landsat data is proposed to adjust the temperature range for different times of captured images within the same range. In this chapter, 11 satellite images acquired by Landsat 4, 5, 7 and 8 during the period from 1992 to 2013 are used to retrieve LST. The results indicate that between 1992 and 2013 55.3 km² of city land cover changed from bare soil and field without vegetation to urban. Consequently the mean daytime LST of the new urbanised area decreased by 2.28°C. From 1992 to 2013, the NDVI of S.A. Park increased from 0.09 ± 0.01 to 0.32 ± 0.11 , resulting in a decrease of the mean daytime LST by 7.29°C. This study demonstrates that the NRS method is appropriate for detecting temperature trends from urbanisation using Landsat remote sensing data for changes of greater than 2°C. Urban expansion may cause a decrease of daytime LST in a dry climate zone and an urban cool island may then be formed.

Chapter 7 : General Discussion, Conclusions and Research Contributions

7.1 Introduction

This chapter consists of five sections. The first section (7.2) identifies the contributions of knowledge of this research and presents the major findings. General discussion and the main conclusions drawn from the study are captured by section 7.3 and 7.4. Section 7.5 explains the limitations of the research in relation to data and methodology. Directions of future research, which are expected to build from this study, based on presented findings and limitations will be discussed in section 7.6.

7.2 Original research contributions

This thesis has presented new results for Erbil, progressing from studies over a summer period to seasonal and decadal change. Both higher resolution (100 m) and lower resolution (1 km) have been used with success. This thesis advances urban climate and urban heat islands study through innovative contributions for each chapter of results. Chapter 4 contributed through using a combination of images of Landsat TIRS to assess SUCI of Erbil as a case study of cities situated in a semi-arid climate. Furthermore, it determined the spatial distribution of the patterns of LST and SUCI in the different LULC and districts of the city of Erbil. Using wetness, brightness and greenness components derived from Landsat OLI by Tasseled Cap transformation (TCT), it found key factors marking out spatial LST variations. In summer time with low vegetation, wetness index and greenness were good reasons for LST change.

Contributions of Chapter 5 are the determination of the seasonal and diurnal variation of the patterns of LST and SUCI/SUHI in a city with a semi-arid climate. In addition, better vegetation measures with respect to LST assess the seasons have evolved. The quantitative analysis of relationships between LST and NDVI shows good results for the spring season. Moreover, the results from the chapter also highlighted the use of ET, LE and derived fsm to examine how they are related to local LST in cities. MODIS data show clear increases in the magnitude of nighttime SUHI and daytime SUCI with year (decade, 2003 – 2014).

Chapter 6 contributes the proposed application of the Normalised Ratio Scale (NRS) for multi-sensor Landsat data to bring the temperature range of different times of captured images within same range. For changes of greater than 2°C from 1992 to 2013, it is possible to use Landsat to look at change at high resolution. A major finding was that LST decreased with the creation of the new S.A. Park and expanded green area as a

technique of cooling the temperature in that quarter of Erbil. In addition, the decreasing daytime LST as consequence of urban expansion in Erbil was apparent as a case study for cities situated in semi-arid climates. Finally, the effect of LULC change on LST is quantified through investigation of different pixels that are representative of change in Erbil. This first opportunity to quantify the impact of change showed that LST trends were particularly strong for bare soil to housing and asphalt; bare soil to tree/grass; farmland to bare soil.

7.3 General Discussion

In this research, the spatiotemporal structure of SUCI/SUHI and their changes in the urban expansion zone of Erbil were determined. It seems possible to differentiate LST in different LST and SUHI/SUCI with the possibility to assess impact of a vegetation at a larger scale. Landsat images were appropriate to investigate the spatial variation of SUCI/SUHI and the effect of LULC change from different samples of classes on LST, whereas, MODIS LST was effective for studying the temporal variation of SUHI/SUHI (e.g. diurnal, seasonal and decadal). In addition, using quality assured MODIS data in the quality control process helped to achieve results that are more accurate. Using R scripts beside ENVI Software for process MODIS products in this study was timesaving. Applying the NRS technique was effective for avoiding the influence of atmosphere conditions from different times of Landsat image acquisition. As a result of NDBI indicating that bare soil has higher mean NDBI than mean NDBI of built-up areas, it means this index was not able to select urban areas in the study area.

This study used Landsat 8 thermal data (TIRS) that launched in 2013 at the beginning of this research. Most Landsat 8 data are available online while for Landsat 5 and 7 only some images are available. The results showed that it is appropriate to use in a study of LST and SUHI. However, some extra uncertainty results from Landsat channel 11 calibration. In Chapter 5, MODIS Aqua and Terra LST products were used for four time-passes during day and night. The result showed MODIS LST data are effective to show the diurnal cycling of LST in the day and night. Applying MODIS products to the relationship between LST and NDVI investigated for each season in this research adds details to the nature of the relationship between them.

The results indicate that during the daytime, the average LST in built-up areas within the city boundaries is lower than the mean LST in non-urban zones around the

city and the strongest SUHI occurs at night. The results of this study differ in this finding from other published studies of the UHI in wet regions. However, results of this research confirm results from some of the previous studies in dry areas. The reason is rural land in the dry season does not have large evaporation and transpiration effects to mitigate the temperature of the soil. The results indicate that the night-time SUHI is stronger in the spring and summer than the autumn and winter. On the other hand, daytime SUCI intensity in the autumn and summer is higher than the winter effect whilst it turns neutral in the spring. That shows the effect of vegetation in the rural areas to modify daytime LST and the disappearance of SUCI in the growing season of crop and grass, whereas night-time SUHI remains even in spring.

This thesis contributed through added knowledge on the nature of SUHI in semi-arid cities. The results from both Landsat and MODIS LST indicate the existence of SUCI during different times of the day and not only in the morning as stated in literature (Bornstein, 1968; Oke, 1982; Morris and Simmonds, 2000; Miao *et al*, 2009). In addition, this SUCI appearance was noted in all seasons except for spring when the intensity of the SUCI was poor/minimal due to vegetation growth in the surroundings of the city.

It was ascertained that a high bareness value is the significant factor corresponding to an increase in LST. Likewise, the results indicate wetness as a main potentially important factor in determining LST. NDVI of the rural areas was on average higher than the NDVI of the urban areas, especially in spring. The general relationship of LST and NDVI (MODIS) for the 12 year period was weakly negative. The peak of the inverse relationship is located in the spring while during the winter this relationship turns positive confirming the results of Sun and Kafatos (2007). It implies high LST associated with high NDVI in winter.

As expected, analysis of the effects of establishing S.A. Park demonstrated a cooling of 7.29°C in LST. In addition, the mean LST of new urbanised areas decreased by 2.28°C. The rapidly growing city of Erbil has led to a transformation of the surface to new materials that reduce sunlight more than natural soil and increasing green spaces, water bodies and soil moisture content. It implies urban expansion does not usually lead to increased surface temperature in all the cities. In contrast, increases of green areas and water body in the urban led to a significant decrease in LST and comfortable temperature.

7.4 Conclusions

This thesis has investigated (as outlined in Chapter 1) the spatial and temporal variation of the LST and SUCI/SUHI in Erbil - as a case study of cities situated in semi-arid climates - and has explored the influential drivers. In terms of urban climatology, it contributes in explaining dynamics of spatiotemporal LST in a semi-arid city focusing on daytime SUCI. Researchers can use remote sensing techniques which we used in this research and Erbil Governorate and city planners can benefit from results and recommendations of the research and apply them to achieve more temperature lowering, increasing comfort for Erbil dwellers.

In the second chapter of this thesis, the four main research questions that were asked were answered:

1) How does the land surface temperature and surface urban cool island vary spatially over the study area?

The low LST pattern and daytime SUCIs (negative SUHI) were associated with high density urban areas, while high LST patterns and SUHIs were correlated with bare land in rural areas and low density urbanisation in relatively new districts. This investigation of the spatial distribution of surface temperature in Erbil ascertained that there is an inverse relationship between the building density and the surface temperature. Inside the city centre and high-density districts, the surface temperature is reduced in comparison to the surroundings of the city. However, on the outskirts of the city and in the modern districts with low-density housing construction, the surface temperature is increased. A daytime SUCI effect is diagnosed for the city centre and a SUHI effect for the low-density developments.

The result demonstrated that during the daytime, residential areas within the city border recorded an LST of $46.2 \pm 1.74^{\circ}\text{C}$ while rural areas surrounding the city recorded $50.1 \pm 1.76^{\circ}\text{C}$. Urban Cool Island Intensity of the city in the morning (at ~07:40) was approximately -4°C when compared to a 10 km buffer zone around the city. Therefore, a variation from the rural to the compact low-rise areas may lead to decreased daytime surface temperature.

2) How does the land surface temperature and surface urban cool/heat island vary temporally over the study area?

During the 12 years covered by the MODIS time series, the greatest magnitude of SUCI occurs at approximately 11:00. However, the greatest magnitude of SUHI

emerged at ~22:00. In terms of diurnal variation, at ~11:00, the average LST of the city was lower than the rural and the city during the day experienced SUCI with higher intensity at ~11:00 than the SUCI intensity at ~13:00. On the other hand, the average LST of the city in 2014 at ~22:00 was higher than the LST of the rural area and the SUHI intensity was higher at ~22:00 than at ~02:00 at night. In terms of the most extreme SUCI and SUHI during these 12 years, in the morning SUCI was -5.37°C , and in the afternoon it was -5.32°C . The highest SUHI of early night was 4.59°C and it was 4.28°C in the late night.

In terms of seasonal variation, during the night in all seasons the city exhibits a SUHI with the different intensity. In the spring and summer, the intensity of the SUHI in the study area is higher than in autumn and winter. During the day-time the intensity of SUCI (negative SUHI) is higher in autumn and the summer and this intensity decreases in winter and changes to a slight SUCI in the spring, which is the growing season of grasses and cropland in rural areas. For this reason, the rural area absorbs the heat more slowly in spring compared to other seasons. During the summer, which is the hottest and the driest season, at 13:00 the average LST of the city is $50.36 \pm 1.35^{\circ}\text{C}$ and LST of the rural is $52.84 \pm 1.01^{\circ}\text{C}$ and SUCI Intensity is -2.48°C . During the night-time, the city exhibits a SUHI with the intensity around 3°C .

3) What are the main determinant variables of the SUCI/SUHI in Erbil?

The results of Chapter 4 - spatial variation - indicated that there is an inverse relationship between the building density and the surface temperature. The research ascertained a strong relationship between LST/SUCI with the wetness index and the Built-up index. Therefore, wetness and bareness are the main factors alongside building density leading to the SUCI in the semi-arid environment of Erbil. It concludes that in cities such as Erbil the surface wetness is the main marker of the SUCI.

In examining the key factors driven by LST in the study area, it ascertained that during the last 12 years NDVI of the rural area was higher than the NDVI of Erbil. In contrast, fsm in the city is higher than in the rural areas. The reason is that in the urban areas, residents add to the surface wetness by irrigation of urban green spaces, mainly in greener residential areas and urban parks (Souch and Grimmond 2006), while in the rural areas, generally agriculture depends on precipitation rather than irrigation. In the study area 93% of croplands are rain-fed (Fadhil 2011) and therefore the vast majority of croplands are definitely dry in the summer time.

The research ascertained a weak but significant inverse relationship between LST and average NDVI. This relationship is not on the same level in all seasons. During the spring season, the strongest inverse relationship is ascertained between LST and NDVI. This relationship weakened in the summer and was moderately strong (inverse) in autumn. However, in the winter, this relationship turns into a moderate positive relationship. A strong (significant) inverse relationship is ascertained between surface temperature and fsm. Therefore, Soil Moisture, Evapotranspiration and NDVI (during the spring) are the main factors leading to the SUCI/SUHI in the study area.

4) What is the effect of LULC change on LST and SUCI/SUHI in semi-arid climates?

By 2013, the majority of the S.A. Park had been converted to a greenspace and its mean NDVI increased by 0.23 compared to 1992. By contrast, the mean daytime LST of the park decreased by 7.29°C. During the same period, 55.3 km² around the city was transformed principally from 'bare soil' and 'field without vegetation' to 'urban'. The mean daytime LST of the new urbanized area decreased by 2.28°C. This result demonstrates that the LULC change from barren soil to urban areas in cities located in a semi-arid climate can cause a decrease in daytime LST. At the pixel-based level, we concluded that the mean daytime LST of the urbanized zone decreased as a result of transformation from bare soil and soil without vegetation to water body, vegetation, building and asphalt parking. By contrast, daytime LST increased due to a change from vegetation to bare soil by 5.84°C. In addition, this study demonstrates that the NRS method, which is proposed in this research, is appropriate for assessing temperature trends from urbanization using Landsat remote sensing data.

7.5 Limitations of the Research

The reader should bear in mind this research mainly relied on remotely sensed data while field measured data were utilised in the selection of land use classes and pixels in order to explore the effect of climatic elements on LST. Therefore, the research is lack in ground truth data. It has not covered surface LST versus canopy temperature which influences the comfort of city dwellers. The highest spatial resolution data used in this research is 60 m (Landsat ETM+) and the use of sensors with different spatial resolution is another weakness of this research. Thus, it is lack of enough images at high spatial resolution which limits applications. Technically, using

space-born data with higher spatial resolution for spatial variation and using satellite data (within more than four times pass) for temporal variations may give more advantages and contributions to the literature. Another limitation is calibration problem of the sensors such as Landsat 8 TIRS. Thus, NRS is not appropriate technique for LST change smaller than 2°C. Further work is also required to understand moisture indices versus building indices. The limitation of Landsat and MODIS overpass time for the study area does not include before and after sunrise and sunset to assess the highest SUHI at night and select the exact time of turn from daytime SUCI to night-time SUHI. This research therefore has some weaknesses due to the limited satellite view of the ground as well as emissivity of different ground materials. It needs more investigation of satellite characterisation of urban areas. In view of the fact that this study was limited to assessing a subset of all possible factors influencing the UHI effect, future studies should explore more factors that affect LST such as soil types, urban geometry, albedo and building components.

7.6 Future Research Directions

In general, future research should assess UHI in urban areas within the same climatic environment and examine the similarities and differences with the findings in this study. There is a need to utilise remote sensing data in investigating surface temperatures of cities in dry and semi-dry environments on a large scale. That study is a necessary requirement in the description of surface characteristics in this specific environmental climate class and to compare it with the results of this thesis.

Even higher spatial resolution with more temporal sampling and improved better calibrated data would be very useful. The application of higher resolution remote sensing data facilitates study on UHI characteristics and urban climate. Moreover, a future sensor improving on Landsat and aircraft thermal data are some possible options. On the other hand, in order to determine a temporal variation of LST using satellite data at restricted overpass times, it appears necessary to use field data to investigate diurnal UHI in dry environments. Future research should improve methods to simultaneously derive LST and LSE from hyperspectral TIR, multi spectral-temporal, TIR-microwave data, and methods should consider aerosol and cirrus effects (Li *et al.*, 2013).

It is hereby recommended that other research should focus on long-term in situ air temperature measurements for UCI/UHI exploration. This is due to the fact that this

type of UHI may have a more direct effect on the comfort of urban dwellers, especially if obtained from long-term measured data that are drawn from multi metrological stations in the city and surrounding towns.

In addition, another viable angle of future studies should focus on mitigation strategies for night-time SUHI and explore surface materials that can reduce surface temperature in urbanised areas. The result from this research has indicated a decrease in LST in vegetated areas while the variation between tree types should be quantified. Research should look more closely at different parts of the city as shown by the present study. Moreover, the area needs the development of more research on techniques to reduce LST in rural areas surrounding the city such as the effect of irrigated vegetation in the dry season and increased soil moisture through artificial streams.

Finally, as this research has examined and explored many variables that determine LST and SUCI, future research should focus on other factors such as building data, sky view factor, albedo, soil types, population size in each districts, the shape and the height of buildings.

Appendices

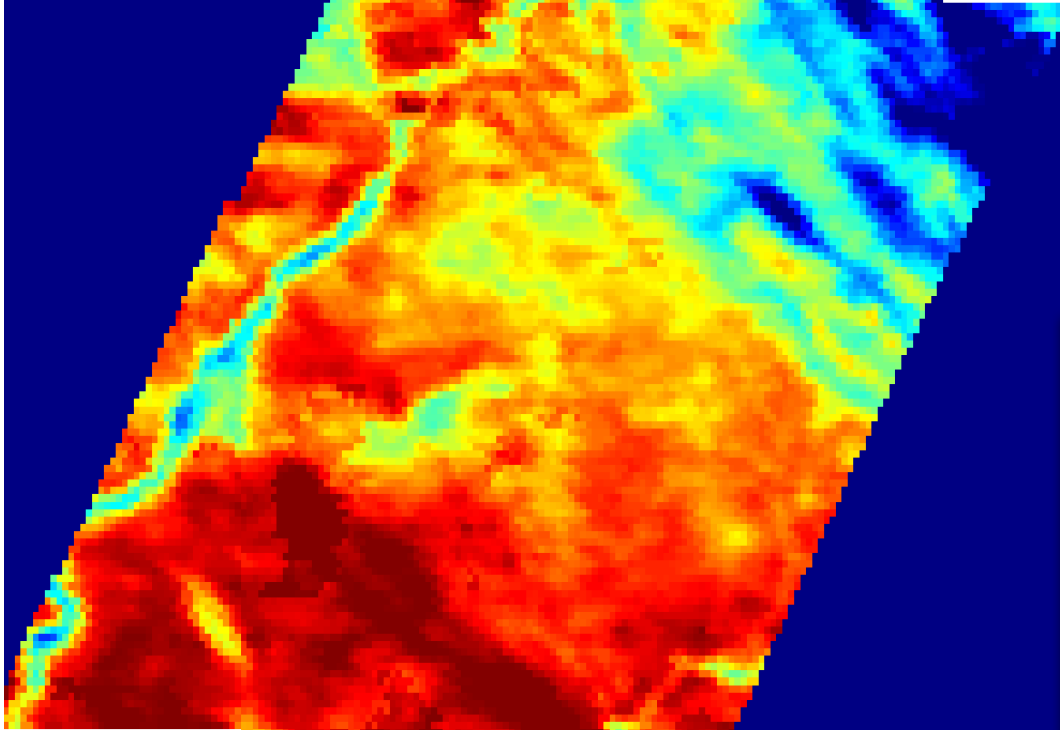


Figure A. 1: MODIS Terra LST daytime product (MOD11A2.A2002153)

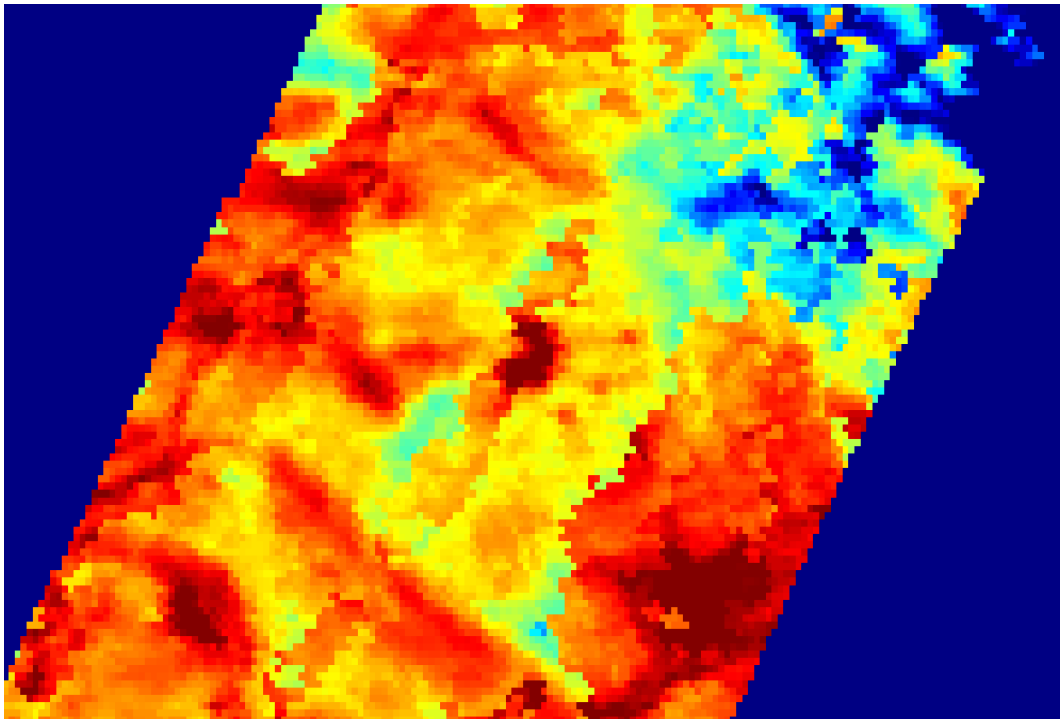


Figure A. 2: MODIS Terra LST night-time product (MOD11A2.A2006089)

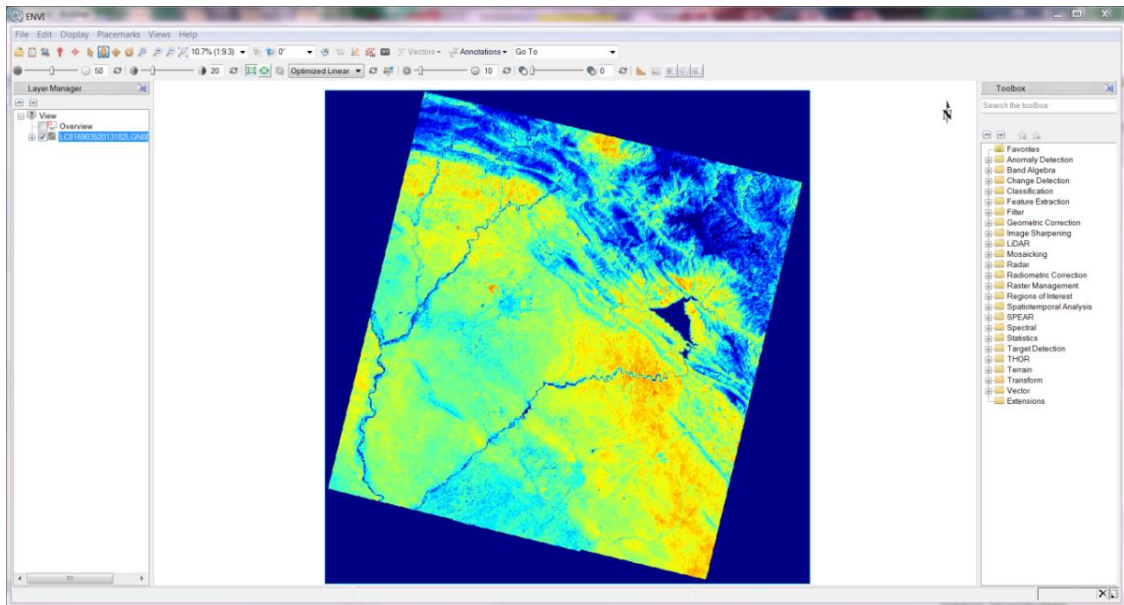


Figure A. 3: Landsat 8 band 10 for 01-07-2013.

View Metadata: LT41690351992213XXX02_MTL_MultiSpectral

	Band Names	Wavelengths	FWHM	Radiance Gains	Radiance Offset
1	Band 1	0.485	0.07	0.67921	-2.19921
2	Band 2	0.569	0.08	1.334	-4.17402
3	Band 3	0.659	0.06	1.0046	-2.17461
4	Band 4	0.841	0.14	0.87602	-2.38602
5	Band 5	1.676	0.2	0.12508	-0.49508
6	Band 7	2.222	0.27	0.065945	-0.21594

Figure A. 4: Metadata of Landsat 4 (LT41690351992213XXX02)

	Band Names	Wavelengths	FWHM	Radiance Gains	Radiance Of
1	Band 1	0.483	0.07	1.181	-7.38071
2	Band 2	0.56	0.08	1.21	-7.60984
3	Band 3	0.662	0.06	0.943	-5.94252
4	Band 4	0.835	0.12	0.969	-6.06929
5	Band 5	1.648	0.2	0.191	-1.19122
6	Band 7	2.206	0.26	0.066	-0.4165

Figure A. 5: Metadata of Landsat 7 (LE71690352002208SGS00)

	Band Names	Wavelengths	FWHM	Radiance Gains	Radiar
1	Coastal aerosol	0.443	0.016	0.012148	-60.738
2	Blue	0.4826	0.0601	0.012439	-62.197
3	Green	0.5613	0.0574	0.011463	-57.314
4	Red	0.6546	0.0375	0.0096661	-48.330
5	Near Infrared (NIR)	0.8646	0.0282	0.0059152	-29.575
6	SWIR 1	1.609	0.0847	0.001471	-7.3552
7	SWIR 2	2.201	0.1867	0.00049582	-2.4791

Figure A. 6: Metadata of Landsat 8 (LC81690352013182LGN00)

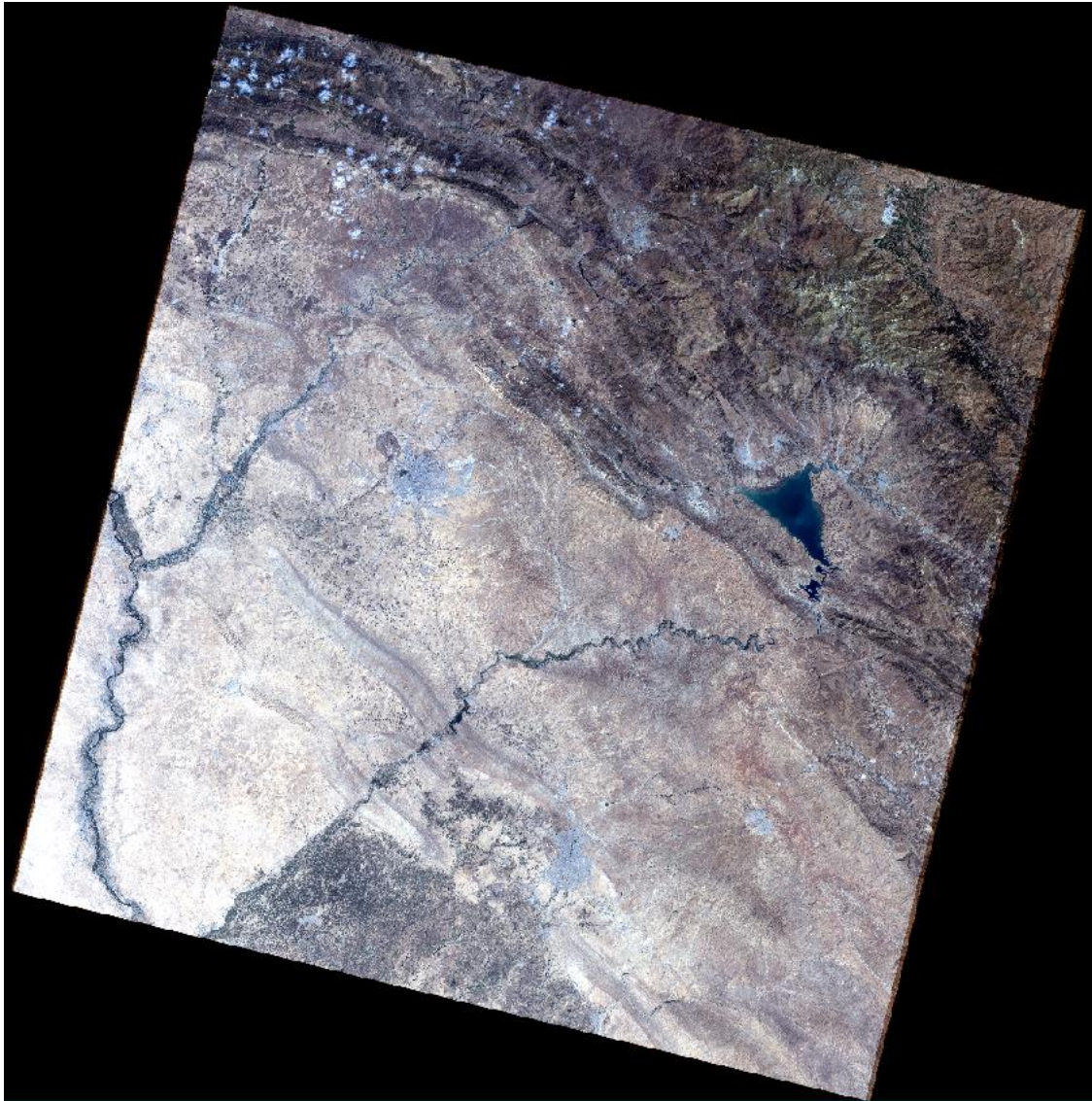


Figure A. 7: Landsat 8 true colour atmospherically corrected with QUAC method.

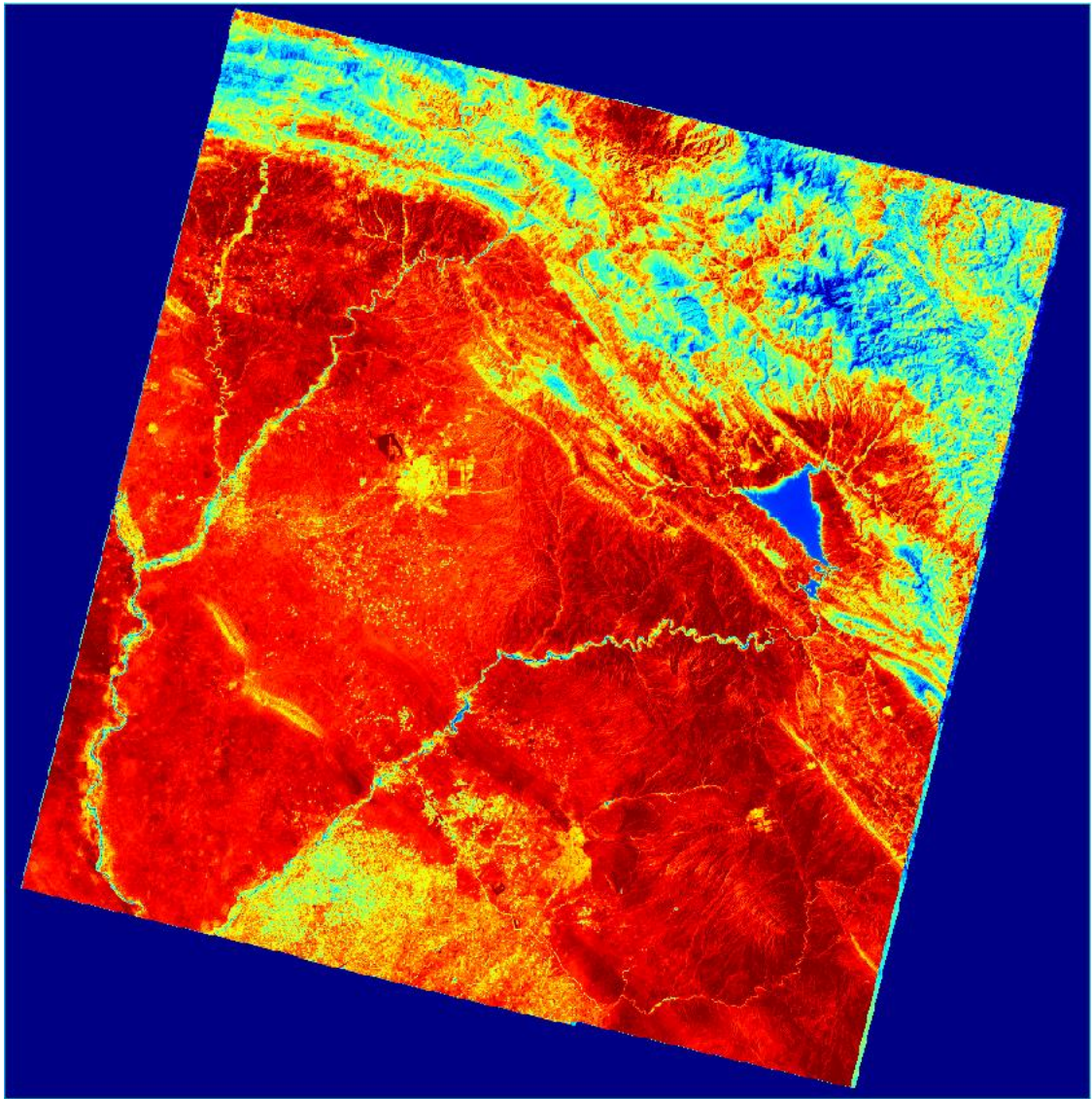


Figure A. 8: Radiance image of Landsat 8 band 10 atmospherically corrected with Thermal Atmospheric Correction method.

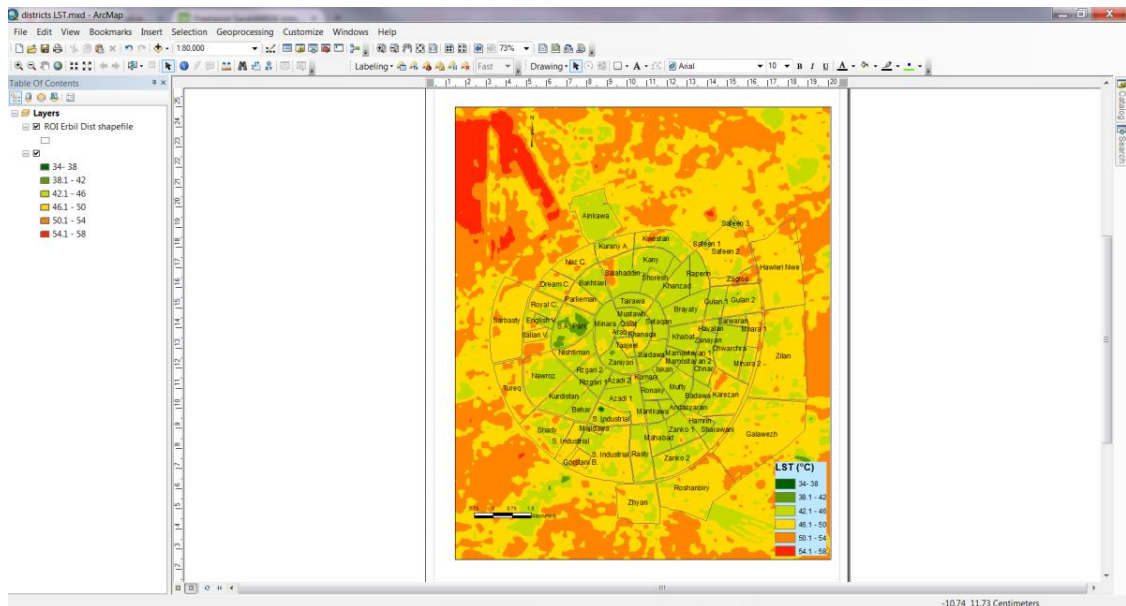


Figure A. 9: Using ArcGIS for create LST map of districts of Erbil from Landsat 8 combination data of 2013.

```

RGui (64-bit) - [Untitled - R Editor]
File Edit Packages Windows Help
library(raster)
#change directory to MODIS Aqua files
## List Aqua Day files
listAN <-list.files(pattern='_LST_Night_1km.tif$')
###Extract file names
S<-paste0(listAN)
S2<-gsub("MYD11A2", "", S)
### Assign file names to file list
names(listAN)<-S2
###Multiplying to the scale factor of LST
funR<-function(x) { D<-raster (x)
  lai<-D * 0.02
# convert 0 to NA data
#lai[lai==0]<-NA
#Convert LST K to C
  lai<-lai - 273.15
S<-paste0(x)
### Change extensions
extension(S) <- 'tif'
### Save list results
writeRaster(lai, filename=S, format="GTiff", file.path("Z:/Desktop Files/Aqua/"),overwrite=T)
###Apply function to list of files
listAN2<-sapply(listAN, funR)
####Stack result of Aqua day list
listANstack<-stack(listAN2)
####save stacked list
writeRaster(listANstack,filename= "ListStacked_AN", format="GTiff")

```

Figure A. 10: R script for processing LST MODIS products.

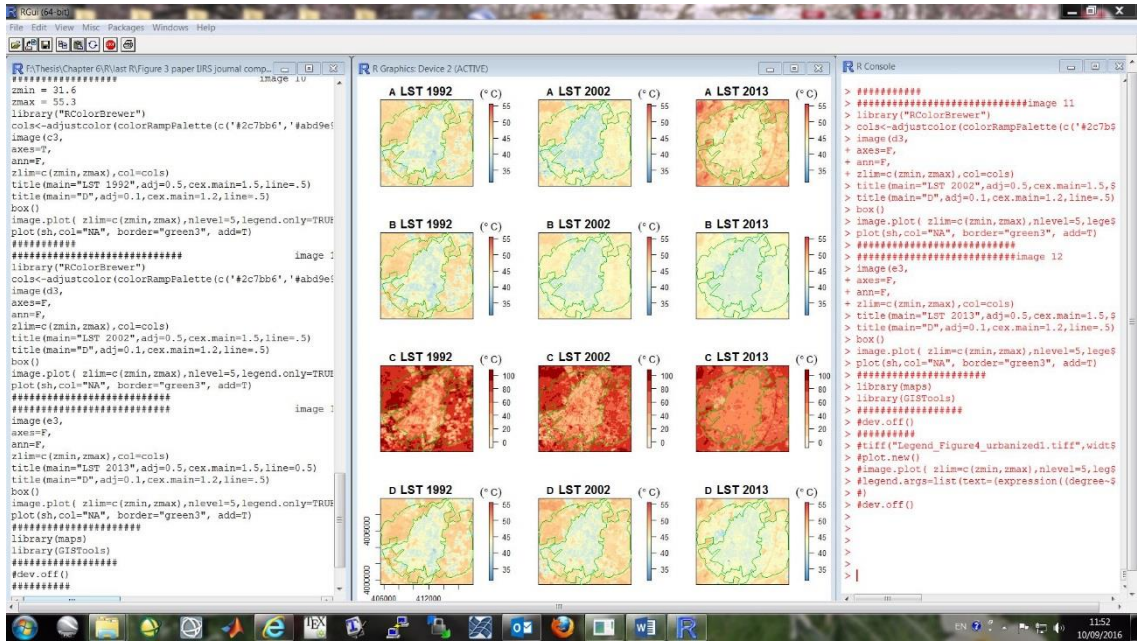


Figure A. 11: R script for produce LST of urbanised areas from 1992 to 2013 through different techniques.

	A	B	C	D	E	F	G	H	I
1		City	City	City	City	Buffer	Buffer	Buffer	Buffer
2	Years	winter	spring	summer	autumn	winter	spring	summer	autumn
3	2003	0.24	0.28	0.14	0.16	0.3	0.4	0.16	0.17
4	2004	0.22	0.25	0.14	0.16	0.28	0.36	0.16	0.18
5	2005	0.25	0.23	0.13	0.13	0.33	0.33	0.14	0.15
6	2006	0.15	0.2	0.13	0.15	0.23	0.32	0.16	0.17
7	2007	0.2	0.22	0.13	0.12	0.28	0.38	0.15	0.15
8	2008	0.12	0.13	0.11	0.13	0.18	0.19	0.12	0.15
9	2009	0.16	0.15	0.12	0.12	0.21	0.23	0.13	0.15
10	2010	0.2	0.18	0.13	0.12	0.36	0.36	0.15	0.15
11	2011	0.15	0.16	0.12	0.13	0.26	0.28	0.14	0.16
12	2012	0.12	0.14	0.12	0.13	0.19	0.23	0.13	0.16
13	2013	0.19	0.17	0.13	0.13	0.36	0.33	0.14	0.16
14	2014	0.16	0.16	0.12	0.16	0.32	0.31	0.14	0.21
15	average	0.18	0.19	0.13	0.14	0.27	0.31	0.14	0.16
16	sd	0.04	0.05	0.01	0.02	0.06	0.07	0.01	0.02

Figure A. 12: Extracted NDVI data for the city and surrounding for different seasons as Excel file.

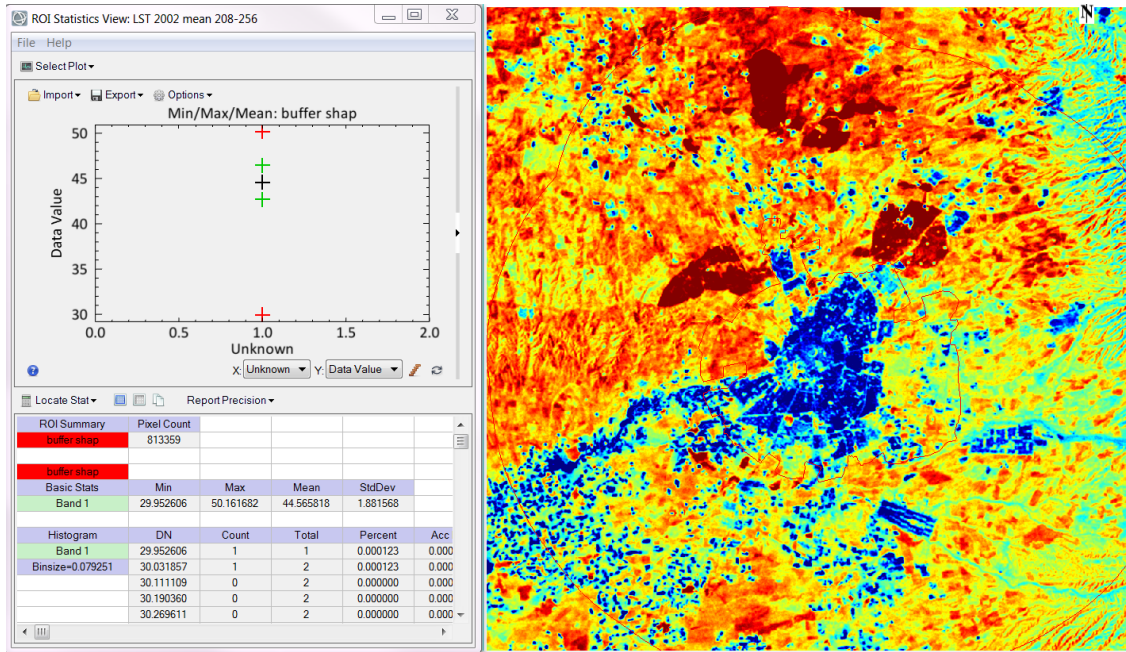


Figure A. 13: Statistical output of LST of 2002 from Landsat for the study area within ENVI software.

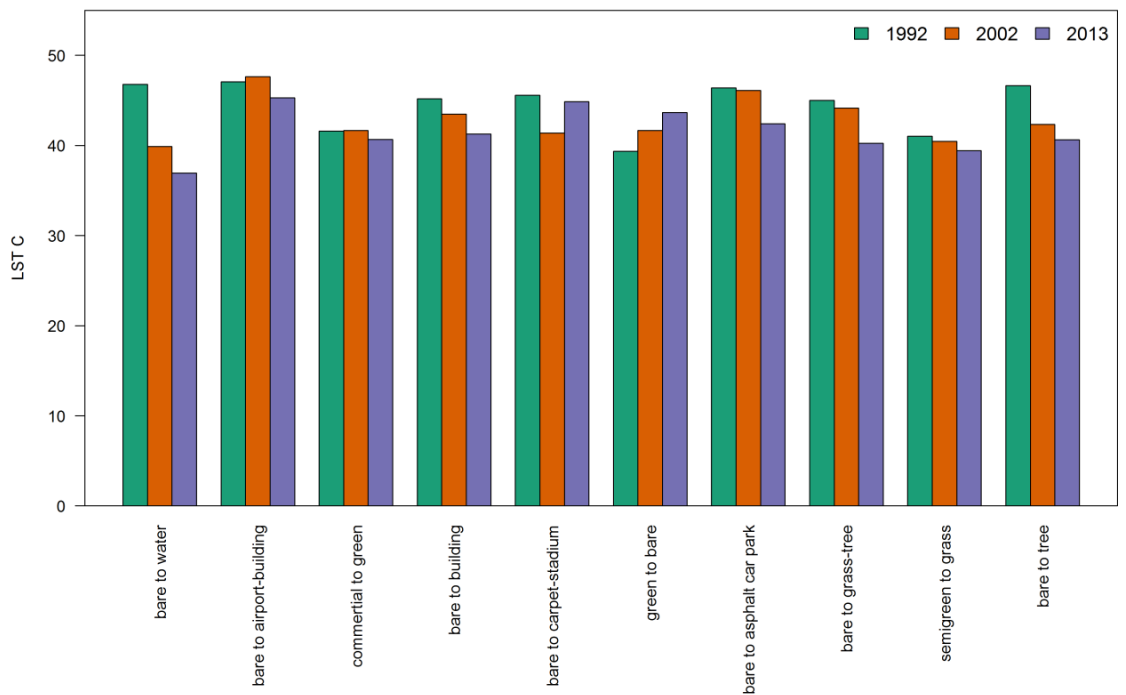


Figure A. 14: LST of pixel samples of LULC change.

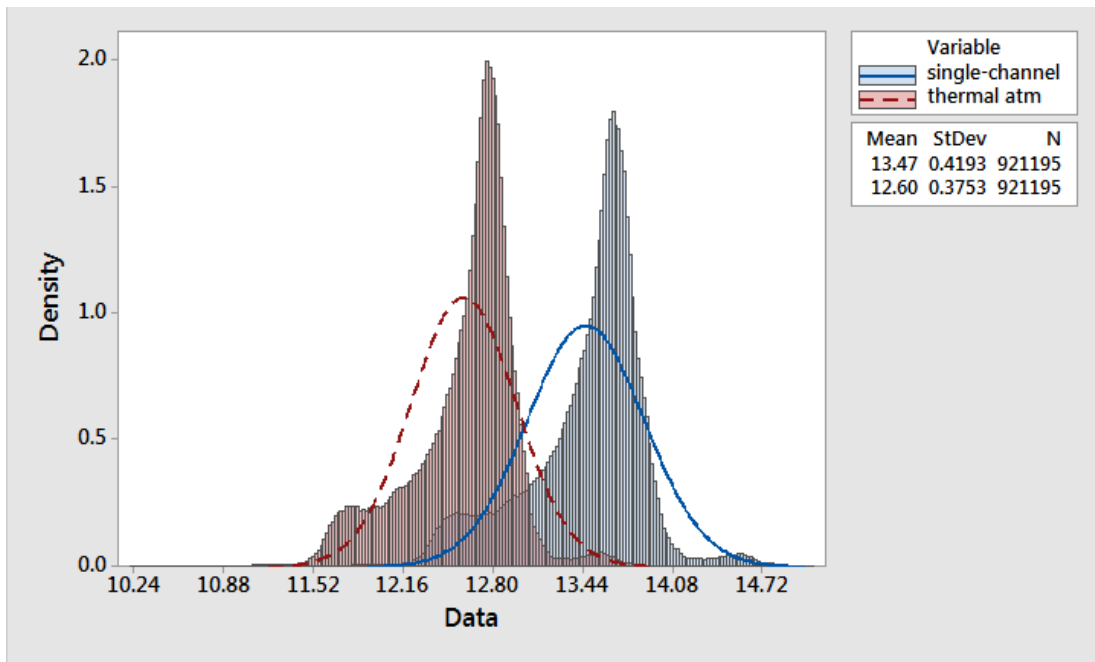


Figure A. 15: Radiance atmospherically corrected from single channel and thermal atmospheric correction.

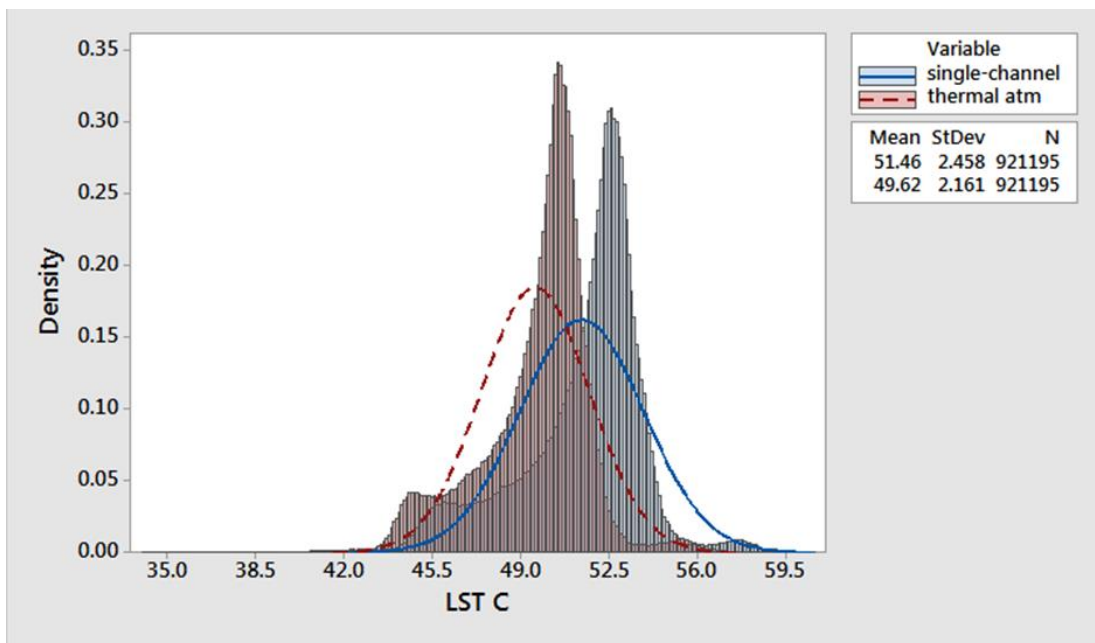


Figure A. 16: LST atmospherically corrected from single channel and thermal atmospheric correction.

Bibliography

- Abdollahi, J., Cheraghi, S. and Rahimian, M. (2008) 'Comparing the environmental effects of land use changes on vegetation cover and emitted land surface temperature in urban and non-urban areas using remote sensing', 34, pp. 85-96.
- Abdullah, H. (2012) *The Use of Landsat 5 TM Imagery to Detect Urban Expansion and Its Impact on Land Surface Temperatures in The City of Erbil, Iraqi Kurdistan*. MSc. University of Leicester.
- Abdulrahman, I. (2014) *Energy efficient buildings in a hot and dry climate*. Master. Mälardalens University. Available at: https://apps.icarda.org/wsInternet/wsInternet.aspx/DownloadFileToLocal?filePath=Working_Paper_Series/working_paper27.pdf&fileName=working_paper27.pdf.
- Akther, M.S. and Hassan, Q.K., 2011. Remote sensing based estimates of surface wetness conditions and growing degree days over northern Alberta, Canada. *Boreal environment research*, 16(5).
- Al-Ali, A.M.H. (2015) *The Effect of Land Cover on the Air and Surface Urban Heat Island of a Desert Oasis*. PhD. Durham University. Available at: <http://etheses.dur.ac.uk/11290/>.
- Alberti, M. and Marzluff, J.M. (2004) 'Ecological resilience in urban ecosystems: linking urban patterns to human and ecological functions', *Urban ecosystems*, 7(3), pp. 241-265.
- Albrecht, F. (1952) 'Mikrometeorologische Temperaturmessungen vom Flugzeug aus', *Ber.Deutsch.Wetterdienst, Bad Kissingen*, 38, pp. 332.
- Al-Hashimi, F.W. and Bandyopadhyay, S. (2015) 'The Persistent Element in the Old Urban Fabric, Erbil Bazar Area', *Journal of Strategic Innovation and Sustainability Vol*, 10(2), pp. 48-57.
- Amiri, R., Weng, Q., Alimohammadi, A. and Alavipanah, S.K. (2009) 'Spatial-temporal dynamics of land surface temperature in relation to fractional vegetation cover and land use/cover in the Tabriz urban area, Iran', *Remote Sensing of Environment*, 113(12), pp. 2606-2617.
- Arnfield, A.J., 1982. An approach to the estimation of the surface radiative properties and radiation budgets of cities. *Physical Geography*, 3(2), pp.97-122.
- Aufmuth, J.L. (2001) *A comparison of the normalized difference and the tasseled cap vegetation indices: a case study of using satellite remote sensing imagery for assessment of environmental impact of a hydroelectric power project on the River*

Danube. Master. University of Florida. Available at:

<http://etd.fcla.edu/UF/ank6404/thesis.pdf>.

- Baboo, S.S. and Devi, M.R., 2010. An analysis of different resampling methods in Coimbatore, District. *Global Journal of Computer Science and Technology*, 10(15).
- Baig, M.H.A., Zhang, L., Shuai, T. and Tong, Q. (2014) 'Derivation of a tasselled cap transformation based on Landsat 8 at-satellite reflectance', *Remote Sensing Letters*, 5(5), pp. 423-431.
- Bajaj, D.N., Inamdar, A.B. & Vaibhav, V. (2012) 'Temporal variation of Urban Heat Island using Landsat data: A case study of Ahmedabad, India', *33rd Asian Conference on Remote Sensing 2012, ACRS 2012 Pattaya, Thailand*, 26-30 November, pp. 797-804.
- Baker, L.A., Brazel, A.T. and Westerhoff, P. (2004) 'Environmental consequences of rapid urbanization in warm, arid lands: Case study of Phoenix, Arizona (USA)', *Sustainable cities*, 18, pp. 155-164.
- Baker, L.A., Brazel, A.J., Selover, N., Martin, C., McIntyre, N., Steiner, F.R., Nelson, A. and Musacchio, L. (2002) 'Urbanization and warming of Phoenix (Arizona, USA): Impacts, feedbacks and mitigation', *Urban ecosystems*, 6(3), pp. 183-203.
- Baper, S., Y., Hassan, A.S. & Ismail, S.T. (2010) 'Modernization Theory and House Garden Transformation: A case Study in Erbil City', *Proceeding Papers of 2nd International Seminar on Tropical Eco-Settlements*, in Denpasar, Bali, Indonesia 3-5 November 2010.
- Barducci, A. and Pippi, I. (1996) 'Temperature and emissivity retrieval from remotely sensed images using the "grey body emissivity" method', *IEEE Transactions on Geoscience and Remote Sensing*, 34(3), pp. 681-695.
- Barring, L., Mattsson, J. and Lindqvist, S. (1985) 'Canyon geometry, street temperatures and urban heat island in Malmö, Sweden', *Journal of Climatology*, 5(4), pp. 433-444.
- Barsi, J.A., Schott, J.R., Hook, S.J., Raqueno, N.G., Markham, B.L. and Radocinski, R.G., 2014. Landsat-8 thermal infrared sensor (TIRS) vicarious radiometric calibration. *Remote Sensing*, 6(11), pp.11607-11626.
- Barsi, J., Barker, J.L. & Schott, J.R. (2003) 'An atmospheric correction parameter calculator for a single thermal band earth-sensing instrument', *Geoscience and Remote Sensing Symposium, 2003 (IGARSS)*. Toulouse, France, 21-25 July.
- Becker, F. and Li, Z.-. (1990) 'Temperature-independent spectral indices in thermal infrared bands', *Remote Sensing of Environment*, 32(1), pp. 17-33.

- Binyan, Y., Wenjie, F., Xin, T. & Xiru, X. (2008) 'Study on Urban Heat Island of Beijing using ASTER Data - A Quantative Remote Sensing Perspective', *International Geoscience and Remote Sensing Symposium (IGARSS)* Boston, MA, United States, 6-11 July.
- Bonan, G.B. (2002) *Ecological climatology: concepts and applications*. Cambridge: Cambridge University Press.
- Borel, C.C. (1997) 'Iterative retrieval of surface emissivity and temperature for a hyperspectral sensor', *First JPL Workshop on Remote Sensing of Land Surface Emissivity* Pasadena, CA, United States, 6-8 May United States: Los Alamos National Lab., NM (United States).
- Borgatti, S., 2016, Normalizing Variables. [ONLINE] Available at:
<http://www.analytictech.com/ba762/handouts/normalization.htm>. [Accessed 27 August 2016].
- Bornstein, R.D. (1968) 'Observations of the urban heat island effect in New York City', *Journal of Applied Meteorology*, 7(4), pp. 575-582.
- Bowler, D.E., Buyung-Ali, L., Knight, T.M. and Pullin, A.S. (2010) 'Urban greening to cool towns and cities: A systematic review of the empirical evidence', *Landscape and Urban Planning*, 97(3), pp. 147-155.
- Brazel, S.W. and Balling Jr, R.C. (1986) 'Temporal analysis of long-term atmospheric moisture levels in Phoenix, Arizona', *Journal of climate and applied meteorology*, 25(2), pp. 112-117.
- Buringh, P. (1960) *Soils and soil conditions in Iraq*. Baghdad, Iraq: Ministry of agriculture.
- Buyantuyev, A. and Wu, J. (2010) 'Urban heat islands and landscape heterogeneity: linking spatiotemporal variations in surface temperatures to land-cover and socioeconomic patterns', *Landscape Ecology*, 25(1), pp. 17-33.
- Ca, V.T., Asaeda, T. and Abu, E.M. (1998) 'Reductions in air conditioning energy caused by a nearby park', *Energy and Buildings*, 29(1), pp. 83-92.
- Carlson, T.N. and Arthur, S.T. (2000) 'The impact of land use-land cover changes due to urbanization on surface microclimate and hydrology: a satellite perspective', *Global and Planetary Change*, 25(1-2), pp. 49-65.
- Carlson, T.N., Dodd, J.K., Benjamin, S.G. and Cooper, J.N. (1981) 'Satellite estimation of the surface energy balance, moisture availability and thermal inertia', *Journal of Applied Meteorology*, 20(1), pp. 67-87.

- Celestian, S.B. and Martin, C.A. (2004) 'Rhizosphere, surface, and air temperature patterns at parking lots in Phoenix, Arizona, US', *Journal of Arboriculture*, 30(4), pp. 245-252.
- Cenedese, A. and Monti, P. (2003) 'Interaction between an inland urban heat island and a sea-breeze flow: A laboratory study', *Journal of Applied Meteorology*, 42(11), pp. 1569-1583.
- Chander, G., and B. Markham, 2003, Revised Landsat-5 TM radiometric calibration procedures and postcalibration dynamic ranges. *IEEE Transactions on Geoscience and Remote Sensing*, 41, pp. 2674-2677.
- Chang, C., Li, M. and Chang, S. (2007) 'A preliminary study on the local cool-island intensity of Taipei city parks', *Landscape and Urban Planning*, 80(4), pp. 386-395.
- Chapman, L., Azevedo, J.A. and Prieto-Lopez, T. (2013) 'Urban heat & critical infrastructure networks: A viewpoint', *Urban Climate*, 3, pp. 7-12.
- Chen, X., Zhao, H., Li, P. and Yin, Z. (2006) 'Remote sensing image-based analysis of the relationship between urban heat island and land use/cover changes', *Remote Sensing of Environment*, 104(2), pp. 133-146.
- Cheval, S., Dumitrescu, A. and Bell, A. (2009) 'The urban heat island of Bucharest during the extreme high temperatures of July 2007', *Theoretical and Applied Climatology*, 97(3-4), pp. 391-401.
- Cheval, S. and Dumitrescu, A., 2009. The July urban heat island of Bucharest as derived from modis images. *Theoretical and applied climatology*, 96(1-2), pp.145-153.
- Chow, W.T., Brennan, D. and Brazel, A.J. (2012) 'Urban heat island research in Phoenix, Arizona: Theoretical contributions and policy applications', *Bulletin of the American Meteorological Society*, 93(4), pp. 517-530.
- Chow, W.T. and Roth, M. (2006) 'Temporal dynamics of the urban heat island of Singapore', *International Journal of Climatology*, 26(15), pp. 2243-2260.
- Chuvieco, E. and Huete, A. (2010) *Fundamentals of satellite remote sensing*. CRC Press Inc. Boca Raton, FL 33487, USA.
- Clark, R.N., Swayze, G.A., Heidebrecht, K., Green, R.O. & Goetz, F.H. (1995) 'Calibration to surface reflectance of terrestrial imaging spectrometry data: Comparison of methods', *Summaries of the Fifth Annual JPL Airborne Earth Science Workshop*. Pasadena, CA, United States, 23 January United States: United States, pp. 41-42.
- Clinton, N. and Gong, P. (2013) 'MODIS detected surface urban heat islands and sinks: Global locations and controls', *Remote Sensing of Environment*, 134, pp. 294-304.

- Coll, C., Galve, J.M., Sanchez, J.M. and Caselles, V. (2010) 'Validation of Landsat-7/ETM thermal-band calibration and atmospheric correction with ground-based measurements', *IEEE Transactions on Geoscience and Remote Sensing*, 48(1), pp. 547-555.
- Coll, C., Caselles, V., Rubio, E., Sospedra, F. and Valor, E. (2001) 'Temperature and emissivity separation from calibrated data of the Digital Airborne Imaging Spectrometer', *Remote Sensing of Environment*, 76(2), pp. 250-259.
- Combs, A.C. (1961) *Techniques and Results of Infrared Surface-temperature Measurements in New Jersey and Greenland*. US Army Signal Research and Development Laboratory.
- Cook, M., Schott, J.R., Mandel, J. and Raqueno, N., 2014. Development of an operational calibration methodology for the Landsat thermal data archive and initial testing of the atmospheric compensation component of a Land Surface Temperature (LST) product from the archive. *Remote Sensing*, 6(11), pp.11244-11266.
- Copernicus (2016) *Land Surface Temperature | Copernicus Global Land Service*. Available at: <http://land.copernicus.eu/global/products/lst>.
- Crist, E.P. and Cicone, R.C. (1984) 'A physically-based transformation of Thematic Mapper data---The TM Tasseled Cap', *IEEE Transactions on Geoscience and Remote Sensing*, GE-22(3), pp. 256-263.
- Crum, S. (2016) *The Geographer's Craft Project, Department of Geography, The University of Colorado at Boulder*. Available at: <http://www.colorado.edu/geography/gcraft/notes/remote/remote.html>.
- Cui, Y.Y. and De Foy, B. (2012) 'Seasonal variations of the urban heat island at the surface and the near-surface and reductions due to urban vegetation in Mexico City', *Journal of Applied Meteorology and Climatology*, 51(5), pp. 855-868.
- DESA, U. 2014 *United Nations, Department of Economic and Social Affairs, Population Division (2014). World Urbanization Prospects: The 2014 Revision, CD-ROM Edition.*, UN DESA, New York, USA.
- Dhorde, A. and Dhorde, A. (2012) *Surface Urban Heat Island*. Saarbrücken, Germany: LAP Lambert Academic Publishing.
- DiStasio Jr., R.J. & Resmini, R.G. (2010) 'Atmospheric compensation of thermal infrared hyperspectral imagery with the emissive empirical line method and the in-scene atmospheric compensation algorithms: a comparison', *SPIE - The International Society for Optical Engineering*. Orlando, FL, United States, 5-8 April.

- Dizayee, R.H. (2014) *Groundwater Degradation and Sustainability of the Erbil Basin, Erbil, Kurdistan Region, Iraq*. Master. Texas Christian University. Available at: <https://repository.tcu.edu/handle/116099117/6044>.
- Du, C., Ren, H., Qin, Q., Meng, J. and Zhao, S. (2015) 'A practical split-window algorithm for estimating land surface temperature from Landsat 8 data', *Remote Sensing*, 7(1), pp. 647-665.
- Elachi, C. and Van Zyl, J. (2006) *Introduction to the physics and techniques of remote sensing*. Second edn. Hoboken, NJ, USA: John Wiley & Sons.
- EPA (2009) 'Reducing Urban Heat Islands: Compendium of Strategies Urban Heat Island Basics', in Anonymous .
- Erbiltourism2014 (2014) *Erbil seeking access to international standards of green areas*. Available at: <http://erbiltourism2014.com/en/erbil/news/113-erbil-seeking-access-to-international-standards-of-green-areas>.
- Etzion, Y. (1990) 'The Thermal Behaviour of Non-Shaded Closed Courtyards in Hot-Arid Zones [1]', *Architectural Science Review*, 33(3), pp. 79-83.
- Fadhil, A.M. (2011) 'Drought mapping using Geoinformation technology for some sites in the Iraqi Kurdistan region', *International Journal of Digital Earth*, 4(3), pp. 239-257.
- Farina, A. (2012) *Exploring the relationship between land surface temperature and vegetation abundance for urban heat island mitigation in Seville, Spain*. Master. Lund University. Available at: <http://lup.lub.lu.se/record/3460284/file/3460402.pdf>.
- Flanagan, M. & Civco, D.L. (2001) 'Subpixel impervious surface mapping', *Proceedings of American Society for Photogrammetry and Remote Sensing Annual Convention* St. Louis, MO, USA, 23-27 April.
- Florio, E., Lele, S., Chi Chang, Y., Sterner, R. and Glass, G. (2004) 'Integrating AVHRR satellite data and NOAA ground observations to predict surface air temperature: a statistical approach', *International Journal of Remote Sensing*, 25(15), pp. 2979-2994.
- Frey, C.M., Rigo, G., Parlow, E. & Marçal, A. (2005) 'The cooling effect of cities in a hot and dry environment', *Global developments in environmental earth observation from space* Porto, Portugal, 6-11 June.
- Frey, C.M., Rigo, G. and Parlow, E. (2012) 'Investigation of the daily Urban Cooling Island (UCI) in two coastal cities in an arid environment: Dubai and Abu Dhabi (UAE)', *City*, 81.

- Gago, E., Roldan, J., Pacheco-Torres, R. and Ordóñez, J. (2013) 'The city and urban heat islands: A review of strategies to mitigate adverse effects', *Renewable and Sustainable Energy Reviews*, 25, pp. 749-758.
- Gallo, K.P. and Owen, T.W. (1998) 'Assessment of urban heat Islands: A multi-sensor perspective for the Dallas-Ft. worth, USA region', *Geocarto International*, 13(4), pp. 35-41.
- Gallo, K., McNab, A., Karl, T., Brown, J., Hood, J. and Tarpley, J. (1993) 'The use of NOAA AVHRR data for assessment of the urban heat island effect', *Journal of Applied Meteorology*, 32(5), pp. 899-908.
- Gao, B., Davis, C.O. & Goetz, A.F.H. (2006) 'A review of atmospheric correction techniques for hyperspectral remote sensing of land surfaces and ocean color', *International Geoscience and Remote Sensing Symposium (IGARSS)* Denver, CO; United States, 31 July - 4 August.
- Gao, B., Heidebrecht, K.B. and Goetz, A.F. (1993) 'Derivation of scaled surface reflectances from AVIRIS data', *Remote Sensing of Environment*, 44(2), pp. 165-178.
- Ghazal, N.K. and Hassoon, K.I. (2012) 'Temperature calculation using thermal bands of (ETM) sensor', *Iraqi Journal of Science*, 53(2), pp. 435-443.
- Ghent, D., Kaduk, J., Remedios, J., Ardö, J. and Balzter, H. (2010) 'Assimilation of land surface temperature into the land surface model JULES with an ensemble Kalman filter', *Journal of Geophysical Research Atmospheres*, 115(19), pp. D19112-1-D19112-16.
- Gillespie, A.R. (1985) 'Lithologic mapping of silicate rocks using TIMS', *Proceedings TIMS Data User's Workshop* Pasadena, CA, USA Jet Propulsion Laboratory.
- Gillespie, A.R., Rokugawa, S., Hook, S.J., Matsunaga, T. and Kahle, A.B. (eds.) (1999) *Temperature/emissivity separation algorithm theoretical basis document*, version 2.4. Greenbelt, MD, USA: NASA/GSFC.
- Golden, J.S., Brazel, A., Salmond, J. and Laws, D. (2006) 'Energy and water sustainability: The role of urban climate change from metropolitan infrastructure', *Journal of Engineering for Sustainable Community Development*, 1(1), pp. 55-70.
- Grossman-Clarke, S., Zehnder, J.A., Loridan, T. and Grimmond, C.S.B. (2010) 'Contribution of land use changes to near-surface air temperatures during recent summer extreme heat events in the Phoenix metropolitan area', *Journal of Applied Meteorology and Climatology*, 49(8), pp. 1649-1664.
- Guoyin, C. & Mingyi, D. (2009) 'Relationship between thermal inertia and urban heat sink in Beijing derived from Satellite images', *2009 Joint Urban Remote Sensing Event* Shanghai, China, 20-22 May.

- Gutman, G. (1999) 'On the monitoring of land surface temperatures with the NOAA/AVHRR: removing the effect of satellite orbit drift', *International Journal of Remote Sensing*, 20(17), pp. 3407-3413.
- Habib, B. (2007) 'The Urban Heat Island of Dammam city, The Study by Using Remote Sensing and GIS', *The second forum of GIS*, Al Khobar, Saudi Arabia, 23-25 April.
- Hafner, J. and Kidder, S.Q. (1999) 'Urban heat island modeling in conjunction with satellite-derived surface/soil parameters', *Journal of Applied Meteorology*, 38(4), pp. 448-465.
- Hama, R., H., Hamad, R., T. & Aziz, F., H. (2014) 'Climate change in relation to rainfall and temperature in Erbil province, Kurdistan, Iraq', *8th Geo Tunis Conference Hammamet*, Tunisia, 2-6 April.
- Hameed, H. (2013) *Water harvesting in Erbil Governorate, Kurdistan region, Iraq: detection of suitable sites using geographic information system and remote sensing*. Master. Lund University. Available at: <http://lup.lub.lu.se/student-papers/record/3737025/file/3737039.pdf>.
- Hansen, P.C. (1998) *Rank-deficient and discrete ill-posed problems: numerical aspects of linear inversion*. SIAM, Philadelphia, PA 19104-2688 USA.
- Hao, X. and Li, W. (2016) 'Oasis cold island effect and its influence on air temperature: a case study of Tarim Basin, Northwest China', *Journal of Arid Land*, 8(2), pp. 172-183.
- Harlan, S.L., Brazel, A.J., Prashad, L., Stefanov, W.L. and Larsen, L. (2006) 'Neighborhood microclimates and vulnerability to heat stress', *Social science & medicine*, 63(11), pp. 2847-2863.
- Hasan, T. (2006) *Geographical Analysis of the Characteristics of the Temperature in the Kurdistan Region of Iraq*. Master. University of Salahaddin.
- Hawkins, T.W., Brazel, A.J., Stefanov, W.L., Bigler, W. and Saffell, E.M., 2004. The role of rural variability in urban heat island determination for Phoenix, Arizona. *Journal of Applied Meteorology*, 43(3), pp.476-486.
- Hawlergov (2012) *Images of Erbil Citadel*. Available at: <http://www.hawlergov.org/ku/album.php?id=21> (Accessed: 24 March 2016).
- Hoffmann, P., Krueger, O. and Schlünzen, K.H. (2012) 'A statistical model for the urban heat island and its application to a climate change scenario', *International Journal of Climatology*, 32(8), pp. 1238-1248.
- Howard, L. (1833) *The climate of London: deduced from meteorological observations made in the metropolis and at various places around it*. Harvey and Darton, J. and A. Arch, Longman, Hatchard, S. Highley [and] R. Hunter.

- Hsu, S. (1984) 'Variation of an urban heat island in Phoenix', *The Professional Geographer*, 36(2), pp. 196-200.
- Ibrahim, R.I., Mushatat, S.A. and Abdelmonem, M.G. (2015) 'Erbil', *Cities*, 49, pp. 14-25.
- Ibrahim, R., Mushatat, S. and Abdelmonem, M.G. (2014) 'Authenticity, indentity and sustainability in post-war Iraq: Reshaping the Urban Form of Erbil City', *Journal of Islamic Architecture*, 3(2), pp. 58-68.
- Imhoff, M.L., Zhang, P., Wolfe, R.E. and Bounoua, L., 2010. Remote sensing of the urban heat island effect across biomes in the continental USA. *Remote Sensing of Environment*, 114(3), pp.504-513.
- IOM Iraq (2015) 'Erbil Governorate Profile'. Available online: http://reliefweb.int/sites/reliefweb.int/files/resources/Erbil_governorate_profile_May_2015.pdf. (Accessed on 26 August 2016).
- Jaggi, S., Quattrochi, D. & Baskin, R. (1992) 'An algorithm for the estimation of bounds on the emissivity and temperatures from thermal multispectral airborne remotely sensed data', *Proceedings of SPIE - The International Society for Optical Engineering* Orlando, FL, USA, 22-24 April Bellingham, WA, United States.
- Jang, K., Kang, S., Lim, Y., Jeong, S., Kim, J., Kimball, J.S. and Hong, S.Y. (2013) 'Monitoring daily evapotranspiration in Northeast Asia using MODIS and a regional Land Data Assimilation System', *Journal of Geophysical Research Atmospheres*, 118(23), pp. 12927-12940.
- Jassim, H.M., Kurdi, Y.A.A. and Al-nidai, F.H.I. (2013) 'Environmental Issues in Erbil City', *International Journal of Engineering Trends and Technology*, 4(8), pp. 3509-3515.
- Jauregui, E. (1997) 'Heat island development in Mexico City', *Atmospheric Environment*, 31(22), pp. 3821-3831.
- Jenerette, G.D., Harlan, S.L., Brazel, A., Jones, N., Larsen, L. and Stefanov, W.L. (2007) 'Regional relationships between surface temperature, vegetation, and human settlement in a rapidly urbanizing ecosystem', *Landscape Ecology*, 22(3), pp. 353-365.
- Ji, M. and Jensen, J.R. (1999) 'Effectiveness of subpixel analysis in detecting and quantifying urban imperviousness from Landsat Thematic Mapper imagery', *Geocarto International*, 14(4), pp. 33-41.
- Jiang, J. and Tian, G. (2010) 'Analysis of the impact of land use/land cover change on land surface temperature with remote sensing', *Procedia environmental sciences*, 2, pp. 571-575.

- Jiménez-Muñoz, J.C. and Sobrino, J.A. (2003) 'A generalized single-channel method for retrieving land surface temperature from remote sensing data', *Journal of Geophysical Research*, 108(22).
- Jin, S. and Sader, S.A. (2005) 'Comparison of time series tasseled cap wetness and the normalized difference moisture index in detecting forest disturbances', *Remote Sensing of Environment*, 94(3), pp. 364-372.
- Johnson, G., Oke, T., Lyons, T., Steyn, D., Watson, I. and Voogt, J.A. (1991) 'Simulation of surface urban heat islands under 'ideal' conditions at night Part 1: theory and tests against field data', *Boundary-Layer Meteorology*, 56(3), pp. 275-294.
- Kahle, A.B., Madura, D.P. and Soha, J.M. (1980) 'Middle infrared multispectral aircraft scanner data: analysis for geological applications', *Applied Optics*, 19(14), pp. 2279-2290.
- Kahraman, L.M. (2004) *Geographical analysis of the characteristics of soils and the problems of the province of Arbil and scalability land productivity*. PhD. Salahaddin University, Erbil, Iraq.
- Kalnay, E. and Cai, M. (2003) 'Impact of urbanization and land-use change on climate', *Nature*, 423(6939), pp. 528-531.
- Kalota, D., 2016. Exploring Relation of Land Surface Temperature with Selected Variables Using Geographically Weighted Regression and Ordinary Least Square Methods in Manipur State, India. *Geocarto International*, pp.1-15.
- Karim, K., H., Fattah, A., I. and Qader, F., M. (2015) 'First record of bedded limestone inside Upper Bakhtiari Formation, Sulaimani Governorate, Kurdistan Region, NE-Iraq', *Journal of Applied Geology and Geophysics*, 3(5), pp. 1-8.
- Karnieli, A., Agam, N., Pinker, R.T., Anderson, M., Imhoff, M.L., Gutman, G.G., Panov, N. and Goldberg, A. (2010) 'Use of NDVI and land surface temperature for drought assessment: merits and limitations', *Journal of Climate*, 23(3), pp. 618-633.
- Kaufmann, R., Zhou, L., Myneni, R., Tucker, C., Slayback, D., Shabanov, N. and Pinzon, J. (2003) 'The effect of vegetation on surface temperature: A statistical analysis of NDVI and climate data', *Geophysical Research Letters*, 30(22).
- Keramitsoglou, I., Kiranoudis, C.T., Ceriola, G., Weng, Q. and Rajasekar, U. (2011) 'Identification and analysis of urban surface temperature patterns in Greater Athens, Greece, using MODIS imagery', *Remote Sensing of Environment*, 115(12), pp. 3080-3090.
- Khalid, N. (2014) *Urban heat island in Erbil City*. Master. Lund University. Available at: <http://lup.lub.lu.se/student-papers/record/4449039>.

- Khandelwal, S., Goyal, R., Kaul, N. & Singhal, V. (2011) 'Study of Land Surface Temperature Variations with Distance from Hot Spots for Urban Heat Island Analysis', *Geospatial World Forum, Theme Dimensions and Directions of Geospatial Industry*. Hyderabad, India, 18-21 January.
- Kidder, S.Q. and Essenwanger, O.M. (1995) 'The effect of clouds and wind on the difference in nocturnal cooling rates between urban and rural areas', *Journal of Applied Meteorology*, 34(11), pp. 2440-2448.
- Kim, Y. and Baik, J. (2005) 'Spatial and temporal structure of the urban heat island in Seoul', *Journal of Applied Meteorology*, 44(5), pp. 591-605.
- Kruse, F.A. (1988) 'Use of airborne imaging spectrometer data to map minerals associated with hydrothermally altered rocks in the northern Grapevine Mountains, Nevada, and California', *Remote Sensing of Environment*, 24(1), pp. 31-51.
- Landsat, N.A.S.A., 7, Science Data Users Handbook. 2011-03-11.
http://landsathandbook.gsfc.nasa.gov/inst_cal/prog_sect8_2.html
- Landsberg, H.E. (1979) 'Atmospheric changes in a growing community', *Urban Ecology*, 4(1), pp. 53-81.
- Landsberg, H.E. (1981) *The urban climate*. Academic press, New York, USA.
- Lauer, D.T., Morain, S.A. and Salomonson, V.V. (1997) 'The Landsat program: Its origins, evolution, and impacts', *Photogrammetric Engineering and Remote Sensing*, 63(7), pp. 831-838.
- Lazzarini, M., Marpu, P.R. and Ghedira, H. (2013) 'Temperature-land cover interactions: the inversion of urban heat island phenomenon in desert city areas', *Remote Sensing of Environment*, 130, pp. 136-152.
- Lee, H. (1993) 'An application of NOAA AVHRR thermal data to the study of urban heat islands', *Atmospheric Environment. Part B, Urban Atmosphere*, 27(1), pp. 1-13.
- Lee, J.S., Kim, J.T. and Lee, M.G. (2014) 'Mitigation of urban heat island effect and greenroofs', *Indoor and Built Environment*, 23(1), pp. 62-69.
- Lee, S. and French, S.P. (2009) 'Regional impervious surface estimation: an urban heat island application', *Journal of Environmental Planning and Management*, 52(4), pp. 477-496.
- Lemonsu, A. and Masson, V. (2002) 'Simulation of a summer urban breeze over Paris', *Boundary-Layer Meteorology*, 104(3), pp. 463-490.

- Lenschow, D.H. and Dutton, J.A. (1964) 'Surface temperature variations measured from an airplane over several surface types', *Journal of Applied Meteorology*, 3(1), pp. 65-69.
- Li, J. and Li, J. (2008) 'Derivation of global hyperspectral resolution surface emissivity spectra from advanced infrared sounder radiance measurements', *Geophysical Research Letters*, 35(15).
- Li, S., Mo, H. and Dai, Y. (2011) 'Spatio-temporal Pattern of Urban Cool Island Intensity and Its Eco-environmental Response in Chang-Zhu-Tan Urban Agglomeration', *Communications in Information Science and Management Engineering*, 1(9), pp. 1-6.
- Li, Y., Zhang, H. and Kainz, W. (2012) 'Monitoring patterns of urban heat islands of the fast-growing Shanghai metropolis, China: Using time-series of Landsat TM/ETM data', *International Journal of Applied Earth Observation and Geoinformation*, 19, pp. 127-138.
- Li, Z., Becker, F., Stoll, M. and Wan, Z. (1999) 'Evaluation of six methods for extracting relative emissivity spectra from thermal infrared images', *Remote Sensing of Environment*, 69(3), pp. 197-214.
- Li, Z. and Becker, F. (1993) 'Feasibility of land surface temperature and emissivity determination from AVHRR data', *Remote Sensing of Environment*, 43(1), pp. 67-85.
- Li, Z., Wu, H., Wang, N., Qiu, S., Sobrino, J.A., Wan, Z., Tang, B. and Yan, G. (2013) 'Land surface emissivity retrieval from satellite data', *International Journal of Remote Sensing*, 34(9-10), pp. 3084-3127.
- Liang, S. & Shi, P. (2009) 'Analysis of the relationship between urban heat island and vegetation cover through Landsat ETM: A case study of Shenyang', *2009 Joint Urban Remote Sensing Event Shanghai*; China, 20-22 May.
- Liang, S., Li, X. and Wang, J. (2012) *Advanced remote sensing*. 1st edn. Amsterdam; Boston: Academic Press.
- Liu, L. and Zhang, Y. (2011) 'Urban heat island analysis using the Landsat TM data and ASTER data: A case study in Hong Kong', *Remote Sensing*, 3(7), pp. 1535-1552.
- Lopezgarcia, M.J., Caselles, V., Melia, J. and Perezcueva, A.J. (1991) 'NOAA-AVHRR contribution to the analysis of urban heat islands', in Guyot G. (ed.) *Physical Measurements and Signatures in Remote Sensing*. Harwood Academic, pp. 501-504.
- Lorenz, D. (1962) *Messungen der Bodenoberflächentemperatur vom Hubschrauber aus:(mit 9 Tabellen im Text)*. Selbstverl. des Deutschen Wetterdienstes.

- Ma, X.L., Wan, Z., Moeller, C.C., Menzel, W.P. and Gumley, L.E. (2002) 'Simultaneous retrieval of atmospheric profiles, land-surface temperature, and surface emissivity from Moderate-Resolution Imaging Spectroradiometer thermal infrared data: extension of a two-step physical algorithm', *Applied Optics*, 41(5), pp. 909-924.
- Ma, X.L., Wan, Z., Moeller, C.C., Menzel, W.P., Gumley, L.E. and Zhang, Y. (2000) 'Retrieval of geophysical parameters from Moderate Resolution Imaging Spectroradiometer thermal infrared data: evaluation of a two-step physical algorithm', *Applied Optics*, 39(20), pp. 3537-3550.
- Magee, N., Curtis, J. and Wendler, G. (1999) 'The urban heat island effect at Fairbanks, Alaska', *Theoretical and Applied Climatology*, 64(1-2), pp. 39-47.
- Majumdar, T., Pal, S. and Bhattacharya, A.K. (2012) 'Generation of emissivity and land surface temperature maps using MODIS TIR data for lithological mapping over the Singhbhum-Orissa Craton', *Journal of the Geological Society of India*, 80(5), pp. 685-699.
- Malinowski, J.C. (2002) *Iraq: A Geography*. ERIC.
- Mallick, Y.K.B. and Kerle, C.A. (2009) 'Satellite-based analysis of the role of land use/land cover and vegetation density on surface temperature regime of Delhi, india', *Journal of the Indian Society of Remote Sensing*, 37(2), pp. 201-214.
- Matson, M., McClain, E.P., McGinnis Jr, D.F. and Pritchard, J.A. (1978) 'Satellite detection of urban heat islands', *Monthly Weather Review*, 106(12), pp. 1725-1734.
- McMillin, L.M. (1975) 'Estimation of sea surface temperatures from two infrared window measurements with different absorption', *Journal of Geophysical Research*, 80(36), pp. 5113-5117.
- Media.tagorg (2013) Available at:
<http://media.tagorg.com/UploadImages/OfficesImages/Erbile%20Office%202013.JPG>
 (Accessed: 24 March 2016).
- Memon, R.A., Leung, D.Y. and Liu, C. (2009) 'An investigation of urban heat island intensity (UHII) as an indicator of urban heating', *Atmospheric Research*, 94(3), pp. 491-500.
- Menberg, K., Bayer, P., Zosseder, K., Rumohr, S. and Blum, P. (2013) 'Subsurface urban heat islands in German cities', *Science of the total environment*, 442, pp. 123-133.
- Miao, S., Chen, F., LeMone, M.A., Tewari, M., Li, Q. and Wang, Y. (2009) 'An observational and modeling study of characteristics of urban heat island and boundary layer structures in Beijing', *Journal of Applied Meteorology and Climatology*, 48(3), pp. 484-501.

- Mo, X., Cheng, C., Zhai, F. & Li, H. (2011) 'Study on temporal and spatial variation of the urban heat island based on Landsat TM/ETM+ in central city and Binhai New Area of Tianjin', *2011 International Conference on Multimedia Technology* Hangzhou; China., 26-28 July.
- Mochida, A., Murakami, S., Ojima, T., Kim, S., Ooka, R. and Sugiyama, H. (1997) 'CFD analysis of mesoscale climate in the Greater Tokyo area', *Journal of Wind Engineering and Industrial Aerodynamics*, 67, pp. 459-477.
- Montanaro, M., Lunsford, A., Tesfaye, Z., Wenny, B. and Reuter, D., 2014. Radiometric calibration methodology of the Landsat 8 thermal infrared sensor. *Remote Sensing*, 6(9), pp.8803-8821.
- Montávez, J.P., Rodríguez, A. and Jiménez, J.I. (2000) 'A study of the urban heat island of Granada', *International Journal of Climatology*, 20(8), pp. 899-911.
- Morris, C. and Simmonds, I. (2000) 'Associations between varying magnitudes of the urban heat island and the synoptic climatology in Melbourne, Australia', *International Journal of Climatology*, 20(15), pp. 1931-1954.
- MSDEG Meteorological and Seismological Department of Erbil Governorate (2014) *Elements Climatic Data of Erbil City*. Unpublished.
- Mu, Q., Zhao, M. and Running, S.W. (2011) 'Improvements to a MODIS global terrestrial evapotranspiration algorithm', *Remote Sensing of Environment*, 115(8), pp. 1781-1800.
- Mu, Q., Zhao, M. and Running, S.W., 2011. Brief introduction to MODIS evapotranspiration data set (MOD16).
- Mukherjee, S., Joshi, P.K. and Garg, R.D., 2015. Regression-Kriging technique to downscale satellite-derived land surface temperature in heterogeneous agricultural landscape. *IEEE Journal of Selected Topics in Applied Earth Observations and Remote Sensing*, 8(3), pp.1245-1250.
- NASA (2016a) *Land Surface Temperature: Global Maps*. Available at: http://earthobservatory.nasa.gov/GlobalMaps/view.php?d1=MOD11C1_M_LSTDA.
- NASA (2016b) *Near Surface Air Temperature — GES DISC - Goddard Earth Sciences Data and Information Services Center*. Available at: http://disc.gsfc.nasa.gov/hydrology/data-holdings/parameters/near_surf_air_temp.shtml.
- Nasrallah, H.A., Brazel, A.J. and Balling, R.C. (1990) 'Analysis of the Kuwait City urban heat island', *International Journal of Climatology*, 10(4), pp. 401-405.
- NGC (2015) Available at: http://www.ngcrealestate.com/realestate_en.php?Action=City&id_city=9 (Accessed: 24 March 2016).

- Nichol, J.E., Fung, W.Y., Lam, K. and Wong, M.S. (2009) 'Urban heat island diagnosis using ASTER satellite images and 'in situ' air temperature', *Atmospheric Research*, 94(2), pp. 276-284.
- Nichol, J. and Wong, M.S. (2005) 'Modeling urban environmental quality in a tropical city', *Landscape and Urban Planning*, 73(1), pp. 49-58.
- Niclòs, R., Caselles, V., Coll, C. and Valor, E., 2007. Determination of sea surface temperature at large observation angles using an angular and emissivity-dependent split-window equation. *Remote Sensing of Environment*, 111(1), pp.107-121.
- Oke, T.R. (1987) *Boundary layer climates*. 2nd edn. London: Routledge.
- Oke, T.R. (1982) 'The energetic basis of the urban heat island', *Quarterly Journal of the Royal Meteorological Society*, 108(455), pp. 1-24.
- Oke, T.R. (1973) 'City size and the urban heat island', *Atmospheric Environment* (1967), 7(8), pp. 769-779.
- Oke, T.R., Crowther, J., McNaughton, K., Monteith, J. and Gardiner, B. (1989) 'The micrometeorology of the urban forest [and discussion]', *Philosophical Transactions of the Royal Society B: Biological Sciences*, 324(1223), pp. 335-349.
- Oke, T.R., Spronken-Smith, R., Jauregui, E. and Grimmond, C. (1999) 'The energy balance of central Mexico City during the dry season', *Atmospheric Environment*, 33(24), pp. 3919-3930.
- Oke, T.R. (1976) 'The distinction between canopy and boundary-layer urban heat islands', *Atmosphere*, 14(4), pp. 268-277.
- Oke, T., Johnson, G., Steyn, D. and Watson, I. (1991) 'Simulation of surface urban heat islands under 'ideal' conditions at night part 2: diagnosis of causation', *Boundary-Layer Meteorology*, 56(4), pp. 339-358.
- One-thirteen (2009) *In and around Erbil City*. Available at: <https://www.flickr.com/photos/one-thirteen/3398097361/> (Accessed: 24 March 2016).
- Onishi, A., Cao, X., Ito, T., Shi, F. and Imura, H. (2010) 'Evaluating the potential for urban heat-island mitigation by greening parking lots', *Urban forestry & Urban greening*, 9(4), pp. 323-332.
- ORNL DAAC (2015) Available at: <http://daac.ornl.gov/MODIS/modis.html>.
- Ottlé, C. and Vidal-Madjar, D. (1992) 'Estimation of land surface temperature with NOAA9 data', *Remote Sensing of Environment*, 40(1), pp. 27-41.
- Pauw, E., D., Saba, M. and Ali, S., H. (2015) *Mapping climate change in Iraq and Jordan*. ICARDA.

- Peres, L.F. and DaCamara, C.C. (2005) 'Emissivity maps to retrieve land-surface temperature from MSG/SEVIRI', *IEEE Transactions on Geoscience and Remote Sensing*, 43(8), pp. 1834-1844.
- Pinheiro, A., Mahoney, R., Privette, J. and Tucker, C. (2006) 'Development of a daily long term record of NOAA-14 AVHRR land surface temperature over Africa', *Remote Sensing of Environment*, 103(2), pp. 153-164.
- Piringer, M., Grimmond, C., Joffre, S., Mestayer, P., Middleton, D., Rotach, M., Baklanov, A., De Ridder, K., Ferreira, J. and Guilloteau, E. (2002) 'Investigating the surface energy balance in urban areas—recent advances and future needs', *Water, Air and Soil Pollution: Focus*, 2(5-6), pp. 1-16.
- Potchter, O., Goldman, D., Kadish, D. and Iluz, D. (2008) 'The oasis effect in an extremely hot and arid climate: The case of southern Israel', *Journal of Arid Environments*, 72(9), pp. 1721-1733.
- Prata, A.J., 2002. *Land surface temperature measurement from space: AATSR algorithm theoretical basis document*. Contract Report to ESA, CSIRO Atmospheric Research, Aspendale, Victoria, Australia, 2002, pp.1-34.
- Price, J.C. (1984) 'Land surface temperature measurements from the split window channels of the NOAA 7 Advanced Very High Resolution Radiometer', *Journal of Geophysical Research*, 89(D5), pp. 7231-7237.
- Price, J.C. (1979) 'Assessment of the urban heat island effect through the use of satellite data', *Monthly Weather Review*, 107(11), pp. 1554-1557.
- Qin, Z., Karnieli, A. and Berliner, P. (2001) 'A mono-window algorithm for retrieving land surface temperature from Landsat TM data and its application to the Israel-Egypt border region', *International Journal of Remote Sensing*, 22(18), pp. 3719-3746.
- Qiu, G., LI, H., Zhang, Q., Wan, C., Liang, X. and Li, X. (2013) 'Effects of evapotranspiration on mitigation of urban temperature by vegetation and urban agriculture', *Journal of Integrative Agriculture*, 12(8), pp. 1307-1315.
- Qu, Z., Goetz, A.F.H. & Heidebrecht, K.B. (2000) 'High-accuracy atmosphere correction for hyperspectral data (HATCH)', *Proceedings of the Ninth JPL Airborne Earth Science Workshop* 1Jet Propul. Lab, Pasadena, USA, 23-25 February.
- R Core Team (ed.) (2014) *R: A language and environment for statistical computing*. R Foundation for Statistical Computing, Vienna, Austria.
- Ragnarsdóttir, K.V. and Banwart, S.A. (2015) *Soil: The Life Supporting Skin of Earth*.

- Rajasekar, U. and Weng, Q. (2009) 'Urban heat island monitoring and analysis using a non-parametric model: A case study of Indianapolis', *ISPRS Journal of Photogrammetry and Remote Sensing*, 64(1), pp. 86-96.
- Rao, P.K. and Winston, J.S. (1963) 'An investigation of some synoptic capabilities of atmospheric "window" measurements from satellite TIROS II', *Journal of Applied Meteorology*, 2(1), pp. 12-23.
- Rao, P. (1972) 'Remote sensing of urban heat islands from an environmental satellite', *Bulletin of the American Meteorological Society*, 53(7), pp. 647.
- Realmuto, V. (1990) 'Separating the effects of temperature and emissivity: Emissivity spectrum normalization', *2nd TIMS Workshop Pasadena, CA, USAJPL Publication*, pp. 23-27.
- Rees, G. and Rees, W.G. (2013) *Physical principles of remote sensing*. Cambridge University Press. Cambridge, CB2 8BS, United Kingdom.
- Rizwan, A.M., Dennis, L.Y. and Chunho, L. (2008) 'A review on the generation, determination and mitigation of Urban Heat Island', *Journal of Environmental Sciences*, 20(1), pp. 120-128.
- Roberts, D., Yamaguchi, Y. and Lyon, R. (1986) 'Comparison of various techniques for calibration of AIS data', *NASA STI/Recon Technical Report N*, 87, pp. 12970.
- Robinson Peter, J. and Ann, H. (1999) *Contemporary Climatology*. Prentice Hall, London, UK.
- Roth, M., Oke, T. and Emery, W. (1989) 'Satellite-derived urban heat islands from three coastal cities and the utilization of such data in urban climatology', *International Journal of Remote Sensing*, 10(11), pp. 1699-1720.
- Runnalls, K. and Oke, T. (2000) 'Dynamics and controls of the near-surface heat island of Vancouver, British Columbia', *Physical Geography*, 21(4), pp. 283-304.
- Saitoh, T., Shimada, T. and Hoshi, H. (1996) 'Modeling and simulation of the Tokyo urban heat island', *Atmospheric Environment*, 30(20), pp. 3431-3442.
- Saleh, S. (2011) 'Impact of urban expansion on surface temperature in Baghdad, Iraq using remote sensing and GIS techniques', *Canadian Journal on Environmental, Construction and Civil Engineering*, 2(8), pp. 193-202.
- Sarrat, C., Lemonsu, A., Masson, V. and Guedalia, D. (2006) 'Impact of urban heat island on regional atmospheric pollution', *Atmospheric Environment*, 40(10), pp. 1743-1758.
- Schönert, M., Zillmann, E., Weichelt, H., Eitel, J.U.H., Magney, T.S., Lilienthal, H., Siegmann, B. and Jarmer, T., 2015. The Tasseled Cap Transformation for

- RapidEye data and the estimation of vital and senescent crop parameters. *The International Archives of Photogrammetry, Remote Sensing and Spatial Information Sciences*, 40(7), p.101.
- Schultz, P. and Halpert, M. (1995) 'Global analysis of the relationships among a vegetation index, precipitation and land surface temperature', *Remote Sensing*, 16(15), pp. 2755-2777.
- Schwarz, N., Schlink, U., Franck, U. and Großmann, K. (2012) 'Relationship of land surface and air temperatures and its implications for quantifying urban heat island indicators - an application for the city of Leipzig (Germany)', *Ecological Indicators*, 18, pp. 693-704.
- SETS 2015 *Erbil Deep Boreholes, Environmental Impact Assessment Report*, World Vision International.
- Shahmohamadi, P., Che-Ani, A., Abdullah, N., Tahir, M., Maulud, K. and Mohd-Nor, M. (2010) 'The Link between urbanization and climatic factors: a concept on formation of urban heat island', *WSEAS Transactions on Environment and Development*, 6(11), pp. 754-768.
- Shahmohamadi, P., Che-Ani, A., Sodoudi, S. and Cubasch, U. (2012) 'Mitigating Urban Heat Island Effects in Tehran Metropolitan Area', in Budi Haryanto (ed.) *Air Pollution - A Comprehensive Perspective*. INTECH Open Access Publisher.
- Sharif, A. (1998) *Climate of the Erbil Region*. PhD. University of Salahadden, Erbil, Iraq.
- Shigeta, Y., Ohashi, Y. & Tsukamoto, O. (2009) 'Urban cool island in daytime - analysis by using thermal image and air temperature measurements', *The Seventh International Conference on Urban Climate* Yokohama, Japan, 29 June - 3 July.
- Skelhorn, C. (2013) *A fine scale assessment of urban greenspace impacts on microclimate and building energy in Manchester*. PhD. University of Manchester. Available at: <https://www.escholar.manchester.ac.uk/api/datastream?publicationPid=uk-ac-man-scw:221895&datastreamId=FULL-TEXT.PDF>.
- Small, C. (2002) 'Multitemporal analysis of urban reflectance', *Remote Sensing of Environment*, 81(2), pp. 427-442.
- Small, C. (2001) 'Estimation of urban vegetation abundance by spectral mixture analysis', *International Journal of Remote Sensing*, 22(7), pp. 1305-1334.
- Smith, J.O. (2010) *Determination of the convective heat transfer coefficients from the surfaces of buildings within urban street canyons*. University of Bath. Available at: http://opus.bath.ac.uk/27547/1/UnivBath_PhD_2010_J_Smith.pdf.

- Smith, W. and Woolf, H. (1976) 'The use of eigenvectors of statistical covariance matrices for interpreting satellite sounding radiometer observations', *Journal of the Atmospheric Sciences*, 33(7), pp. 1127-1140.
- Snyder, W.C., Wan, Z., Zhang, Y. and Feng, Y. (1998) 'Classification-based emissivity for land surface temperature measurement from space', *International Journal of Remote Sensing*, 19(14), pp. 2753-2774.
- Sobrino, J. and Raissouni, N. (2000) 'Toward remote sensing methods for land cover dynamic monitoring: application to Morocco', *International Journal of Remote Sensing*, 21(2), pp. 353-366.
- Sobrino, J.A., Jiménez-Muñoz, J.C., Labeled-Nachbrand, J. and Nerry, F. (2002) 'Surface emissivity retrieval from digital airborne imaging spectrometer data', *Journal of Geophysical Research: Atmospheres (1984–2012)*, 107(D23), pp. ACL 24-1-ACL 24-13.
- Sobrino, J.A., Jiménez-Muñoz, J.C. and Paolini, L. (2004) 'Land surface temperature retrieval from LANDSAT TM 5', *Remote Sensing of Environment*, 90(4), pp. 434-440.
- Sofer, M. and Potchter, O. (2006) 'The urban heat island of a city in an arid zone: the case of Eilat, Israel', *Theoretical and Applied Climatology*, 85(1-2), pp. 81-88.
- Solano, R., Didan, K., Jacobson, A. and Huete, A., 2010. MODIS vegetation index user's guide (MOD13 series). Vegetation Index and Phenology Lab, The University of Arizona, pp.1-38.
- Song, C., Woodcock, C.E. and Li, X. (2002) 'The spectral/temporal manifestation of forest succession in optical imagery: The potential of multitemporal imagery', *Remote Sensing of Environment*, 82(2), pp. 285-302.
- Souch, C. and Grimmond, S. (2006) 'Applied climatology: urban climate', *Progress in Physical Geography*, 30(2), pp. 270.
- Srivanit, M. and Hokao, K. (2012) 'Thermal Infrared Remote Sensing for Urban Climate and Environmental Studies: An Application for the City of Bangkok, Thailand', *JARS Journal of Architectural/Planning Research and Studies*, 9(1), pp. 83-100.
- Srivastava, P., Majumdar, T. and Bhattacharya, A.K. (2009) 'Surface temperature estimation in Singhbhum Shear Zone of India using Landsat-7 ETM thermal infrared data', *Advances in space research*, 43(10), pp. 1563-1574.
- Stathopoulou, M. and Cartalis, C. (2007) 'Daytime urban heat islands from Landsat ETM and Corine land cover data: An application to major cities in Greece', *Solar Energy*, 81(3), pp. 358-368.

- Steenefeld, G., Koopmans, S., Heusinkveld, B. and Theeuwes, N. (2014) 'Refreshing the role of open water surfaces on mitigating the maximum urban heat island effect', *Landscape and Urban Planning*, 121, pp. 92-96.
- Steinecke, K. (1999) 'Urban climatological studies in the Reykjavik subarctic environment, Iceland', *Atmospheric Environment*, 33(24), pp. 4157-4162.
- Stevens, S., S., 1946, On the Theory of Scales of Measurement. *Science*, 103 (2684), pp. 677–680. doi:10.1126/science.103.2684.677.
- Stewart, I.D. (2011) *Redefining the urban heat island*. PhD. University of British Columbia. Available at:
<https://open.library.ubc.ca/cIRcle/collections/ubctheses/24/items/1.0072360>.
- Stewart, I.D., Oke, T. and Krayenhoff, E.S. (2014) 'Evaluation of the 'local climate zone' scheme using temperature observations and model simulations', *International Journal of Climatology*, 34(4), pp. 1062-1080.
- Stewart, I. & Oke, T. (2009) 'Newly developed "thermal climate zones" for defining and measuring urban heat island magnitude in the canopy layer', Eighth Symposium on Urban Environment, Phoenix, AZ, USA.
- Streutker, D.R. (2002) 'A remote sensing study of the urban heat island of Houston, Texas', *International Journal of Remote Sensing*, 23(13), pp. 2595-2608.
- Su, Y., Foody, G.M. and Cheng, K. (2012) 'Spatial non-stationarity in the relationships between land cover and surface temperature in an urban heat island and its impacts on thermally sensitive populations', *Landscape and Urban Planning*, 107(2), pp. 172-180.
- Sun, D. and Kafatos, M. (2007) 'Note on the NDVI-LST relationship and the use of temperature-related drought indices over North America', *Geophysical Research Letters*, 34(24).
- Susca, T., Gaffin, S. and Dell'Osso, G. (2011) 'Positive effects of vegetation: Urban heat island and green roofs', *Environmental Pollution*, 159(8), pp. 2119-2126.
- Susskind, J., Barnet, C.D. and Blaisdell, J.M. (2003) 'Retrieval of atmospheric and surface parameters from AIRS/AMSU/HSB data in the presence of clouds', *IEEE Transactions on Geoscience and Remote Sensing*, 41(2), pp. 390-409.
- Szymanowski, M. and Kryza, M. (2012) 'Local regression models for spatial interpolation of urban heat island - an example from Wrocław, SW Poland', *Theoretical and Applied Climatology*, 108(1-2), pp. 53-71.
- Szymanowski, M. and Kryza, M. (2009) 'GIS-based techniques for urban heat island spatialization', *Climate Research*, 38(2), pp. 171.

- Taha, H. (1997) 'Urban climates and heat islands: albedo, evapotranspiration, and anthropogenic heat', *Energy and Buildings*, 25(2), pp. 99-103.
- Taha, H., Akbari, H. and Rosenfeld, A. (1991) 'Heat island and oasis effects of vegetative canopies: micro-meteorological field-measurements', *Theoretical and Applied Climatology*, 44(2), pp. 123-138.
- Tan, J., Zheng, Y., Tang, X., Guo, C., Li, L., Song, G., Zhen, X., Yuan, D., Kalkstein, A.J. and Li, F. (2010) 'The urban heat island and its impact on heat waves and human health in Shanghai', *International journal of biometeorology*, 54(1), pp. 75-84.
- Tarle, M. (2010) *Application of GIS in Defining Urban Heat Island Using Transect Data: Urban Heat Island Using GIS Mapping*. Saarbrücken, Germany: Lambert Academic Publishing.
- Tarleton, L.F. and Katz, R.W. (1995) 'Statistical explanation for trends in extreme summer temperatures at Phoenix, Arizona', *Journal of Climate*, 8(6), pp. 1704-1708.
- Tempfli, K., Huurneman, G., Bakker, W., Janssen, L., Bakker, W., Feringa, W., Gieske, A., Grabmaier, K., Hecker, C. and Horn, J. (2009) *Principles of remote sensing: an introductory textbook*. 4th Edition edn. Enschede, Netherlands: ITC.
- Terjung, W.H. and O'Rourke, P.A. (1980a) 'Simulating the causal elements of urban heat islands', *Boundary-Layer Meteorology*, 19(1), pp. 93-118.
- Terjung, W.H. and O'Rourke, P.A. (1980b) *Energy exchanges in urban landscapes: selected climatic models*. CW Thornthwaite Associates, Laboratory of Climatology.
- Tiangco, M., Lagmay, A. and Argete, J. (2008) 'ASTER-based study of the night-time urban heat island effect in Metro Manila', *International Journal of Remote Sensing*, 29(10), pp. 2799-2818.
- Todd, S., Hoffer, R. and Milchunas, D. (1998) 'Biomass estimation on grazed and ungrazed rangelands using spectral indices', *International Journal of Remote Sensing*, 19(3), pp. 427-438.
- Tomlinson, C., Prieto-Lopez, T., Bassett, R., Chapman, L., Cai, X., Thornes, J. and Baker, C. (2013) 'Showcasing urban heat island work in Birmingham—measuring, monitoring, modelling and more', *Weather*, 68(2), pp. 44-49.
- Tonkaz, T. and Cetin, M. (2007) 'Effects of urbanization and land-use type on monthly extreme temperatures in a developing semi-arid region, Turkey', *Journal of Arid Environments*, 68(1), pp. 143-158.

- Tran, H., Uchihama, D., Ochi, S. and Yasuoka, Y. (2006) 'Assessment with satellite data of the urban heat island effects in Asian mega cities', *International Journal of Applied Earth Observation and Geoinformation*, 8(1), pp. 34-48.
- Trenberth, K.E. (2004) 'Climatology (communication arising): rural land-use change and climate', *Nature*, 427(6971), pp. 213-213.
- Tupin, F., Inglada, J. and Nicolas, J. (2014) *Remote Sensing Imagery*. Hoboken, NJ, USA: John Wiley & Sons.
- Ukwattage, N. and Dayawansa, N. (2012) 'Urban Heat Islands and the Energy Demand: An Analysis for Colombo City of Sri Lanka Using Thermal Remote Sensing Data', *International Journal of Remote Sensing and GIS*, 1(2), pp. 124-131.
- Ulivieri, C., Castronuovo, M., Francioni, R. and Cardillo, A. (1994) 'A split window algorithm for estimating land surface temperature from satellites', *Advances in Space Research*, 14(3), pp. 59-65.
- Unger, J., Gál, T., Rakonczai, J., Musci, L., Szatman, J. & Tobak, Z. (2009) 'Air temperature versus surface temperature in urban environment', *7th international conference on urban climate* Yokohama, Japan, 29 June - 3 July.
- Upmanis, H., Eliasson, I. and Lindqvist, S. (1998) 'The influence of green areas on nocturnal temperatures in a high latitude city (Göteborg, Sweden)', *International Journal of Climatology*, 18(6), pp. 681-700.
- Ur, J., De Jong, L., Giraud, J., Osborne, J.F. and MacGinnis, J. (2013) 'Ancient cities and landscapes in the kurdistan region of Iraq: The Erbil plain archaeological survey 2012 season', *Iraq*, 75, pp. 89-117.
- urbanheatlands.com (2010) *Heat Island Types*. Available at: <http://www.urbanheatlands.com/heat-island-types> (Accessed: 30 March 2016).
- USGS (2016) *Landsat Data*. Available at: <http://earthexplorer.usgs.gov/>.
- USGS (2013) *Using the USGS Landsat 8 Product*. Available at: http://landsat.usgs.gov/Landsat8_Using_Product.php.
- Van de Griend, A. and Owe, M. (1993) 'On the relationship between thermal emissivity and the normalized difference vegetation index for natural surfaces', *International Journal of Remote Sensing*, 14(6), pp. 1119-1131.
- Voogt, J. (2002) *Urban heat island: Causes and consequences of global environmental change*. Chichester: John Wiley and Sons, Ltd.
- Voogt, J.A. (2004) *Urban heat islands: hotter cities*. Available at: <http://www.actionbioscience.org/environment/voogt.html>.

- Voogt, J.A. and Oke, T.R. (2003) 'Thermal remote sensing of urban climates', *Remote Sensing of Environment*, 86(3), pp. 370-384.
- Vowles G. (2013) *Urban Heat Islands*. Available at: <http://www.sustainablecitiescollective.com/glenn-vowles/165241/urban-heat-islands>.
- Wan, Z., 2007. Collection-5 MODIS land surface temperature products users' guide. *ICESSE, University of California, Santa Barbara*.
- Wan, Z. and Dozier, J. (1996) 'A generalized split-window algorithm for retrieving land-surface temperature from space', *IEEE Transactions on Geoscience and Remote Sensing*, 34(4), pp. 892-905.
- Wan, Z. and Li, Z. (1997) 'A physics-based algorithm for retrieving land-surface emissivity and temperature from EOS/MODIS data', *IEEE Transactions on Geoscience and Remote Sensing*, 35(4), pp. 980-996.
- Wang, F., Qin, Z., Song, C., Tu, L., Karnieli, A. and Zhao, S. (2015) 'An Improved Mono-Window Algorithm for Land Surface Temperature Retrieval from Landsat 8 Thermal Infrared Sensor Data', *Remote Sensing*, 7(4), pp. 4268-4289.
- Wark, D.Q., Yamamoto, G. and Lienesch, J. (1962) 'Methods of estimating infrared flux and surface temperature from meteorological satellites', *Journal of the Atmospheric Sciences*, 19(5), pp. 369-384.
- Watson, C. (2012) *Analysis of urban heat island climates along the I-85/I-40 corridor in central North Carolina*. PhD. University of North Carolina at Greensboro. Available at: https://libres.uncg.edu/ir/uncg/f/Watson_uncg_0154D_11024.pdf.
- Watson, K. (1992) 'Two-temperature method for measuring emissivity', *Remote Sensing of Environment*, 42(2), pp. 117-121.
- Wen, L., Lü, S., Chen, S., Meng, X. and Bao, Y. (2005) 'Numerical simulation of cold island effect in Jinta Oasis summer', *Plateau Meteorology*, 24(6), pp. 865-871.
- Weng, Q. (2009) 'Thermal infrared remote sensing for urban climate and environmental studies: Methods, applications, and trends', *ISPRS Journal of Photogrammetry and Remote Sensing*, 64(4), pp. 335-344.
- Weng, Q. (2001) 'A remote sensing? GIS evaluation of urban expansion and its impact on surface temperature in the Zhujiang Delta, China', *International Journal of Remote Sensing*, 22(10), pp. 1999-2014.
- Weng, Q. and Lu, D. (2008) 'A sub-pixel analysis of urbanization effect on land surface temperature and its interplay with impervious surface and vegetation coverage in Indianapolis, United States', *International journal of applied earth observation and geoinformation*, 10(1), pp. 68-83.

- Weng, Q., Lu, D. and Schubring, J. (2004) 'Estimation of land surface temperature–vegetation abundance relationship for urban heat island studies', *Remote Sensing of Environment*, 89(4), pp. 467-483.
- Wickham, H. (2009) *ggplot2: elegant graphics for data analysis*. Springer Science & Business Media.
- Witherick, M., Ross, S.R. and Small, R.J. (2001) *A modern dictionary of geography*. Oxford University Press. Oxford, OX2 6DP, UK.
- Wong, N.H. and Yu, C. (2005) 'Study of green areas and urban heat island in a tropical city', *Habitat International*, 29(3), pp. 547-558.
- Wu, C. and Murray, A.T. (2003) 'Estimating impervious surface distribution by spectral mixture analysis', *Remote Sensing of Environment*, 84(4), pp. 493-505.
- Wu, W. (2014) 'The generalized difference vegetation index (GDVI) for dryland characterization', *Remote Sensing*, 6(2), pp. 1211-1233.
- Wuertz, D. and Chalabi, Y. (2009) '*timeSeries: Rmetrics-Financial Time Series Objects*', R package version, 2100.
- Xiao, H. and Weng, Q. (2007) 'The impact of land use and land cover changes on land surface temperature in a karst area of China', *Journal of environmental management*, 85(1), pp. 245-257.
- Xu, H. (2007) 'Extraction of urban built-up land features from Landsat imagery using a thematic-oriented index combination technique', *Photogrammetric Engineering & Remote Sensing*, 73(12), pp. 1381-1391.
- Xu, Y., Qin, Z. & Lv, J. (2008) 'Comparative analysis of urban heat island and associated land cover change based in Suzhou City using Landsat data', *International Workshop on Education Technology and Training and International Workshop on Geoscience and Remote Sensing* Shanghai; China, 21-22 December.
- Yamashita, S., Sekine, K., Shoda, M., Yamashita, K. and Hara, Y. (1986) 'On relationships between heat island and sky view factor in the cities of Tama River basin, Japan', *Atmospheric Environment (1967)*, 20(4), pp. 681-686.
- Yao, Y., Liang, S., Cheng, J., Liu, S., Fisher, J.B., Zhang, X., Jia, K., Zhao, X., Qin, Q. and Zhao, B. (2013) 'MODIS-driven estimation of terrestrial latent heat flux in China based on a modified Priestley–Taylor algorithm', *Agricultural and Forest Meteorology*, 171, pp. 187-202.
- Youneszadeh, J.S. (2013) *The effect of land use on land surface temperature in the Netherlands*. Master. Lund University. Available at: <http://lup.lub.lu.se/luur/download?func=downloadFile&recordOid=4081671&fileOid=4090512>.

- Young, S.J., Johnson, B.R. and Hackwell, J.A. (2002) 'An in-scene method for atmospheric compensation of thermal hyperspectral data', *Journal of Geophysical Research: Atmospheres (1984–2012)*, 107(D24), pp. ACH 14-1-ACH 14-20.
- Yu, C. and Hien, W.N. (2006) 'Thermal benefits of city parks', *Energy and Buildings*, 38(2), pp. 105-120.
- Yuan, F. and Bauer, M.E. (2007) 'Comparison of impervious surface area and normalized difference vegetation index as indicators of surface urban heat island effects in Landsat imagery', *Remote Sensing of Environment*, 106(3), pp. 375-386.
- Zakaria, S., Al-Ansari, N., Mustafa, Y.T., Alshibli, M.D.J. and Knutsson, S., 2013. Macro Rain Water Harvesting Network to Estimate Annual Runoff at Koysinjak (Koya) District, Kurdistan Region of Iraq. *Engineering*, 5(12), p.956.
- Zha, Y., Gao, J. and Ni, S. (2003) 'Use of normalized difference built-up index in automatically mapping urban areas from TM imagery', *International Journal of Remote Sensing*, 24(3), pp. 583-594.
- Zhang, H., Qi, Z., Ye, X., Cai, Y., Ma, W. and Chen, M. (2013) 'Analysis of land use/land cover change, population shift, and their effects on spatiotemporal patterns of urban heat islands in metropolitan Shanghai, China', *Applied Geography*, 44, pp. 121-133.
- Zhang, J., Wang, Y. and Wang, Z. (2007) 'Change analysis of land surface temperature based on robust statistics in the estuarine area of Pearl River (China) from 1990 to 2000 by Landsat TM/ETM data', *International Journal of Remote Sensing*, 28(10), pp. 2383-2390.
- Zhang, Z., Ji, M., Shu, J., Deng, Z. and Wu, Y. (2008) 'Surface urban heat island in Shanghai, China: Examining the relationship between land surface temperature and impervious surface fractions derived from Landsat ETM imagery', *The International Archives of the Photogrammetry, Remote Sensing and Spatial Information Sciences*, 37, pp. 601-606.
- Zhao, L., Lee, X., Smith, R.B. and Oleson, K. (2014) 'Strong contributions of local background climate to urban heat islands', *Nature*, 511(7508), pp. 216-219.
- Zhao, W., Li, Z., Wu, H., Tang, B., Zhang, X., Song, X. and Zhou, G. (2013) 'Determination of bare surface soil moisture from combined temporal evolution of land surface temperature and net surface shortwave radiation', *Hydrological Processes*, 27(19), pp. 2825-2833.
- Zhou, L., Dickinson, R.E., Tian, Y., Fang, J., Li, Q., Kaufmann, R.K., Tucker, C.J. and Myneni, R.B. (2004) 'Evidence for a significant urbanization effect on climate in China', *Proceedings of the National Academy of Sciences of the United States of America*, 101(26), pp. 9540-9544.